RESILIENCE OF BALLASTED RAILWAY TRACKS EXPOSED TO EXTREME TEMPERATURE

By

CHAYUT NGAMKHANONG

A thesis submitted to the University of Birmingham

for the degree of DOCTOR OF PHILOSOPHY

School of Engineering

College of Engineering and Physical Sciences

University of Birmingham

December 2020

UNIVERSITY OF BIRMINGHAM

University of Birmingham Research Archive

e-theses repository

This unpublished thesis/dissertation is copyright of the author and/or third parties. The intellectual property rights of the author or third parties in respect of this work are as defined by The Copyright Designs and Patents Act 1988 or as modified by any successor legislation.

Any use made of information contained in this thesis/dissertation must be in accordance with that legislation and must be properly acknowledged. Further distribution or reproduction in any format is prohibited without the permission of the copyright holder.

Abstract

At present, railway track buckling, caused by extreme heat, is a serious concern that can lead to the huge loss of lives and assets. With increasing exposures to high temperatures globally, a greater expansion in Continuous Welded Rails (CWRs) can induce higher risk of track buckling, especially when track defects exist. Note that track lateral stability is one of the most critical considerations for safe and reliable railway infrastructures. In ballasted railway tracks, ballast layer holds sleepers in place and provides lateral resistance and stiffness to the track. This doctoral thesis aims at investigating the buckling behaviour of ballasted railway tracks under extreme temperatures to clearly understand this vulnerability in order to improve the ballast track's resilience to extreme temperatures.

This doctoral thesis first presents 3D Finite Element Modelling (FEM) of traditional and interspersed railway tracks exposed to extreme temperatures, through realistic modelling. The new findings highlight the buckling phenomena and failure mechanism of interspersed railway tracks, which are usually adopted during railway transformations from timber to concrete sleepered tracks in real-life practices around the world. All possible phenomena observed in the field are captured. The novel in-depth insight unprecedentedly instigates vulnerability and resilience of traditional and interspersed railway track systems exposed to extreme weather conditions. Moreover, the coupling DEM-FEM modelling are developed to deeply investigate the effect of ballast degradation and vulnerability on track lateral stability. This shows that the inspection of ballast profile is essential even though ballast condition seems to be good according to a visual inspection, as the hidden degraded ballast in the bottom layer can still undermine the buckling strength unexpectedly, resulting in increasing vulnerability to track buckling. The obtained results can be used for stability

and misalignment management of ballasted railway tracks. The key findings will enhance the development of inspection criteria for lateral resistance and support conditions, improve safety and reliability of rail network, and mitigate the risk of delays due to track buckling leading to unplanned maintenance. Lastly, this doctoral thesis also proposes a new type of resilient material to effectively increase track resilience and reduce the likelihood of track buckling.

Acknowledgements

I would like to take a moment to say thank you to the people who have contributed to this doctoral thesis and supported me throughout the years. First, I would like to express my deepest appreciation to my supervisor, Dr Sakdirat Kaewunruen for giving me the opportunities to study at the University of Birmingham and work as a teaching assistant and graduate research assistant under his supervision. I truly appreciate his guidance and patience in completing this doctoral thesis. He also taught me how to unlock my potential and be the best of myself. I am very pleased and proud that I had the opportunity to be his student. I would also like to thank my second supervisor, Prof Charalampos Baniotopoulos for his cheerful comments and continuous support during my time in Birmingham.

I would like to take this opportunity to thank Dr Mayorkinos Papaelias and Dr Xueyu Geng – my examiners, for the valuable comments and suggestions to improve this thesis.

Special thanks to Dr Keiichi Goto, Prof Ping Liu and Assistant Prof You Ruilin, visiting scholars at the University of Birmingham from Railway Technical Research Institute (RTRI), Jiangsu University of Science and Technology, and China Academic of Railway Science (CARS) for their kind assistance and guidance with the modelling and advanced computer simulation approach.

Special thanks to Dr Serdar Dindar and Dr Mohd Haniff Bin Osman, my senior colleagues from TOFU research group for their guidance on the PhD research

progression. Many thanks to all my friends in room N121, TOFU research group, Civil Engineering and BCRRE for the friendship and memorable times during my stay in Birmingham, in particular, Panrawee Rungskunroch, Dan Li, Xu Huang, Andre Luis Oliveira de Melo, Fatma Seyma Keskin, Mehmet Zahid Hamarat, Hamad Alawad, Jessada Sresakoolchai, and Pasakorn Sengsri.

I would like to offer my sincere gratitude to Dr Rodolfo Martins, and my colleagues at EVOLEO technologies company in Porto, Portugal for being a great host during my stay in Portugal. Special thanks to Dr Bruno J. Afonso Costa for his technical support on trackside monitoring and his contribution on the research paper.

My Sincere gratitude to Prof Erol Tutumluer, my supervisor at the University of Illinois at Urbana-Champaign for his support and guidance on the Discrete Element Modelling which is a part of my thesis. I would also like to acknowledge Prof Youssef M A Hashash and Bin Feng for their contributions and valuable comments on my research paper. Thanks to all my friends and colleagues at the University of Illinois at Urbana-Champaign for their friendship.

Special thanks to the School of Engineering, University of Birmingham for the PhD scholarship award. Also, I wish to express my gratitude to the European Commission for the financial sponsorship of the H2020-MSCA-RISE Project No. 691135 “RISEN: Rail Infrastructure Systems Engineering Network, (www.risen2rail.eu)”. I would like to thank everyone who has been involved in this project.

Finally, I would like to thank my parents for their encouragement, and support, and love through the years. Without them, it would not be possible to have this doctoral thesis. I dedicate this doctoral thesis to my family as an appreciation for their endless love.

List of Publications

This doctoral thesis is written in the format of collection of articles. This doctoral thesis is predominantly constituted of the following significant scientific articles:

Journal papers

Ngamkhanong, C., Kaewunruen, S., and Baniotopoulos, C. A Review on Modelling and Monitoring of Railway Ballast. *Structural Monitoring and Maintenance* **2017**, *4*(3), 195-220.

Ngamkhanong, C., Kaewunruen, S., and Afonso Costa, B. J. State-of-the-Art Review of Railway Track Resilience Monitoring. *Infrastructures* **2018**, *3*(1).

Ngamkhanong, C., Wey, C. M., and Kaewunruen, S. Buckling Analysis of Interspersed Railway Tracks. *Applied Sciences (Switzerland)* **2020**, *10*(9).

Ngamkhanong, C., Kaewunruen, S., and Baniotopoulos, C. Nonlinear Buckling Instabilities of Interspersed Railway Tracks. *Computer and Structures* **2021**, 249, 106516

Ngamkhanong, C., Feng, B., Tutumluer, E., Hashash, Y.M.A., and Sakdirat Kaewunruen, S. Evaluation of Lateral Stability of Railway Tracks due to Ballast Degradation. *Construction and Building Materials* **2021,** 278, 122342.

Ngamkhanong, C., Kaewunruen, S., and Baniotopoulos, C. Influences of Ballast Degradation on Railway Track Buckling. *Engineering Failure Analysis* **2021**, 122, 105252

Ngamkhanong, C., and Kaewunruen, S. Effects of under Sleeper Pads on Dynamic Responses of Railway Prestressed Concrete Sleepers Subjected to High Intensity Impact Loads. *Engineering Structures* **2020**, 214.

Conference papers

Ngamkhanong, C., Goto, K., and Kaewunruen, S. Sensitivity of Dynamic Responses of Railway Prestressed Concrete Sleepers with under Sleeper Pads to Impact Energy. Paper presented at the Proceedings of ISMA 2018 - International Conference on Noise and Vibration Engineering and USD 2018 - International Conference on Uncertainty in Structural Dynamics 2018.

Ngamkhanong, C., Nascimento, A. T., and Kaewunruen, S. Economics of Track Resilience. Paper presented at the IOP Conference Series: Materials Science and Engineering 2019.

Ngamkhanong, C., Kaewunruen, S., and Baniotopoulos, C. Thermal buckling behaviour of degraded railway tracks. Civil Engineering for a Disaster Resilient Society: Select Proceedings of VCDRR 2021.

Presentations/Invited talks

Ngamkhanong, C. Buckling analysis of ballasted railway track subjected to extreme high temperature. PGR symposium 2019. University of Birmingham, UK. ***(People's choice award)***

Ngamkhanong, C. Buckling analysis of ballasted railway track subjected to extreme high temperature. RISEN ECR Workshop 2019, Tampere University, Tampere, Finland. ***(Best presentation award)***

Ngamkhanong, C. Kaewunruen, S., and Baniotopoulos, C. Dynamic Responses of Railway Prestressed Concrete Sleepers with Under Sleeper Pads Subjected to Extreme Impact Loads. Poster Research Conference 2019. University of Birmingham, UK.

Ngamkhanong, C. Under Sleeper Pads (USPs) for Ballasted Railway Track. Thailand-World Rail Expansion Conference 2020, Bangkok, Thailand.

Ngamkhanong, C. Under Sleeper Pads (USPs) for Ballasted Railway Track. Online WEBINAR series 2020, Malabor Institute of Technology, India.

In addition, during the period of postgraduate study, the following papers were published:

Journal papers

You, R., Li, D., **Ngamkhanong**, C., Janeliukstis, R., and Kaewunruen, S. Fatigue Life Assessment Method for Prestressed Concrete Sleepers. *Frontiers in Built Environment* **2017**, *3*.

Kaewunruen, S., **Ngamkhanong, C.**, and Lim, C. H. Damage and Failure Modes of Railway Prestressed Concrete Sleepers with Holes/Web Openings Subject to Impact Loading Conditions. *Engineering Structures* **2018**, *176*, 840-48.

Kaewunruen, S., **Ngamkhanong, C.**, Papaelias, M., and Roberts, C. Wet/Dry Influence on Behaviors of Closed-Cell Polymeric Cross-Linked Foams under Static, Dynamic and Impact Loads. *Construction and Building Materials* **2018**, *187*, 1092-102.

Kaewunruen, S., Wang, Y., and **Ngamkhanong, C.** Derailment-Resistant Performance of Modular Composite Rail Track Slabs. *Engineering Structures* **2018**, *160*, 1-11.

Mansell, B., **Ngamkhanong, C.**, and Kaewunruen, S. Evaluating the Residual Life of Aged Railway Bridges. *Proceedings of the Institution of Civil Engineers: Forensic Engineering* **2018**, *171*(4), 153-62.

Ngamkhanong, C., and Kaewunruen, S. The Effect of Ground Borne Vibrations from High Speed Train on Overhead Line Equipment (Ohle) Structure Considering Soil-Structure Interaction. *Science of The Total Environment* **2018**, *627*, 934-41.

Ngamkhanong, C., Kaewunruen, S., and Baniotopoulos, C. Far-Field Earthquake Responses of Overhead Line Equipment (Ohle) Structure Considering Soil-Structure Interaction. *Frontiers in Built Environment* **2018**, *4*.

Kaewunruen, S., **Ngamkhanong, C.**, and Liu, X. Spectro-Temporal Responses of Curved Railway Tracks with Variable Radii of Arc Curves. *International Journal of Structural Stability and Dynamics* **2019**, *19*(4).

Kaewunruen, S., **Ngamkhanong, C.**, and Ng, J. Influence of Time-Dependent Material Degradation on Life Cycle Serviceability of Interspersed Railway Tracks Due to Moving Train Loads. *Engineering Structures* **2019**, *199*.

Ngamkhanong, C., Li, D., Remennikov, A. M., and Kaewunruen, S. Dynamic Capacity Reduction of Railway Prestressed Concrete Sleepers Due to Surface Abrasions Considering the Effects of Strain Rate and Prestressing Losses. *International Journal of Structural Stability and Dynamics* **2019**, *19*(1).

You, R., Goto, K., **Ngamkhanong, C.**, and Kaewunruen, S. Nonlinear Finite Element Analysis for Structural Capacity of Railway Prestressed Concrete Sleepers with Rail Seat Abrasion. *Engineering Failure Analysis* **2019**, *95*, 47-65.

Ngamkhanong, C., Ming, Q. Y., Li, T., and Kaewunruen, S. Dynamic Train-Track Interactions over Railway Track Stiffness Transition Zones Using Baseplate Fastening Systems. *Engineering Failure Analysis* **2020**, *118*.

Sengsri, P., **Ngamkhanong, C.**, Melo, A. L. O., and Kaewunruen, S. Experimental and Numerical Investigations into Dynamic Modal Parameters of Fiber-Reinforced Foamed Urethane Composite Beams in Railway Switches and Crossings. *Vibration* **2020**, *3*, 174-188.

Sengsri, P., **Ngamkhanong, C.**, Melo, A.L.O., Papaelias, M., and Kaewunruen, S. Damage Detection in Fiber-Reinforced Foamed Urethane Composite Railway Bearers Using Acoustic Emissions. *Infrastructures* **2020**, *5*, 50.

Kaewunruen, S., **Ngamkhanong, C.**, Yang, T. Large-Amplitude Vibrations of Spider Web Structures. *Applied Sciences (Switzerland)* **2020**, 10, 6032.

Kaewunruen, S., **Ngamkhanong, C.**, Sengsri, P., Ishida, M. On hogging bending test specifications of railway composite sleepers and bearers. *Frontiers in Built Environment* **2020**.

Kaewunruen, S., **Ngamkhanong, C.,** Xu, S. Large-amplitude free vibrations of imperfect spider web structures. *Scientific Reports* **2020**. *10(1)*, 1-9.

Conference papers

Kaewunruen, S., **Ngamkhanong, C.**, Janeliukstis, R., and You, R. Dynamic Amplification Factors for Railway Turnout Bearers in Switches and Crossings. Paper presented at the COMPDYN 2017 - Proceedings of the 6th International Conference on Computational Methods in Structural Dynamics and Earthquake Engineering 2017.

Kaewunruen, S., **Ngamkhanong, C.**, Janeliukstis, R., and You, R. Influences of Surface Abrasions on Dynamic Behaviours of Railway Concrete Sleepers. Paper presented at the 24th International Congress on Sound and Vibration, ICSV 2017 2017.

Lawrence, V., **Ngamkhanong, C.**, and Kaewunruen, S. An Investigation to Optimize the Layout of Protective Blast Barriers Using Finite Element Modelling. Paper presented at the IOP Conference Series: Materials Science and Engineering 2017.

Li, D., **Ngamkhanong, C.**, and Kaewunruen, S. Time-Dependent Topology of Railway Prestressed Concrete Sleepers. Paper presented at the IOP Conference Series: Materials Science and Engineering 2017.

Li, D., **Ngamkhanong, C.**, Kaewunruen, S. Influence of Surface Abrasion on Creep and Shrinkage of Railway Prestressed Concrete Sleepers. Paper presented at the IOP Conference Series: Materials Science and Engineering 2017.

Li, D., **Ngamkhanong, C.**, Kaewunruen, S. Influence of Vertical Holes on Creep and Shrinkage of Railway Prestressed Concrete Sleepers. Paper presented at the IOP Conference Series: Materials Science and Engineering 2017.

Liu, X., **Ngamkhanong, C.**, and Kaewunruen, S. Nonlinear Dynamic of Curved Railway Tracks in Three-Dimensional Space. Paper presented at the IOP Conference Series: Materials Science and Engineering 2017.

Ngamkhanong, C., Kaewunruen, S., Baniotopoulos, C., and Papaelias, M. Crossing Phenomena in Overhead Line Equipment (Ohle) Structure in 3d Space Considering Soil-Structure Interaction. Paper presented at the IOP Conference Series: Materials Science and Engineering 2017.

Ngamkhanong, C., Kaewunruen, S., and Remennikov, A. M. Static and Dynamic Behaviours of Railway Prestressed Concrete Sleepers with Longitudinal through Hole. Paper presented at the IOP Conference Series: Materials Science and Engineering 2017.

Ngamkhanong, C., Li, D., and Kaewunruen, S. Impact Capacity Reduction in Railway Prestressed Concrete Sleepers with Surface Abrasions. Paper presented at the IOP Conference Series: Materials Science and Engineering 2017.

Ngamkhanong, C., Li, D., Kaewunruen, S. Impact Capacity Reduction in Railway Prestressed Concrete Sleepers with Vertical Holes. Paper presented at the IOP Conference Series: Materials Science and Engineering 2017.

Ngamkhanong, C., Li, D., Remennikov, A., and Kaewunruen, S. Capacity Reduction in Railway Prestressed Concrete Sleepers Due to Dynamic Abrasions. Paper presented at 15th East-Asia Pacific Conference on Structural Engineering and Construction 2017.

Kaewunruen, S., **Ngamkhanong, C.**, Goto, K., and Janeliukstis, R. Asymmetrical Effects on Railway Turnout Bearers Due to Wheelset Impact over a Crossing Nose.

Proceedings of the International Conference on Road and Rail Infrastructure CETRA 2018.

Ngamkhanong, C., and Kaewunruen, S. Influence of Prestress Losses on the Dynamic over Static Capacity Ratios of Railway Concrete Sleepers. Presented at SynerCrete'18 International Conference on Interdisciplinary Approaches for Cement-based Materials and Structural Concrete 2018.

Ngamkhanong, C., Kaewunruen, S., Calçada, R., and Martin, R. Condition Monitoring of Overhead Line Equipment (Ohle) Structures Using Ground-Bourne Vibrations from Train Passages. 2018. In: Rodrigues H., Elnashai A. (eds) Advances and Challenges in Structural Engineering. GeoMEast 2018. Sustainable Civil Infrastructures. Springer

Ngamkhanong, C., Tang, T., and Kaewunruen, S. Dynamic Properties Evaluation of Railway Ballast Using Impact Excitation Technique. *Multidisciplinary Digital Publishing Institute Proceedings* **2018**, *2*(16), 1149.

Ngamkhanong, C., Kaewunruen, S., Calçada, R., and Martin, R. Failure of Overhead Line Equipment (Ohle) Structure under Hurricane. 2019. In: El-Naggar H., El-Zahaby K., Shehata H. (eds) Innovative Solutions for Soil Structure Interaction. GeoMEast 2019. Sustainable Civil Infrastructures. Springer

Kaewunruen, S., **Ngamkhanong, C.**, and Remennikov, A. M. Dynamic Responses of Railway Sleepers to Coupling Vertical and Lateral Forces. Paper presented at the

Proceedings of the 26th International Congress on Sound and Vibration, ICSV 2019.

Ngamkhanong, C., Goto, K., and Kaewunruen, S. Dynamic Responses of Railway Ballasted Track Considering Rail Pad Deterioration. Paper presented at the Journal of Physics: Conference Series 2018.

Goto, K., Minoura, S., Watanabe, T., **Ngamkhanong, C.**, and Kaewunruen, S. Impact Load Response of Pc Rail Joint Sleeper under a Passing Train. Paper presented at the Journal of Physics: Conference Series 2018.

Kaewunruen, S., Janeliukstis, R., and **Ngamkhanong, C.** Dynamic Properties of Fibre Reinforced Foamed Urethane Composites in Wet and Dry Conditions. Materials Today: Proceedings **2020**, 29, 7-10.

CONTENTS

CHAPTER 1 INTRODUCTION 1

1.1 Background and Motivation 1

1.2 Statement of Problems and Significance of Research 8

1.3 Scope of Work 12

1.4 Aim and Objectives 14

1.5 Thesis Structure 15

1.6 References 19

CHAPTER 2 A REVIEW OF BALLASTED RAILWAY TRACKS 27

2.1 Introduction 27

2.2 Ballasted Railway Tracks 28

2.2.1 Rail 29

2.2.2 Fastening systems 30

2.2.3 Rail pad 30

2.2.4 Sleeper 31

2.2.5 Under Sleeper Pad (USP) 34

2.2.6 Ballast 37

2.2.7 Sub-ballast 38

2.2.8 Subgrade 39

2.3 Interspersed Railway Track 39

2.4 A Review of Railway Track Modelling 42

2.4.1 Finite Element Method (FEM) 42

2.4.2 Discrete Element Method (DEM) 45

2.5 Summary 50

2.6 References 51

CHAPTER 3 A REVIEW OF VULNERABILITY OF BALLASTED RAILWAY TRACK BUCKLING TO EXTREME HEAT 60

3.1 Introduction 60

3.2 Axial Force in Rail due to Temperature Change 60

3.3 Track Buckling Theory 64

3.3.1 Buckling path and buckling regime 64

3.3.2 Buckling mode shapes 67

3.4 Track Buckling Analysis 74

3.5 Lateral Resistance of Ballasted Railway Tracks 79

3.6 Summary 86

3.7 References 87

CHAPTER 4 LINEAR BUCKLING ANALYSIS OF BALLASTED RAILWAY TRACKS 94

4.1 Introduction 94

4.2 Finite Element Modelling (FEM) 95

4.2.1 Boundary conditions 101

4.3 Linear Eigenvalue Buckling Analysis 102

4.3.1 Model validation 105

4.4 Results and Discussions 107

4.4.1 Buckling shape 107

4.4.2 Effects of torsional resistance and lateral resistance 120

4.4.3 Buckling temperature reduction 123

4.4.4 Recommendations for interspersed approach 125

4.5 Summary 128

4.6 Reference 132

CHAPTER 5 NONLINEAR BUCKLING ANALYSIS OF BALLASTED RAILWAY TRACKS 134

5.1 Introduction 133

5.2 Finite Element Modelling (FEM) 134

5.2.1 Boundary conditions 136

5.3 Nonlinear Buckling Analysis 138

5.4 Buckling Path 140

5.4.1 Safe temperature evaluation 141

5.5 Results and Discussions 148

5.5.1 Buckling shape 148

5.5.2 Rail axial force 156

5.5.3 Effects of lateral resistance 160

5.5.4 Effects of track misalignment 166

5.5.5 Buckling Criteria 171

5.6 Summary 174

5.7 References 177

CHAPTER 6 LATERAL RESISTANCE OF BALLASTED RAILWAY TRACKS 179

6.1 Introduction 179

6.2 Discrete Element Modelling (DEM) 182

6.2.1 Ballast particle shapes 183

6.2.2 DEM parameters 184

6.2.3 Physical model 186

6.3 Ballast Fouling Mechanism 188

6.4 Ballast Layer Preparation 191

6.5 Results and Discussions 195

6.6 Summary 208

6.7 References 210

CHAPTER 7 INFLUENCES OF BALLAST DEGRADATION ON BALLASTED TRACK BUCKLING 212

7.1 Introduction 212

7.2 Modelling 213

7.3 Simulation Approach 216

7.4 Results and Discussions 219

7.4.1 Buckling temperature 219

7.4.2 Rail axial force 224

7.4.3 Safety criteria and allowable temperature 229

7.5 Summary 236

7.6 References 238

CHAPTER 8 UNDER SLEEPER PADS (USPs) SUBJECTED TO EXTREME IMPACT LOADING 239

8.1 Introduction 239

8.2 Life Cycle Cost Analysis (LCCA) 241

8.3 Finite Element Modelling (FEM) 245

8.3.1 Model validation 249

8.4 Results and Discussions 250

8.4.1 Mode shapes and frequencies 250

8.4.2 Impact loads 253

8.4.3 Sleeper responses 256

8.4.4 Ballast responses 264

8.5 Summary 269

8.6 References 273

CHAPTER 9 CONCLUSIONS AND RECOMMENDATIONS 277

9.1 Introduction 277

9.2 Research Findings 277

9.2.1 Parametric studies to identify critical parameters influencing buckling strength 278

9.2.2 Coupling method FEM-DEM for lateral vulnerability influencing track buckling phenomena 281

9.2.3 Under Sleeper Pad (USPs) for ballast protection from extreme impact loads 282

9.3 Recommendations for Future Research 284

LIST OF FIGURES

Figure 1.1 Heat incidents by asset type from 15 June to 19 July 2015 (Ferranti et al., 2018). 3

Figure 1.2 Number of track buckling incidents in the UK from 2012 to 2018 (Edgley, 2018). 4

Figure 1.3 Passengers at Waterloo station on the hottest day of the year in the UK (Hawken and Akbar, 2018). 5

Figure 1.4 Schematic representation of the thesis structure. 16

Figure 2.1 Typical cross section of ballasted railway track. 28

Figure 2.2 Ballasted railway track with rotten timber sleepers. 32

Figure 2.3 Ballasted railway track with concrete sleepers. 33

Figure 2.4 Typical ballasted railway track and its components with USP (Kaewunruen et al., 2017). 35

Figure 2.5 Load distribution of railway track: (a) with USPs and (b) without USPs. 36

Figure 2.6 Problems in interspersed railway tracks: (a) mud pumping and (b) ballast pulverisation and dilation. 42

Figure 2.7 Particle shapes for DEM: (a) sphere, (b) spherical clump, and (c) polyhedral. 46

Figure 3.1 Bar extension due to increase in temperature. 61

Figure 3.2 Restrained bar. 61

Figure 3.3 Force in the bar due to increase in temperature if both ends are restrained. ... 62

Figure 3.4 Buckling of restrained bar due to the force P. 63

Figure 3.5 Axial force in rails in ballasted railway track. 64

Figure 3.6 Buckling path: (a) snap-through buckling and (b) progressive buckling. 65

Figure 3.7 Symmetrical buckling shape (Lankyrider, 2014). 68

Figure 3.8 Asymmetrical buckling shape (Clark, 2018). 69

Figure 3.9 Sinusoidal buckling shape. 69

Figure 3.10 First symmetrical buckling shape (Kerr, 1978). 70

Figure 3.11 First asymmetrical buckling shape (Kerr, 1978). 71

Figure 3.12 Second symmetrical buckling shape (Kerr, 1978). 72

Figure 3.13 Second asymmetrical buckling shape (Kerr, 1978). 73

Figure 3.14 Contribution of sleeper–ballast contact force on lateral resistance. 79

Figure 3.15 Lateral resistance and benchmarked values. 85

Figure 4.1 Spring model for lateral ballast resistance: (a) normal springs with no movement, (b) linear elastic spring with stiffness k at both ends, (c) linear elastic spring with stiffness k at one end, and (d) nonlinear tensionless spring with stiffness 2k at both ends. 97

Figure 4.2 Ballasted railway track modelling. 98

Figure 4.3 Railway track models: (a) timber sleepered track, (b) ‘1 in 2’ interspersed track, (c) ‘1 in 3’ interspersed track, (d) ‘1 in 4’ interspersed track, and (e) concrete sleepered track..... 101

Figure 4.4 Boundary conditions..... 102

Figure 4.5 Linear bifurcation buckling path (Strand7 Pty Ltd, 2005). 104

Figure 4.6 Buckling shape of railway tracks under different conditions and with 6-m unconstrained length: (a) Lateral resistance = 200 N/mm and (b) Lateral resistance = 2000 N/mm 112

Figure 4.7 Buckling shape of railway tracks under different conditions and with 12-m unconstrained length: (a) Lateral resistance = 200 N/mm and (b) Lateral resistance = 2000 N/mm. 113

Figure 4.8 Buckling shape of railway tracks under different conditions and with 18-m unconstrained length: (a) Lateral resistance = 200 N/mm and (b) Lateral resistance = 2000 N/mm. 114

Figure 4.9 Buckling shape of railway tracks under different conditions with 24-m unconstrained length: (a) Lateral resistance = 200 N/mm and (b) Lateral resistance = 2000 N/mm. 115

Figure 4.10 Buckling shape of railway tracks under different conditions with 30-m unconstrained length: (a) Lateral resistance = 200 N/mm and (b) Lateral resistance = 2000 N/mm. 116

Figure 4.11 Buckling temperature over neutral and unconstrained length of railway tracks with lateral resistance of (a) 200 N/mm, (b) 800 N/mm, (c) 1400 N/mm, and (d) 2000 N/mm. 119

Figure 4.12 Effects of ballast lateral and fastening torsional resistance of (a) timber sleepered track, (b) 1 in 2 interspersed track, (c) 1 in 3 interspersed track, (d) 1 in 4 interspersed track, and (e) concrete sleepered track. 122

Figure 4.13 Buckling temperature over neutral difference relative to timber sleepered track: (a) 6-m unconstrained length, (b) 12-m unconstrained length, and (c) 30-m unconstrained length..... 125

Figure 4.14 Railway track with concrete sleeper consisting of unconstrained and constrained lengths: (a) boundary condition and (b) buckling shape 126

Figure 4.15 Spot replacement approach every 20 spans: (a) boundary condition and (b) buckling shape. 128

Figure 5.1 Nonlinear tensionless spring with stiffness 2k at both ends..... 135

Figure 5.2 Ballasted railway track modelling. 136

Figure 5.3 Initial misalignment..... 137

Chapter 5. Figure 5.4 Elastoplastic model for ballast tensionless spring. 139

Figure 5.5 Thermal load defined in LS-DYNA. 139

Figure 5.6 Buckling path..... 141

Figure 5.7 Elastoplastic model for lateral ballast spring..... 143

Figure 5.8 Safe temperature evaluation using indirect method from progressive buckling curves. 144

Figure 5.9 Rail axial force against temperature rise above neutral: (a) snap-through buckling and (b) progressive buckling..... 146

Figure 5.10 Safe temperature evaluation using rail axial force-temperature rise curves.147

Figure 5.11 Measured elements. 148

Figure 5.12 Lateral displacement of railway tracks due to temperature rise: (a) 8mm misalignment and (b) 32mm misalignment. 149

Figure 5.13 Buckling of timber sleepered track (Misalignment = 8mm, Lateral resistance = 200N/mm, W_p = 1mm) exposed to: (a) 20°C, (b) 50°C, (c) 100°C, and (d) 150°C.... 152

Figure 5.14 Buckling of timber sleepered track (Misalignment = 8mm, Lateral resistance = 2000N/mm, W_p = 1mm) exposed to: (a) 50°C, (b) 90°C, (c) 100°C, and (d) 150°C.. 153

Figure 5.15 Buckling of timber sleepered track (Misalignment = 32mm, Lateral resistance = 200N/mm, W_p = 1mm) exposed to: (a) 20°C, (b) 50°C, (c) 100°C, and (d) 150°C.... 154

Figure 5.16 Buckling of timber sleepered track (Misalignment = 32mm, Lateral resistance = 2000N/mm, W_p = 1mm) exposed to: (a) 20°C, (b) 50°C, (c) 100°C, and (d) 150°C.. 156

Figure 5.17 Axial force-temperature relationship of railway tracks with 8mmmisalignment: (a) timber sleepered tracks and (b) concrete sleepered tracks. 158

Figure 5.18 Axial force-temperature relationship of railway tracks with 32mm misalignment: (a) timber sleepered tracks and (b) concrete sleepered tracks. 159

Figure 5.19 Buckling and safe temperatures of railway tracks with track lateral resistance with Wp = 1mm and lateral misalignment amplitude of: (a) 8mm, (b) 16mm, (c) 24mm, and (d) 32mm. 163

Figure 5.20 Buckling and safe temperatures of railway tracks with track lateral resistance with Wp = 2mm and initial misalignment amplitude of: (a) 8mm, (b) 16mm, (c) 24mm, and (d) 32mm. 165

Figure 5.21 Effects of track lateral misalignment on buckling temperature of railway tracks with lateral stiffness of: (a) 200N/mm, (b) 800N/mm, (c) 1400N/mm, and (d) 2000N/mm. 168

Figure 5.22 Effects of track lateral misalignment on safe temperature of railway tracks with lateral stiffness of: (a) 200N/mm, (b) 800N/mm, (c) 1400N/mm, and (d) 2000N/mm.. 170

Figure 5.23 Allowable temperature considering lateral misalignment and lateral resistance with 1mm displacement limit: (a) timber sleepered track, (b) 1 in 2, (c) 1 in 3, d) 1 in 4, and (e) concrete sleepered track 172

Figure 5.24 Allowable temperature considering lateral misalignment and lateral resistance with 2mm displacement limit: (a) timber sleepered track, (b) 1 in 2, (c) 1 in 3, (d) 1 in 4, and (e) concrete sleepered track. 173

Figure 6.1 Contribution of sleeper–ballast contact force on lateral resistance. 179

Figure 6.2. Ballast Particle Size Distribution (PSD) based on AREMA No. 24. 184

Figure 6.3 Sleeper and ballast layer geometry with no ballast crib and shoulder: (a) timber sleeper and (b) concrete sleeper. 187

Figure 6.4 Schematic view of ballast layer with ballast crib and shoulder..... 188

Figure 6.5. Critical ballast fouling phases: (a) Phase 1: clean ballast, (b) Phase 2: partially fouled ballast, and (c) Phase 3: heavily fouled ballast (Huang et al., 2009)..... 189

Figure 6.6 Schematic view of (a) clean ballast layer, (b) 100-mm fouled ballast layer, (c) 200-mm fouled ballast layer, and (d) fully fouled ballast layer..... 191

Figure 6.7 Ballast layer preparation step 1. 192

Figure 6.8 Ballast layer preparation step 2. 193

Figure 6.9 Ballast layer preparation step 3. 193

Figure 6.10 Ballast layer preparation step 4. 194

Figure 6.11 Ballast layer preparation step 5. 194

Figure 6.12 Ballast layer preparation step 6. 195

Figure 6.13 Lateral force–displacement: (a) timber sleeper and (b) concrete sleeper.... 196

Figure 6.14 Lateral resistance of ballasted track at 2-mm sleeper displacement with benchmarked values..... 198

Figure 6.15. Timber/concrete sleeper lateral resistance ratio. 199

Figure 6.16. Lateral force–displacement of timber sleeper considering fouled ballast: (a) timber sleeper with no ballast shoulder and (b) timber sleeper with ballast shoulder.... 201

Figure 6.17. Lateral force–displacement of concrete sleeper considering fouled ballast: (a) concrete sleeper with no ballast shoulder and (b) concrete sleeper with ballast shoulder. 202

Figure 6.18. Lateral resistance reduction due to ballast fouling. 202

Figure 6.19. Contribution of each component: (a) timber sleeper and (b) concrete sleeper. 204

Figure 6.20 Contact force chain of ballast layer with timber sleeper with different conditions: (a) clean ballast, (b) 100-mm fouled ballast, (c) 200-mm fouled ballast, and (d) fully fouled ballast. 206

Figure 6.21 Contact force chain of ballast layer with concrete sleeper with different conditions: (a) clean ballast, (b) 100-mm fouled ballast, (c) 200-mm fouled ballast, and (d) fully fouled ballast. 207

Figure 7.1 (a) Finite Element modelling of ballasted railway track (b) Nonlinear lateral ballast spring representing sleeper-ballast lateral resistance. 215

Figure 7.2 Ballast fouling conditions: (a) 100 mm fouled layer (b) 200 mm fouled layer (c) fully fouled. 216

Figure 7.3 Lateral force-displacement curve for: (a) Timber sleepers (b) Concrete sleepers. 218

Figure 7.4 Buckling temperature over neutral and buckling axial force of railway tracks with timber sleepers: (a) misalignment = 8 mm (b) misalignment = 16 mm (c) misalignment = 24 mm (d) misalignment = 32 mm. 222

Figure 7.5 Buckling temperature over neutral and buckling axial force of railway tracks with concrete sleepers (a) misalignment = 8 mm (b) misalignment = 16 mm (c) misalignment = 24 mm (d) misalignment = 32 mm. 224

Figure 7.6 Rail axial force – temperature rise above neutral of tracks with concrete sleepers and clean ballast: (a) 6 m unconstrained length (b) 30 m unconstrained length..... 226

Figure 7.7 Rail axial force – temperature rise above neutral of tracks considering ballast fouling conditions: (a) 6 m unconstrained length, 8 mm misalignment (b) 6 m unconstrained length, 32 mm misalignment (c) 30 m unconstrained length, 8 mm misalignment (d) 30 m unconstrained length, 32 mm misalignment..... 229

Figure 7.8 Buckling temperature and safe temperature of railway tracks with timber sleepers: (a) unconstrained length = 6 m (b) unconstrained length = 12 m (c) unconstrained length = 18 m (d) unconstrained length = 24 m (e) unconstrained length = 30 m. 231

Figure 7.9 Buckling temperature and safe temperature of railway tracks with concrete sleepers: (a) unconstrained length = 6 m (b) unconstrained length = 12 m (c) unconstrained length = 18 m (d) unconstrained length = 24 m (e) unconstrained length = 30 m. 232

Figure 7.10 Allowable temperature rise of railway tracks with timber sleepers: (a) unconstrained length = 6 m (b) unconstrained length = 12 m (c) unconstrained length = 18 m (d) unconstrained length = 24 m (e) unconstrained length = 30 m..... 234

Figure 7.11 Allowable temperature rise of railway tracks with concrete sleepers: (a) unconstrained length = 6 m (b) unconstrained length = 12 m (c) unconstrained length = 18 m (d) unconstrained length = 24 m (e) unconstrained length = 30 m..... 235

Figure 8.1 USP glued to the sleeper (Kaewunruen et al., 2017)..... 241

Figure 8.2 Comparison of the annual cost of railway tracks with and without USP..... 244

Figure 8.3 Cumulative present values (NPV) of two projects..... 245

Figure 8.4 Finite element model of sleeper with USP..... 248

Figure 8.5 Comparison between numerical and experimental results: (a) contact shock load and (b) acceleration at rail seat (top) and mid-span (bottom)..... 250

Figure 8.6 Impact loads of with initial velocities of drop mass of (a) 0.74 m/s (A), (b) 1.94 m/s (B), and (c) 3.14 m/s (C). 255

Figure 8.7 Von Mises stress contour of sleeper: (a) without USP and (b) with USP. 257

Figure 8.8 von Mises stress under impact load case C: (a) rail seat and (b) mid span. .. 258

Figure 8.9 Stress contour of sleeper with USP under impact load case C at each time point. 259

Figure 8.10 Maximum von Mises stress at: (a) rail seat and (b) mid span. 260

Figure 8.11 Sleeper maximum displacement ratio at rail seat 262

Figure 8.12 Insertion loss due to USP under load cases: (a) case A, (b) case B, and (c) case C. 264

Figure 8.13 Sleeper-ballast contact force: (a) case A, (b) case B, and (c) case C. 266

Figure 8.14 Sleeper-ballast contact force reduction. 267

Figure 8.15 Ballast responses: (a) sleeper-ballast contact force, (b) von Mises stress at rail seat over time, and (c) von Mises stress distributions. 269

LIST OF TABLES

Table 2.1 Advantages and disadvantages of timber sleepers. 33

Table 2.2 Advantages and disadvantages of concrete sleepers. 34

Table 2.3 USP applications and characterisations (International Union of Railway, 2013). 37

Table 2.4 Summary of advantages and disadvantages of particle shapes for DEM. 49

Table 3.1 Safety criteria and allowable temperature (European Rail Research Institute Committee D202, 1995). 67

Table 3.2 Description of research gap. 76

Table 3.3 Previous research on lateral resistance of ballasted tracks. 82

Table 4.1 Material properties. 99

Table 4.2 Buckling load factor (BLF). 105

Table 4.3 Buckling temperatures for model validation (°C). 106

Table 4.4 Buckling shapes of timber sleepered tracks. 109

Table 4.5 Buckling shapes of timber sleepered tracks (Contd.). 110

Table 6.1 Imaging-based shape indices of ballast particles as discrete elements in DEM model. 184

Table 6.2 DEM parameters. 186

Table 6.3 Sleeper characteristics. 187

Table 7.1 Material properties. 214

Table 7.2 Lateral force-displacement equations. 218

Table 8.1 Initial cost construction (Guedelha, 2012). 243

Table 8.2 Maintenance cost. 243

Table 8.3 Sleeper dimension (Austrack Broad Gauge Sleeper). 247

Table 8.4 Material properties. 248

Table 8.5 Mode shapes and natural frequencies (dynamic strength, $f'_{c,d}$= 90 MPa)..... 252

Table 8.6 Contact force and impulse. 256

CHAPTER 1

INTRODUCTION

1.1 Background and Motivation

At present, railway systems play a vital role in modern transportation systems by quickly and safely transporting large amounts of cargoes and large numbers of passengers. Due to an increase in capacity and the growth of investment in railway infrastructure improvement, railway infrastructure has become a valuable asset throughout the world. It is interesting to note that the rapid increase in rail traffic is a major challenge as an approximate 10% reduction in road traffic means a 100% increase in railway traffic (Powrie, 2014). Not only the increase in passengers and freight but also the changes in the global climate have become the main reason that compels railway infrastructures to frequently undertake maintenance operations (Oslakovic et al., 2012, Koetse and Rietveld, 2009, Leviäkangas et al., 2011). Because of the increased demand, railway track infrastructure needs significantly higher capacity to carry passengers and freight while ensuring its good conditions. Apart from increasing traffic demands, many natural hazards, such as storms, earthquakes, snowstorms, extreme temperatures, and flash floods, can be a cause of failure of ageing railway infrastructures.

Extreme events, generally rare occurrences, have become a serious concern and more common under present climate condition (Field et al., 2012). The likelihood of extreme events is described by the return period, which is the average interval between one such event and its recurrence. Normally, the extreme events are of high intensity with a short duration with sometimes no signs of early warning. Nonetheless, a number of extreme events tend to increase in both magnitude and frequency, which will greatly create impacts that can cause damage or problems to any transportation system, namely, concerning the

infrastructure, operations, freight, and passengers. Note that the effects of climate change cause a slight deterioration of the railway infrastructure and may significantly affect its performance when extreme events occur (Dobney et al., 2009, Sogabe et al., 2013). As for the existing tracks, railway traffic together with the poor construction and progressive degradation of the railway tracks is compounded with the effects of extreme events, leading to frequent and severe disruptions to the railway system (Armstrong et al., 2016). Some of the common damages to rail assets subjected to such extreme events are damaged track components, track geometry misalignment, track buckling, and shear tunnelling cracks. These could significantly lead to a progressive failure of key structural systems, such as switches and crossings, railway bridges and tunnels, and even open railway tracks. It is important to note that about 5–10% of all failures are weather related, being mostly caused by extreme temperatures (Oslakovic et al., 2012). It is important to note that an increase in the frequency of high temperature occurrences will lead to more track buckling problems, which can induce train derailments and other dangerous accidents.

Presently, global temperatures have been increasing continuously by the average of 0.7 °C per year. Due to the rise in temperature, this can cause damage and loss to the railway infrastructure around the globe. It is found that the failures of rail infrastructure are weather-related. This failure due to extreme weathers tend to be more frequently. The future incidents of railway tracks can be predicted by the correlated data about the performance of rail infrastructure such as past failure with related weather conditions (Oslakovic et al., 2012). It is consequently seen that the extreme temperature tends to have the significant impact not only on the railway tracks but also the other railway infrastructure assets in the entire network, as shown in Figure 1.1. Note that track buckling

is the second major incident caused by extremely high temperatures in summer, while signalling incidents are the most serious problem, as reported by Ferranti et. al. (2018).

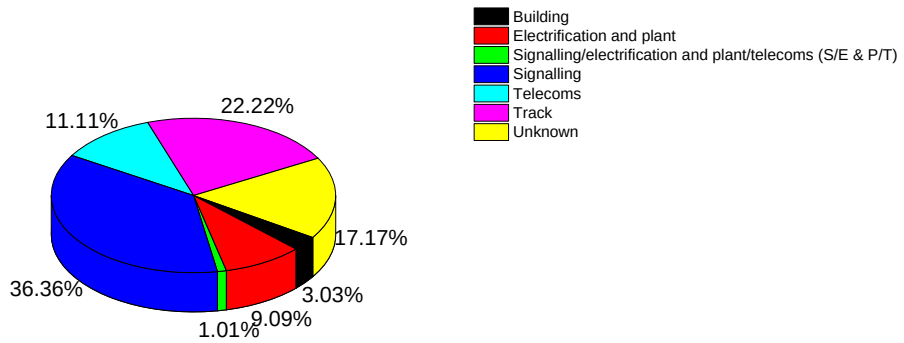

Figure 1.1 Heat incidents by asset type from 15 June to 19 July 2015 (Ferranti et al., 2018).

In summer, as found in many reports and open literature, the number of hot days (over 20 °C air temperature) is proportional to the number of track buckles (Edgley, 2018). Note that, in 2017/18, although there were fewer very hot days than in the previous years, the number of track buckling incidents increased, as the hottest day was observed in 2017/18. This was due to not only an increase in the air temperature but also a lack of appropriate railway track conditions. It was reported that the factors causing track buckling in summer include the lack of ballast support, insufficient confinement, incorrect rail stress, and track misalignment that can significantly undermine the buckling strength of a railway track; in other words, buckling could easily occur when exposed to extreme heat.

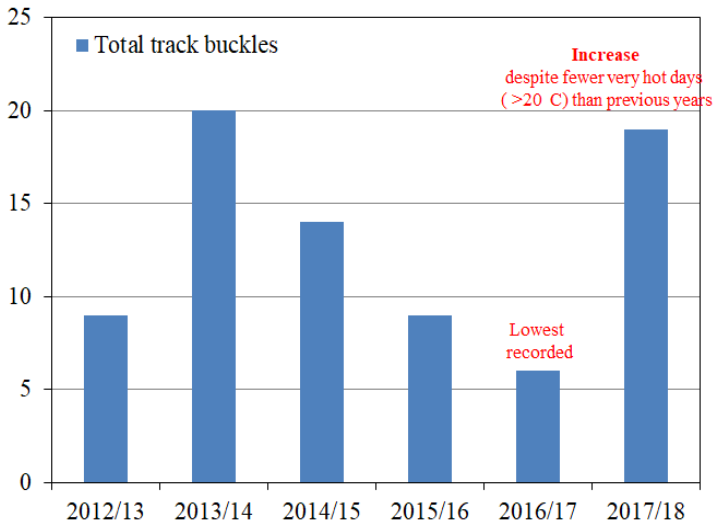

Figure 1.2 Number of track buckling incidents in the UK from 2012 to 2018 (Edgley, 2018).

Moreover, many research studies have indicated that track buckling is one of the causes of train derailments, which has led to the huge loss of lives and assets, as illustrated by many evidences (Ling et al., 2014, Kaewunruen et al., 2018, Ngamkhanong et al., 2018). The derailment risk of trains at railway turnouts was studied (Dindar et al., 2016); the researchers found that the number of train derailments at railway turnouts was relatively high in summer because of the heat-related irregularities and the buckling of tracks. Approximately 40 to 140 incidents of train derailments found in the USA between 1975 and 1989 were caused by track buckling (Thompson, 1991). It has also been reported that in 2006, track buckling caused 50 incidents of derailment with the reported damage of USD 13 million. Even though the buckling-related derailment events reduced to 34 incidents as compared to the year before, the reported loss increased to USD 34 million.

Importantly, in the regions where the rail temperature tends to exceed the limit, the train speed needs to be restricted to prevent or reduce the likelihood of track buckling, as the

additional force can be applied to the rails by the train. Note that speed restrictions are normally applied after the maintenance activities until the track stabilisation is achieved. This may cause train delays and disruptions, as can be seen in the news in summer. For instance, the Waterloo station in the UK was packed with passengers because of the train delays and cancellations on the hottest day in 2018 (Figure 1.3). Note that train speed restriction policies have been drafted and proposed over the railway network in different countries on the basis of the air temperature, expected rail temperature, sleeper types, and maintenance activities (Network Rail, 2006, Network Rail, 2008, RailCorp, 2013, Queensland Railways, 1988) For example, in the UK, Network Rail proposed the speed restrictions of 45 mph and 90 mph that need to be applied on timber and concrete sleepered tracks, respectively, when the air temperature reaches 36 °C, while the expected rail temperature is 53°C (Network Rail, 2006).

Figure 1.3 Passengers at Waterloo station on the hottest day of the year in the UK (Hawken and Akbar, 2018).

As mentioned earlier, a railway track buckling has become one of the serious concerns for track engineers because of the higher average summer temperatures observed globally and the increasing risk of track buckling noted around the world (Quinn, 2017). Theoretically,

an increase in the global temperatures can induce higher rail temperatures and build up the compression force in the Continuous Welded Rail (CWR). Despite the fact that CWR provides a smoother ride and has a relatively low maintenance cost, CWR suffers from the drawbacks in which the track can buckle easily when the rail temperature reaches the safe temperature or buckling strength. It has been found that the track components developing resistance to rail buckling are the sleeper and the supporting ballast. Lateral ballast resistance not only resists track buckling but also helps to maintain the lateral track alignment, which is one of the reasons for the lateral force in the rails. The ballast providing lateral resistance can be stated as the most significant factor in resisting the buckling forces during the expansion of the rail. The lateral resistance of a ballast consists of the following three main components: bottom friction of sleeper, side friction of sleeper, and ballast shoulder restraint (Kish and Samavedam, 2013).

Many researchers have reported the effects of the sleeper and the ballast on the track's lateral resistance by using Single Sleeper (Tie) Push Tests (STPTs). This method has been proven to be the most suitable method to quantify the lateral resistance of tracks, as recommended by (American Railway Engineering and Maintenance-of-Way Association, 2004). Considerable research has been conducted on the STPTs of sleepers to obtain the lateral resistance–displacement curve of the sleepers for the ballasted track (Jing and Aela, 2020). This method can measure the lateral resistance of the sleeper–ballast interaction. Researchers in the past have conducted STPTs using both numerical and experimental methods to obtain the lateral resistance of tracks. As for numerical methods, different methods have been applied for quantifying the lateral resistance force through Finite Element Method (FEM) and Discrete Element Method (DEM). The lateral resistance of

ballasted tracks can be reduced by the loss of compaction of the ballast layer. Moreover, note that maintenance activities, such as sleeper removals, ballast tamping, and track realignment, have a significant impact by reducing the buckling resistance, as the ballast is disturbed and has less compaction (Huang, 2010). As the ballast is a major factor affecting the lateral resistance of a track, it is clear that ballast degradation leads to insufficient confinement for maintaining the stability of the track. However, it has been widely reported that track buckling can occur even if the railway track and ballast seem to in a good condition, according to a visual inspection. In fact, degraded ballast particles and the accumulation of ballast breakdown due to the impact loads or outside contamination, such as subgrade intrusion or coal dust, often may not be seen visually as these particles can be hidden in the bottom layer (Sussmann et al., 2012). Its presence would undoubtedly have a negative impact on the vertical stiffness of the railway tracks and cause potential track geometry defects. No quantifiable data currently exist on the extent to which the degraded ballast can influence the lateral stiffness of the ballasted track and the percentage of fine particles generated in a fouled ballast that would decrease the lateral support through direct contact with the sleeper. Accordingly, there is a clear need to study and quantify the effect of the progressive degradation of the ballast influencing the lateral resistance by appropriately considering the contributions of the different frictional components in a ballasted track. The influences of the progressive degradation of the ballast may undermine the buckling strength leading to the significant need to evaluate its effects on buckling temperature of ballasted railway tracks. Note that major cause of ballast breakage is the impact loads which are generated from the irregularities of either wheel or rail. Hence, it is important to prevent ballast breakage from impact loads in order to maintain the stiffness

and stability of ballasted railway tracks (Remennikov and Kaewunruen, 2008). As the major causes of ballast breakage is the impact loads which are generated from the irregularities of either wheel or rail, many methods (e.g. rail pad, Under Sleeper Pad (USP), Under Ballast Mat (UBM)) have been proposed to reduce the transmitted load from train to the ballast and underlying substructure (Setsobhonkul et al., 2017). Recent studies mostly adopted the USPs to reduce noise and vibration of the tracks and moderate track stiffness at transition zone (Paixão et al., 2015, Le Pen et al., 2018, Mottahed et al., 2018). They mostly focused on the performance of USPs under static, quasi-static, and normal dynamic loads. It is crucial to study its effects on the tracks under extreme impact loads in order to improve the design to prevent ballast breakage.

This doctoral thesis aims at investigating the buckling phenomena of ballasted railway tracks exposed to extreme temperatures, through realistic modelling. This study combines two methods, namely FEM and DEM, to potentially create a realistic modelling. Lastly, this doctoral thesis also proposes the method to improve track resilience and prevent the progressive degradation of the ballast from impact loads using USP. The insight into the railway track buckling analysis derived from this doctoral thesis will underpin the life cycle design, maintenance, and construction strategies related to the ageing railway track systems.

1.2 Statement of Problems and Significance of Research

Previous investigations have shown that the buckling strength of ballasted railway tracks is influenced by the track conditions, track layer geometries, and types of elements and materials used (fasteners, sleepers, and ballast). According to previous studies on the track

buckling analysis, the most significant factor that influences the buckling strength is the track's lateral resistance, which is provided by the sleeper and the ballast (Kish, 2011). The lateral resistance of tracks consists of the sleeper base–ballast friction, sleeper side–ballast friction, and ballast shoulder end force. Importantly, different types of sleepers provide different values of lateral resistance, and the contribution of lateral resistance of each part is attributed to its geometry and properties (Zakeri and Bakhtiary, 2014, Kish et al., 1995, Lichtberger, 2007, Tutumluer et al., Jing et al., 2019, Guo et al., 2020, Jing et al., 2018). Note that buckling usually occurs on ageing railway tracks with purely timber sleepers. This is attributed to the lightweight of timber and its ease to degrade over time that may reduce the lateral resistance of tracks (Zarembski, 2016). To improve the buckling strength of ageing railway tracks, many researchers have proposed compacting the ballast, increasing the torque of the fastening system, and replacing the old sleepers by the heavier ones (Jing and Aela, 2020, Zarembski, 2016). Many researchers have studied the STPTs to obtain the lateral resistance of different types of sleepers. As for ageing railway tracks, many studies have proposed replacing the rotten sleepers by heavier sleepers such as concrete to the whole track; however, this may incur a huge cost. Thus, a spot replacement approach, which is a cost-effective method to improve track performance, may help increase the buckling strength if a heavier sleeper such as a concrete one is used. Note that this type of track has never been proposed and studied for track buckling analysis and prevention despite the common uses in various countries.

As for track modelling that consists of a series of beam and discrete spring elements, most of the previous studies modelled the ballast as a spring; however, most researchers used a normal spring, taking both compression and tension into account, to represent the ballast.

By nature, a ballast is a coarse aggregate that provides the tensionless elastic support to the superstructure (Nguyen et al., 2003). Thus, a tensionless spring must be used to reflect the actual behaviour of a ballast that only resists compression. This could significantly affect the results, leading to unreliable predictions. Note that such a spring should be applied to all the directions, including vertical, longitudinal, and transverse.

As observed in many studies on the lateral resistance of ballasted tracks, the displacement limit of the lateral force–displacement obtained by STPTs is usually lower than that used in the previous buckling analysis. However, none of the previous studies on track buckling used the actual value from STPTs for track modelling. For instance, 2 mm and 5 mm were used as a displacement limit for the lateral resistance of a ballast in the latest research papers (Villalba Sanchis et al., 2018, Pucillo, Carvalho et al., 2013), while the displacement limit obtained in STPTs is likely to be smaller than the above values (Jing et al., 2018, Khatibi et al., 2017). This implies that the previous studies slightly overestimated the buckling temperature of the ballasted tracks, which might mislead the practitioners in using their findings for a buckling temperature estimation. Hence, there is a clear need to investigate the buckling behaviour of railway tracks by using the actual properties and resistance values. Although track buckling has been widely investigated numerically in the past (Villalba et al., 2017, Villalba Sanchis et al., 2018, Cuadrado et al., 2008, Carvalho et al., 2013, Prud'Homme and Janin, 1969, Kerr, 1978, Kerr, 1980, Samavedam et al., 1993, Sussmann et al., 2003, Ole, 2008), interspersed tracks and their inconsistency have never been fully analysed. Hence, there is still a significant need to fully address the benefits of interspersed tracks in improving the resilience and the buckling prevention of ballasted tracks.

Note that the buckling shapes of railway tracks that have been analysed in the previous numerical approaches were the symmetrical and anti-symmetrical shapes only; however, in reality, bucking shapes can be sinusoidal waves creating a more severe and wider area of rail damage. This aspect has never been addressed before, raising a question which condition of the ballast tracks can lead to this phenomenon. Moreover, note that previous analytical solutions only provided the mathematical solution for the first few typical shapes, which did not cover the sinusoidal shape (Kerr, 1978).

Furthermore, as evidenced in the UK and worldwide, railway track buckling can still occur even when the railway tracks are fully supported and the ballast layer seems to be in a good condition according to a visual inspection. In fact, degraded ballast particles and the accumulation of ballast breakdown or outside contamination, such as subgrade intrusion or coal dust, often may not be seen visually (Sussmann et al., 2012, Anbazhagan et al., 2012). Their presence undoubtedly would have a negative impact on the vertical stiffness of the railway tracks and cause potential track geometry defects. No quantifiable data currently exist on the extent to which a degraded ballast could influence the lateral stiffness of the ballasted track and what percentage of the fine particles generated in a fouled ballast would decrease the lateral support through direct contact with the sleeper. Accordingly, there is a need to study and quantify the effect of the progressive degradation of the ballast influencing the lateral resistance by appropriately considering the contributions of the different frictional components in a ballasted track. The bucking analysis of ageing railway tracks is conducted in this doctoral thesis to identify the buckling regime that could potentially help to inspect the ballast conditions that encounter extreme temperatures.

Several methods have been used to improve lateral resistance, e.g. heavier sleepers and USPs. USPs were proposed to increase the contact area between a sleeper and a ballast. It was reported that the lateral resistance of a ballasted track could be increased significantly by using USPs (Sol-Sánchez et al., 2014). There have been many studies showing that USPs can help to reduce noise and vibration and redistribute the load to the ballast (Paixão et al., 2018, Schneider et al., 2011, Setsobhonkul et al., 2017). Note that not only does this study focus on the normal serviceability condition, but it also investigates an extreme condition, which can usually occur when there are coupled effects of short- and long-wavelength defects (Kaewunruen and Chiengson, 2018). These events may cause ballast breakage that can possibly undermine the lateral stability of ballasted railway tracks. However, the field measurement data showed that the sleepers with USPs could have lesser flexures, contact force, and impact energy, but sleeper vibration could be amplified by installing USPs, which is more likely to be seen at areas prone to impact loading (Kaewunruen, 2012). Although the effects of USPs on railway tracks have been widely studied, the performance of USPs under extreme impact loads has never been investigated in the open literature. It is essential to improve the design of USP for dynamic and impact problems. An alternative USP is also proposed in this doctoral thesis to overcome the drawbacks of the traditional ones.

1.3 Scope of Work

This study illustrates the buckling phenomenon of ballasted railway tracks under extreme heat by using the coupling methods between FEM and DEM. Firstly, this study reviews the modelling procedures for a ballasted railway track for the buckling analysis in order to

understand and minimise the computational time and memory consumption, while maintaining the quality of the model and the appropriate amount of data. After a review of the previous models of ballasted tracks, the coupling model between FEM and DEM was found to be the most suitable for the buckling analysis, as it could help to provide a realistic model and reduce the simulation time and storage. The FEM part is conducted using the commercial software 'LS-DYNA', while the DEM part uses the 'BLOKS3D' DEM software developed and extensively used at the University of Illinois at Urbana-Champaign in the last three decades. Note that the DEM part is undertaken under the H2020-MSCA-RISE Project No. 691135 RISEN: Rail Infrastructure Systems Engineering Network. Note that this study mainly focuses on the numerical simulation of the behaviour of ballasted railway tracks under extreme temperatures, as the experimental results and field measurement data have rarely been reported and are very limited, as such analyses require massive facilities for the full-scale tracks. Thus, in this study, the numerical results were first validated against the previous analytical solutions and numerical approaches. The parametric studies are conducted using both linear and nonlinear analyses to evaluate the major factor influencing the track buckling phenomena.

The STPT using DEM, is carried out at the University of Illinois at Urbana-Champaign under the RISE program. The DEM software called BLOSK3D developed by the University of Illinois at Urbana-Champaign is used for analysing the lateral resistance of ballasted track, considering the progressive degradation of the ballast. The DEM simulation results are validated against the benchmarking STPT values proposed by a recent European review and the previous STPT results reported by other researchers. These STPT results obtained from DEM are then applied in FEM to analyse the effects of ballast degradation

on the buckling behaviour. Various factors related to track degradation are considered, including the progressive fouling of the ballast and track misalignment. Lastly, the FEM of a single span ballasted track for the impact experiment is built using LS-DYNA to investigate the dynamic responses of the ballasted track. This part includes USP to study its influences on the track behaviour under extreme impact conditions which are the major cause of ballast breakage. The sleeper vibrations and ballast contact pressure are also obtained. Furthermore, this thesis proposes an alternative USP for use in areas prone to extreme conditions.

1.4 Aim and Objectives

This study aims at investigating the buckling behaviour of ballasted railway tracks under extreme temperatures to clearly understand this vulnerability in order to improve the ballast track's resilience to extreme temperatures. The FEM coupled with DEM of the ballasted railway tracks is investigated. The aims of this study are achieved by completing the following objectives:

- Review the problem and the gap of previous studies on the buckling of ballasted railway tracks to extreme heat.
- Identify the critical parameters and conditions of the ballasted tracks influencing track buckling.
- Investigate the buckling phenomena of a railway ballasted track subjected to extreme temperatures by using the coupling method FEM–DEM considering various track and component conditions, e.g. ballast conditions, boundary conditions, fastening system, and track degradation.

- Propose a cost-effective method to help improve the buckling strength and the resilience of ballasted tracks.
- Analyse the buckling behaviour of a ballasted track, considering the progressive fouling conditions of the ballast to further help to inspect the ballast conditions in summer.
- Analyse the dynamic responses of a ballasted track with USP to appropriately identify the effects on USP on the areas prone to extreme loading conditions.

1.5 Thesis Structure

This doctoral thesis consists of nine chapters, including the introduction and the conclusion. Figure 1.4 clarifies the structure of this thesis and helps the reader find the correct focus of the work. This doctoral thesis is written in the format of article collection (‘called compilation thesis’). The thesis structure is based on an alternative format thesis 7.4.1 from the University of Birmingham regulation. Chapter 1 presents a general introduction and background of this doctoral thesis. The main structure of this doctoral thesis excluding Chapter 1 can be divided into three main parts: critical review, original studies, and conclusion. The critical review section consists of two chapters: a review of a ballasted railway track (Chapter 2) and a review of railway track buckling (Chapter 3).

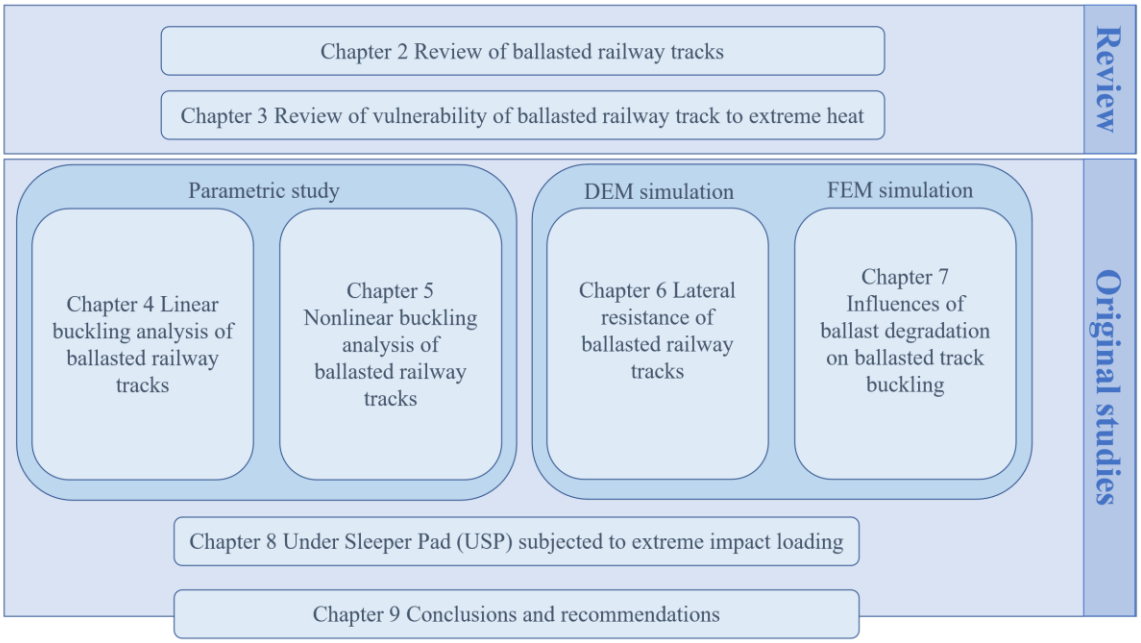

Figure 1.4 Schematic representation of the thesis structure.

Chapter 2 reviews the main components of the railway ballasted track and their functions and contributions to the railway systems. This is followed by the literature review on an interspersed railway track, which is an effective short-term solution for an ageing ballasted track. At the end of Chapter 2, the review of the ballasted track modelling for different aspects is presented. This will help the readers determine the appropriate method to use for modelling a railway track and its components for different purposes. Chapter 3 reviews the previous studies on railway track buckling. This chapter also provides the factors affecting track vulnerability that have been studied in the previous literature. This chapter reports that there are some research gaps on railway track buckling that researchers have not fully investigated. Furthermore, the original studies in this thesis are presented in Chapters 4–8. In Chapters 4 and 5, the buckling phenomena of ballasted railway tracks are investigated using FEM on the basis of parametric studies. Chapter 4 uses a linear buckling analysis to analyse the buckling shape and the corresponding buckling temperature of railway tracks.

The major factors affecting track buckling are taken into account. However, this method cannot analyse the whole behaviour of railway track buckling because of the limitations of the linear analysis, and hence, only the pre-buckling stage is discussed. This chapter also proposes a cost-effective solution to improve the buckling strength of railway tracks. In Chapter 5, a nonlinear analysis is proposed to overcome the drawbacks of the linear analysis described in Chapter 4. This method can capture both the pre- and the post-buckling stages. The actual material properties can be included in this analysis, resulting in a more realistic behaviour of ballasted track buckling. The buckling and the safe temperatures of ballasted railway tracks are analysed. It is known from the outcome of Chapters 4 and 5 that the major factor influencing the buckling resistance is the lateral resistance of a ballast. The coupling DEM–FEM is presented in Chapters 6 and 7. According to the critical review in Chapter 3, even though the lateral resistance of a ballasted track has been widely analysed, a research gap has been found, and more importantly, an appropriate lateral resistance has never been applied in the track buckling analysis. Chapter 6 presents the DEM simulations of the Single Sleeper (Tie) Push Test (STPT) with the consideration of the progressive fouling conditions of a ballast. In accordance, the results are input in Chapter 7 as a lateral spring in track models to analyse the buckling phenomenon of the ballasted tracks. Chapter 8 presents the effects of an Under Sleeper Pad (USP) on the overall track performance subjected to extreme impact loading. Note that previous researchers found that USPs could potentially help attenuate vibration and increase the lateral resistance. However, a few recent studies have illustrated that USPs may induce higher sleeper vibrations when used in the areas prone to impact loading. This chapter focuses on the effects of USPs on the dynamic responses of ballasted track under

extreme impact loads, which are the main cause of ballast breakdown. Lastly, the conclusions of the thesis and the recommendations for future study are presented in Chapter 9.

1.6 References

AMERICAN RAILWAY ENGINEERING AND MAINTENANCE-OF-WAY ASSOCIATION 2004. Manual for Railway Engineering.

ANBAZHAGAN, P., BHARATHA, T. P. & AMARAJEEVI, G. 2012. Study of Ballast Fouling in Railway Track Formations. *Indian Geotechnical Journal,* 42**,** 87-99.

ARMSTRONG, J., PRESTON, J. & HOOD, I. Adapting railways to provide resilience and sustainability. 2016 2016. Thomas Telford Ltd, 225-234.

CARVALHO, J., DELGADO, J., CALÇADA, C. & DELGADO, R. 2013. A new methodology for evaluating the safe temperature in continuous welded rail tracks. *International Journal of Structural Stability and Dynamics* 13**,** 1350016.

CUADRADO, M., ZAMORANO, C., GONZÁLEZ, P., NASARRE, J. & ROMO, E. Analysis of buckling in dual-gauge tracks. 2008 2008. Thomas Telford Ltd, 177-184.

DINDAR, S., KAEWUNRUEN, S., AN, M. & MOHD, O. 2016. Natural Hazard Risks on Railway Turnout Systems. *Procedia Engineering* 161**,** 1254–1259.

DOBNEY, K., BAKER, C. J., QUINN, A. D. & CHAPMAN, L. 2009. Quantifying the effects of high summer temperatures due to climate change on buckling and rail related delays in south-east United Kingdom. *Meteorological Applications: A journal of forecasting, practical applications, training techniques and modelling,* 16**,** 245-251.

EDGLEY, J. 2018. Summer Track Engineering Conference.

FERRANTI, E., CHAPMAN, L., LEE, S., JAROSZWESKI, D., LOWE, C., MCCULLOCH, S. & QUINN, A. 2018. The hottest J uly day on the railway network: insights and thoughts for the future. *Meteorological Applications,* 25**,** 195-208.

FIELD, C. B., BARROS, V., STOCKER, T. F. & DAHE, Q. 2012. *Managing the risks of extreme events and disasters to advance climate change adaptation: special report of the intergovernmental panel on climate change*, Cambridge University Press.

GUO, Y., FU, H., QIAN, Y., MARKINE, V. & JING, G. 2020. Effect of sleeper bottom texture on lateral resistance with discrete element modelling. *Construction and Building Materials,* 250.

HAWKEN, A. & AKBAR, J. 2018. SUNSET UK Weather – Travel chaos as sweltering commuters pack Waterloo on hottest day of 2018 – but MORE heat to come. The Sun, UK, 27 June. Avaliable at: https://www.thesun.co.uk/news/6617442/uk-weather-forecast-met-office-warning-temperature-heatwave/

HUANG, H. 2010. *Discrete Element Modeling of Railroad Ballast Using Imaging Based Aggregate Morphology Characterization.* Doctor of Philosophy PhD Thesis, University of Illinois at Urbana-Champaign.

JING, G. & AELA, P. 2020. Review of the lateral resistance of ballasted tracks. *Proceedings of the Institution of Mechanical Engineers, Part F: Journal of Rail and Rapid Transit,* 234**,** 807-820.

JING, G., AELA, P. & FU, H. 2019. The contribution of ballast layer components to the lateral resistance of ladder sleeper track. *Construction and Building Materials,* 202**,** 796-805.

JING, G., AELA, P., FU, H. & YIN, H. 2018. Numerical and experimental analysis of single tie push tests on different shapes of concrete sleepers in ballasted tracks. *Proceedings of the Institution of Mechanical Engineers, Part F: Journal of Rail and Rapid Transit,* 233**,** 666-677.

KAEWUNRUEN, S. 2012. In situ performance of under-sleeper pads (USPs) at glued insulated joints (GIJs). *Technical Rep. TR,* 208.

KAEWUNRUEN, S. & CHIENGSON, C. 2018. Railway track inspection and maintenance priorities due to dynamic coupling effects of dipped rails and differential track settlements. *Engineering Failure Analysis,* 93**,** 157-171.

KAEWUNRUEN, S., WANG, Y. & NGAMKHANONG, C. 2018. Derailment-resistant performance of modular composite rail track slabs. *Engineering Structures,* 160**,** 1-11.

KERR, A. D. 1978. Analysis of thermal track buckling in the lateral plane. *Acta Mechanica,* 30**,** 17-50.

KERR, A. D. 1980. An improved analysis for thermal track buckling. *International Journal of Non-Linear Mechanics,* 15**,** 99-114.

KHATIBI, F., ESMAEILI, M. & MOHAMMADZADEH, S. 2017. DEM analysis of railway track lateral resistance. *Soils and Foundations,* 57**,** 587-602.

KISH, A. 2011. On the Fundamentals of Track Lateral Resistance. *Annual Conference.* Minneapolis, USA.

KISH, A., CLARK, D. W. & THOMPSON, W. 1995. Recent Investigations on the Lateral Stability of Wood and Concrete Tie Tracks. *AREA Bulletin,* 752**,** 248-265.

KISH, A. & SAMAVEDAM, G. 2013. Track buckling prevention: theory, safety concepts, and applications. John A. Volpe National Transportation Systems Center (US).

KOETSE, M. J. & RIETVELD, P. 2009. The impact of climate change and weather on transport: An overview of empirical findings. *Transportation Research Part D: Transport and Environment,* 14**,** 205-221.

LE PEN, L., WATSON, G., HUDSON, A. & POWRIE, W. 2018. Behaviour of under sleeper pads at switches and crossings–Field measurements. *Proceedings of the Institution of Mechanical Engineers, Part F: Journal of rail and rapid transit,* 232**,** 1049-1063.

LEVIÄKANGAS, P., TUOMINEN, A., MOLARIUS, R., SCHABEL, J., TOIVONEN, S., KERÄNEN, J., TÖRNQVIST, J., MAKKONEN, L., VAJDA, A. & TUOMENVIRTA, H. 2011. Extreme weather impacts on transport systems. Finland: VTT Technical Research Centre of Finland.

LICHTBERGER, B. 2007. The lateral resistance of the track (Part 2). *European Railway Review*.

LING, L., XIAO, X. B. & JIN, X. S. 2014. Development of a simulation model for dynamic derailment analysis of high-speed trains. *Acta Mechanica Sinica,* 30**,** 860-875.

MOTTAHED, J., ZAKERI, J. A. & MOHAMMADZADEH, S. 2018. Field and numerical investigation of the effect of under-sleeper pads on the dynamic behavior of railway bridges. *Proceedings of the Institution of Mechanical Engineers, Part F: Journal of Rail and Rapid Transit,* 232**,** 2126-2137.

NETWORK RAIL 2006. Continuous Welded Rail (CWR) Track. London.

NETWORK RAIL. 2008. *Why rails buckle in Britain* [Online]. Available: https://www.networkrail.co.uk/stories/why-rails-buckle-in-britain/ [Accessed].

NGAMKHANONG, C., KAEWUNRUEN, S. & COSTA, B. J. A. 2018. State-of-the-art review of railway track resilience monitoring. *Infrastructures,* 3**,** 3.

NGUYEN, V.-H., DUHAMEL, D. & NEDJAR, B. 2003. A continuum model for granular materials taking into account the no-tension effect. *Mechanics of materials,* 35**,** 955-967.

OLE, Z. K. 2008. *Track stability and buckling-rail stress management.* Unversity of Southern Queensland.

OSLAKOVIC, I. S., TER MAAT, H., HARTMANN, A. & DEWULF, G. 2012. Climate Change and Infrastructure Performance: Should We Worry About? *Procedia - Social and Behavioral Sciences,* 48**,** 1775-1784.

PAIXÃO, A., ALVES RIBEIRO, C., PINTO, N., FORTUNATO, E. & CALÇADA, R. 2015. On the use of under sleeper pads in transition zones at railway underpasses: experimental field testing. *Structure and Infrastructure Engineering,* 11**,** 112-128.

PAIXÃO, A., VARANDAS, J. N., FORTUNATO, E. & CALÇADA, R. 2018. Numerical simulations to improve the use of under sleeper pads at transition zones to railway bridges. *Engineering structures,* 164**,** 169-182.

POWRIE, W. 2014. On track: the future for rail infrastructure systems. *Proceedings of the Institution of Civil Engineers - Civil Engineering,* 167**,** 177-185.

PRUD'HOMME, M. A. & JANIN, M. G. 1969. The stability of tracks laid with long welded rails. *RAIL INTERNATIONAL,* 46**,** 459-487.

PUCILLO, G. P. 2019. Train-Induced Load Effects on the Thermal Track Buckling. Joint Rail Conference, April 9–12, 2019 Utah, USA. American Society of Mechanical Engineers Digital Collection.

QUEENSLAND RAILWAYS 1988. Track Buckling In: COMMITTEE, R. O. A. T. D. A. A. (ed.) Railways of Australia.

QUINN, A., JACK, A.; HODGKINSON, S.; FERRANTI, E., BECKFORD J., DORA J. 2017. RAIL ADAPT Adapting the railway for the future. Paris, France: International Union of Railways (UIC).

RAILCORP 2013. TMC211 TRACK GEOMETRY & STABILITY. *Engineering Manual.* Australia.

REMENNIKOV, A. M. & KAEWUNRUEN, S. 2008. A review of loading conditions for railway track structures due to train and track vertical interaction. *Structural Control and Health Monitoring: The Official Journal of the International Association for Structural Control and Monitoring and of the European Association for the Control of Structures,* 15**,** 207-234.

SAMAVEDAM, G., KISH, A., PURPLE, A. & SCHOENGART, J. 1993. Parametric Analysis and Safety Concepts of CWR Track Buckling. United States. Federal Railroad Administration.

SCHNEIDER, P., BOLMSVIK, R. & NIELSEN, J. C. O. 2011. In situ performance of a ballasted railway track with under sleeper pads. *Proceedings of the Institution of Mechanical Engineers, Part F: Journal of Rail and Rapid Transit,* 225**,** 299-309.

SETSOBHONKUL, S., KAEWUNRUEN, S. & SUSSMAN, J. M. 2017. Lifecycle assessments of railway bridge transitions exposed to extreme climate events. *Frontiers in built environment,* 3**,** 35.

SOGABE, M., ASANUMA, K., NAKAMURA, T., KATAOKA, H., GOTO, K. & TOKUNAGA, M. 2013. Deformation behavior of ballasted track during earthquakes. *Quarterly Report of RTRI,* 54**,** 104-111.

SOL-SÁNCHEZ, M., MORENO-NAVARRO, F. & RUBIO-GÁMEZ, M. C. 2014. Viability of using end-of-life tire pads as under sleeper pads in railway. *Construction and Building Materials,* 64**,** 150-156.

SUSSMANN, T., KISH, A. & TROSINO, M. 2003. Influence of track maintenance on lateral resistance of concrete-tie track. *Transportation research record,* 1825**,** 56-63.

SUSSMANN, T. R., RUEL, M. & CHRISMER, S. M. 2012. Source of ballast fouling and influence considerations for condition assessment criteria. *Transportation Research Record: Journal of the Transportation Research Board***,** 87-94.

THOMPSON, W. C. 1991. Union pacific's approach to preserving lateral track stability. *Transportation research record,* 1289**,** 64-70.

TUTUMLUER, E., HUANG, H., HASHASH, Y. & GHABOUSSI, J. 2006. Aggregate shape effects on ballast tamping and railroad track lateral stability. AREMA 2006 Annual Conference, September 17-20, 2006 Louisville, KY, USA.

VILLALBA, I., INSA, R., SALVADOR, P. & MARTINEZ, P. 2017. Methodology for evaluating thermal track buckling in dual gauge tracks with continuous welded rail. *Proceedings of the Institution of Mechanical Engineers, Part F: Journal of Rail and Rapid Transit,* 231**,** 269-279.

VILLALBA SANCHIS, I., INSA, R., SALVADOR, P. & MARTÍNEZ, P. 2018. An analytical model for the prediction of thermal track buckling in dual gauge tracks. *Proceedings of the Institution of Mechanical Engineers, Part F: Journal of Rail and Rapid Transit,* 232**,** 2163-2172.

ZAKERI, J. A. & BAKHTIARY, A. 2014. Comparing lateral resistance to different types of sleeper in ballasted railway tracks. *Scientia Iranica,,* 21**,** 101-107.

ZAREMBSKI, A. M. 2016. Survey of techniques and approaches for increasing the lateral resistance of wood tie track. *Newark: Department of Civil and Environmental Engineering, University of Delaware*.

CHAPTER 2

A REVIEW OF BALLASTED RAILWAY TRACKS

2.1 Introduction

Presently, there are two types of modern railway tracks used in railway systems: conventional ballasted track and ballastless track (also called “slab track”) which have different types of support structures. Conventional ballasted track has been widely being used around the world for both normal and high-speed train up to the operational speed of 250km/h. At present, slab tracks have been a rational choice for highspeed railways globally because of its advantages for higher stability, lower track deformation, and minimal maintenance compared with conventional ballasted tracks. However, ballasted tracks are still being used and have a major share in the railway market as it provides lower initial construction cost than slab tracks. It is important to note that ballasted railway tracks are more prone to buckling due to extreme temperature compared to slab tracks and so ballasted railway tracks will be considered in this study. This chapter reviews the functions of traditional ballasted railway track and its components, which will be further used for simulation in the next chapters. A critical review into the functions, advantages and disadvantages of the properties of each component of ballasted railway tracks is presented. This chapter first introduces ballasted railway tracks and their components from top to bottom layers including rail, fastening system, rail pad, sleeper, ballast, sub-ballast and subgrade. This is followed by a literature review of previous studies of interspersed railway track (also called the “spot replacement approach”), which has been adopted to replace rotten timber sleepers to provide a cost effective short term solution to solve the deterioration problems for traditional ballasted tracks. Lastly, the methods for modelling ballasted railway tracks are presented, comprising Finite Element Method (FEM) and

Discrete Element Method (DEM). This chapter presents a literature review of the track and component models used for different purposes of studies.

2.2 Ballasted Railway Tracks

Ballasted railway tracks are the traditional railway track widely used around the world. A ballasted railway track mainly consists of a superstructure of rail, fastening system, sleeper and ballast; and substructure of sub-ballast, subgrade and underlying soil. In some areas, the ballasted track sometimes has an additional resilient material to improve the performance and prolong its service life, such as Under Sleeper Pad (USP), Under Ballast Mat (UBM) etc. A typical cross section of ballasted railway track can be seen in Figure 2.1.

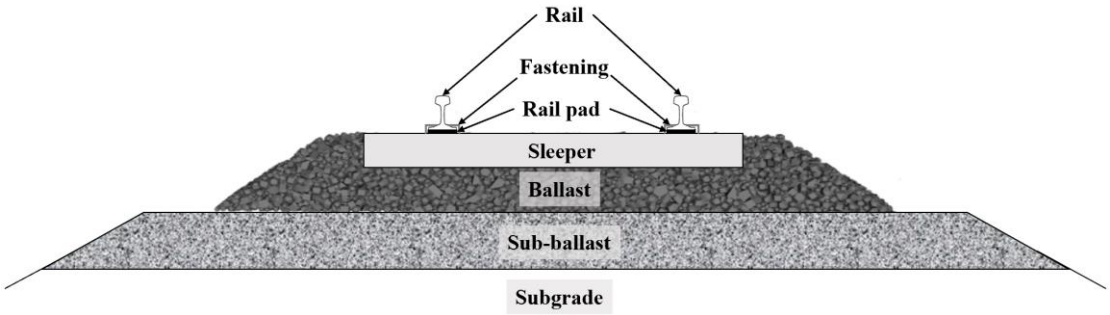

Figure 2.1 Typical cross section of ballasted railway track.

The advantages of ballasted railway tracks over slab tracks are concluded as follows:

- Simplicity in design and construction
- Relatively low initial and constriction cost
- Ease of maintenance work
- Provides a better drainage system

- Good elasticity
- Better noise and vibration suppression

However, a ballasted railway track is easy to settle over a time resulting in the loss of track geometry and irregularity. Although a ballasted railway track has lower construction cost than slab track, frequent maintenance activities and inspections may be required due to the higher rate of track deterioration. Routine activities are always required to restore track geometry and clean or renew ballast regularly.

2.2.1 Rail

Rail, the longitudinal members, is normally made of hot-rolled steel to guide and support the wheels and transfer wheel loads to the underlying components. There are different types and shapes of steel rails which are used for different tracks, such as flat-bottom, construction rail, grooved rail, block rail, and crane rail. In ballasted track, flat bottom rail, which consists of rail head, rail web, and rail foot, is generally used. Rail head provides a contact to wheel so the rail must be smooth and have a high wear resistance. Rail web serves an adequate bending stiffness and connection to the adjacent rail while the rail foot is fastened to the sleeper by the fastening system. The main functions of rails are as follows:

- To guide the wheels in lateral directions.
- To distribute the train load to the underlying sleepers.
- To provide signal current and electricity to the electric train
- To provide ride comfort and distribute the acceleration and braking force.

2.2.2 Fastening systems

The functions of fastening systems are to secure the rails to the sleepers and provide longitudinal and torsional resistances. The fastening system normally consists of rail anchors, chairs, fasteners, insulators, clips, washers, spikes, screws, bolts, base plates, rail pads. There are various types of fastening system. There applications depend on the rail and sleeper types. It should be noted that the stiffness of fastening system for timber sleepers is generally higher than that of concrete sleepers. The functions of fastening systems are as follows:

- To maintain the track gauge and rail inclination within an acceptable range.
- To transfer the rail force to the sleeper.
- To provide longitudinal and torsional resistance.
- To absorb vibrations and impacts by the train load.

2.2.3 Rail pad

Rail pad is an elastic resilient material mounted on rail seats in between rail and sleeper. It is normally made of polyurethane, santoprene rubber, EVA etc. to isolate track vibration and attenuate the load transferred to sleepers. It is important to note that rail pad can be deteriorated and worn over a service time. The stiffness and damping properties of rail pad could be worsened, resulting in the poorer performance in attenuating dynamic stress from trains (Kaewunruen and Remennikov, 2005). Thus, it is necessary to replace worn pads with new ones regularly.

2.2.4 Sleeper

Railway sleepers (or 'railroad ties' in North America) are a main part of railway track structures. It is important to note that railway sleepers are a structural and safety-critical component in railway track systems (Gustavson, 2004, Remennikov et al., 2012, Kaewunruen and Remennikov, 2009, Kaewunruen and Remennikov, 2013). Railway sleepers can be made of timber, concrete, steel, composite materials or other engineering materials (Esveld, 2001). They have been systemically introduced to the railway industry and currently are present in almost every railway network in the world. Railway sleepers have been developed to provide a better performance, longer life cycles and cost effectiveness. The main duties of sleepers are as follows:

- To distribute loads from the rail foot to the underlying ballast and substructure.
- To hold the rails at the proper gauge through the rail fastening system.
- To maintain rail inclination and rail gauge for safe passages of rolling stocks.
- To anchor track against longitudinal, lateral, and vertical movements of the rails.

Note that the sleeper design and analysis must be ascertained to assure public safety and operational reliability. Critical performance criteria such as static capacity, dynamic strength and ultimate capacity should be evaluated properly as each property is mutually important and interconnected. Two typical types of sleepers that are usually used for conventional straight railway lines are timber (hardwood) and concrete sleepers.

Timber railway sleepers have been being used in the rail industry worldwide (Hamzah and Din, 2008, Kaewunruen and Chamniprasart, 2014). It should be noted that this is particularly the case in the US, where wood has a 93% share of the market making up about

16 million timber sleepers laid every year (RailwayTechnology, 2010). Timber railway sleepers are expected to serve about 15 to 20 service years, but their strength and serviceability is easily degraded due to environmental weathering over time. The advantages and disadvantages of timber sleepers are presented in Table 2.1. The limited availability of reliable and high-quality timbers, and restrictions on deforestation led to the exploration of more appropriate alternative materials such as concrete, and composite materials (AGICO GROUP, 2020).

Figure 2.2 Ballasted railway track with rotten timber sleepers.

Table 2.1 Advantages and disadvantages of timber sleepers.

Advantages	Disadvantages
• Easy to handle, transport and construct due to being lightweight • Suitable for circuited railway tracks • Can be used in coastal areas or salty regions • Flexible for any track gauge and section of rail • Easy to handle and place • They are barely corroded • Relatively cheap	• Has shorter service life span of 10-20 years compared to concrete sleepers • Prone to environmental deterioration such as toxic deterioration, rot, fungi, and insect infestation • Susceptible to wear and tear • Due to their lightweight, timber sleepers provide less lateral stability of track

It is remarkable that concrete sleepers have been widely used in railway industry for more than 50 years as they provide longer service life than traditional timber sleepers. An example of ballasted railway track is shown in Figure 2.3. The advantages and disadvantages of concrete sleepers are shown in Table 2.2.

Figure 2.3 Ballasted railway track with concrete sleepers.

Table 2.2 Advantages and disadvantages of concrete sleepers.

Advantages	Disadvantages
• Has longer life span, from 30-70 years • They can be produced in large quantities by installing a temporary plant • Heavier than other types of sleeper, thus providing greater lateral resistance to the track resulting in less chance of being buckled • Suitable for use in track circuited lines. • Require less maintenance activities resulting in long term cost effectiveness • Efficient in controlling creep • Not prone to environmental degradation • Suitable for welded tracks • Effectively and strongly hold the track to gauge • Inflammable and fire resistant	• Difficult to handle due to their heavy weight. • Cannot be used in bridges and crossings due to its difficulties in manufacturing process in different sizes • Can be damaged easily when loading and unloading • Require skilled labor to equip them, especially for pre-stressed concrete sleepers.

2.2.5 Under Sleeper Pad (USP)

Under Sleeper Pads (USPs), that can be made of polyurethane, elastomers, rubber, EVA etc. with a foam structure including encapsulated air voids, have been recently adopted and installed underneath sleepers in ballasted tracks as shown in Figure 2.4. They can be treated

as another component of ballasted track to adjust track stiffness and redistribute the axle load over a greater number of sleepers, as shown in Figure 2.5. It should be noted that USPs usually have two layers combined into one: upper layer for attenuating noise and vibration and a lower layer for protecting the sleepers from repeated impact load with ballast (Dahlberg, 2010, Schneider et al., 2011, Müller-Boruttau and Kleinert, 2001). USP can increase the contact surface between sleepers and ballast. This can help to stabilise the top layer of ballast. Note that USPs can lead to long-term higher railway track economic values and to substantial wider social benefits (Markine et al., 2011, Ortega et al., 2018) (Setsobhonkul et al., 2017) since USPs can significantly reduce the unplanned maintenance and annual maintenance cost over the service life.

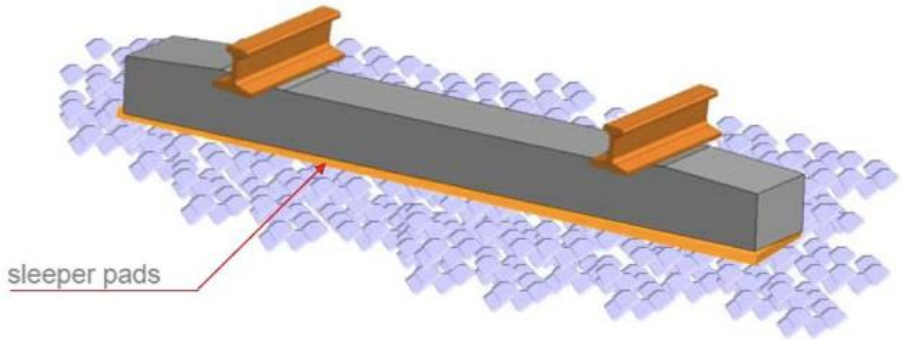

Figure 2.4 Typical ballasted railway track and its components with USP (Kaewunruen et al., 2017).

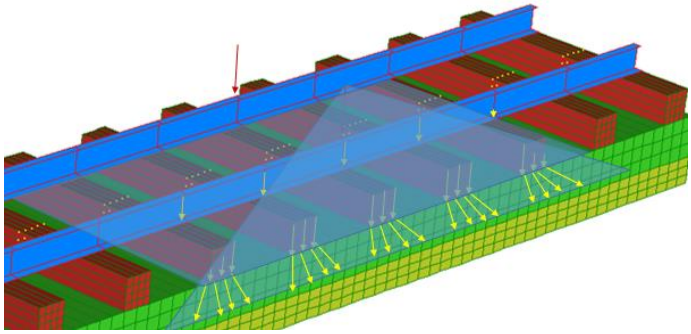

(a)

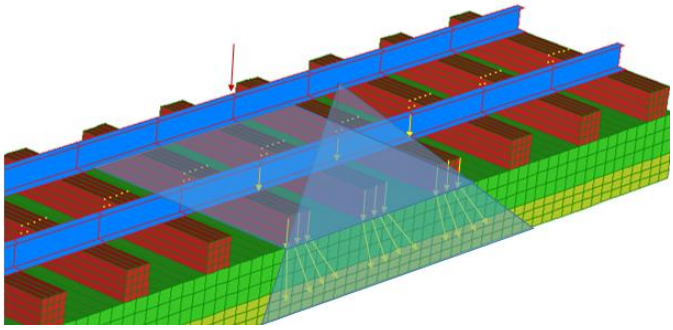

(b)

Figure 2.5 Load distribution of railway track: (a) with USPs and (b) without USPs.

The USP can be classified into stiff, medium, soft and very soft categories of bedding modulus, as shown in Table 2.3. Different types of USPs are linked to different purposes of use. The benefits of USP are summarised as follows (Schilder, 2013, Setsobhonkul et al., 2017):

- Improves track quality and prolongs track service life
- Increases contact area between sleeper and ballast leading to reduced stress distributed on ballast and underlying layers
- Reduces ballast thickness while maintaining good track performance
- Reduces ground borne noise and vibration
- Adjusts track stiffness at transition zones creating smoother railway tracks

- Reduces long pitch rail corrugation in tight curves as rail pad can modify the natural frequencies of track components
- Increases lateral resistance of sleepers

Table 2.3 USP applications and characterisations (International Union of Railway, 2013).

Fields of application of USP	USP			
	Very soft	Soft	Medium stiff	Stiff
	$C_{stat} \leq 0.10$	$0.10 < C_{stat} \leq 0.15$	$0.15 < C_{stat} \leq 0.25$	$0.25 < C_{stat} \leq 0.35$
Improve track quality (reduce ballast breakage and track/turnout pressure)			✓	✓
Transition zones			✓	✓
On existing structures with reduced ballast thickness			✓	✓
Reduction of long-pitch low-rail corrugation in tight curves			✓	✓
Reduction of ground-borne vibration		✓	✓	

2.2.6 Ballast

Railway ballast is the crushed stone, gravel and crushed gravel providing the support to the superstructure of ballasted tracks. Generally, ballast must be angular, uniformly graded, strong, hard, and durable to provide strength to the tracks. The important ballast properties include particle size, shape, distribution, compressive strength, cleanable and workability for alignment adjustments. As the ballast is basically a tensionless elastic support for

sleepers, it is important to note that the ballast component is a major factor causing track irregularities due to its particle nature and high levels of nonlinearities that can easily cause plastic track deformation.

The functions of ballast are as follows (Selig and Waters, 1994, Indraratna et al., 2011):

- To transmit and reduce the load from sleeper/ballast interface to the sub-ballast and subgrade by spreading it over a wider interface.
- Provide stability to the track by withstanding vertical, longitudinal, and lateral forces.
- Support sleepers uniformly.
- Provide adequate permeability for drainage and keep the sleepers in a dry condition.
- Absorb noise, vibration and energy
- Provide adequate electrical resistance between rails

2.2.7 Sub-ballast

The sub-ballast layer (also called “capping layer”) gives a solid support for the top crushed stone ballast and reduces the water seepage from the underlying subgrade and soil. The sub-ballast layer has the primary function of reducing the impact of traffic loads on the track subgrade and underlying soil without requiring excessive increase in thickness of the ballast. It can also help to protect frost-susceptible soils from frost and water susceptible soil from water (Navikas et al., 2016).

2.2.8 Subgrade

The subgrade acts as a foundation of railway systems. This part is located between subsoil and sub-ballast or ballast. It is important to note that subgrade has a significant influence on the track quality as the settlement of subgrade leads to track settlement to an undesirable level (McHenry and Rose, 2012). The performance of subgrade is governed by two indicators: strength and deformation (Selig and Lutenegger, 1991). Strength refers to shear strength and bearing capacity of soil while deformation refers to settlement in the subgrade layer, which can be either elastic or plastic (permanent). These two indicators are important for subgrade performance.

2.3 Interspersed Railway Track

For the problems of ageing railway tracks with degraded timber sleepers, interspersed railway track ("spot replacement method") is an alternative short-term approach to maintain track quality and solve the problem of rotten timber sleepers by replacing the rotten sleepers by new types of sleepers. Due to the limited availability of reliable and high-quality timbers, and restrictions on deforestation as previously presented in Table 2.1, most countries have adopted steel, concrete, composite sleepers to replace ageing timber sleepers (Manalo et al., 2013, Gustavson, 2004, Ferdous et al., 2015). This approach provides sufficient short time solutions (less than 10 years) for solving the problem of timber deterioration that could be cheaper, quicker, more effective, and more agile than other methods. This approach has been widely adopted to enrich the performance of lower-class tracks with low operational speed. Such a method is used in many countries such as UK, Japan, Australia, and USA (Kaewunruen et al., 2014). There are many types of materials

that have been used to replace rotten timber sleeper such as steel, concrete, composite materials etc. In modernised railway lines, concrete sleepers are the most popular due to their performance and resistance compared with others (Kohoutek, 1991). The advantages and disadvantages have been previously presented in Table 2.2

Recently, steel sleepers have been used for spot replacements and partial resleepering on timber sleeper track, for example in Australia (Birks et al., 1989). The different patterns of steel sleepers interspersed with degraded timber sleepers were studied to measure deflection, vertical rail seat load, rail creep and track buckling before and after installing the steel sleepers. It was found that both timber and steel sleepers had quite similar deflection amplitudes when the installation process was performed properly. Moreover, the installation of steel sleepers helped the railway track to reduce rail creep and track buckling due to the increase in lateral and longitudinal resistances provided by sleepers and ballast, and torsional resistance provided by fastening system. However, higher deflections of steel sleeper could be observed when the sleeper and ballast were not well packed. Mostly, the degraded timber sleepers are replaced by concrete sleepers as seen in many countries such as Australia, Japan, United Kingdom, United States etc (Kohoutek, 1991). Although a partial replacement of aged and rotten timber sleepers is obviously more economical than complete track renewal or reconstruction, it can be seen from the field investigations that the long-term performance of interspersed track could possibly be impaired due to the soil foundation failure, track stiffness inconsistency leading to mud pumping, ballast dilation and pulverisation. The deterioration of interspersed tracks due to mud pumping, ballast dilation and pulverisation, can be seen in Figure 2.6. This figure presents the conditions of interspersed track under an operational speed of less than 25 km/h that serves as a link from

mainline to a maintenance depot in Australia. There have been numerous studies and evidences provided about the dynamic responses of railway tracks with concrete sleepers interspersed by timber sleepers using Finite Element Modelling (FEM) by applying the moving train loads along the interspersed tracks (Kaewunruen et al., 2018b, Kaewunruen et al., 2018a). In the study, 4 typical types of interspersed tracks were considered. The results showed that the uplift behaviours of timber sleepers were observed in 1 in 3 and 1 in 4 interspersed railway tracks. Furthermore, the material degradation over time was considered to study the time-dependent behaviour of ballasted tracks (Kaewunruen et al., 2019). The dynamic responses of interspersed tracks from year 0 to year 20 were taken into consideration in the simulations. It was clearly seen that in year 20, timber sleepered tracks had higher structural responses in comparison to new timber sleepered track. Although the replacements of timber sleepers by concrete sleepers can reduce the displacement and acceleration, uplift behaviour can possibly be induced by concrete sleepers depending on types of interspersed tracks and local spot areas resulting in worsened long-term performance. It was confirmed in field investigations that aggressive uplift behaviour caused by interspersing was the major cause of long-term track deterioration. Due to the stiffness inconsistency differentials of railway track, rail pad sensitivity has been proposed to adjust track stiffness and improve the problem of stiffness inconsistency (Kaewunruen et al., 2018c). It could be seen that rail pads have little effect on the displacement reduction of spot replacement sleepers. Thus, softer rail pads do not improve the performance of interspersed track systems. On this ground, it can be concluded that the interspersed approach can provide a cost-effective short-term solution for certain track types while it can cause long-term deterioration due to inconsistent stiffness problems, and the different track decay rate can cause differential settlement and foundation failure.

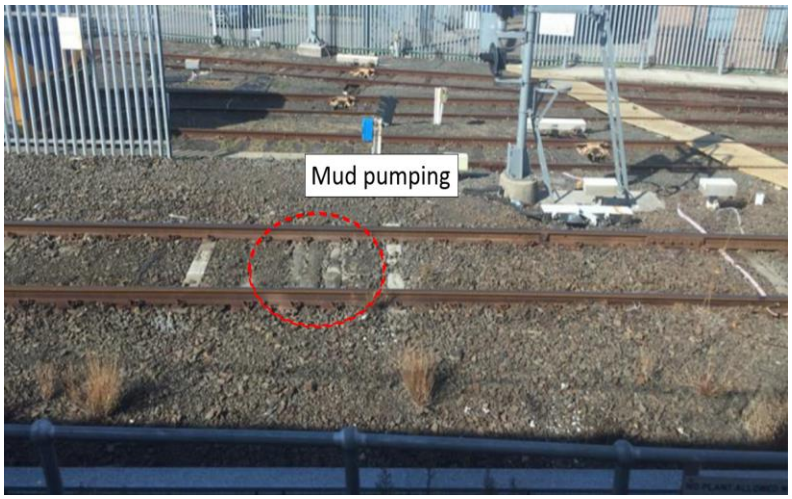

(a)

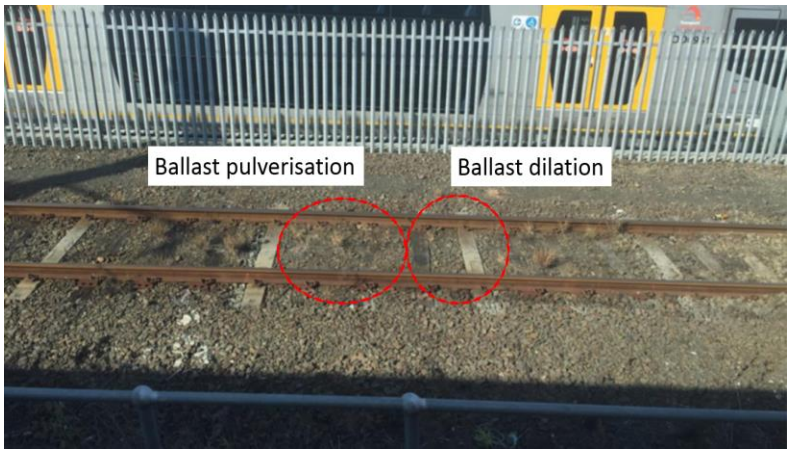

(b)

Figure 2.6 Problems in interspersed railway tracks: (a) mud pumping and (b) ballast pulverisation and dilation.

2.4 A Review of Railway Track Modelling

2.4.1 Finite Element Method (FEM)

The Finite Element Method (FEM) is a discretisation technique for analysing problems in structural and mechanical behaviours (Turner et al., 1956). This technique has been proven to be an effective method and has widely used for decades. The FEM is expressed by

differential equations and boundary conditions within a domain of interest represented as an assembly of finite elements. In FEM, the element types normally consist of truss, beam, shell, plate and solid element, which provide different types of structures used for different structural problems. This approach is made up of several steps, starting from discretising the continuum structure into small elements and connected via nodes. A local stiffness matric is first formed for each element and then these element's matrices are assembled for a global stiffness matrix. Then load and boundary conditions are applied to solve the nodal forces and stresses (Rao, 2017).

As for railway track modelling, each element can be modelled differently depending on the purposes of simulations. Rails can be modelled as either a beam or solid elements depending on the size and purposes of structure. It is important to note that for predicting the global behaviour with large modelling such as train-track interaction, buckling analysis etc., a beam element is more efficient due to their lower computational cost than solid element as beam elements take axial, shear and bending into account. Whereas modelling rail as a solid element can offer a better local behaviour along the depth and cross section of the rail than a beam element. It is also noted that sleepers can be modelled as similar to rail as either beam or solid. It should be noted that rail and sleepers should be modelled as solid elements when a single or a few spans are considered (Kaewunruen et al., 2018d).

As for ballast and substructure layers, two or three-dimensional multilayer systems have been modelled as a group of layers using solid elements (Sasaoka and Davis, 2005, Gallego et al., 2011). The layers were initially considered as a continuum model by assuming ballast as infinitesimal in size (Nguyen et al., 2003). The size of the model depends on the purposes of the simulations. The 2D plane strain model has been used for simulating the responses

of multilayers track system across the section (transverse and vertical directions) under the simplified train point loads while the longitudinal direction along the rails cannot be fully simulated (Indraratna et al., 2007, Jiang and Nimbalkar, 2019). The 2D plane strain model mostly focuses on the geotechnical aspects or substructure of the deep depth of subgrade layer. As for the track model under moving load, the 2.5D model has been proposed as an alternative to significantly reduce the computational time compared to the 3D model (Yang and Hung, 2001, Bian et al., 2011, Bian et al., 2018). However, this method has some limitations, as the material and geometry of the track must be assumed to be constant and is used for vertical response only. The 3D model is used for any purposes and the model can be built in full-scale. Several studies have presented the 3D track models considering train-track-soil interaction by modelling the layers of substructure using solid elements (Sayeed and Shahin, 2016, Li et al., 2020, Connolly et al., 2013).

Alternatively, to properly model a track structure considering global track behaviours, discrete springs can be used to simulate the interaction between ballast and sleepers. It is important to note that the spring properties should have been validated and calibrated with field measurements or any full track modelling as one spring layer placed uniformly underneath sleepers represents the stiffness of the whole substructure. As for the lateral behaviour, buckling can occur in the lateral plane and thus lateral spring properties of ballast, representing the lateral resistance of ballast and sleeper interaction, should be obtained from Single Sleeper (Tie) Push/Pull Tests (STPTs) (Esmaeili et al., 2018, Jing et al., 2018). Importantly, springs for ballast and substructure must be modelled with compression only to reflect the actual behaviour of these materials. This model has been confirmed by the comparison between experiments and FEA models using nonlinear elastic

model of ballast with and without tension under the vertical quasi static load (Nguyen et al., 2003).

However, it is important to note that ballast and substructure are granular and heterogenous materials. However, FEM can only demonstrate stress-strain distribution and is not able to perform a detail into its granular behaviour and particle interactions and local discontinuities. Hence, another technique should be employed to overcome the drawbacks of FEM in order to study the particle behaviours influencing the whole ballast layer.

2.4.2 Discrete Element Method (DEM)

In reality, ballast particles generally comprise a number of large particle sizes approximately between 40mm and 60mm and it is difficult to accurately treat such a material in a continuum model. To correctly model the ballast layer, the DEM is an alternative method that can accurately provide the realistic behaviour of railway ballast. This method is a numerical method for computing the motion and effect of a large number of small particles with their interactions in a granular assembly including the discontinuities and nonlinearities. The DEM for granular material was first introduced by (Cundall, 1971) for rock and soil. DEM can provide insight into the micro-mechanical behaviour and interactions of railway ballast. Each particle can be represented as a rigid particle. However, there are generally certain disadvantages of DEM including high computational time and memory consumption in comparison to continuum or FEM model. This is because this method calculates every single contact of the complex realistic shape of particles resulting in higher computational time and memory space being required. This leads to a limitation in modelling more than a single span of railway track. There are several

types of particle shapes that can be modelled using DEM: circular, circular cluster and polygonal for 2D and spherical, spherical clump and polyhedral for 3D as shown in Figure 2.7.

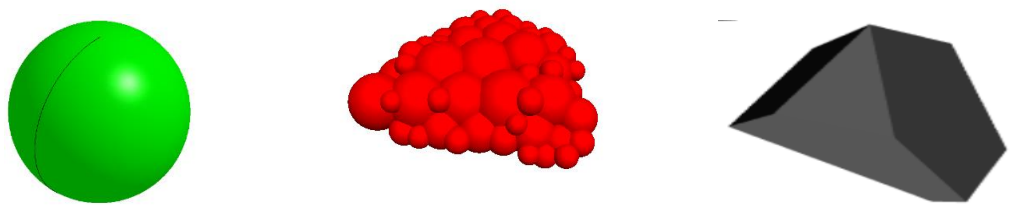

(a) **(b)** **(c)**

Figure 2.7 Particle shapes for DEM: (a) sphere, (b) spherical clump, and (c) polyhedral.

Firstly, circular for 2D and spherical for 3D, these methods form the ballast particles as circular or sphere and require less computational time compared to later methods (Lobo-Guerrero et al., 2006). However, these methods provide unrealistic shapes of ballast that have no angularity, resulting in weak interlocking ballast particles and unrealistic behaviour. The rolling resistance has been suggested to be applied to the particles to compensate the roughness of particles and can correctly present accurate results of the whole ballast layer (Irazábal González, 2017). However, it is not clear how this property can correctly link to every particle as each particle should have different surface textures and roughness. Even though the calibration of contact and rolling parameters have been accurately conducted, resulting in the same results with the experimental results of small scale tests, spherical DEM has never been simulated and further investigation is essential for ballast degradation (Guo et al., 2020).

Secondly, the use of a circular and spherical clump or cluster can overcome the limitations of the first model as this can provide more accurate and complex shapes of ballast particles (Thakur et al., 2009, Ngo et al., 2014). These approaches consist of small sphere particles of various sizes assembled into one actual particle making an irregular shape ballast. These approaches can also include the effects of ballast breakage and abrasion showing their effectiveness in analysing ballast degradation as the small particles are bonded and can be released presenting particle breakage. However, to improve the ballast shape to be more realistic, the number of spheres assembled should be increased, which will lead to an increase in number of contact points between particles. This significantly increases the computational time as the responses at each contact point have to be updated in every step.

Lastly, polyhedral particles represent the most realistic shape of particle of all the methods, with sharp edges and corners as the shape is formed based on actual photography (Elias, 2013). The shapes can perform a high contact interlocking between particles. The polyhedron particles are normally assumed to be rigid and undeformable. It should be noted that the contact algorithm between particles is complicated as it is hard to detect. Due to its computational time from contact detection, several researchers have studied the new contact algorithms to reduce the time consuming starting from common plane method (Cundall, 1988), fast common plane method (Nezami et al., 2004) and end up with short link method (G. Nezami et al., 2006) that provides the shortest simulation time compared to the previous ones. However, the study of ballast degradation using polyhedral shape is very limited for full scale ballast layer.

The comparison between each shape including pros and cons is presented in Table 2.4. It can be concluded that DEM should be used if the focus is on ballast particle interactions

and degradation, while it is not necessary for full scale track models, due to the computational time being limited and the limitations on the commercial software for coupled FEM-DEM methods. DEM is important for ballast and geotechnical aspects while other elements for superstructure should be modelled and analysed using FEM.

Table 2.4 Summary of advantages and disadvantages of particle shapes for DEM.

	Circular	Circular cluster	Spherical	Spherical clump	Polygonal and Polyhedral
Dimensions	2D	2D	3D	3D	2D, 3D
Shape	Unrealistic, Simplified shape	Irregular More element required to form a particle for more realistic	Unrealistic	Irregular More element required to form a particle for more realistic	Realistic
Contact interlocking	Weak (Rolling resistance should be applied to compensate the rough surface)	Strong	Weak (Rolling resistance should be applied to compensate the rough surface)	Strong	Strong
Computational time and memory consumption	Medium	High (Depends on number of elements)	High	High (Depends on number of elements)	High

2.5 Summary

Ballasted railway track is composed of a superstructure made up of rail, rail pad, fastening system, sleeper and ballast; and a substructure made up of sub-ballast, subgrade and underlying soil. Rails are normally made of steel while sleepers can be made of a wide range of material such as timber, concrete, steel, and composite material. The functions of each component have been reviewed and summarised. It should be noted that, at present, prestressed concrete sleepers have been used for decades to replace aged timber sleepers which have a shorter service life and tend to be degraded easily over time. However, in some cases, the concrete sleeper replaces the timber sleeper in some spans especially where a high deterioration rate is observed. This spot replacement is believed to elongate the service life of railway track, however, it induces inconsistency of railway track properties and stiffness. Previous studies of works on interspersed railway tracks have been discussed. Lastly, railway track modelling has been presented including both finite element modelling (FEM) and discrete element modelling (DEM). According to the discussions on the previous modelling, ballasted railway track modelling will be built for buckling analysis in the next chapters.

2.6 References

AGICO GROUP. 2020. *How Much Do You Know About the Types of Rail Sleepers* [Online]. Available: http://www.rail-fastener.com/types-of-rail-sleepers.html [Accessed].

BIAN, X.-C., CHAO, C., JIN, W.-F. & CHEN, Y.-M. 2011. A 2.5 D finite element approach for predicting ground vibrations generated by vertical track irregularities. *Journal of Zhejiang University-Science A,* 12**,** 885-894.

BIAN, X.-C., CHAO, C., JIN, W.-F. & CHEN, Y.-M. 2018. A 2.5 D Finite Element Approach for Predicting Ground Vibrations Generated by Vertical Track Irregularities. *China's High-Speed Rail Technology.* Springer.

BIRKS, F. J., TEW, G. P. & CHITTY, G. B. 1989. Narrow gauge track with interspersed steel sleepers. *Fourth International Heavy Haul Railway Conference* Institution of Engineers, Australia.

CONNOLLY, D., GIANNOPOULOS, A. & FORDE, M. C. 2013. Numerical modelling of ground borne vibrations from high speed rail lines on embankments. *Soil Dynamics and Earthquake Engineering,* 46**,** 13-19.

CUNDALL, P. A. 1971. A computer model for simulating progressive, large-scale movement in blocky rock system. *Proceedings of the International Symposium on Rock Mechanics.*

CUNDALL, P. A. 1988. Formulation of a three-dimensional distinct element model—Part I. A scheme to detect and represent contacts in a system composed of many

polyhedral blocks. *International Journal of Rock Mechanics and Mining Sciences & Geomechanics* 25**,** 107-116.

DAHLBERG, T. 2010. Railway track stiffness variations–consequences and countermeasures. *International journal of civil engineering,* 8**,** 1-12.

ELIAS, J. 2013. DEM simulation of railway ballast using polyhedral elemental shapes. PARTICLES III: proceedings of the III International Conference on Particle-Based Methods: fundamentals and applications, 2013. CIMNE, 247-256.

ESMAEILI, M., MAJIDI-PARAST, S. & HOSSEINI, A. 2018. Comparison of dynamic lateral resistance of railway concrete, wooden and steel sleepers subjected to impact loading. *Road Materials and Pavement Design,* 20**,** 1779-1806.

ESVELD, C. 2001. *Modern railway track,* MRT-productions Zaltbommel, Netherlands.

FERDOUS, W., MANALO, A., VAN ERP, G., ARAVINTHAN, T., KAEWUNRUEN, S. & REMENNIKOV, A. 2015. Composite railway sleepers–Recent developments, challenges and future prospects. *Composite Structures,* 134**,** 158-168.

G. NEZAMI, E., MA HASHASH, Y., ZHAO, D. & GHABOUSSI, J. 2006. Shortest link method for contact detection in discrete element method. *International Journal for Numerical and Analytical Methods in Geomechanics,* 30**,** 783-801.

GALLEGO, I., MUÑOZ, J., RIVAS, A. & SÁNCHEZ-CAMBRONERO, S. 2011. Vertical track stiffness as a new parameter involved in designing high-speed railway infrastructure. *Journal of transportation engineering,* 137**,** 971-979.

GUO, Y., ZHAO, C., MARKINE, V., SHI, C., JING, G. & ZHAI, W. 2020. Discrete element modelling of railway ballast performance considering particle shape and rolling resistance. *Railway Engineering Science*, 1-26.

GUSTAVSON, R. P. G. 2004. *Structural behaviour of concrete railway sleepers.* Doctoral thesis, Chalmers University of Technology.

HAMZAH, S. H. & DIN, K. 2008. Appraisal of used wooden railway sleeper. *Journal of Engineering Science and Technology,* 3, 224-233.

INDRARATNA, B., SALIM, W. & RUJIKIATKAMJORN, C. 2011. *Advanced rail geotechnology-ballasted track,* CRC press.

INDRARATNA, B., SHAHIN, M. A. & SALIM, W. 2007. Stabilisation of granular media and formation soil using geosynthetics with special reference to railway engineering. *Proceedings of the Institution of Civil Engineers-Ground Improvement,* 11, 27-43.

INTERNATIONAL UNION OF RAILWAY 2013. USP recommendations, Under Sleeper Pads, Recommendations for Use. *UIC-Leaflet, Draft Document.* Paris, France: International Union of Railway.

IRAZÁBAL GONZÁLEZ, J. 2017. *Numerical analysis of railway ballast behaviour using the Discrete Element Method.* Master, Universitat Politècnica de Catalunya.

JIANG, Y. & NIMBALKAR, S. 2019. Finite Element Modeling of Ballasted Rail Track Capturing Effects of Geosynthetic Inclusions. *Frontiers in Built Environment,* 5, 69.

JING, G., AELA, P., FU, H. & YIN, H. 2018. Numerical and experimental analysis of single tie push tests on different shapes of concrete sleepers in ballasted tracks. *Proceedings of the Institution of Mechanical Engineers, Part F: Journal of Rail and Rapid Transit,* 233**,** 666-677.

KAEWUNRUEN, S., AIKAWA, A. & REMENNIKOV, A. M. 2017. Vibration attenuation at rail joints through under sleeper pads. *Procedia Engineering,* 189**,** 193-198.

KAEWUNRUEN, S. & CHAMNIPRASART, K. 2014. Damage analysis of spot replacement sleepers interspersed in ballasted railway tracks. *Proceedings of the 29th Nordic Seminar on Computational Mechanics.* Chalmers University of Technology, Gothenburg, Sweden.

KAEWUNRUEN, S., LEWANDROWSKI, T. & CHAMNIPRASART, K. 2018a. Dynamic responses of interspersed railway tracks to moving train loads. *International Journal of Structural Stability and Dynamics,* 18**,** 1850011.

KAEWUNRUEN, S., LEWANDROWSKI, T. & CHAMNIPRASART, K. 2018b. Nonlinear modelling and analysis of moving train loads on interspersed railway tracks.

KAEWUNRUEN, S., NG, J. & AIKAWA, A. 2018c. Sensitivity of rail pads on dynamic responses of spot replacement sleepers interspersed in ballasted railway tracks. *Proceedings of the 25th International Congress on Sound and Vibration.* Hiroshima, Japan.

KAEWUNRUEN, S., NGAMKHANONG, C. & LIM, C. H. 2018d. Damage and failure modes of railway prestressed concrete sleepers with holes/web openings subject to impact loading conditions. *Engineering Structures,* 176**,** 840-848.

KAEWUNRUEN, S., NGAMKHANONG, C. & NG, J. 2019. Influence of time-dependent material degradation on life cycle serviceability of interspersed railway tracks due to moving train loads. *Engineering Structures,* 199**,** 109625.

KAEWUNRUEN, S. & REMENNIKOV, A. 2005. Monitoring structural degradation of rail pads in laboratory using impact excitation technique.

KAEWUNRUEN, S. & REMENNIKOV, A. 2013. On the residual energy toughness of prestressed concrete sleepers in railway track structures subjected to repeated impact loads.

KAEWUNRUEN, S., REMENNIKOV, A., AIKAWA, A. & SAKAI, H. 2014. Free vibrations of interspersed railway track systems in three-dimensional space.

KAEWUNRUEN, S. & REMENNIKOV, A. M. 2009. Structural safety of railway prestressed concrete sleepers. *Australian Journal of Structural Engineering,* 9**,** 129-140.

KOHOUTEK, R. Dynamic and static performance of interspersed railway track. 1991 1991. Institution of Engineers, Australia, 153.

LI, T., SU, Q. & KAEWUNRUEN, S. 2020. Influences of piles on the ground vibration considering the train-track-soil dynamic interactions. *Computers and Geotechnics,* 120**,** 103455.

LOBO-GUERRERO, S., VALLEJO, L. E. & VESGA, L. F. 2006. Visualization of crushing evolution in granular materials under compression using DEM. *International Journal of Geomechanics,* 6**,** 195-200.

MANALO, A. C., ARAVINTHAN, T. & KARUNASENA, W. 2013. Analysis of a railway turnout system with a spot replacement sleeper. Proceedings of the 22nd Australasian Conference on the Mechanics of Structures and Materials (ACMSM 22), 2013. Taylor & Francis (CRC Press)/Balkema, 841-846.

MARKINE, V. L., STEENBERGEN, M. & SHEVTSOV, I. Y. 2011. Combatting RCF on switch points by tuning elastic track properties. *Wear,* 271**,** 158-167.

MCHENRY, M. T. & ROSE, J. G. 2012. Railroad subgrade support and performance indicators: a review of available laboratory and in-situ testing methods.

MÜLLER-BORUTTAU, F. H. & KLEINERT, U. 2001. Betonschwellen mit elastischer Sohle: Erfahrungen und Erkenntnisse mit einem neuen Bauteil: Fahrbahn der Zukunft. *ETR. Eisenbahntechnische Rundschau,* 50**,** 90-98.

NAVIKAS, D., BULEVIČIUS, M. & SIVILEVIČIUS, H. 2016. Determination and evaluation of railway aggregate sub-ballast gradation and other properties variation. *Journal of Civil Engineering and Management,* 22**,** 699-710.

NEZAMI, E. G., HASHASH, Y. M. A., ZHAO, D. & GHABOUSSI, J. 2004. A fast contact detection algorithm for 3-D discrete element method. *Computers and geotechnics,* 31**,** 575-587.

NGO, N. T., INDRARATNA, B. & RUJIKIATKAMJORN, C. 2014. DEM simulation of the behaviour of geogrid stabilised ballast fouled with coal. *Computers and Geotechnics,* 55**,** 224-231.

NGUYEN, V.-H., DUHAMEL, D. & NEDJAR, B. 2003. A continuum model for granular materials taking into account the no-tension effect. *Mechanics of materials,* 35**,** 955-967.

ORTEGA, A., BLAINEY, S. & PRESTON, J. 2018. Installation of under sleeper pads on ballasted railway tracks: An economic analysis of their potential implementation. *Proceedings of the Institution of Mechanical Engineers, Part F: Journal of Rail and Rapid Transit,* 232**,** 1800-1813.

RAILWAYTECHNOLOGY. 2010. *At a Glance: Railway Sleeper Materials* [Online]. Available: https://www.railway-technology.com/features/feature92105/ [Accessed].

RAO, S. S. 2017. *The finite element method in engineering,* Butterworth-heinemann.

REMENNIKOV, A. M., MURRAY, M. H. & KAEWUNRUEN, S. 2012. Reliability-based conversion of a structural design code for railway prestressed concrete sleepers. *Proceedings of the Institution of Mechanical Engineers, Part F: Journal of Rail and Rapid Transit,* 226**,** 155-173.

SASAOKA, C. D. & DAVIS, D. 2005. Implementing track transition solutions for heavy axle load service. AREMA Annual Conference, 2005 Chicago, IL. Citeseer.

SAYEED, M. A. & SHAHIN, M. A. 2016. Three-dimensional numerical modelling of ballasted railway track foundations for high-speed trains with special reference to critical speed. *Transportation Geotechnics,* 6**,** 55-65.

SCHILDER, R. 2013. USP (Under Sleeper Pads): a contribution to save money in track maintenance. *AusRAIL PLUS 2013, Driving the Costs out of Rail.* Canberra, ACT, Australia.

SCHNEIDER, P., BOLMSVIK, R. & NIELSEN, J. C. O. 2011. In situ performance of a ballasted railway track with under sleeper pads. *Proceedings of the Institution of Mechanical Engineers, Part F: Journal of Rail and Rapid Transit,* 225**,** 299-309.

SELIG, E. T. & LUTENEGGER, A. J. 1991. *Assessing Railroad Track Subgrade Performance Using in Situ Tests*, Department of Civil Engineering, University of Massachusetts.

SELIG, E. T. & WATERS, J. M. 1994. *Track geotechnology and substructure management,* London, UK.

SETSOBHONKUL, S., KAEWUNRUEN, S. & SUSSMAN, J. M. 2017. Lifecycle assessments of railway bridge transitions exposed to extreme climate events. *Frontiers in built environment,* 3**,** 35.

THAKUR, P. K., INDRARATNA, B. & VINOD, J. S. J. S. 2009. DEM simulation of effect of confining pressure on ballast behaviour. 17th International Conference on Soil Mechanics and Geotechnical Engineering, 2009 Amsterdam, Netherlands. IOS Press, 602-605.

TURNER, M. J., CLOUGH, R. W., MARTIN, H. C. & TOPP, L. J. 1956. Stiffness and deflection analysis of complex structures. *journal of the Aeronautical Sciences,* 23**,** 805-823.

YANG, Y. B. & HUNG, H. H. 2001. A 2.5 D finite/infinite element approach for modelling visco-elastic bodies subjected to moving loads. *International Journal for Numerical Methods in Engineering,* 51**,** 1317-1336.

CHAPTER 3

A REVIEW OF VULNERABILITY OF BALLASTED RAILWAY TRACK BUCKLING TO EXTREME HEAT

3.1 Introduction

This chapter presents a critical review of theories and previous studies related to railway track bucklings due to extreme heat. Firstly, this chapter discusses the general concept of railway track bucklings, including the concept of stress in a beam because of a temperature change, track bucklings on the basis of the beam theory, and the track buckling paths and regimes. Secondly, previous studies on railway track buckling are reviewed from the early 70s to the latest research including analytical and numerical approaches. Lastly, the lateral resistance analysis of ballasted railway tracks, which are vulnerable, are critically reviewed. The research gap of the buckling analysis and the lateral resistance of ballasted railway tracks has been identified. It is observed that despite the fact that a number of track buckling analyses using FEM have been widely performed, the previously published papers have mostly focused on a plain ballasted track or a dual gauge track considering the specific length of the railway tracks. Note that the possible buckling mode shapes observed in real life have not been fully investigated in the past, as the recent studies have only demonstrated a symmetrical buckling shape considering the specific length of the railway track model. As a result, the novel findings presented in this chapter will enable the most suitable time-effective technique to be adopted for the methodologies for the track buckling analysis and lateral resistance analysis in Chapters 4–7.

3.2 Axial Force in Rail due to Temperature Change

Since a rail is made of steel, this type of materials deforms due to the changes in the temperature, resulting in expansion (increase) or contraction (decrease). In general, the rails can be buckled at the critical axial buckling force. Figure 3.1 presents a steel bar with

a length *l*, fixed at the left end while the right end is free to move. It is subjected to a temperature increase leading to the elongation of the steel bar *Δl*.

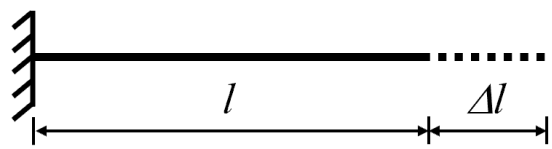

Figure 3.1 Bar extension due to increase in temperature.

Note that the change in the length of the bar is directly influenced by the material characteristic called 'thermal expansion coefficient, *α*'. The increase in length can be calculated on the basis of the increase in temperature (ΔT, T_{after}-T_{before}) by using Eq. (3.1).

$$\Delta l = \alpha \Delta T l \tag{3.1}$$

The above equation can also be written in term of the axial strain (*ε*) as follows:

$$\varepsilon = \alpha \Delta T \tag{3.2}$$

As for the restrained bar at both the ends (Figure 3.2), the bar is prevented from movement by the increase in the temperature, and thus, the stress in the bar is generated.

Figure 3.2 Restrained bar.

The force (*P*) is generated at the one end to prevent the movement of the bar to maintain its original length (*l*) as Figure 3.1. The force generates the axial force or stress in the bar in the cases of the restrained bar, as shown in Figure 3.3.

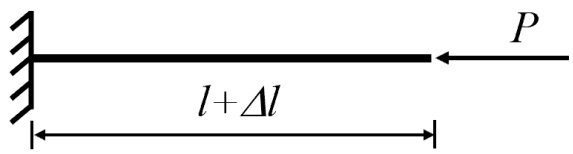

Figure 3.3 Force in the bar due to increase in temperature if both ends are restrained.

The axial stress can be calculated from the axial force and the cross-sectional area, as shown in Eq. (3.3).

$$\sigma = \mathrm{P}/\mathrm{A} \tag{3.3}$$

where σ is the axial stress and A is the cross-sectional area of the bar.

On the basis of the modulus of elasticity equation ($\mathrm{E} = \sigma/\varepsilon$), the axial force in terms of the temperature change and the thermal expansion coefficient can be written as follows:

$$\mathrm{E} = \frac{\mathrm{P}}{\mathrm{A}\alpha\Delta\mathrm{T}} \qquad \text{or} \qquad \mathrm{P} = \mathrm{EA}\alpha\Delta\mathrm{T} \tag{3.4}$$

As the stress developed by the increase in the temperature reaches the critical stress, the buckling occurs if the bar is restrained, as shown in Figure 3.4.

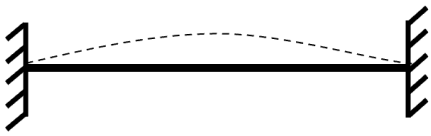

Figure 3.4 Buckling of restrained bar due to the force P.

As for the rails in the railway track, the above equation can be used for the evaluation of the axial force generated in the rails by the increase in the rail temperature before it buckles. In this case, the increase in the temperature is the rail temperature subtracted by the rail neutral temperature or the stress-free temperature, which is set depending on the country. The neutral temperature is a reference condition for the force build up in the rail at which the net longitudinal force in this rails is zero.

Meanwhile, the critical force, which can buckle the structure, was first proposed by Leonhard Euler in 1757 for a column structure (Timoshenko and Gere, 2009). This formula evaluates the critical load that causes the sudden change in the lateral deflection of the column. This causes the loss of stability, which is independent of the material strength and usually occurs within the elastic range of the material. Note that if the load applied is less than the critical load, it generates the axial force in the structure while the structure remains straight. If the load applied is larger than the critical load, the structure will suddenly bend or buckle. There are several factors related to the structural geometries and materials affecting the critical buckling load: elastic modulus, moment of inertia, structural length, and support condition. It is important to note that a railway track can also be treated as a column structure with more elements and much complexity; therefore, Euler's critical load cannot be used directly as a rail buckling force.

3.3 Track Buckling Theory

3.3.1 Buckling path and buckling regime

In general, if the rail temperature is higher than the neutral temperature, the compression axial force in the rails builds up. The built-up axial force can be estimated using Eq. (3.4) presented in Section 3.3. Note that the axial force can be estimated only in the pre-buckling stage before its limit. With the consideration of a long CWR, the axial force due to the temperature increase in the rails is shown in Figure 3.5.

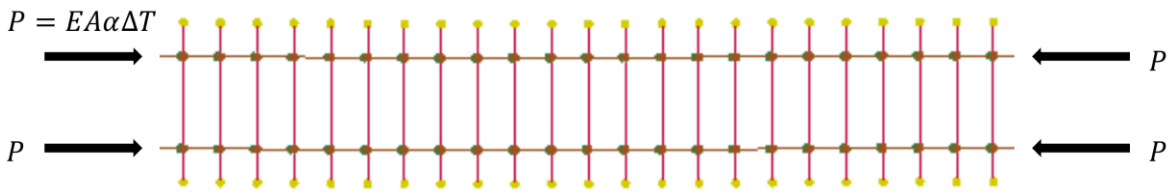

Figure 3.5 Axial force in rails in ballasted railway track.

The rails may buckle when the compression force reaches its limit or the buckling resistance. Note that the buckling resistance is highly influenced by the track type, element type, and track conditions. The relationship between the rail temperature and the lateral displacement is typically plotted as shown in Figure 3.6. It can be seen that there are two types of buckling failure modes: snap-through buckling and progressive buckling. In the pre-buckling stage, the rails are exposed to a higher temperature than the neutral temperature and the axial force is linearly increased. As for the snap-through buckling mode (also called 'sudden buckling' or 'explosive buckling') (Figure 3.6a), the track buckles explosively with no external energy after reaching its maximum temperature (upper critical temperature, T_{max}) and becomes unstable in its post-buckling stages. T_{min}

represents the lower bound, which can buckle the track if sufficient energy is supplied. It can also be defined as a safe temperature, as the track cannot buckle if it experiences a temperature below this temperature. Moreover, progressive buckling (Figure 3.6b) can occur when T_{min} cannot be differentiated from T_{max}, as the peak cannot be seen clearly. In this case, the track's lateral displacement gradually increases after buckling, and the critical temperature is defined as T_P.

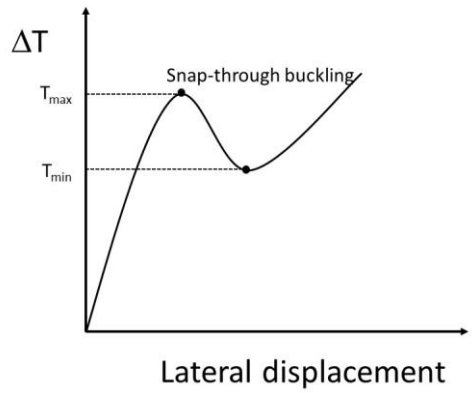

(a)

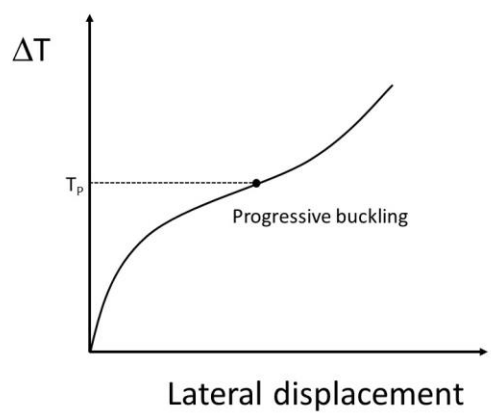

(b)

Figure 3.6 Buckling path: (a) snap-through buckling and (b) progressive buckling.

The safety criteria of railway track buckling have been determined from the difference between the buckling temperature and the safe temperature (European Rail Research Institute Committee D202, 1995). The train operations should be minimised when the rail temperature exceeds the certain temperature level called 'Allowable temperature, T_{all}'. The allowable temperature above neutral temperature, where the rail has zero stress, can be evaluated as shown in Table 3.1. The allowable temperature is generally calculated using the safe temperature. Note that the difference in the buckling criteria depends on ΔT or the buckling failure modes. The allowable temperature of a progressive buckling track, which falls into the last criterion, is generally lower than that of a snap-through buckling failure. This implies that tracks should not be buckled under conditions which can possibly buckle them progressively.

Table 3.1 Safety criteria and allowable temperature (European Rail Research Institute Committee D202, 1995).

Criteria	Allowable temperature (°C)	Buckling paths
$\Delta T > 20°C$	$T_{all} = T_{min} + 0.25\Delta T$	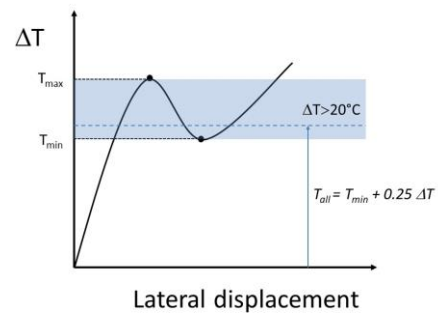
$5°C \leq \Delta T \leq 20°C$	$T_{all} = T_{min}$	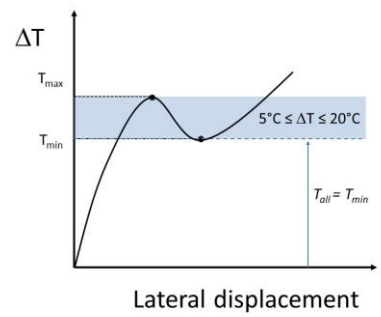
$0°C \leq \Delta T < 5°C$	$T_{all} = T_{min} - 5$	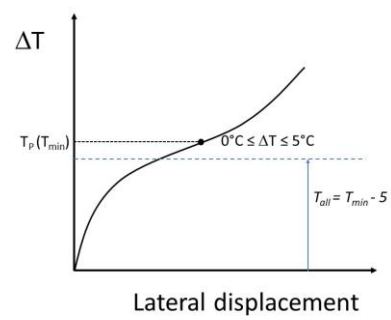

Note: Here, $\Delta T = T_{max}$-T_{min}.

3.3.2 Buckling mode shapes

In general, buckling mode shapes can be often found in the field as symmetrical or asymmetrical mode shapes, as presented in Figures 3.7 and 3.8, respectively. Moreover,

sometimes, buckling shape can be found in the wider length of track showing the sinusoidal shapes as can be seen in Figure 3.9. Previous study has presented certain analytical solutions for predicting the buckling mode shape and the corresponding buckling temperature by using the concept of beam theory (Kerr, 1978). In general, for buckled track, there are two main regions, namely buckled region and adjoining region. The buckled region is the zone of deformation in the shape of the track geometry in the lateral plane, while the rails are deformed longitudinally in the adjoining region. The differential equations are solved to obtain the resulting equations for different buckling mode shapes. Note that, for the asymmetrical buckling shape, the governing equations are identical to those derived for the symmetrical buckling shape except for the boundary conditions.

Figure 3.7 Symmetrical buckling shape (Lankyrider, 2014).

Figure 3.8 Asymmetrical buckling shape (Clark, 2018).

Figure 3.9 Sinusoidal buckling shape.

For Shape #1 (First symmetrical shape) (Figure 3.10): In the analytical solutions for the first symmetrical shape, the track consists of a buckled region ($0 \leq x \leq l$) and an adjoining region ($l \leq x \leq l_0$) with length *a*. Subscript *1* and *a* represent buckled region 1 and the adjoining regions, respectively.

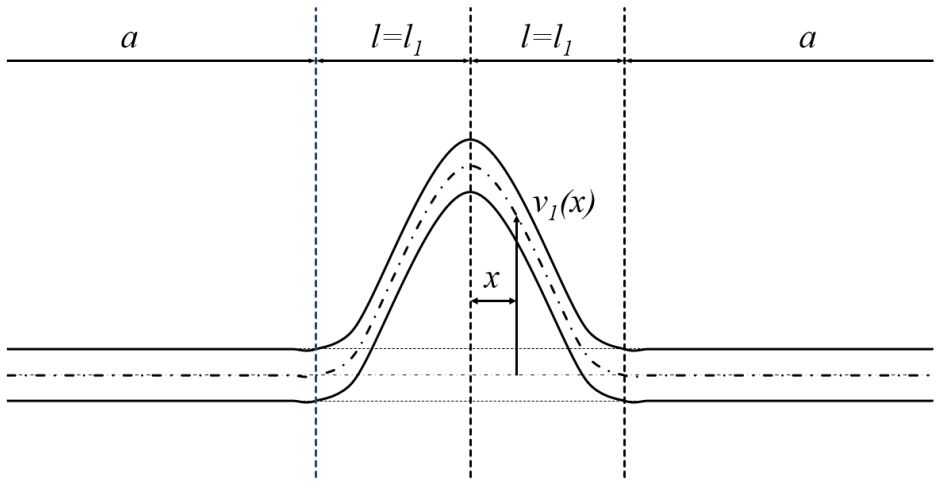

Figure 3.10 First symmetrical buckling shape (Kerr, 1978).

After solving the differential equation integrated with the boundary and the constraint conditions, the general solution for the lateral deformation and the first symmetrical buckling shape can be expressed as Eqs. (3.5) and (3.6), respectively:

$$v_1(x) = \frac{\varrho^* l^4}{2(\lambda l)^2}\left[1 - \frac{x^2}{l^2} - \frac{2(\cos\lambda x - \cos\lambda l)}{\lambda l \sin\lambda l}\right] \tag{3.5}$$

$$EA\alpha T_0 = \widetilde{N}_t + l r_0\left[-1 \pm \sqrt{1 + \frac{EA}{l^2 r_0}\left[\int_0^{l_1} v_1'^2 dx\right]}\right] \tag{3.6}$$

where $\lambda = \sqrt{\frac{\widetilde{N}_t}{EI}}$; $\varrho^* = \frac{\varrho_0}{EI}$; $\int_0^l v_1'^2 dx = 20.45 \times 10^{-4} \varrho^{*2/7}$.

Furthermore, *v(x)* is lateral displacement at location x, *u(x)* is the axial displacement at location x, ϱ_0 is the lateral resistance (always opposite to the direction of *v(x)*), $r_0(x)$ is the axial resistance at location x, *E* is the modulus of elasticity of the rail steel, I is the moment of inertia of the rail steel, *A* is the cross-sectional area of the rail steel, α is the thermal

expansion coefficient, T_0 is the temperature increase, and $\widetilde{N}_t$ is the axial force in the post-buckling stage corresponding to T_0.

Note that $E, A, I, \alpha, r_0,$ and ϱ_0 are the known values and that the unknown $\widetilde{N}_t$ is chosen for determining the corresponding T_0 in order to plot the buckling path. This is also used for evaluating other buckling mode shapes.

For Shape #2 (First asymmetrical shape) (Figure 3.11): The initial formulation is identical to that for Shape #1 except for the boundary condition at $x = 0$, which states that there is no lateral deformation. As it is an asymmetrical shape, solving only the part for $x \geq 0$ is sufficient. The general solution for the lateral deformation and the first symmetrical buckling shape is expressed in Eqs. (3.7) and (3.8), respectively.

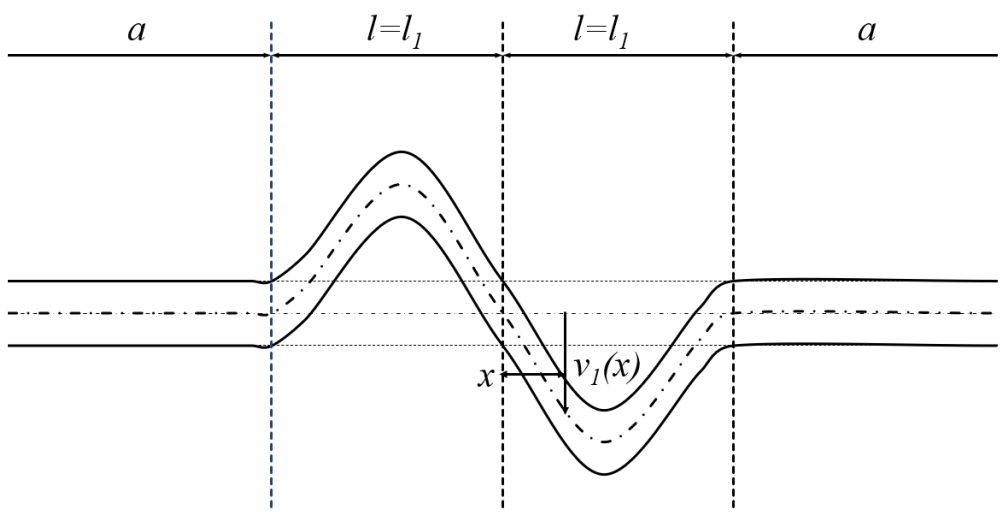

Figure 3.11 First asymmetrical buckling shape (Kerr, 1978).

$$v_1(x) = \frac{\varrho^* l^4}{16\pi^4}\left\{1 - \cos\left(\frac{2\pi x}{l}\right) + \pi \sin\left(\frac{2\pi x}{l}\right) - 2\pi^2\left[\left(\frac{x}{l}\right)^2 - \frac{x}{l}\right]\right\} \quad (3.7)$$

$$EA\alpha T_0 = \widetilde{N}_t + lr_0[-1 + \sqrt{1 + \frac{EA}{l^2 r_0}[\int_0^{l_1} v_1'^2 dx]}] \quad (3.8)$$

where $\int_0^l v_1'^2 dx = 17.40 \times 10^{-5} \varrho^{*2/7}$.

For Shape #3 (Second symmetrical shape) (Figure 3.12): The assumed symmetrical shape of the buckled track is adopted from that for Shape #1 with three buckled regions. The second symmetrical shape consists of a buckled region ($0 \leq x \leq l$) and an adjoining region ($l \leq x \leq l_0$) with length *a*. Subscripts *1*, *2*, and *a* represent buckled region *1*, buckled region *2*, and the adjoining regions, respectively. The final general solution for Shape #3 can be written as shown in Eq. (3.9).

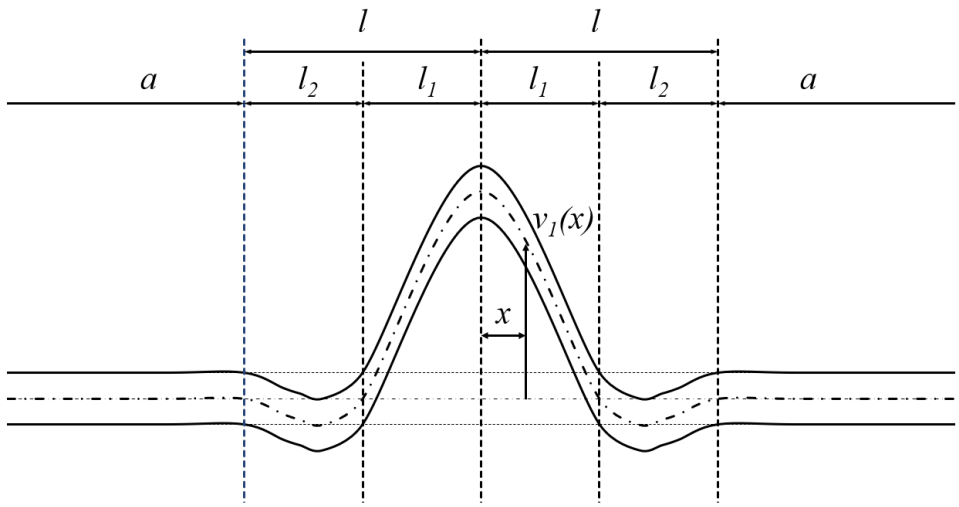

Figure 3.12 Second symmetrical buckling shape (Kerr, 1978).

$$EA\alpha T_0 = \widetilde{N}_t + lr_0[-1 + \sqrt{1 + \frac{EA}{l^2 r_0}[\int_0^{l_1} v_1'^2 dx + \int_{l_1}^{l} v_2'^2 dx]}] \quad (3.9)$$

where $\int_0^{l_1} v_1'^2 dx = 3.09\text{x}10^{-2}\, \varrho^{*2} l_1^7$ and $\int_{l_1}^{l} v_2'^2 dx = 6.25\text{x}10^{-6}\, \varrho^{*2} l^7$.

For Shape #4 (Second asymmetrical shape) (Figure 3.13): The initial formulation is identical to that for Shape #3 except for the boundary condition at $x = 0$, which states that there is no lateral deformation. As it is an asymmetrical shape, solving only the part for $x \geq 0$ is sufficient. The general solution for the lateral deformation and the first symmetrical buckling shape is presented in Eq. (3.10).

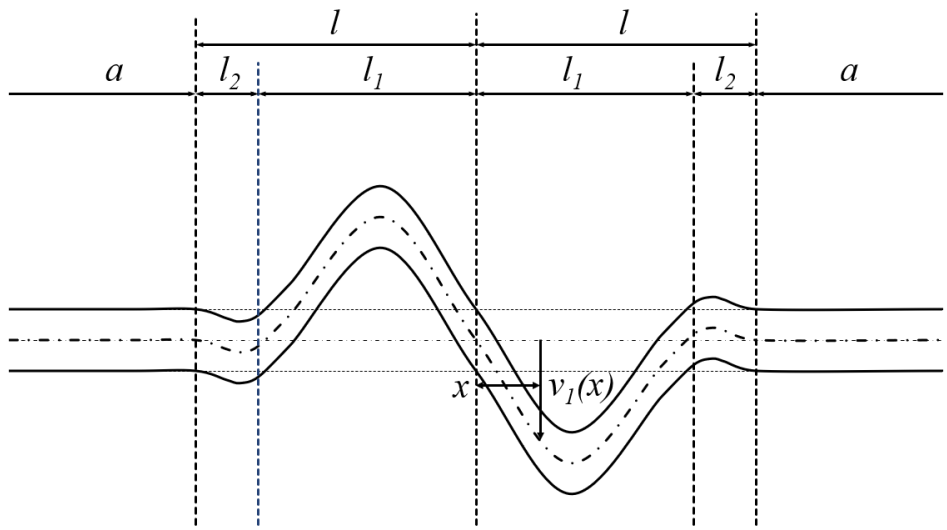

Figure 3.13 Second asymmetrical buckling shape (Kerr, 1978).

$$EA\alpha T_0 = \widetilde{N}_t + lr_0[-1 + \sqrt{1 + \frac{EA}{l^2 r_0}[\int_0^{l_1} v_1'^2 dx + \int_{l_1}^{l} v_2'^2 dx]}] \tag{3.10}$$

where $\int_0^{l_1} v_1'^2 dx = 5.49x10^{-4}\, \varrho^{*2} l_1^7$ and $\int_{l_1}^{l} v_2'^2 dx = 1.91x10^{-7}\, \varrho^{*2} l^7$.

From the analytical solutions, the buckling of the track in an asymmetrical shape generally leads to a wider buckled region than in the case of track buckling in a symmetrical shape because of the larger unconstrained length. However, a general solution is only provided for the first four buckling mode shapes, while the railway tracks can be observed with more cycles of sinusoidal curves in the field.

3.4 Track Buckling Analysis

This section reviews the previous studies on track buckling analyses. These studies can be classified into two solutions: analytical solutions and numerical solutions. An analytical solution was first proposed on the basis of the theory of beam. As the FEM software was developed in the last decade, most of the studies since then used FEM to investigate the buckling behaviour of a railway track. The first method is far more complicated, as it requires many variables, assumptions, and equations to completely analyse the buckling behaviour of railway tracks.

In the late 70s, a research on railway track buckling was first conducted by Kerr (Kerr, 1978, Kerr, 1980). A series of studies provided the concept of track buckling on the basis of the beam theory for the first time. The analytical solutions were presented by assuming the two types of regions in the buckled tracks beforehand: buckled regions and adjoining regions. Note that the lateral displacement occurred only in the buckled regions, while the longitudinal displacement occurred only in the adjoining regions. Kish and Samavedam (Kish, 1985, Samavedam et al., 1993) presented a series of papers on the instability of the American railway track, investigated using the beam model of a single rail, associated with rail imperfections, while the sleeper and the fastener were not taken into account in the model.

A two-dimensional rail–sleeper model of a segment of the track, which represented a length equal to the spacing between the sleepers, was then presented (Jackson et al., 1986, Jackson et al., 1988, Ramesh, 1985). This method also determined the final shape of the track after buckling, unlike the modelling using a beam model. However, several parameters were not

taken into account, such as fastener stiffness, ballast vertical stiffness, and the requirement of consistent track properties along the track.

In 2006, Grissom and Kerr (Grissom and Kerr, 2006) included the torsional resistance of the fasteners and the flexural rigidity of the sleeper in the beam model that was previously introduced by Kerr (1970); however, this model did not include the nonlinearity of the material properties. The 2D model on the basis of the beam theory and the rail–sleeper model has been proven to overestimate the buckling temperature, as the lateral stability of the railway track is a 3D problem (Lim et al., 2003, Lim et al., 2008).

Since the late 2000s, the FEM software has been used more frequently for evaluating the buckling phenomena of ballasted tracks, as it can provide capability and accuracy. This method can help to easily provide the actual buckling phenomena and significantly overcome the drawback of the analytical method that needs complicated differential equations to correctly include all the parameters. The description of the research gap using FEM along with the model descriptions is presented in Table 3.2.

Table 3.2 Description of research gap.

Research	Description	Gap/issue
(Lim et al., 2003, Lim et al., 2008)	This paper presented a preliminary study comparing the 2D and 3D models for buckling analysis using FEM.	This paper first suggested the use of a 3D model over that of a 2D model, as the 2D model overestimated the buckling temperature. Two nonlinear springs were connected to the sleeper ends. The peak displacement limit of the lateral resistance curve was very high.
(Cuadrado et al., 2008)	Simplified dual gauge track model was developed in ANSYS.	The peak displacement limit was set as 5 mm, which was slightly larger than that obtained from the STPTs.
(Carvalho et al., 2013)	This study aimed at investigating the safe temperature of 60-m ballasted tracks by using an indirect method to cope with the drawback of the ANSYS solver in the thermal analysis. The authors modelled the track as one beam with a spacing of 1 m that consisted of 6 DOFs.	The model was simplified. Only a few cases of results were presented.
(Yang and Bradford, 2016)	They considered symmetric and asymmetric modes for buckling and concluded that, for very long members, the final buckling modes were the same if the lateral	The cases when the symmetrical and asymmetrical shapes existed were analysed.

	resistance was consistent along the track.	
(Villalba et al., 2017)	This study developed a 3D finite element model of 60-m dual gauge tracks using ANSYS. Solid and beam models of the rails were compared.	Only the first buckling shape was obtained. The lateral springs of the ballast were applied at both ends of the sleepers, but how the ballast spring was modelled was not clear. The safe temperature was not analysed.
(Villalba Sanchis et al., 2018)	This study developed a 3D finite element model of 60-m dual gauge tracks using ANSYS.	The displacement limit of the lateral spring for sleeper and ballast was not mentioned. It was not clear how they compensated for the effect of the actual tensionless support of the ballast. The safe temperature was not analysed.
(Pucillo, 2019)	The 24-m-long ballasted track was modelled in ABAQUS considering various parameters.	In reality, buckling can be observed with ballasted tracks longer than 24 m; therefore, this study did not cover the whole phenomenon in the field. The displacement elastic limit of the lateral spring of ballast was slightly larger than that obtained by the actual STPTs.
(Miri et al., 2020)	The model developed in ABAQUS consisted of two 50-m UIC60 rails with a narrow gauge of 1.067 m and	They studied the effects of the train load on the buckling behaviour by

	standard B70 concrete sleepers with a central spacing of 0.70 m. It was coupled with a multi-body train track model for accounting for the effects of the train load.	applying vertical and lateral loads on the rails.
(Khatibi et al., 2020)	The authors used the lateral resistance curves obtained from the DEM simulation of STPTs (PFC3D) as an input to the FEM track models (ABAQUS).	The study focused on the effects of the ballast layer geometries on the track buckling.

Table 3.2 clearly shows that most of the recent researches used FEM to analyse the buckling phenomena since the last decade. These studies mostly used ABAQUS, which can potentially provide a full analysis of the buckling, including the buckling and safe temperatures, while ANSYS can directly obtain only the buckling temperature Note that the safe temperature has not been fully analysed in ANSYS because of the limitation of the ANSYS solver in converging the results in the thermal analysis during the post-buckling stage. However, the safe temperature could be achieved using an indirect method as that proposed by Carvalho et al. (2013). Furthermore, it is found that previous studies mostly paid attention to the normal ballasted and dual gauge tracks with the consideration of the various parameters affecting the buckling phenomena. None of them have studied the influences of the track stiffness inconsistency, which is usually seen at an interspersed track, on the track buckling. However, Khatibi et al. (2020) proposed a coupling method that combined FEM and DEM to correctly analyse the buckling phenomena considering

the actual lateral resistances of the tracks obtained from the DEM simulation of the STPTs. The study considered the influences of the ballast layer geometries on the track buckling (Khatibi et al., 2020). This doctoral thesis first analyses the buckling phenomena of ballasted railway tracks capturing the possible buckling shapes observed in the field using FEM to clearly understand the physical behaviour. The coupling method FEM-DEM is then used, as described in Chapters 6 (DEM) and 7 (FEM). This doctoral thesis considers the effects of the progressive degradation of a railway ballast, which, to the best of my knowledge, has never been investigated thus far. It will provide more evidences for railway track buckling and enhance the inspection criteria to mitigate the risk of track buckling in the field.

3.5 Lateral Resistance of Ballasted Railway Tracks

As commonly known, the main factor that influences the buckling strength is the lateral resistance of the railway tracks. The resistance forces can be calculated from the total contact force between the sleeper and the ballast against the movement of the sleeper in the lateral plane. The contact forces include those at three different locations: sleeper bottom, sleeper crib, and sleeper end force, as illustrated in Figure 3.14.

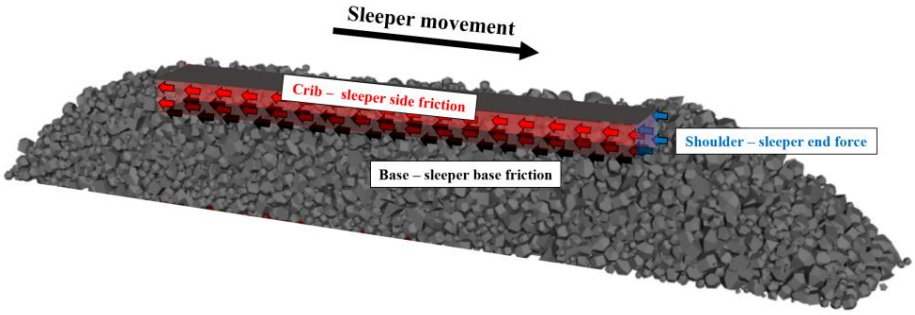

Figure 3.14 Contribution of sleeper–ballast contact force on lateral resistance.

Researchers in the past have conducted both numerical and experimental studies to obtain the lateral resistance of a track. The previous research papers on the lateral resistance of a ballasted track are summarised in Table 3.3. The methods used and the model descriptions are presented to analyse the research gap that has never been investigated. For the numerical analyses, different methods have been applied for quantifying the lateral resistance force through the FEM and DEM approaches by considering different contact parameters and types of particle shapes. The FEM was first used for a lateral resistance evaluation by Kabo (2006), who considered different ballast layer geometries. Several parameters were assumed, particularly for the FEM (Zakeri et al., 2014, Kabo, 2006) and DEM spherical shapes (González, 2015). In addition, a spherical clump has been widely used previously for STPT simulations in the DEM (Huang, 2010, Khatibi et al., 2017, Jing et al., 2018, Guo et al., 2020), while only one study has been carried out using the polyhedral particle (Huang, 2010). The previous studies mostly considered the tracks when the ballast was well compacted, and the ballast shapes were assumed to be clumps of spherical particles. Both the textured sleepers (Huang, 2010, Zakeri et al., 2014) and the ladder sleepers (Jing et al., 2019a) were considered to improve the lateral resistance of the ballasted track. Furthermore, many researchers studied the effects different dimensions and profiles of the ballast layer (Khatibi et al., 2017, Jing and Aela, 2020). It was found that the frictional components of the sleeper bottom and sides played a major role in determining a track's lateral resistance. Moreover, widening the ballast shoulder could help increase the lateral resistance. Nonetheless, only a few studies using DEM focused on the effect of the ballast particle shape, e.g. the angularity (Huang, 2010). It was found that a ballast with angular aggregates provided better shear resistance than a ballast with round

particle shapes; however, these results were not fully indicative, as only the sleeper base friction was considered (Huang, 2010). Different geometries of the ballast layer were factored only for the ballast thickness and shoulder length (Khatibi et al., 2017).

Moreover, measurements for lateral resistance have been widely conducted through field experiments (European Rail Research Institute Committee D202, 1995, Kish, 2011, Le Pen and Powrie, 2011, Khatibi et al., 2017, Jing et al., 2018, Zakeri et al., 2012, Zakeri and Bakhitiary, 2013). Although the STPTs were carried out in both the laboratory and the field experiments, it was found that the lateral resistance of the track in the laboratory experiments was generally less than that in the field because of the lower compaction levels (Zakeri et al., 2012). Note that the lateral resistance in the field tended to be larger, as the tracks had been operated at some point before the tests took place and thus, were well compacted. Note that most of the previous studies with field experiments focused on the effects of sleepers on the lateral resistance of a ballasted track with a clean ballast. The methods of improving the lateral resistance by using more detailed sleeper geometries and dimensions, such as the different types of frictional sleepers and ladder sleepers, were studied in the field. These different sleeper types and features could significantly improve the lateral stiffness of a railway track (Jing et al., 2019a, Jing et al., 2019b, Guo et al., 2020, Zakeri and Mirfattahi, 2020). Moreover, Under Sleeper Pads (USPs) were adopted as another elastic layer to the sleeper with the aim to improve the lateral resistance of the track (Sol-Sánchez et al., 2014). It was found that sleepers with USPs have a slightly higher mean value of the lateral resistance that those without USPs. As for the ballast layer contribution, some type of ballast particle gluing was applied to railway tracks to improve the lateral stability (Xiao and Ling, 2017, Jing et al., 2019b). Moreover, different types of

ballast materials, e.g. limestone and steel slag, with a similar gradation were considered in the field measurements (Esmaeili et al., 2016), and the steel slag was found to provide better lateral resistance than the limestone ballast because of its higher bulk specific gravity. It was found that none of them considered the degradation of the ballast, which can be widely observed on the existing railway tracks. As a ballast can be progressively degraded over time because of the impact load from the train that are distributed via the sleeper to the ballast, it can generate a ballast fouling layer that significantly undermines the track stiffness.

Table 3.3 Previous research on lateral resistance of ballasted tracks.

Research	Method		Parameters
	Numerical	Experimental	
(Kabo, 2006)	✓ FEM (Abaqus)		Ballast layer geometries, variation of FEM contact parameters
(Kish, 2011)		✓	Concrete and timber sleepers, effects of maintenance activities
(Le Pen and Powrie, 2011)		✓	Contribution of base, crib, and shoulder ballast
(Huang, 2010, Huang and Tutumluer, 2011)	✓ DEM polyhedral (BLOSK3D)		Angularity of ballast particle, tamping
(Zakeri et al., 2012)		✓	Frictional sleepers

(Zakeri et al., 2014)	✓ FEM		Frictional sleepers
(Le Pen et al., 2014)		✓	Ballast at shoulder on sleeper end resistance
(Koike et al., 2014)		✓	Sleeper shape, sleeper spacing
(Sol-Sánchez et al., 2014)		✓	Under sleeper pads (USPs)
(Bakhtiary et al., 2015)		✓	Different types of sleepers
(González, 2015)	✓ DEM spherical		Ballast layer geometries, frictional parameters
(Esmaeili et al., 2016)		✓	Compared limestone and steel slag as ballast
(Zakeri and Talebi, 2016)		✓	Steel sleeper
(Khatibi et al., 2017)	✓ DEM spherical clump (PFC3D)		Ballast layer geometries

(Xiao and Ling, 2017)	✓ DEM spherical clump (PFC3D)	✓	Ballast gluing
(Jing et al., 2018, Jing et al., 2019a)	✓ DEM spherical clump (PFC3D)		Different shapes of concrete sleeper
(Jing et al., 2019b)	✓ DEM spherical clump (PFC3D)		Polyurethane-reinforced ballast
(Guo et al., 2020)	✓ DEM spherical clump (PFC3D)		Sleeper bottom texture

A recent European review provided some benchmarked STPT results for the lateral resistance of a ballasted track with mono-block concrete sleeper during different ballast construction and in-service stages (Lichtberger, 2007). On a basis of this benchmarking, Figure 3.15 presents a comparison of the results from various STPT research studies for mono-block concrete sleepers. The different track conditions and the ballast construction and in-service stages correspond to the unballasted track or lying free; loosely filled track, tamped, and lined track; dynamically stabilised track; and well-filled and fully stabilised

track according to (Lichtberger, 2007). The typical values of the lateral resistance of a ballasted track with a concrete sleeper are presented at the sleeper displacement of 2 mm, which tends to be over the yielding point (Lichtberger, 2007). Note that this yielding point is when the lateral stiffness is reduced after the sleeper is displaced; this has been reported in the literature to be between 0.5 mm and 2 mm. The lateral contact force changes very slightly and is likely to be constant after the yielding point or the elastic limit. Note that the value shown in Figure 3.15 is used as the benchmarked value for the model validation in this doctoral thesis, which will be presented in Chapter 6.

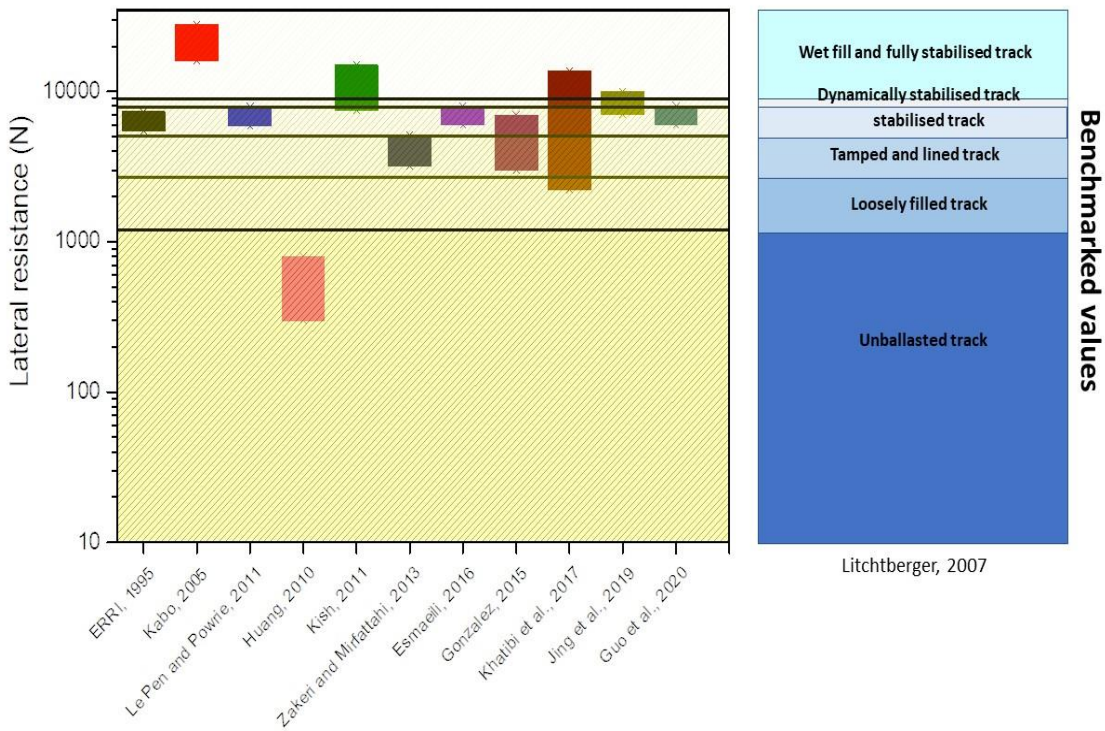

Figure 3.15 Lateral resistance and benchmarked values.

3.6 Summary

This chapter identifies previous studies, which represent the past and current knowledge, including substantive findings, as well as theoretical and methodological contributions to the buckling analysis of railway tracks due to extreme heat. The chapter summarises a wide range of studies, including experimental and numerical studies on the lateral stability of a ballasted railway track. To the best of my knowledge, there are several research gaps that have never been captured and need to be filled fully to cover all the buckling phenomena due to extreme heat.

To fully understand the behaviour of the ballasted railway track due to extreme heat, the parametric studies covering all the significant parameters will be conducted in Chapters 4 and 5. Furthermore, the coupled DEM–FEM method, which has been used only once in the past, will be investigated in Chapters 6 and 7.

3.7 References

BAKHTIARY, A., ZAKERI, J. A., FANG, H. J. & KASRAIEE, A. 2015. An experimental and numerical study on the effect of different types of sleepers on track lateral resistance. *International Journal of Transportation Engineering,* 3**,** 7-15.

CARVALHO, J., DELGADO, J., CALÇADA, C. & DELGADO, R. 2013. A new methodology for evaluating the safe temperature in continuous welded rail tracks. *International Journal of Structural Stability and Dynamics* 13**,** 1350016.

CLARK, J. 2018. *Roads melt and rail tracks buckle as UK heatwave strikes* [Online]. Available: https://www.newcivilengineer.com/latest/roads-melt-and-rail-tracks-buckle-as-uk-heatwave-strikes-27-06-2018/?post_id=141949&access=off [Accessed].

CUADRADO, M., ZAMORANO, C., GONZÁLEZ, P., NASARRE, J. & ROMO, E. 2008. Analysis of buckling in dual-gauge tracks. *Proceedings of the Institution of Civil Engineers-Transport,* 161**,** 177-184.

ESMAEILI, M., NOURI, R. & YOUSEFIAN, K. 2016. Experimental comparison of the lateral resistance of tracks with steel slag ballast and limestone ballast materials. *Proceedings of the Institution of Mechanical Engineers, Part F: Journal of Rail and Rapid Transit,* 231**,** 175-184.

EUROPEAN RAIL RESEARCH INSTITUTE COMMITTEE D202 1995. Improved knowledge of forces in CWR track (including switchws). *Report2, review of existing experimental work in behaviour of CWR track.* Utrecht, Netherlands: European Rail Research Institute

GONZÁLEZ, J. I. 2015. *Numerical modelling of railway ballast using the discrete element method.* Master Thesis, Escola de Camins.

GRISSOM, G. T. & KERR, A. D. 2006. Analysis of lateral track buckling using new frame-type equations. *International Journal of Mechanical Sciences,* 48**,** 21-32.

GUO, Y., FU, H., QIAN, Y., MARKINE, V. & JING, G. 2020. Effect of sleeper bottom texture on lateral resistance with discrete element modelling. *Construction and Building Materials,* 250.

HUANG, H. 2010. *Discrete Element Modeling of Railroad Ballast Using Imaging Based Aggregate Morphology Characterization.* Doctor of Philosophy PhD Thesis, University of Illinois at Urbana-Champaign.

HUANG, H. & TUTUMLUER, E. 2011. Discrete Element Modeling for fouled railroad ballast. *Construction and Building Materials,* 25**,** 3306-3312.

JACKSON, J. E., BAULD, N. R. & RAMESH, M. 1986. A Finite Element Model for the Lateral Strength of Railroad Track Structures. *In:* YAGAWA, G. & ATLURI, S. N. (eds.) *Computational Mechanics.* Tokyo, Japan: Springer

JACKSON, J. E., BAULD, N. R., RAMESH, M. S. & MENON, S. C. 1988. A superelement for lateral track deformation. *Applied Mechanics Rail Transportation Symposium.* Chicago, USA: ASME.

JING, G. & AELA, P. 2020. Review of the lateral resistance of ballasted tracks. *Proceedings of the Institution of Mechanical Engineers, Part F: Journal of Rail and Rapid Transit,* 234**,** 807-820.

JING, G., AELA, P. & FU, H. 2019a. The contribution of ballast layer components to the lateral resistance of ladder sleeper track. *Construction and Building Materials,* 202**,** 796-805.

JING, G., AELA, P., FU, H. & YIN, H. 2018. Numerical and experimental analysis of single tie push tests on different shapes of concrete sleepers in ballasted tracks. *Proceedings of the Institution of Mechanical Engineers, Part F: Journal of Rail and Rapid Transit,* 233**,** 666-677.

JING, G., ZHANG, X. & JIA, W. 2019b. Lateral resistance of polyurethane-reinforced ballast with the application of new bonding schemes: Laboratory tests and discrete element simulations. *Construction and Building Materials,* 221**,** 627-636.

KABO, E. 2006. A numerical study of the lateral ballast resistance in railway tracks. *Proceedings of the Institution of Mechanical Engineers, Part F: Journal of Rail and Rapid Transit,* 220**,** 425-433.

KERR, A. D. 1978. Analysis of thermal track buckling in the lateral plane. *Acta Mechanica,* 30**,** 17-50.

KERR, A. D. 1980. An improved analysis for thermal track buckling. *International Journal of Non-Linear Mechanics,* 15**,** 99-114.

KHATIBI, F., ESMAEILI, M. & MOHAMMADZADEH, S. 2017. DEM analysis of railway track lateral resistance. *Soils and Foundations,* 57**,** 587-602.

KHATIBI, F., ESMAEILI, M. & MOHAMMADZADEH, S. 2020. Numerical investigation into the effect of ballast properties on buckling of continuously

welded rail (CWR). *Proceedings of the Institution of Mechanical Engineers, Part F: Journal of Rail and Rapid Transit*.

KISH, A. 2011. On the Fundamentals of Track Lateral Resistance. *Annual Conference.* Minneapolis, USA.

KISH, A. S., G.; JEONG, D. 1985. INFLUENCE OF VEHICLE INDUCED LOADS ON THE LATERAL STABILITY OF CWR TRACK. USA: Federal Railroad Administration, Office of Research and Development.

KOIKE, Y., NAKAMURA, T., HAYANO, K. & MOMOYA, Y. 2014. Numerical method for evaluating the lateral resistance of sleepers in ballasted tracks. *Soils and Foundations,* 54**,** 502-514.

LANKYRIDER. 2014. *Buckled rails on the Yarra Valley Railway* [Online]. Available: https://commons.wikimedia.org/wiki/File:Buckled_rails_on_the_Yarra_Valley_Railway.JPG#file [Accessed].

LE PEN, L., BHANDARI, A. R. & POWRIE, W. 2014. Sleeper End Resistance of Ballasted Railway Tracks. *Journal of Geotechnical and Geoenvironmental Engineering,* 140.

LE PEN, L. M. & POWRIE, W. 2011. Contribution of Base, Crib, and Shoulder Ballast to the Lateral Sliding Resistance of Railway Track: A Geotechnical Perspective. *Proceedings of the Institution of Mechanical Engineers, Part F: Journal of Rail and Rapid Transit,* 225**,** 113-128.

LICHTBERGER, B. 2007. The lateral resistance of the track. *European Railway Review.* Plasser & Theurer.

LIM, N.-H., PARK, N.-H. & KANG, Y.-J. 2003. Stability of continuous welded rail track. *Computers & Structures,* 81**,** 2219-2236.

LIM, N., HAN, S.-Y., HAN, T. & KANG, Y. 2008. Parametric Study on Stability of Continuous Welded Rail Track-Ballast Resistance and Track Irregularity. *Steel Structures,* 8**,** 171-181.

MIRI, A., DHANASEKAR, M., THAMBIRATNAM, D., WESTON, B. & CHAN, T. H. T. 2020. Analysis of Buckling Failure in Continuously Welded Railway Tracks. *Engineering Failure Analysis***,** 104989.

PUCILLO, G. P. 2019. Train-Induced Load Effects on the Thermal Track Buckling. Joint Rail Conference, April 9–12, 2019 Utah, USA. American Society of Mechanical Engineers Digital Collection.

RAMESH, M. S. 1985. *A nonlinear finite element approach to the analysis of lateral thermal and mechanical buckling of railroad tracks.* Master thesis, Clemson University.

SAMAVEDAM, G., KISH, A., PURPLE, A. & SCHOENGART, J. 1993. Parametric Analysis and Safety Concepts of CWR Track Buckling. United States. Federal Railroad Administration.

SOL-SÁNCHEZ, M., MORENO-NAVARRO, F. & RUBIO-GÁMEZ, M. C. 2014. Viability of using end-of-life tire pads as under sleeper pads in railway. *Construction and Building Materials,* 64**,** 150-156.

TIMOSHENKO, S. P. & GERE, J. M. 2009. *Theory of elastic stability,* Courier Corporation.

VILLALBA, I., INSA, R., SALVADOR, P. & MARTINEZ, P. 2017. Methodology for evaluating thermal track buckling in dual gauge tracks with continuous welded rail. *Proceedings of the Institution of Mechanical Engineers, Part F: Journal of Rail and Rapid Transit,* 231**,** 269-279.

VILLALBA SANCHIS, I., INSA, R., SALVADOR, P. & MARTÍNEZ, P. 2018. An analytical model for the prediction of thermal track buckling in dual gauge tracks. *Proceedings of the Institution of Mechanical Engineers, Part F: Journal of Rail and Rapid Transit,* 232**,** 2163-2172.

XIAO, H. & LING, X. 2017. Experiment and DEM Analysis of Lateral Resistance of Glued Ballast. *Xinan Jiaotong Daxue Xuebao/Journal of Southwest Jiaotong University,* 52**,** 1046-1054.

YANG, G. & BRADFORD, M. A. 2016. Thermal-induced buckling and postbuckling analysis of continuous railway tracks. *International Journal of Solids and Structures,* 97**,** 637-649.

ZAKERI, J.-A. & TALEBI, R. 2016. Experimental investigation into the effect of steel sleeper vertical stiffeners on railway track lateral resistance. *Proceedings of the Institution of Mechanical Engineers, Part F: Journal of Rail and Rapid Transit,* 231**,** 104-110.

ZAKERI, J. A. & BAKHITIARY, A. 2013. Experimental investigation on effects of frictional sleeper in lateral resistance of railway tracks. *Trans Res. J. (TRJ),* 10**,** 159-169.

ZAKERI, J. A., ESMAEILI, M., KASRAEI, A. & BAKHTIARY, A. 2014. A numerical investigation on the lateral resistance of frictional sleepers in ballasted railway tracks. *Proceedings of the Institution of Mechanical Engineers, Part F: Journal of Rail and Rapid Transit,* 230**,** 440-449.

ZAKERI, J. A. & MIRFATTAHI, B. 2020. Field investigation on the lateral resistance of railway tracks with frictional sleepers *IOP Conf. Series: Materials Science and Engineering,* 671.

ZAKERI, J. A., MIRFATTAHI, B. & FAKHARI, M. 2012. Lateral resistance of railway track with frictional sleepers. *Proceedings of the Institution of Civil Engineers - Transport,* 165**,** 151-155.

CHAPTER 4

LINEAR BUCKLING ANALYSIS OF BALLASTED RAILWAY TRACKS

4.1 Introduction

This chapter first analyses the buckling temperature of traditional ballasted railway tracks. The first type of traditional ballasted tracks consists of timber sleepers which are still being used nowadays. Because of the fast degradation of timber sleepers, the short-term solution of replacing rotten timber sleepers with other types of sleepers has been proposed by making a new type of ballasted track called 'interspersed railway track'. This method is a temporary approach to maintain the performance of a conventional timber track for a low to moderate operational speed train. More details and previous studies on interspersed railway tracks were discussed in Chapter 2. This chapter presents the three-dimensional finite element modelling of interspersed railway tracks subjected to a temperature change by using a linear buckling analysis based on eigenvalues and eigenvectors. The eigenvalue analysis is primarily used to analyse the buckling temperature and the corresponding buckling shape at the bifurcation point of railway tracks on the basis of the assumption of the linear properties of each component. Note that this method can provide an estimation for the maximum or buckling temperature and help to save computational time. The buckling analysis of conventional and interspersed railway tracks is carried out. Five types of railway tracks are considered: plain timber sleepered track, 1 in 2 interspersed track, 1 in 3 interspersed track, 1 in 4 interspersed track, and plain concrete sleepered track. The linear eigenvalue analysis is used to simulate the buckling temperature and the buckling shape of a railway track with purely timber sleepers, and the timber sleepers are then replaced by concrete sleepers for interspersed tracks. The results obtained from the first model are then compared with interspersed tracks and concrete sleepered tracks.

The new key findings highlight the buckling phenomena of interspersed railway tracks, which are usually adopted during railway transformations from degraded timber to concrete sleepered tracks in real-life scenarios around the world. The results provide a recommendation for tracks with different parameters to improve the buckling strength and resilience of ballasted railway track for extreme temperature.

4.2 Finite Element Modelling (FEM)

In this chapter, ballasted railway tracks with standard gauge are modelled in LS-DYNA (Livermore Software Technology Coporation (LSTC), 2018). Steel rails UIC60 and sleepers are modelled as beam elements, which take into account shear and flexural deformations (Cai, 1994). Rails and sleepers are constructed using SECTION_BEAM and MAT_ELASTIC. The MAT_ADD_THERMAL_EXPANSION property is assigned to the steel rails. The rail pads and fasteners are modelled as the series of spring elements by using SECTION_DISCRETE and SPRING_ELASTIC in the connections between the sleepers and the rails. At the rail seat, a rail pad and a fastener, consisting of three translational springs to represent the pad stiffness in three directions and one rotational spring to represent the fastener resistance, are applied. For the ballast, the tensionless support spring should be considered and connected to both the sleeper ends instead of a normal spring, as it allows the beam to move over the support while the tensile support is neglected (Ngamkhanong et al., 2020). This presents the realistic behaviour of the ballast. However, in the linear analysis, a nonlinear user-defined spring is not allowed. Hence, SPRING_ELASTIC is used in the linear analysis. Note that the stiffness value in the system is doubled when the sleeper is moved. However, the results presented are based on the

actual stiffness derived using the input value divided by two. Figure 4.1 presents the relationship between the sleeper and the ballast contact models represented by the beam and the spring elements. Figure 4.1a presents the sleeper with linear elastic springs connected at both ends of the sleeper in the equilibrium state. When the sleeper is moved laterally, one spring is compressed, while the other is tensioned. In this case, the summation of lateral stiffness is equal to 2k, which implies that the springs are in series. This is equivalent to Figure 4.1c, wherein the linear elastic spring with 2k stiffness is connected at one end. In fact, the nonlinear tensionless springs with 2k stiffness should be connected instead to represent the actual ballast behaviour in the lateral plane, as presented in Figure 4.1d.

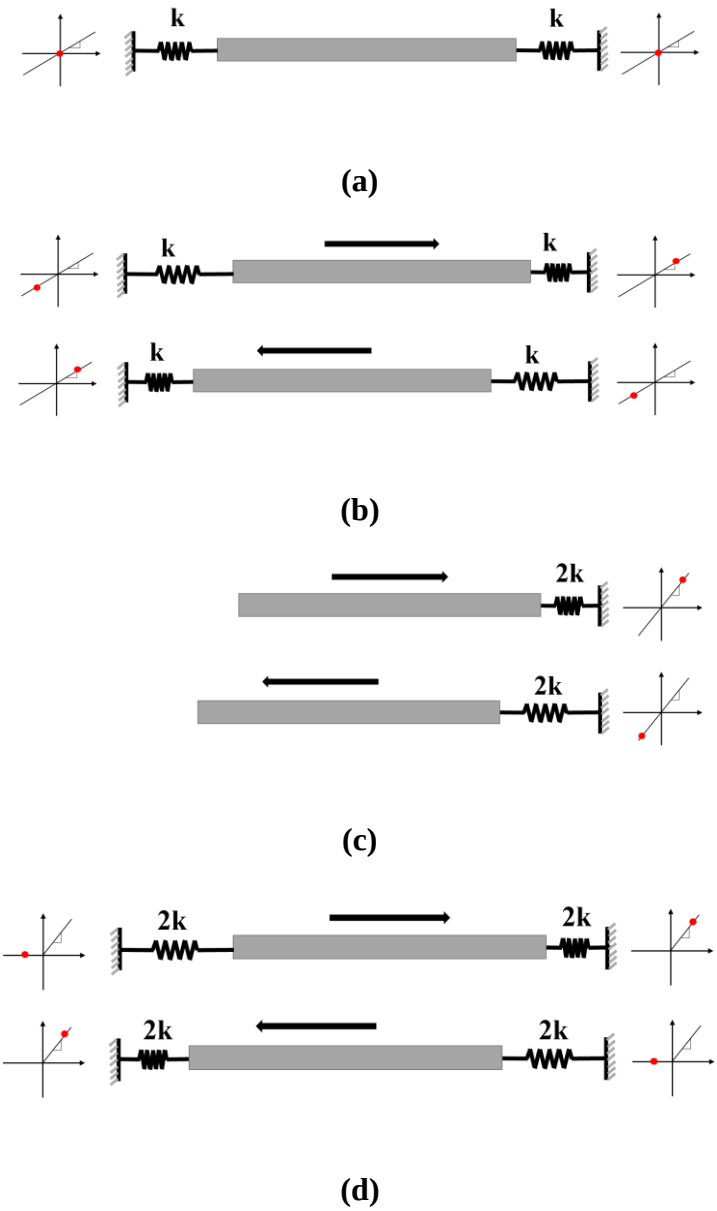

Figure 4.1 Spring model for lateral ballast resistance: (a) normal springs with no movement, (b) linear elastic spring with stiffness k at both ends, (c) linear elastic spring with stiffness k at one end, and (d) nonlinear tensionless spring with stiffness 2k at both ends.

For the track buckling analysis, 60-m-long ballasted railway tracks are modelled to analyse the effects of the temperature rise on the track, as shown in Figure 4.2. The model consists of 100 spans with a spacing of 0.6 m. Note that 60m is sufficiently long to capture the track buckling phenomena and covers the buckling length observed in practice.

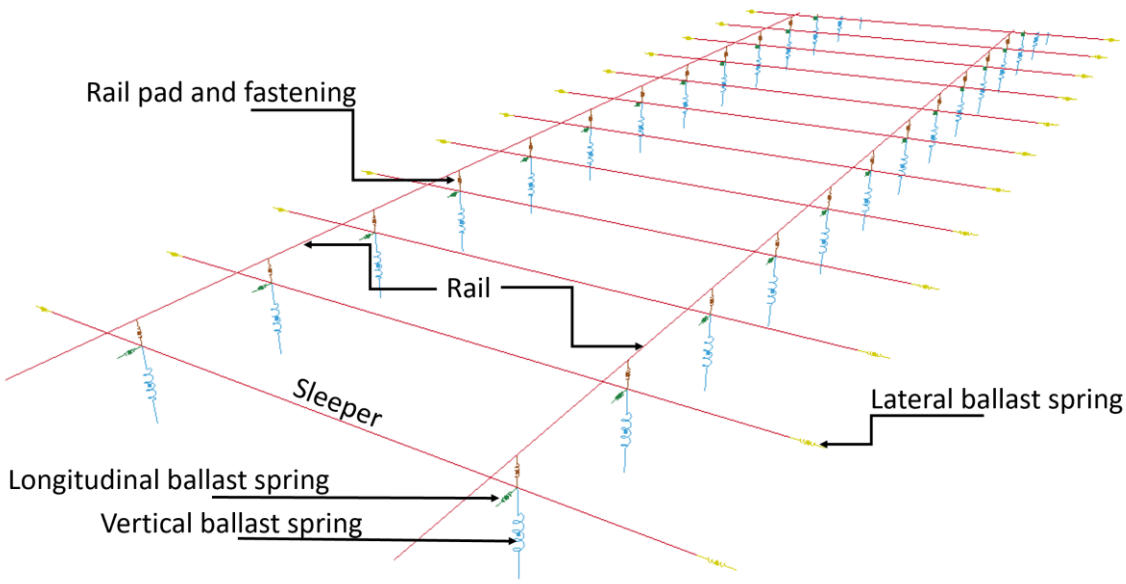

Figure 4.2 Ballasted railway track modelling.

The material properties shown in Table 4.1 are applied to the elements. Note that the properties including elastic modulus, density, and Poisson's ratio, are based on the common use in railway system while the resistances are considered according to the previous tests. In this study, it is assumed that the lateral resistance of the timber sleeper is approximately 60% of that of the concrete sleeper based on the results obtained from the previous STPTs (CRC for Rail Innovation, 2009, Kish, 2011). In contrast, the torsional fastening resistance at the rail seat of the timber sleeper is approximately 2.5 times of that of the concrete sleeper (Esveld, 2001, Kish and Samavedam, 2013). The assumptions of these properties have been described in Chapter 3.

Table 4.1 Material properties.

Parameter list	Characteristic value	Unit
Rail (UIC60)		
Modulus	2×10^5	MPa
Density	7850	kg/m^3
Poisson's ratio	0.25	
Thermal expansion	1.17×10^{-5}	1/°C
Concrete sleeper		
Modulus	3.75×10^4	MPa
Shear modulus	1.09×10^4	MPa
Density	2740	kg/m^3
Poisson's ratio	0.2	
Lateral resistance	200–2000	N/mm
Torsional fastening resistance	75	kNm/rad
Timber sleeper (Hardwood)		
Modulus	1.02×10^4	MPa
Shear modulus	3.93×10^3	MPa
Density	1100	kg/m^3
Poisson's ratio	0.2	
Lateral resistance	120–1200	N/mm
Torsional fastening resistance	225	kNm/rad

In this study, the conventional ballasted track with a plain timber sleeper is first constructed. Then, the timber sleepers are substituted by the concrete sleepers depending on the track types in order to build three types of commonly interspersed railway tracks and the plain concrete sleepered track, as shown in Figure 4.3. They are identified as follows:

- Timber sleepered track

- 1 in 2 interspersed track
- 1 in 3 interspersed track
- 1 in 4 interspersed track
- Concrete sleepered track

By definition, 'XinY' implies that for every Y span of the conventional timber sleepered track, the timber sleepers are replaced by X concrete sleepers. For instance, '1 in 4' indicates that one concrete sleeper is seated alongside every three timber sleepers. For clearer understanding, the configurations of all the tracks are presented by showing the section of each component with different colours to classify the timber and the concrete sleepers as shown in Figure 4.3.

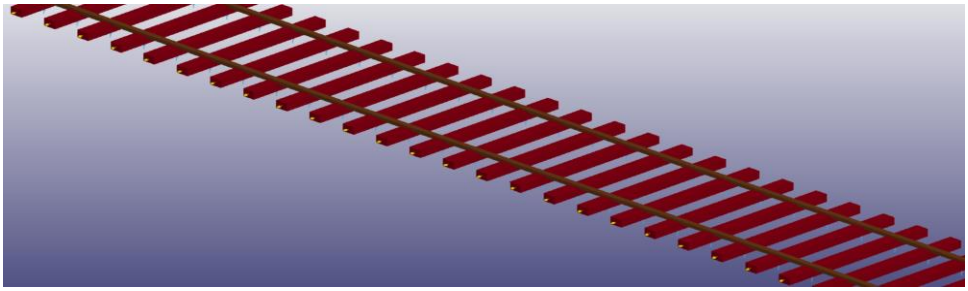

(a)

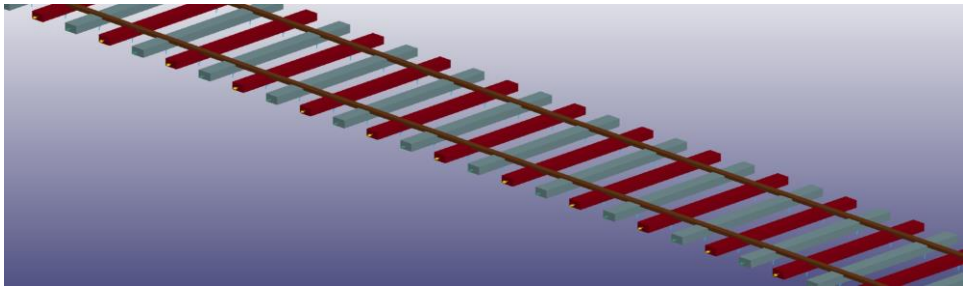

(b)

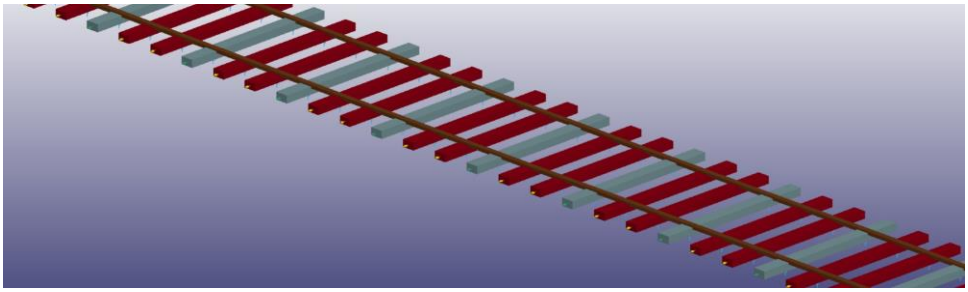

(c)

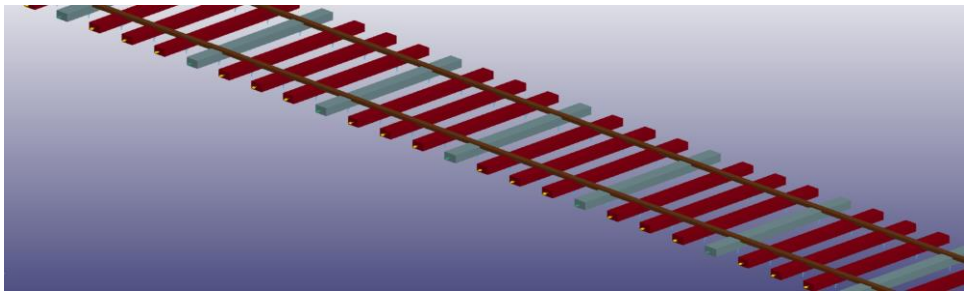

(d)

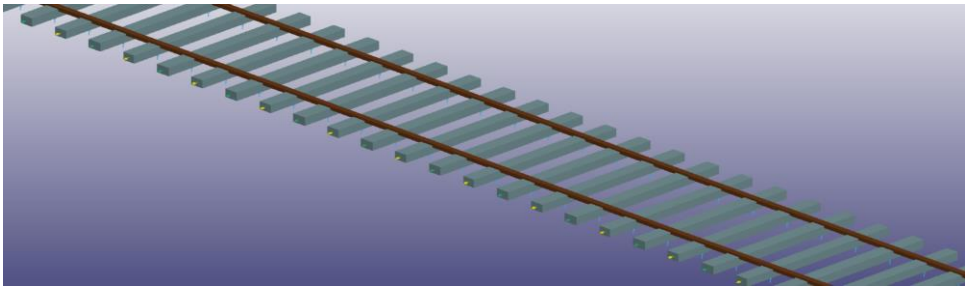

(e)

Figure 4.3 Railway track models: (a) timber sleepered track, (b) '1 in 2' interspersed track, (c) '1 in 3' interspersed track, (d) '1 in 4' interspersed track, and (e) concrete sleepered track.

4.2.1 Boundary conditions

In an actual track, there are two regions in a buckled track: buckled regions (positive and negative lateral displacement) and adjoining regions. Because of the extreme temperature, the large lateral displacement of the rails normally occurs in the transverse direction: if the tracks have imperfection, the rails are deformed longitudinally in the adjoining region.

Note that the buckling shapes of a track are often symmetrical or anti-symmetrical. The buckling shape and the buckling length in an actual track differ under different track conditions. Note that the buckled region is normally in a relatively weak zone of the tracks. The fixed end supports are applied to the end nodes of the rails. The roller supports are applied on the rails to generate the stiff track area so that the rails are constrained and not allowed to move transversally. In LS-DYNA, the nodes are constrained using the BOUNDARY_SPC_SET keyword. Hence, the unconstrained length is presented as a characteristic of a relatively weak track, and thus, the buckled region is expected in this area. In this study, the track originally had a length of 60 m, which was sufficient for the track buckling analysis. As observed in the field, the buckling length was normally less than 30 m; therefore, the largest unconstrained length of 30 m was chosen, and the track beyond this length was considered as the adjoining zone. The boundary conditions of the track models are presented in Figure 4.4. In this study, the unconstrained length started from 6 m and was increased to 12 m, 18 m, 24 m, and 30 m.

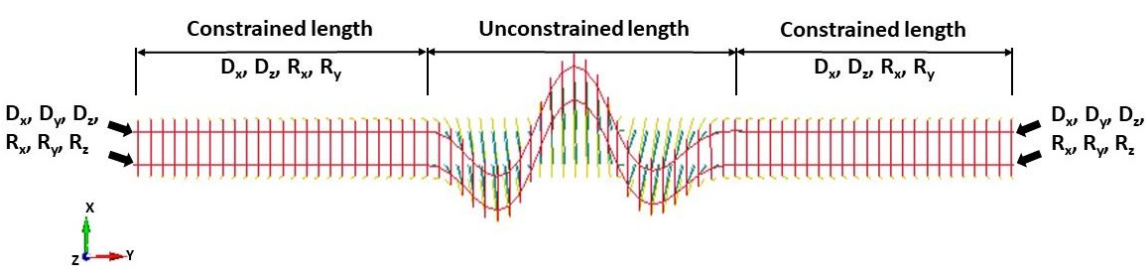

Figure 4.4 Boundary conditions.

4.3 Linear Eigenvalue Buckling Analysis

In the linear buckling analysis, the buckling temperature and the corresponding mode shapes for the railway track are calculated using the CONTROL_IMPLICIT_BUCKLE

keyword in LS-DYNA on the basis of the eigenvalues and the eigenvectors. This keyword uses the Block Shift and Invert Lanczos methods to extract the buckling modes of the structure. It should be noted that Buckling Load Factor (BLF), which is an indicator of the safety factor or the proportion of the given load, is analysed. This factor is then multiplied by the given load to compute the buckling temperature. The buckling path in the linear analysis is shown in Figure 4.5. The buckling temperature is calculated on the basis of the bifurcation point, which is the intersection between the primary and the secondary (post-buckling) loads' path at which the structure became unstable; this could occur at more than one equilibrium positions at this point (El-Ghazaly et al., 1991, Yang and Bradford, 2016). After buckling, the post-buckling state does not follow the primary path. At this stage, the secondary slope can be either positive (post-buckling strength) or negative (simply collapse). Note that the stresses occurred in direct proportion to the load factor before reaching the bifurcation point. However, the buckling analysis does not include the nonlinearities and the initial imperfection of the structure. The governing equation used for evaluating the buckling temperature and the corresponding buckling shapes is shown in Equation (4.1).

$$\left|K + \lambda K_g\right| = 0 \tag{4.1}$$

This equation is equivalent to the eigenvalue solution shown in Equation (4.2):

$$Kx = -\lambda K_g x \tag{4.2}$$

where K is the global stiffness matrix, x is the buckling mode vector, λ is the buckling load factor (BLF), and K_g is the global geometric stiffness matrix known as the initial stress

stiffness matrix depending on the stress level of the element. Note that the element force vector at each state changed the geometric stiffness of the element.

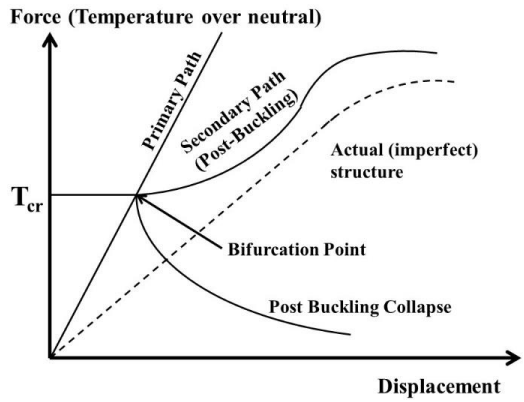

Figure 4.5 Linear bifurcation buckling path (Strand7 Pty Ltd, 2005).

Note that the BLF is an indicator of the factor of safety (FOS) against buckling or the ratio of the critical buckling load to the applied loads. With Equation (4.2), the BLFs are calculated and then multiplied by the applied temperature to determine the buckling temperature. It should be noted that buckling is predicted when the applied thermal loads are higher than the estimated critical loads (BLF < 1). In contrast, the track does not buckle under the applied temperature when the BLF is beyond 1. However, the buckling temperature can still be calculated using this method by extrapolating to reach the buckling temperature, despite the possible buckling temperature is higher than the applied temperature. The interpretations of BLFs are summarised in Table 4.2. In this study, the temperature is set to 200°C for the whole system.

Table 4.2 Buckling load factor (BLF).

BLF	Status	Note
<1	Buckling is predicted under applied load.	The applied load is larger than the critical buckling load. Buckling is expected. Critical buckling load = BLF × Applied load
1	Buckling is predicted under applied load.	The applied load is equal to critical buckling load. Buckling is expected. Critical buckling load = Applied load
>1	Buckling is not predicted under applied load.	The applied load is less than the critical buckling load. Buckling is not expected. However, the critical buckling load can be predicted. Critical buckling load = BLF × Applied load

4.3.1 Model validation

As the buckling of the interspersed railway track has never been evaluated in the past and the field data on interspersed tracks are very limited, the traditional ballasted track with purely concrete sleepers is first considered for the model validation. The result is first validated against two different previous analytical solutions and two different finite element analysis (FEA) results. Note that a straight ballasted railway track with only concrete sleepers with the lateral stiffness of 200 N/mm and the torsional stiffness of 75k Nm/rad is considered to compare the initial result with previous studies, as these values

represent similar track conditions and properties. The analytical solutions calculate buckling temperature on the basis of bending beam theory and principle of the virtual displacement equation. The results are solved by assuming the buckling shape and applying the chosen track parameters to the equation. The buckling temperature is then calculated from the corresponding critical axial force (Prud'Homme and Janin, 1969, Kerr, 1980). The previous finite element approach in ANSYS used a simplified model by combining two rails into one idealised continuous beam with four springs representing the fastening system and ballast support with a spacing of 1 m along the continuous beam (Carvalho et al., 2013). Another FEA model of the ballasted track built in STRAND7 is also compared to the current model in this chapter (Ngamkhanong et al., 2020). Table 4.3 presents a comparison between the previous studies and the current study. It is found that the result obtained in this study is within the acceptable range of the previous studies as the percentage difference of the buckling temperature of the example model is only 3.7%, and thus, the models can be appropriately used further.

Table 4.3 Buckling temperatures for model validation (°C).

Analytical solutions		FEM		Average	This study	Difference (%)
Prud'Homme and Janin 1969	Kerr 1980	Carvalho et al. 2013	Ngamkhanong, Wey, and Kaewunruen 2020			
57.7	47.8	50.0	53.0	52.1	54.1	3.7

4.4 Results and Discussions

4.4.1 Buckling shape

In this section, the unconstrained length represents the weaker area of the track with the poorer track conditions where buckling occurs, while the area beyond this demonstrates the stiffer area or better track conditions representing the adjoining zones. Five cases of unconstrained lengths are considered to understand the physical behaviours of track buckling, including the buckling shape and the buckling temperature. The first global buckling modes of the conventional timber sleepered tracks considering different unconstrained lengths and lateral resistance are presented in Table 4.4; the first mode represents the lowest temperature that can buckle the tracks. Clearly, the symmetrical shape, which is presented as mode 1 in Chapter 3, is observed in tracks with an unconstrained length of 6 m. The bucking shape is shifted from a symmetrical shape to an anti-symmetrical shape when the lateral resistance increases to 2000 N/m for the 6-m-long unconstrained length tracks.

Hence, the buckling shapes can be changed by either increasing or reducing the track's lateral resistance. The buckling modes are also shifted from first symmetrical to anti-symmetrical when the unconstrained length increases from 6 m to 12 m, whereas the first anti-symmetrical shape are shifted to the second symmetrical mode shape when the lateral resistance increases from 200 N/m to 800 N/mm for tracks with an unconstrained length of 12 m. Moreover, the number of buckling regions increase with an increase in the unconstrained length. Hence, the analytical solutions confirm that the shape of buckling mainly depends on the boundary conditions and the lateral resistance. It is important to

note that although the lateral resistance can significantly increase the buckling strength and the buckling temperature, the buckling shape of a track with higher lateral resistance tends to be sinusoidal shapes and have more buckled regions than that of a track with lower lateral resistance, as the track buckles because of the higher temperature or axial compression force.

Table 4.4 Buckling shapes of timber sleepered tracks.

Unconstrained length (m)	Lateral stiffness			
	200 N/mm	800 N/mm	1400 N/mm	2000 N/mm
6	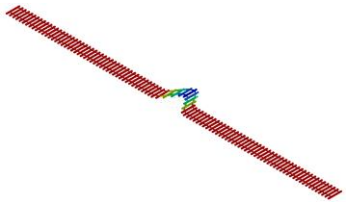	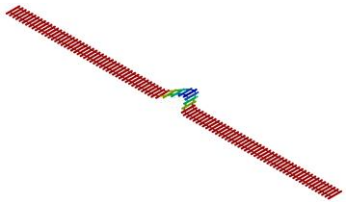	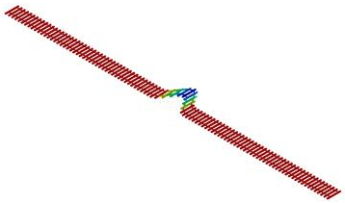	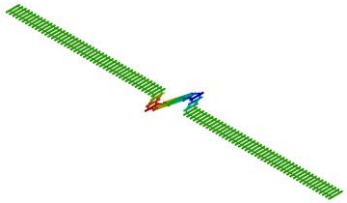
12	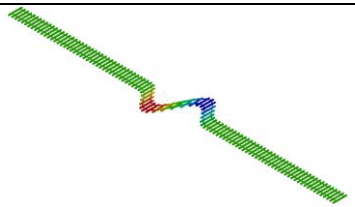	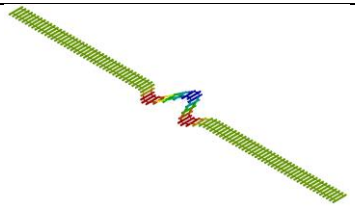	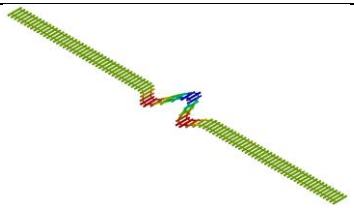	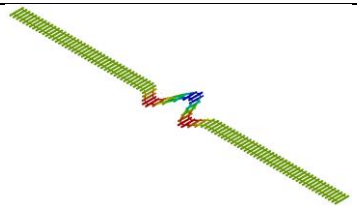
18	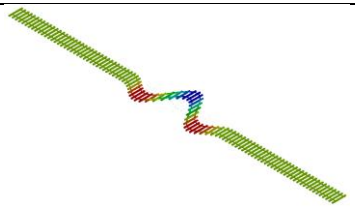	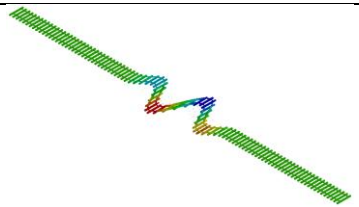	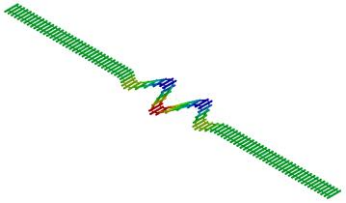	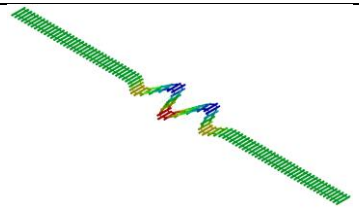

Table 4.5 Buckling shapes of timber sleepered tracks (Contd.).

Unconstrained length (m)	Lateral stiffness			
	200 N/mm	800 N/mm	1400 N/mm	2000 N/mm
24	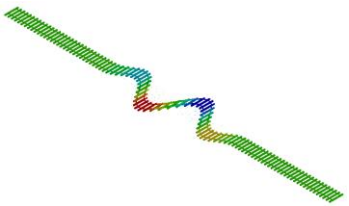	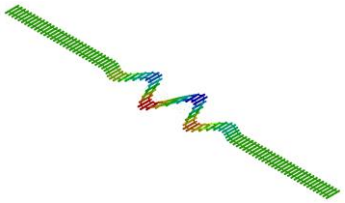	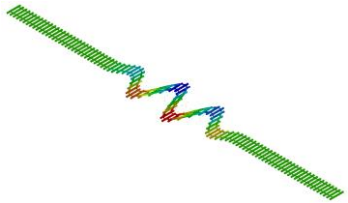	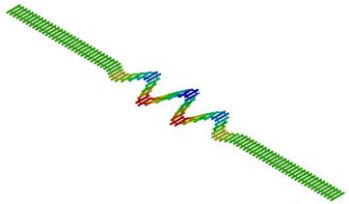
30	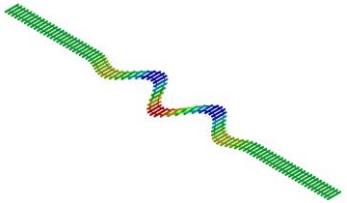	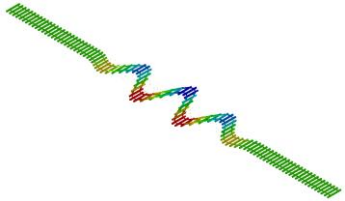	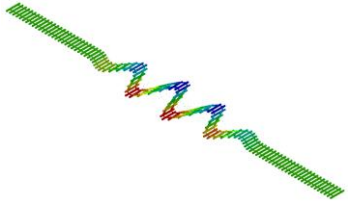	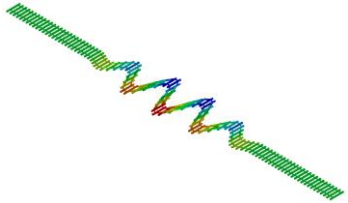

Figures 4.6–4.10 present the effects of the unconstrained length on the buckling shapes considering the low and the high lateral resistances. It is observed that the first symmetrical buckling shape is observed in the tracks with an unconstrained length of 6 m and a lateral stiffness of 200 N/mm, as shown in Figure 4.6a. In contrast, the first anti-symmetrical buckling shape is observed in all the track types with an unconstrained length of 6 m and a lateral stiffness of 2000 N/mm (Figure 4.6b) and those with an unconstrained length of 12 m and a lateral stiffness of 200 N/mm (Figure 4.7a). In case of a lateral resistance of 2000 N/mm, the concrete sleepered track is likely to have a larger number of buckled regions than the other types of tracks (Figure 4.7b). Note that, in the model, the ballast springs are connected in parallel to the sleepers; therefore, the larger number of concrete sleepers represents a higher track lateral resistance. It is found that a larger unconstrained length results in a larger number of buckled regions particularly when the lateral resistance is high (Figures 4.8–4.10).

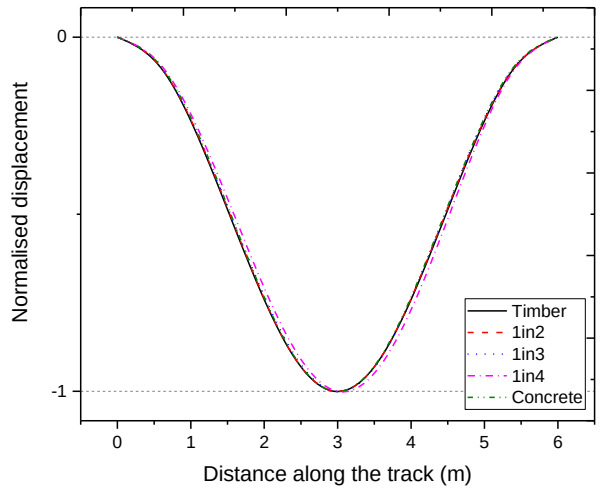

(a)

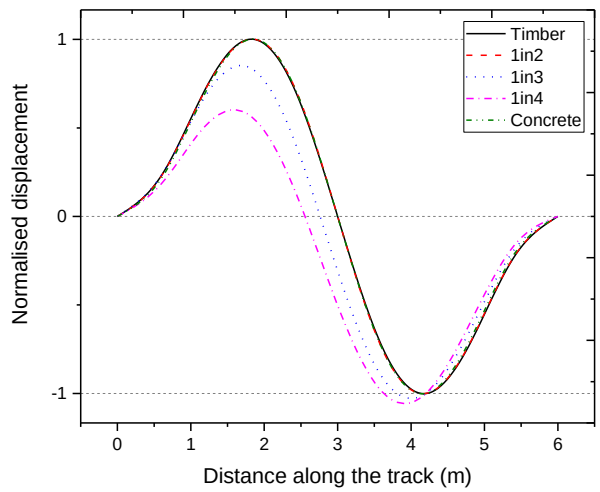

(b)

Figure 4.6 Buckling shape of railway tracks under different conditions and with 6-m unconstrained length: (a) Lateral resistance = 200 N/mm and (b) Lateral resistance = 2000 N/mm

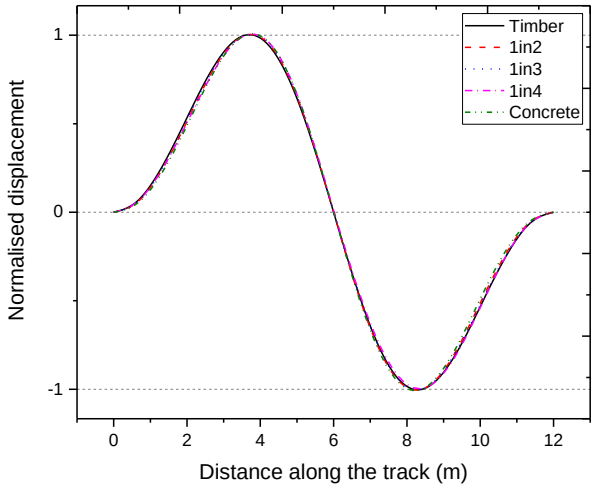

(a)

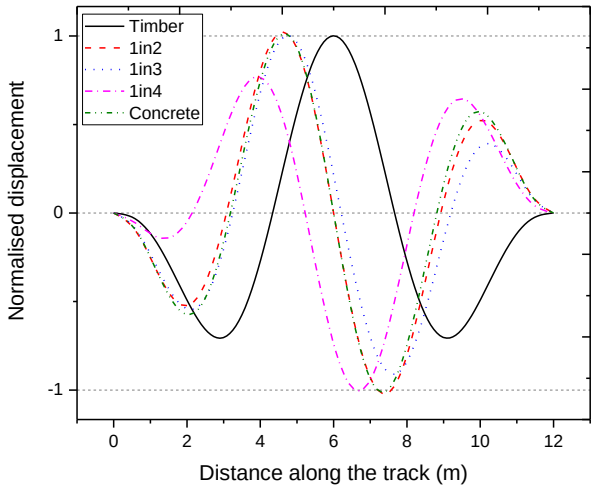

(b)

Figure 4.7 Buckling shape of railway tracks under different conditions and with 12-m unconstrained length: (a) Lateral resistance = 200 N/mm and (b) Lateral resistance = 2000 N/mm.

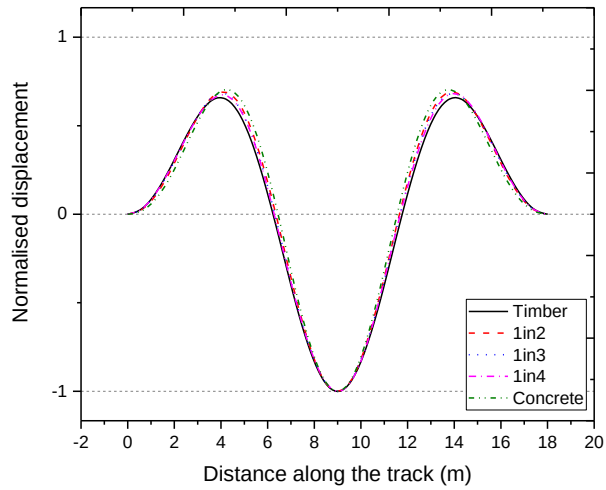

(a)

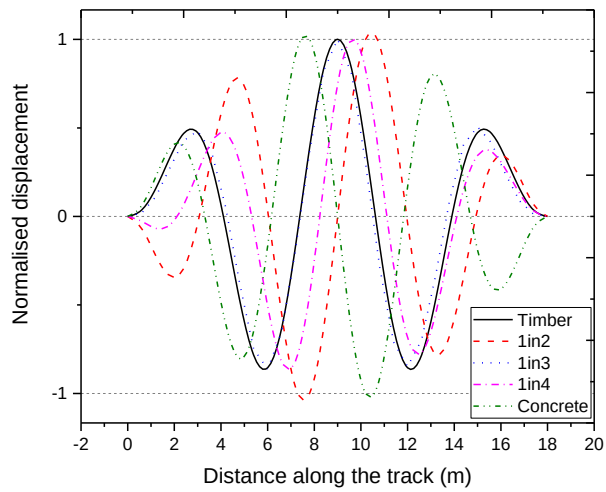

(b)

Figure 4.8 Buckling shape of railway tracks under different conditions and with 18-m unconstrained length: (a) Lateral resistance = 200 N/mm and (b) Lateral resistance = 2000 N/mm.

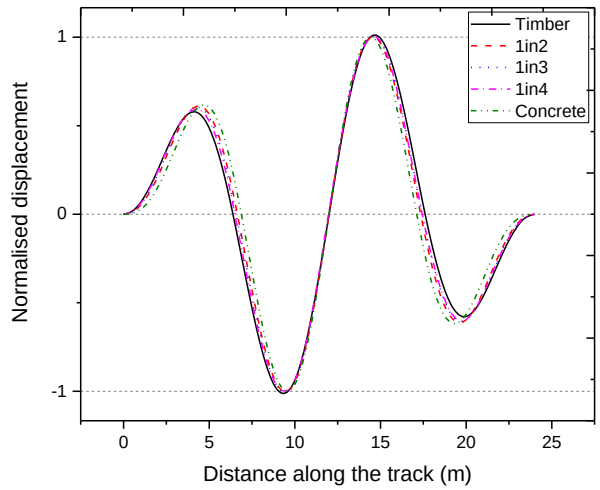

(a)

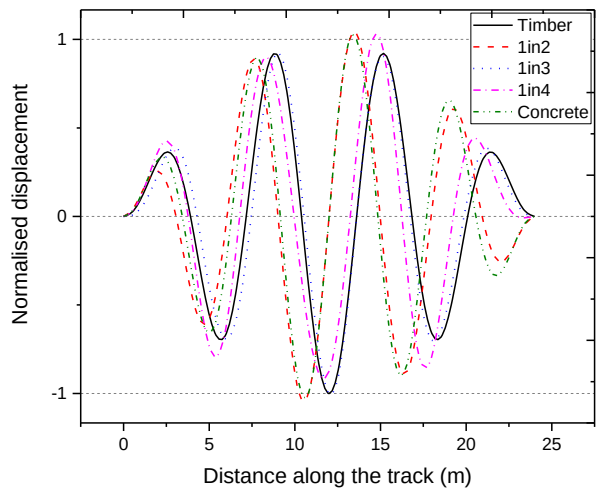

(b)

Figure 4.9 Buckling shape of railway tracks under different conditions with 24-m unconstrained length: (a) Lateral resistance = 200 N/mm and (b) Lateral resistance = 2000 N/mm.

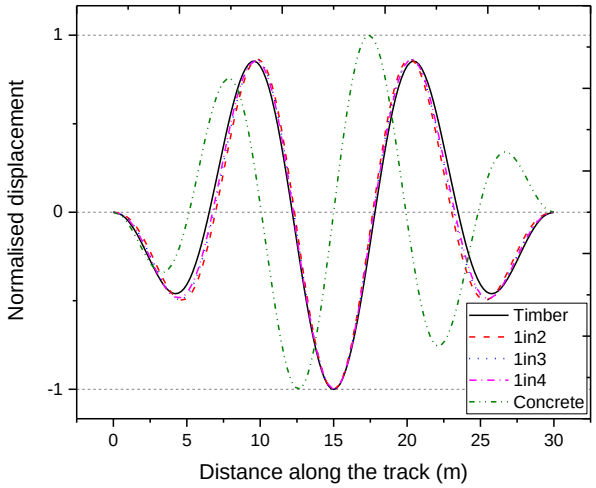

(a)

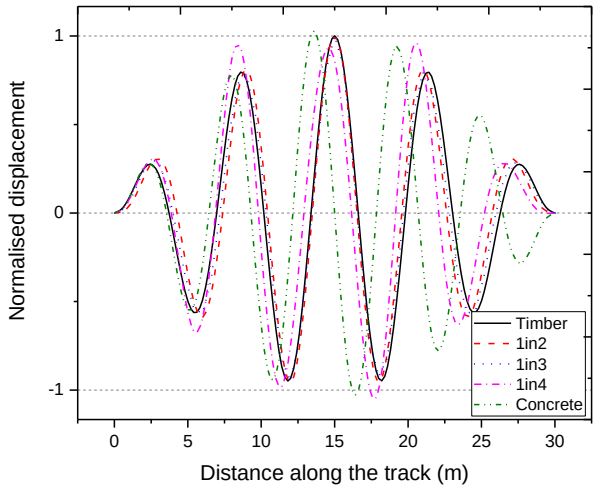

(b)

Figure 4.10 Buckling shape of railway tracks under different conditions with 30-m unconstrained length: (a) Lateral resistance = 200 N/mm and (b) Lateral resistance = 2000 N/mm.

Figure 4.11 presents the effects of the unconstrained length on the buckling temperature. Note that the original results are initially obtained as BLF and the values are then multiplied by the applied temperature to obtain the buckling temperature. It is clear that the larger unconstrained length can buckle the tracks earlier than the shorter unconstrained length, as

for the 6-m unconstrained length of the tracks, the buckling temperature for all the tracks is considerably higher than that in the other cases. In the case of the 12-m unconstrained length, the buckling temperature is slightly affected by the boundary conditions. The buckling temperature tends to be constant when the unconstrained length reached the certain length. It is obvious that the railway tracks can be buckled when subjected to the same temperature and an unconstrained length of more than 24 m. As for the buckling temperature in general, the concrete sleepered track demonstrates the best buckling prevention performance, resulting in a higher buckling temperature. In terms of the interspersed railway tracks, the 1 in 2 track has better performance than 1 in 3 and 1 in 4 because of the larger number of concrete sleepers that has a higher lateral resistance than the timber sleepers. However, when the track stiffness is 200 N/mm, the reverse result is observed that the concrete sleepered track is worse than the other tracks, as the rotation stiffness of the fastening system of the concrete sleeper is one-third of that of the timber sleeper and the lateral resistance does not help the track to prevent buckling. Thus, an unconstrained length of 30 m for the railway tracks is chosen for the nonlinear analysis to analyse the buckling temperature.

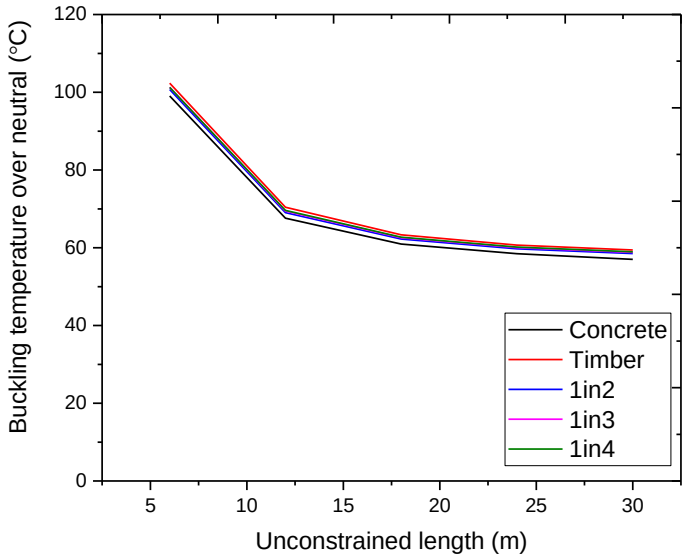
Buckling temperature over neutral (°C)
Unconstrained length (m)
Concrete
Timber
1in2
1in3
1in4

(a)

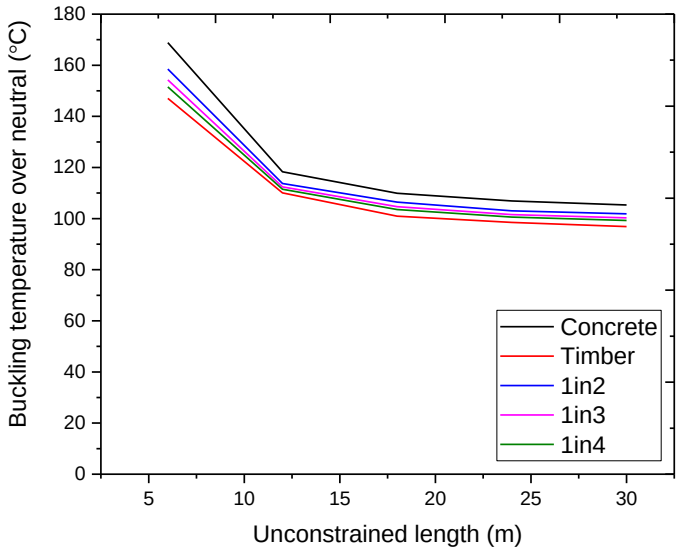
Buckling temperature over neutral (°C)
Unconstrained length (m)
Concrete
Timber
1in2
1in3
1in4

(b)

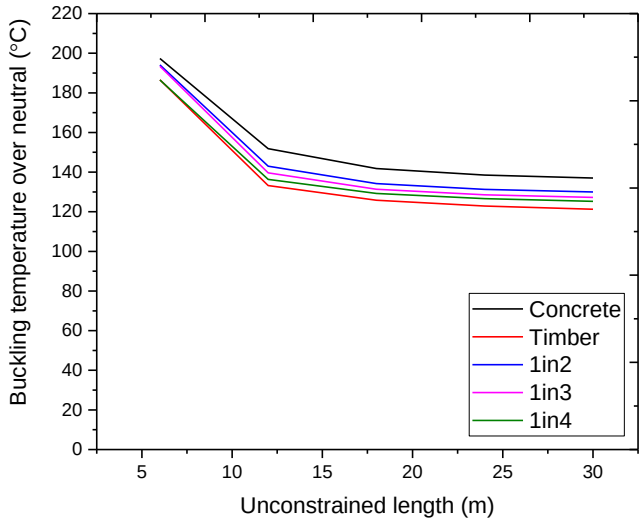

(c)

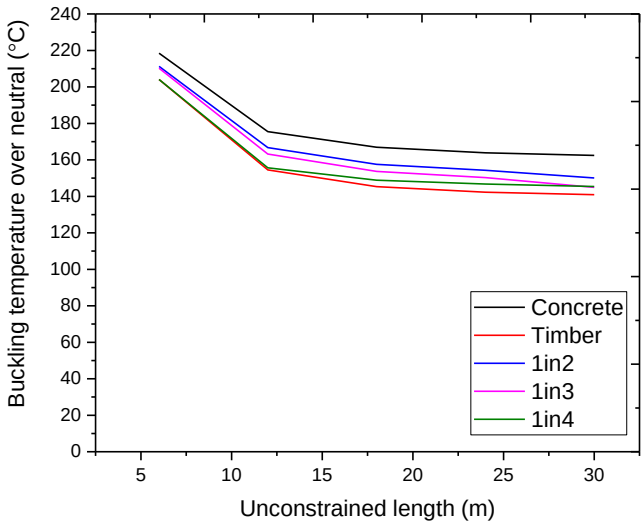

(d)

Figure 4.11 Buckling temperature over neutral and unconstrained length of railway tracks with lateral resistance of (a) 200 N/mm, (b) 800 N/mm, (c) 1400 N/mm, and (d) 2000 N/mm.

4.4.2 Effects of torsional resistance and lateral resistance

Figure 4.12 presents the buckling temperature rise above the neutral temperature considering the unconstrained length, lateral resistance, and torsional resistance. It should be noted that the lower and the upper bounds of torsional resistance are the nominal values times 0.5 and 1.5, respectively. These are represented as the effects of the torsional fastening resistance by the dot and dash lines in Figure 4.12. It is clear that the lateral resistance plays a very significant role while the torsional fastening resistance plays a small role in improving the buckling resistance. All the tracks show the similar trends in terms of the lateral resistance. However, the torsional fastening resistance in the concrete sleepered track can hardly influence the buckling temperature, while the fastening systems can potentially help the timber sleepered track to improve the buckling resistance, as seen in the wider range between the upper and the lower bounds of the buckling temperature.

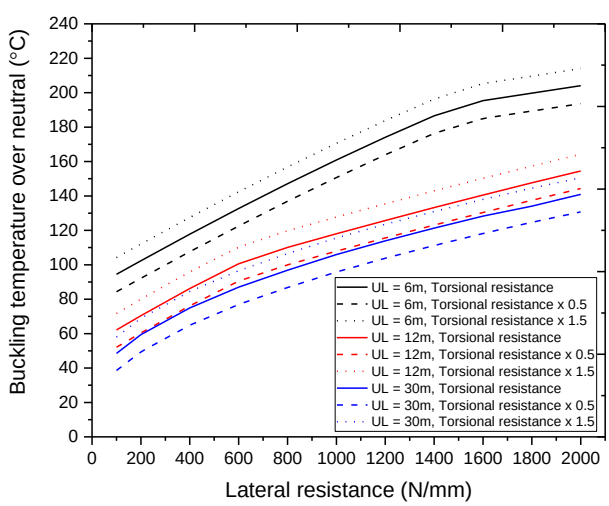

(a)

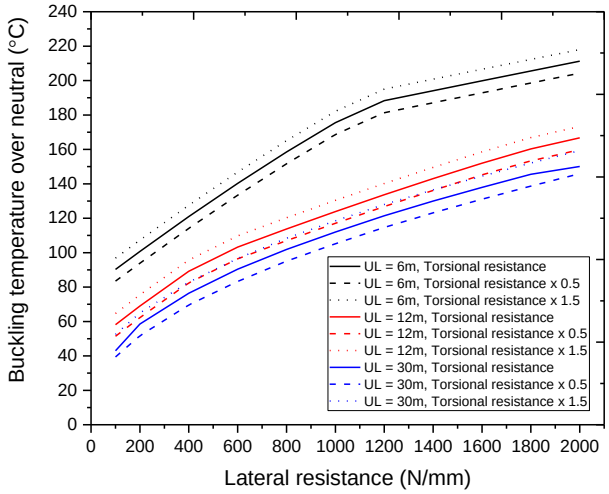
Buckling temperature over neutral (°C)
Lateral resistance (N/mm)
0
20
40
60
80
100
120
140
160
180
200
220
240
0
200
400
600
800
1000
1200
1400
1600
1800
2000
UL = 6m, Torsional resistance
UL = 6m, Torsional resistance x 0.5
UL = 6m, Torsional resistance x 1.5
UL = 12m, Torsional resistance
UL = 12m, Torsional resistance x 0.5
UL = 12m, Torsional resistance x 1.5
UL = 30m, Torsional resistance
UL = 30m, Torsional resistance x 0.5
UL = 30m, Torsional resistance x 1.5

(b)

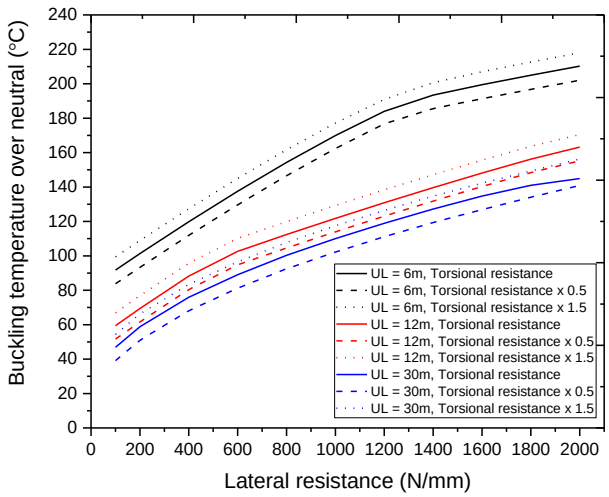
Buckling temperature over neutral (°C)
Lateral resistance (N/mm)
0
20
40
60
80
100
120
140
160
180
200
220
240
0
200
400
600
800
1000
1200
1400
1600
1800
2000
UL = 6m, Torsional resistance
UL = 6m, Torsional resistance x 0.5
UL = 6m, Torsional resistance x 1.5
UL = 12m, Torsional resistance
UL = 12m, Torsional resistance x 0.5
UL = 12m, Torsional resistance x 1.5
UL = 30m, Torsional resistance
UL = 30m, Torsional resistance x 0.5
UL = 30m, Torsional resistance x 1.5

(c)

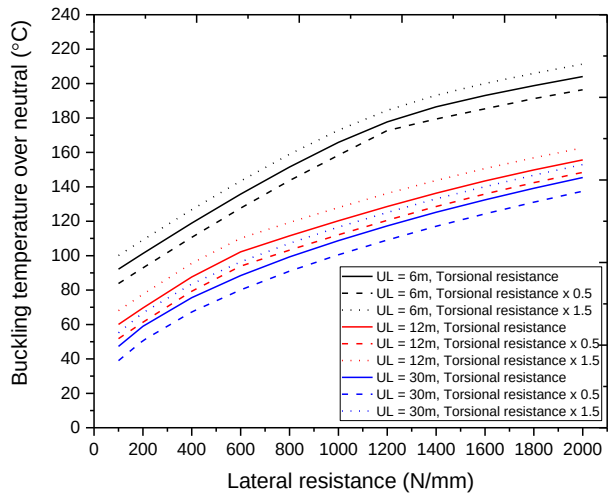

(d)

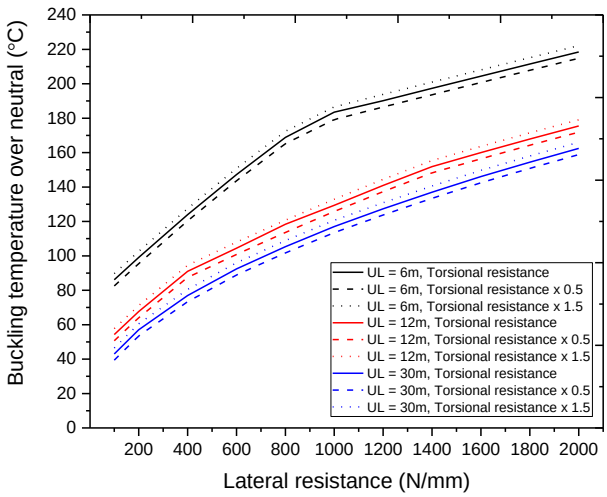

(e)

Figure 4.12 Effects of ballast lateral and fastening torsional resistance of (a) timber sleepered track, (b) 1 in 2 interspersed track, (c) 1 in 3 interspersed track, (d) 1 in 4 interspersed track, and (e) concrete sleepered track.

4.4.3 Buckling temperature reduction

Figure 4.13 presents the differences in the temperature rise above the neutral for the interspersed and concrete tracks to the timber track. It demonstrates the replacement of timber sleepers by concrete sleepers in terms of the temperature differences with the consideration of the lateral resistance. There are significant changes in the buckling temperature when the timber sleepers are replaced by the concrete sleepers. As can be seen, in general, the concrete sleepered track can significantly increase the buckling temperature by 15% maximum. Assuming the similar track conditions with similar lateral resistance of concrete sleeper, concrete sleepered track provides the best results and is followed by 1in2, 1in3, and 1in4 interspersed tracks, respectively. However, when the lateral resistance decreases to the level that ballast could not provide the sufficient confinement, the timber sleepered track may have better buckling strength compared to railway tracks with more concrete sleepers. This is due to the effect of torsional resistance provided by fasteners that play a significant role in this case instead of the lateral resistance provided by sleeper and ballast.

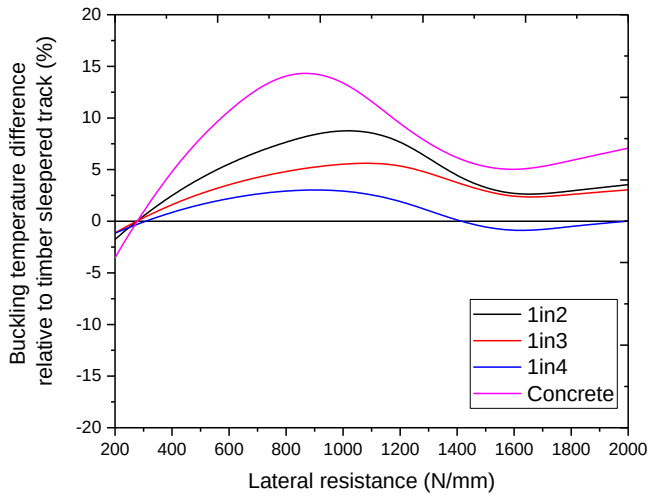
Buckling temperature difference relative to timber sleepered track (%)
Lateral resistance (N/mm)
1in2
1in3
1in4
Concrete

(a)

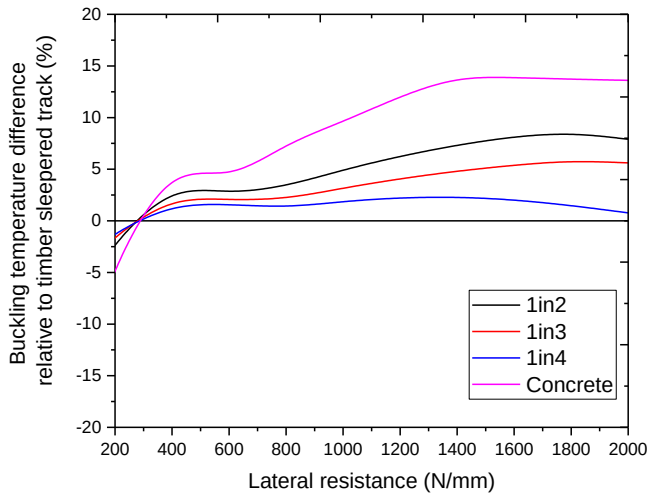
Buckling temperature difference relative to timber sleepered track (%)
Lateral resistance (N/mm)
1in2
1in3
1in4
Concrete

(b)

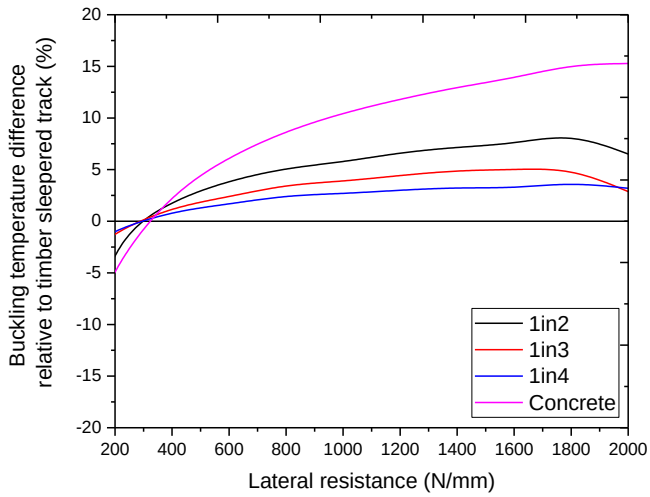

(c)

Figure 4.13 Buckling temperature over neutral difference relative to timber sleepered track: (a) 6-m unconstrained length, (b) 12-m unconstrained length, and (c) 30-m unconstrained length.

4.4.4 Recommendations for interspersed approach

As discussed in the previous section, the buckling temperature derived from different unconstrained lengths can be used to optimise the span number that can potentially be strengthened as a spot replacement. This can also significantly help to minimise the renewal cost of the sleeper at specific spans for increasing the buckling strength instead of increasing the whole track or larger area. From the previous sections that analysed the effects of the unconstrained lengths of 6 m, 12 m, 18 m, 24 m, and 30 m, an unconstrained length of more than 18 m yields a lower buckling temperature of the track than that of 6 m and 12 m. The results can be used as a recommendation for the interspersed approach or spot replacement. This section studies the unconstrained length of 12 m for a railway track for the possible use of the interspersed approach every 12 m instead of the previous types

of interspersed tracks. This track is compared with the tracks that consists of two different boundary conditions: strong and weak areas. A railway track with a weak area or an unconstrained length of 12 m is used for this comparison, as shown in Figure 4.14a. The lateral resistance applied is set as 200 N/mm in the unconstrained length area. The buckling shape is anti-symmetrical, as shown in Figure 4.14b. Note that, for this track, the buckling temperature is evaluated as 67.62°C, as previously presented in Figure 4.11e.

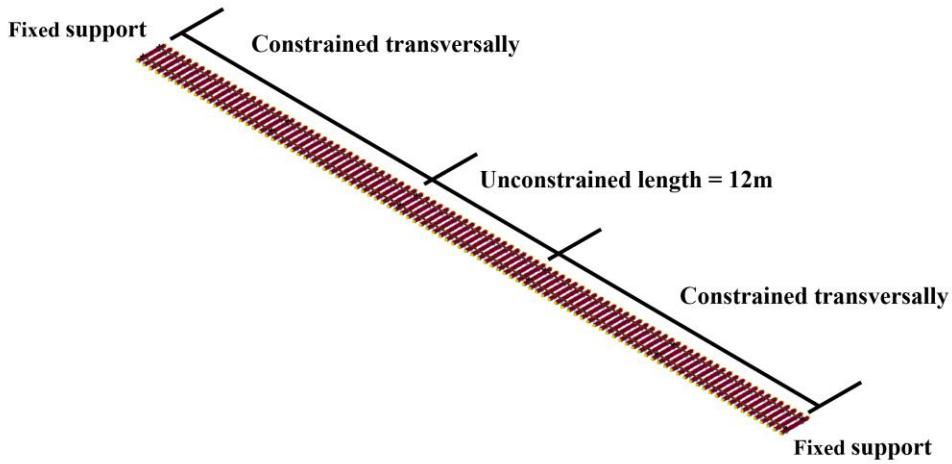

(a)

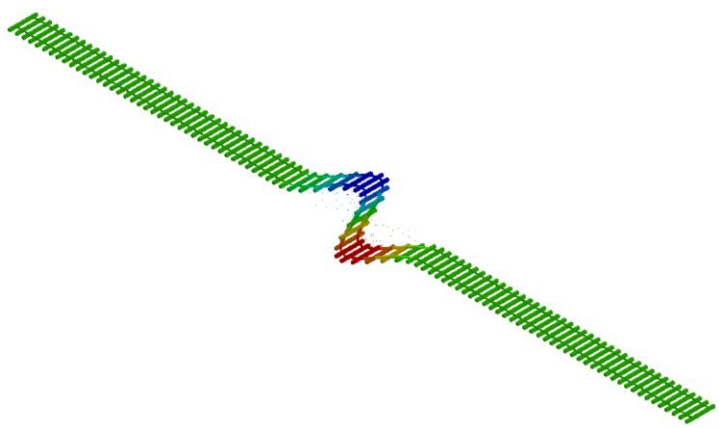

(b)

Figure 4.14 Railway track with concrete sleeper consisting of unconstrained and constrained lengths: (a) boundary condition and (b) buckling shape

The rails at every 20 spans (12 m) are fully restrained in the transverse plane. Note that, in reality, the ageing sleepers at these spans can be replaced by new types of sleepers, such as frictional sleepers, which provide considerably larger lateral resistance than the usual concrete sleepers. The spans at every 20 spans are fully restrained transversally, as shown in Figure 4.15a. It should be noted that the buckling temperature obtained for this case by using the linear analysis is 67.62°C, which is exactly the same as in the previous case. Furthermore, the buckling shape tends to be multiple curves because of the larger unconstrained length overall, as shown in Figure 4.15b. The analysis of unconstrained length can suggest an appropriate spot replacement that can significantly improve the buckling strength.

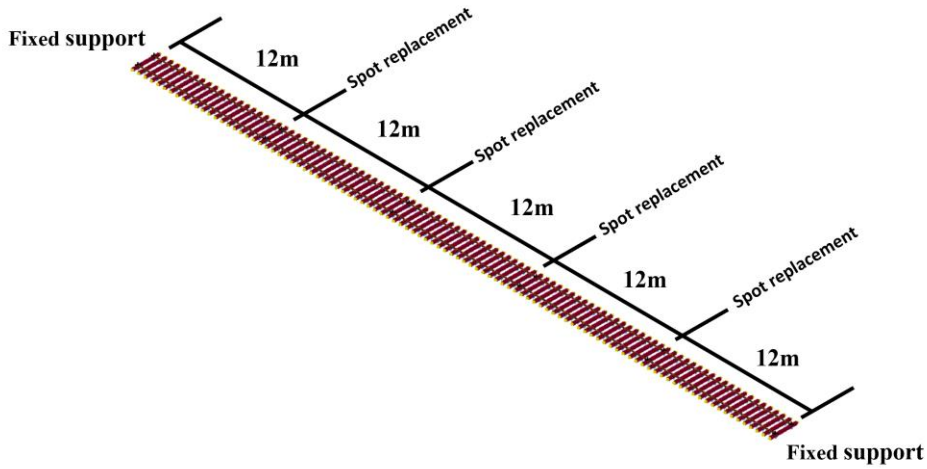

(a)

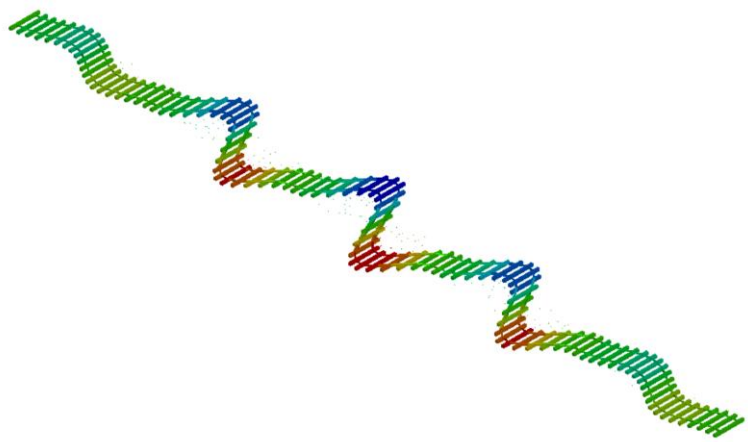

(b)

Figure 4.15 Spot replacement approach every 20 spans: (a) boundary condition and (b) buckling shape.

Strengthening every 12 m or 20 spans can vitally increase the buckling temperature, resulting in reducing the risk of track buckling. Moreover, note that the method used on the basis of the unconstrained length can be represented by the interspersed approach in the case of a replacement with highly restrained elements in the transverse direction.

4.5 Summary

This chapter presents the 3D finite element model of conventional ballasted and interspersed railway tracks developed to investigate the buckling behaviour by using a linear buckling analysis based on eigenvalues and eigenvectors. Note that this method can only provide the buckling temperature, which is predicted at the bifurcation point. In the past, only the buckling behaviour of either a plain timber sleepered track or a concrete sleepered track has been investigated. To the best of my knowledge, this study is the first to propose a buckling analysis of conventional plain railway tracks and interspersed railway tracks that have never been fully studied. Note that an interspersed railway track

has an issue of stiffness inconsistency and material properties that can lead to track degradation, as the uplift behaviour of the track has been normally observed for passing trains. Nonetheless, an interspersed track seems to have a positive effect by preventing track buckling, as the concrete sleeper can increase the lateral resistance, thereby increasing the buckling temperature. The following key findings are revealed from the parametric studies and obtained results in this chapter:

- The ‘1 in 2’ interspersed track provides better buckling strength than the ‘1 in 3’ and ‘1 in 4’ interspersed tracks and the timber track, as more timber sleepers are replaced by concrete sleepers. Besides, plain concrete sleepered railway track provides higher buckling strength than all the other tracks. Hence, the buckling resistance of railway tracks from high to low can be presented in order as plain concrete sleepered track, ‘1 in 2’, ‘1 in 3’, ‘1 in 4’, and plain timber sleepered track.
- The replacement of timber sleepers by concrete sleepers tends to increase the buckling temperature.
- The plain concrete sleepered track can significantly increase the buckling temperature by about 25% in comparison to the plain timber sleepered track.
- The unconstrained length has a significant effect on the track buckling shapes, which causes various defects and misaligns the track.
- It is important to minimise the length of the weaker area (unconstrained length) and keep the tracks restrained laterally, as these can significantly help to increase the buckling temperature.
- The unconstrained length suggests the location of spot replacement that can actually increase buckling temperature. This means that unconstrained length of x m

equalises to interspersing the traditional timber sleepers every x m. For instance, the 12-m unconstrained length equals to the interspersing span every 12m.

- In case of low lateral resistance, the buckling trends can be inversed as the ballast can no longer help mitigate the buckling. The torsional fastening resistance can rather help in this case, and thus, the timber sleepered track has a higher buckling temperature than interspersed tracks.

Note that the current chapter mainly focuses on the parametric studies of conventional and interspersed railway tracks, and the results could be relatively compared with each other. Even though, the results could be slightly overestimated, this approach is best used for a preliminary study and investigating the effects of various parameters. Nevertheless, the replacement approach of sleepers should be performed carefully as this activity probably induces ballast disturbance, resulting in a loose track, which may lead to lesser lateral resistance at the beginning.

The insight into interspersed railway tracks derived from this chapter will underpin the life cycle design, maintenance, and construction strategies related to the use of concrete sleepers as spot replacement sleepers in ageing railway track systems. The outcome of this study will help track engineers to improve the inspection of the lateral stiffness of interspersed tracks in an area prone to extreme temperatures.

Next chapter will analyse the buckling phenomena of conventional plain railway tracks and interspersed railway tracks using nonlinear analysis. To overcome the drawback of linear analysis, geometric and material nonlinearities will be taken into account. Both

buckling and allowable temperature of ballasted railway tracks will be evaluated in the next chapter.

4.6 Reference

CAI, Z. 1994. *Modelling of rail track dynamics and wheel/rail interaction.* PhD Thesis, Queen's University.

CARVALHO, J., DELGADO, J., CALCADA, R. & DELGADO, R. 2013. A new methodology for evaluating the safe temperature in continuous welded rail tracks. *International Journal of Structural Stability and Dynamics,* 13**,** 1350016.

CRC FOR RAIL INNOVATION 2009. Track Stability Management – Literature Review: Theories and Practices Brisbane, Australia: CRC for Rail Innovation

EL-GHAZALY, H. A., SHERBOURNE, A. N. & ARBABI, F. 1991. Strength and stability of railway tracks—II Deterministic, finite element stability analysis. *Computers & structures,* 39**,** 23-45.

ESVELD, C. 2001. *Modern railway track*, MRT-productions Zaltbommel, Netherlands.

KERR, A. D. 1980. An improved analysis for thermal track buckling. *International Journal of Non-Linear Mechanics,* 15**,** 99-114.

KISH, A. 2011. On the fundamentals of track lateral resistance. American Railway Engineering and Maintenance of Way Association, September 18-21, 2011 Minneapolis, MN, USA.

KISH, A. & SAMAVEDAM, G. 2013. Track buckling prevention: theory, safety concepts, and applications. John A. Volpe National Transportation Systems Center (US).

LIVERMORE SOFTWARE TECHNOLOGY COPORATION (LSTC) 2018. *LS-DYNA KEYWORD USER'S MANUAL* LIVERMORE SOFTWARE TECHNOLOGY CORPORATION (LSTC)

NGAMKHANONG, C., WEY, C. M. & KAEWUNRUEN, S. 2020. Buckling Analysis of Interspersed Railway Tracks. *Appl. Sci.,* 10**,** 3091.

PRUD'HOMME, M. A. & JANIN, M. G. 1969. The stability of tracks laid with long welded rails. *RAIL INTERNATIONAL,* 46**,** 459-487.

STRAND7 PTY LTD 2005. Using Strand7—Introduction to the Strand7 finite-element analysis system.

YANG, G. & BRADFORD, M. A. 2016. Thermal-induced buckling and postbuckling analysis of continuous railway tracks. *International Journal of Solids and Structures,* 97**,** 637-649.

CHAPTER 5

NONLINEAR BUCKLING ANALYSIS OF BALLASTED RAILWAY TRACKS

5.1 Introduction

This chapter analyses the buckling temperature of conventional ballasted railway track and interspersed railway tracks using the nonlinear buckling approach. This chapter extends the three-dimensional Finite Element Modelling (FEM), that was developed in Chapter 4, of interspersed railway tracks subjected to temperature change using nonlinear analysis to overcome the limitations of linear analysis. It is important to note that only buckling temperature is captured in linear buckling analysis in which only the pre-buckling stage can be obtained by assuming linear function linking between starting point and buckling point. Moreover, safe temperature, which can be measured in the post-buckling stage, is evaluated in this chapter. Nonlinear analysis can analyse both pre- and post-buckling stages so that the overall response from the beginning to after buckling can be presented. This approach can potentially propose more realistic buckling behaviour of structures due to the increase in temperature as nonlinear properties are taken into consideration. Even though studies on track buckling have been conducted, interspersed tracks and their inconsistency have never been fully analysed using advanced FEM. It is also important to note that, as seen in many studies on lateral resistance of ballasted tracks, the displacement limit of the lateral force-displacement of sleepers obtained by STPTs is usually lower than that used in buckling analysis in previous studies (Samavedam et al., 1993, Carvalho et al., 2013, Cuadrado et al., 2008, Villalba Sanchis et al., 2018). The actual values of the displacement limit for lateral displacement of sleepers are roughly between 1mm and 2mm. This point is usually measured at the yield point where the lateral stiffness drops significantly. It should be noted that previous studies on track buckling mostly use bigger values than these values (Jing and Aela, 2020). This implies that previous studies have slightly overestimated

the buckling temperature of ballasted tracks. More details related to lateral resistance are presented in Chapter 3. In this chapter, various parameters including torsional resistance, lateral resistance, and initial misalignment are considered based on the actual values obtained from previous experimental results for buckling analysis. Both buckling temperature and safe temperature are analysed in this chapter. The insights will help track engineers to improve track buckling mitigation methods for conventional ballasted and interspersed railway tracks.

5.2 Finite Element Modelling (FEM)

The modelling constructed in Chapter 4 is adopted in this chapter in LS-DYNA (Livermore Software Technology Coporation (LSTC), 2018). Steel rails UIC60 and sleepers are modelled as beam elements, which take into account shear and flexural deformations (Cai, 1994). Rails and sleepers are constructed using SECTION_BEAM and MAT_ELASTIC. The MAT_ADD_THERMAL_EXPANSION property is assigned to the steel rails. The rail pads and fasteners are modelled as a series of spring elements using SECTION_DISCRETE and SPRING_ELASTIC in the connections between sleepers and rails. At rail seat, rail pad and fastener, three translational springs to represent pad stiffness in three directions and one rotational spring to represent the fastener resistance, are applied. For ballast, the tensionless support spring should be considered and connected to both sleeper ends instead of the normal spring since it allows the beam to lift and move over the support while the tensile support is neglected (Ngamkhanong et al., 2020). This presents realistic behaviour of the ballast. The properties and dimensions of conventional railway tracks are previously presented in Table 4.1. It should be noted that the model has been

validated already as shown in Chapter 4. However, in the linear analysis, the nonlinear user-defined spring property is disabled. Hence, SPRING_ELASTIC is used in linear analysis while various keywords or methods in LS-DYNA can be used for nonlinear spring in nonlinear analysis e.g. SPRING_ELASTOPLASTIC, SPRING_INELASTIC. As for lateral spring, it is important to note that the stiffness value in the system is doubled when the sleeper is moved. However, the results presented are based on the actual stiffness which are derived by the input value divided by two. Figure 5.1 presents the relationship between the sleeper and ballast contact models represented by beam and spring elements. When the sleeper is moved laterally, one spring is compressed while another is tensioned. In this case, the summation of lateral stiffness is equal to 2k which means that the springs are in series. This is equivalent to Figure 4.1c where the linear elastic spring with 2k stiffness is connected at one end. In fact, the nonlinear tensionless springs with 2k stiffness should be connected instead to represent the actual ballast behaviour in lateral plane, as presented in Figure 5.1.

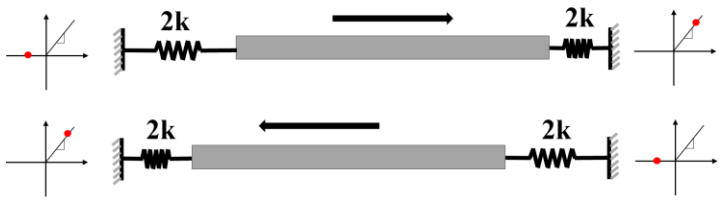

Figure 5.1 Nonlinear tensionless spring with stiffness 2k at both ends.

In this chapter. the model of 60m long railway track is similarly constructed as that in Chapter 4 as shown in Figure 5.2 while the properties of springs are nonlinear. It is important that the initial lateral alignment of track is not straight as that in Chapter 4 since the curvature is applied in the middle of the track to trigger the lateral force in rails.

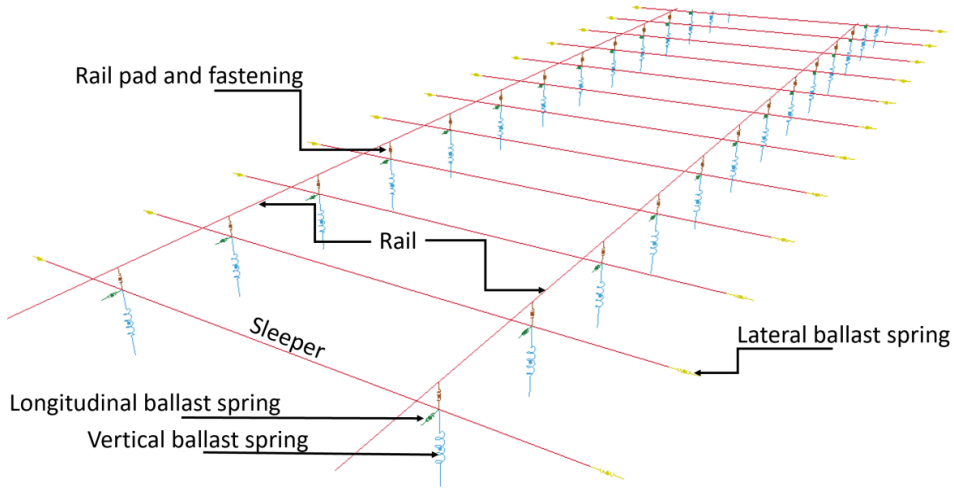

Figure 5.2 Ballasted railway track modelling.

5.2.1 Boundary conditions

The boundary conditions of track models are set in the same way as those in Chapter 4. They consist of two main regions in buckled track: buckled regions (positive and negative lateral displacements) and adjoining regions. Due to the increasing temperature, the large lateral displacement of rails occurs in a transverse direction if the tracks have imperfections, which can trigger the lateral force in steel rails, leading to buckled track in the buckled region. The rails are deformed longitudinally in the adjoining region. It is noted that the buckling shapes of a track is often symmetrical or anti-symmetrical as already evidenced in Chapter 4. Buckling shape and buckling length in actual track can be shifted within the same track profile and properties due to different track conditions. It is important to note that a buckled region is normally in the weaker zone of a track which can be separated from the stronger zone by applying different element constraints. The boundary conditions of track models are presented in Figure 5.3. The fully fixed supports are applied to the end nodes of the rails. The roller supports are applied longitudinally on the rails to

generate a stiff track area representing adjoining regions so that the rails are constrained and not allowed to move transversally. In LS-DYNA, nodes are constrained using BOUNDARY_SPC_SET keyword. Hence, the unconstrained length is presented as a weaker track and thus the buckled region is expected to be found in this area. In this study, the track was originally made to be 60 m in length with buckled regions of 30m as track buckling length is always roughly from a very short to 30m (Pucillo, 2019). In Chapter 4, it was shown that the critical buckling temperature also largely depends on unconstrained length which is directly relied to the boundary conditions. The results obviously illustrated that the critical buckling temperature is not affected by the effects of unconstrained length when it is longer than 30 m. Thus, the unconstrained length of 30m is a control case and chosen for nonlinear analysis. It is important to note that, in nonlinear buckling analysis, imperfection or misalignment must be applied as an initial condition since the structures cannot be buckled theoretically without imperfection. The initial misalignment amplitude of 8-32 mm is applied to both rails at the nodes of the centre span of the full railway tracks as shown in Figure 5.3. It is noted that, in reality, the allowable misalignment can be allowed up to over 30mm depending on class of track (CRC for Rail Innovation, 2009, Federal Railroad Administration (FRA), 2010).

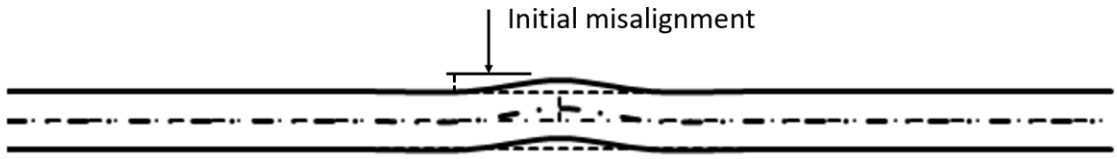

Figure 5.3 Initial misalignment.

5.3 Nonlinear Buckling Analysis

In nonlinear buckling analysis, the solution method uses the nonlinear approach with BFGS quasi newton algorithm in LS-DYNA. This iterative method is used to solve unconstrained nonlinear optimisation problems (Hallquist, 2006). This approach is more accurate than linear analysis since it can include the geometric and material nonlinearities and analyse both pre- and post-buckling of a structure. Note that, geometric nonlinearity arises when changes in geometry, large or small, have a significant effect on the load deflection characteristics of the structure. However, it has been known that structures without imperfections theoretically cannot be buckled. It should be noted that perfectly straight tracks always remain straight even when they are exposed to the buckling temperature. Hence, the initial track imperfection needs to be applied to trigger the initial lateral follower force in the rails. It should also be noted that initial misalignments are usually seen in the field because of the incorrect stress adjustment, loss of track geometry, and loss of lateral resistance (De Rosa et al., 2019).

It is noted that, based on previous STPTs on ballast lateral resistance, the load-displacement curves are likely to be bi-linear. Thus, the elastoplastic curve is used as the lateral resistance curve applied to the lateral springs connected to the sleeper ends to create the lateral resistance of the track. The elastoplastic curve of tensionless spring is presented in Figure 5.4 where F_p represents the lateral force limit and W_p represents the displacement limit. The keyword used in LS-DYNA is MAT_SPRING_INELASTIC with the consideration of tension only. This study presents two cases (1mm and 2mm) of yielding displacement of

ballast. The lateral resistance is presented by the initial stiffness which is the peak lateral force over displacement limit.

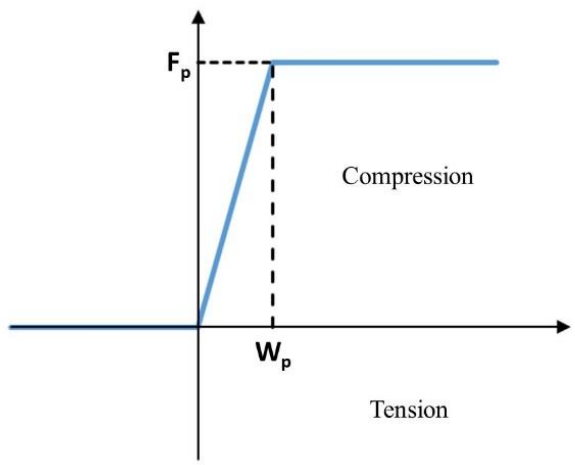

Figure 5.4 Elastoplastic model for ballast tensionless spring.

To create the temperature load curve, the curve is first made in the keyword DEFINE_CURVE in LS-DYNA as shown in Figure 5.5. After that, this load-curve is assigned in the keyword LOAD_THERMAL_LOAD_CURVE to apply the temperature to the system. It is noted that the system is heated up to 200°C.

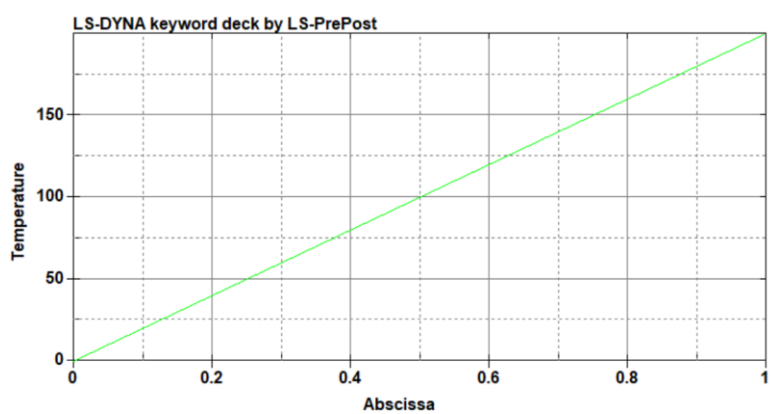

Figure 5.5 Thermal load defined in LS-DYNA.

5.4 Buckling Path

Generally, if rail temperature is higher than the neutral temperature or stress-free temperature, the compression axial force in the rails builds up. The rail can be buckled when the compression force reaches its limit or buckling resistance. It should be noted that buckling resistance is affected by track type, element type, and track conditions. The relationship between rail temperature over lateral displacement is typically plotted as seen in Figure 3.6. It can be seen that there are two types of buckling failure modes: sudden buckling and progressive buckling. In the pre-buckling stage, the rails are exposed to a higher temperature than the neutral temperature and the axial force is linearly increased. As for the sudden buckling mode (also called "Snap-through"), the track buckles explosively with no external energy after reaching its maximum temperature (upper critical temperature, T_{Bmax}) and becomes unstable in its post-buckling stages. T_{Bmin} represents the lower bound which can buckle the track if sufficient energy is supplied. It can also be defined as a safe temperature since the track cannot buckle if it experiences a temperature below this temperature. Moreover, progressive buckling can occur when the T_{Bmin} cannot be differentiated from T_{Bmax} as the peak cannot be clearly seen. In this case, track lateral displacement is gradually increased after buckling and the critical temperature is defined as T_P.

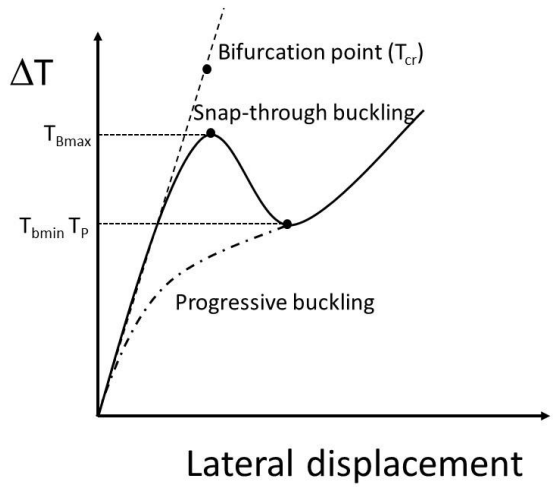

Figure 5.6 Buckling path.

5.4.1 Safe temperature evaluation

5.4.1.1 Direct method for safe temperature evaluation

Safe temperature can be evaluated directly from the minimum point of the relationship between the rise in temperature and lateral displacement of rail after buckling as can be seen in Figure 3.6 for snap-through buckling curve. It is important to note that, in nonlinear analysis, some numerical solvers do not allow negative load increment. These methods include the Newton Raphson method (also known as the nonlinear stabilisation or load control method). This results in difficulties in analysing safe temperature in buckling analysis. Hence, displacement control methods are used to determine the safe temperature, using the nonlinear arc-length method. However, the arc-length method is not suitable for temperature load due to the serious convergence problem, which has been discussed previously in relation to thermal loading in any structures (Junior et al., 2006). It is noted that the arc-length method in the ANSYS software family is not able to obtain convergence and trace negative load increment in the post-buckling path for thermal loading (Carvalho

et al., 2013). Previous studies have suggested that the combination of load control and displacement control methods using the branch-switching technique can overcome the problem (Junior et al., 2006, Yang et al., 2008).

5.4.1.2 Indirect method for safe temperature evaluation

The indirect method can be used when the safe temperature cannot be evaluated directly from the temperature rise above neutral and rail lateral displacement curve. This is because of the limitations of the many solver algorithms that cannot obtain the negative slope of the structural responses due to thermal loading. It is noted that temperature responses in the post buckling stage, which lead to snap-through buckling failure (Figure 3.6), cannot be fully obtained with negative slope by some numerical algorithm. This leads to being unable to directly evaluate safe temperature. Nonetheless, there are two methods that can alternatively evaluate the safe temperature for buckling analysis in case of snap-through buckling failure.

5.4.1.2.1 Progressive buckling failure curves

Cavallo et al. (2013) proposed the indirect method to evaluate the safe temperature of the idealised beam element. It was suggested that the safe temperature can be estimated from the intersection of various progressive buckling curves of railway tracks with similar F_p but different W_p of the lateral spring model. It was found that beam models with different W_p can fail in either snap-through or progressive buckling. This depends on the W_p where beams with larger W_p are likely to buckle in progressive failure mode while snap-through buckling occurs with small W_p. Larger W_p means lower lateral stiffness. The intersection

point of the buckling path of those beam models with different W_p values represents the safe temperature of the corresponding beam model with smaller W_p but similar F_p.

This study adopts the indirect method to evaluate the safe temperature of idealised track model for full railway track modelling. To ensure that this method can be used properly, ballasted railway tracks with concrete sleepers are first proposed with a lateral resistance force limit of 2000kN. The displacement limit of lateral resistance is varied from 1mm to 90mm. It should be noted that the higher W_p should be taken in order to obtain the progressive buckling failure mode. Various elastoplastic curve models for lateral springs are presented in Figure 5.7. The temperature rise above neutral against rail lateral displacement is obtained as shown in Figure 5.8.

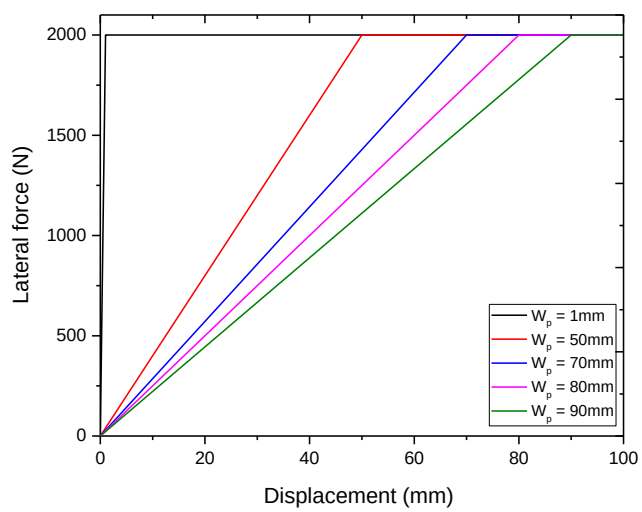

Figure 5.7 Elastoplastic model for lateral ballast spring.

This study shows that a safe temperature can be obtained from the intersection of the progressive buckling curves. The buckling temperature of railway track with lateral spring properties of 2000 N F_p and 1mm W_p, which is buckled in snap-through mode, is about

80°C. The safe temperature of this track model is estimated from the intersection point of the progressive failure curves which can be seen in Figure 5.8. It is observed that the safe temperature, where the intersection point occurs, is around 34°C. From this, it can be concluded that, as for track with F_p of 2000N and W_p of 1mm, snap-through buckling occurs between 34°C and 79°C. However, as for track with higher W_p, buckling occurs progressively. It is interesting to note that this crossing point represents the buckling temperature for progressive buckling mode of tracks with W_p of 50-90 mm. It is noted that previous studies have not clearly mentioned the calculation of buckling temperature for progressive buckling failure.

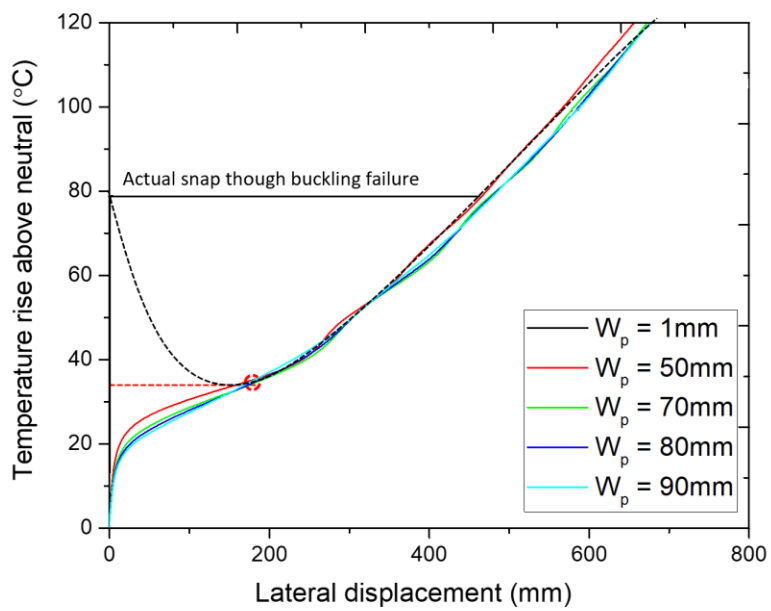

Figure 5.8 Safe temperature evaluation using indirect method from progressive buckling curves.

5.4.1.2.2 Rail axial compression force

Safe temperature or minimum temperature can be calculated indirectly from the rail axial compression force against rail temperature rise above neutral. This method provides a faster and more convenient method than the first indirect method as there is no need to analyse the buckling path of multiple curves in order to find the intersection point.

It should be noted that, rail axial force drops immediately after buckling and track enters the post-buckling stage as presented in Figure 5.9a. In post-buckling stages, there is a lateral excitation in the beginning and then track becomes stable showing the progressive reduction trend of axial force. When projecting a trend line of axial force in post-buckling toward the pre-buckling stage, the line intersects the axial force in the pre-buckling stage. The intersection point represents the minimum axial force that can buckle the track. The projection of this point to the x axis represents the minimum temperature over neutral or safe temperature. However, as for progressive buckling failure (Figure 5.9b), axial force does not drop simultaneously but progressively. It is noted that there is no clear intersection point between the trend line of the axial force in the post buckling stage and the axial force in pre-buckling stage, however, it is likely to intersect at the maximum axial force. Thus, it is clear that the maximum temperature is equal to the minimum temperature for progressive buckling. This shows that the buckling temperature for progressive buckling failure can be measured from the point where maximum axial force occurs. It is noted that this cannot be measured directly from the temperature-lateral displacement curve mentioned in the previous method.

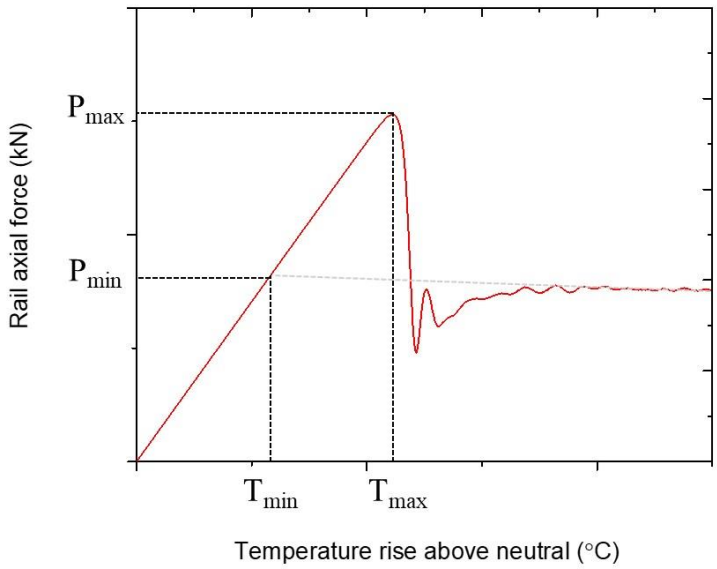

(a)

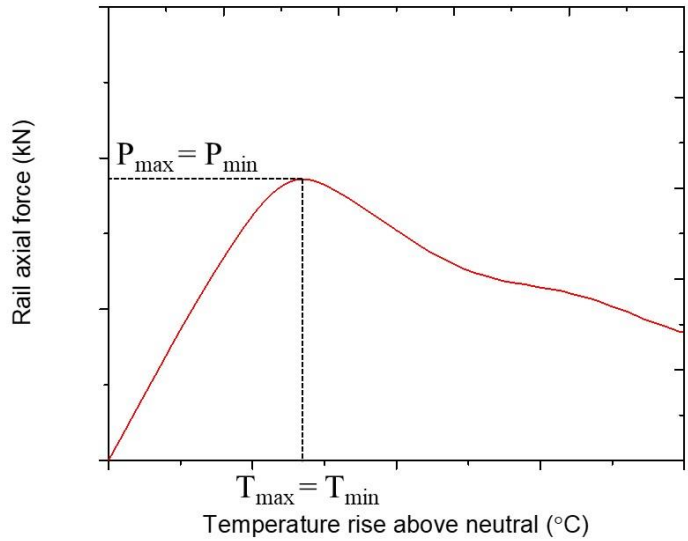

(b)

Figure 5.9 Rail axial force against temperature rise above neutral: (a) snap-through buckling and (b) progressive buckling.

To calculate the safe temperature of track models that have been presented in the first indirect method, the axial compression force is measured in the time history analysis in

LS-DYNA in which the time is directly proportional to the rail temperature. From Figure 5.10, it can be seen clearly that, after buckling, the axial force drops and tends to maintain a similar trend. The trend line can be drawn and it is found that the axial force trends are all obvious in the same trend line. Moreover, it is recommended to obtain the relationship between rail axial force and temperature rise as it can detect the maximum axial force that clearly separate the pre- and post-buckling stages even if buckling occurs progressively. This method can potentially calculate the buckling temperature for both types of buckling failures. Moreover, there is no need to run multiple simulations to obtain the safe temperature as the safe temperature can be directly obtained from the axial force-temperature rise curve.

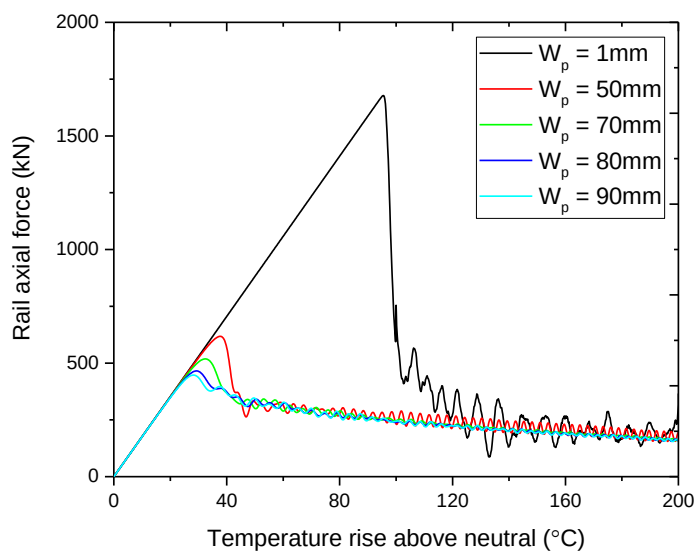

Figure 5.10 Safe temperature evaluation using rail axial force-temperature rise curves.

5.5 Results and Discussions

5.5.1 Buckling shape

In this study, the measured node is located at mid span to represent track lateral displacement while the beam that is connected to this node is considered for axial force evaluation. The locations and members of measured elements are presented in Figure 5.11.

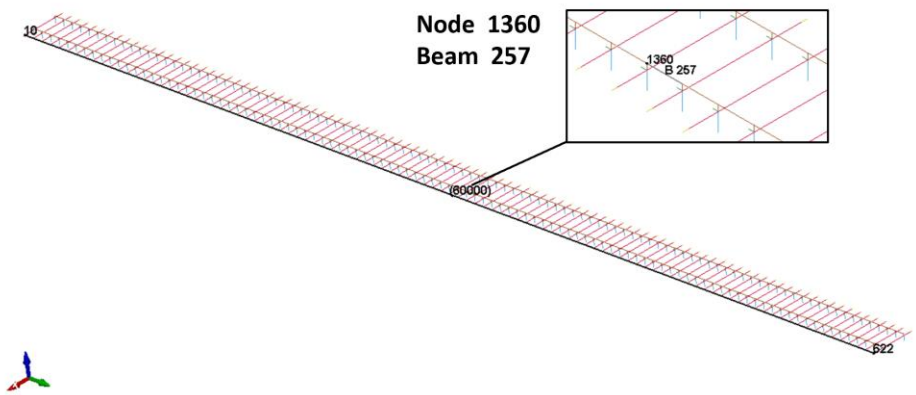

Figure 5.11 Measured elements.

The lateral displacement of mid-span node is measured while the whole track is heated up to 200°C. To study the physical behaviour in both pre- and post-buckling stages, railway tracks with pure timber sleepers between 200N/mm and 2000N/mm lateral resistances are considered in terms of the effects on lateral movement of railway tracks. Moreover, the effects of misalignment amplitudes are also compared to study the buckling behaviour. The temperature rise over neutral against lateral displacement curves is presented in Figure 5.12 considering lateral resistance and initial misalignments. Generally, it is found that tracks with lower misalignments are buckled with higher temperature and axial force, inducing excitation in the post-buckling stage until tracks become stable.

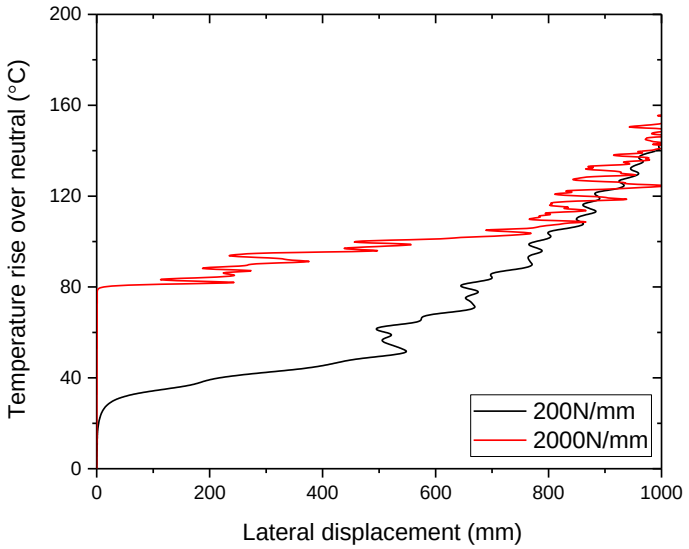

(a)

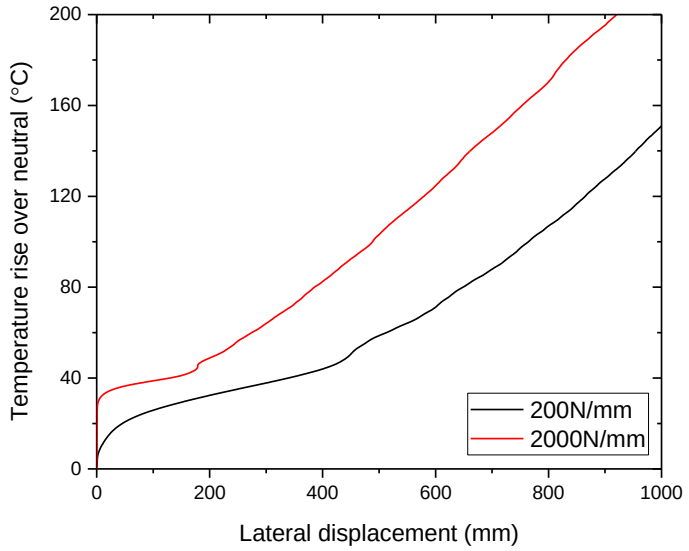

(b)

Figure 5.12 Lateral displacement of railway tracks due to temperature rise: (a) 8mm misalignment and (b) 32mm misalignment.

The lateral displacement of tracks at different temperature levels of 4 different track conditions are presented in Figures 5.13-5.16. It is noted that the displacement is scaled up to 5 for a better visualization and clarification. In Figure 5.13, it is observed that the lateral displacement of track with 200N/mm lateral resistance and 8mm misalignment is progressively increased even though there is an excitation in post-buckling stage as observed in Figure 5.12a, however, the overall trend is still progressive. When the lateral resistance is large (2000N/mm), the buckling shape can be varied according to different temperature levels. Track displacement trend becomes stable when the track is heated up to 150°C. It is noted that once the track becomes stable in post-buckling stage, the buckling shape is likely to be similar which directly follow the misalignment shape. Moreover, as for the misalignment of 32mm (Figures 5.15-5.16), the buckling shapes tend to be progressive as the lateral displacement is progressively increased with no change of direction. It is found that the buckling shapes are relevant to Figure 5.12b in that the lateral displacement increases smoothly with no excitation as in tracks with 8mm misalignment. Figures 5.15-5.16 are found to have a similar trend. This implies that the buckling shape of tracks with progressive buckling failure tends to follow the misalignment shape for all temperatures. Meanwhile, tracks with snap-through buckling failure can be buckled in different shapes depending on the temperature exposed to the tracks.

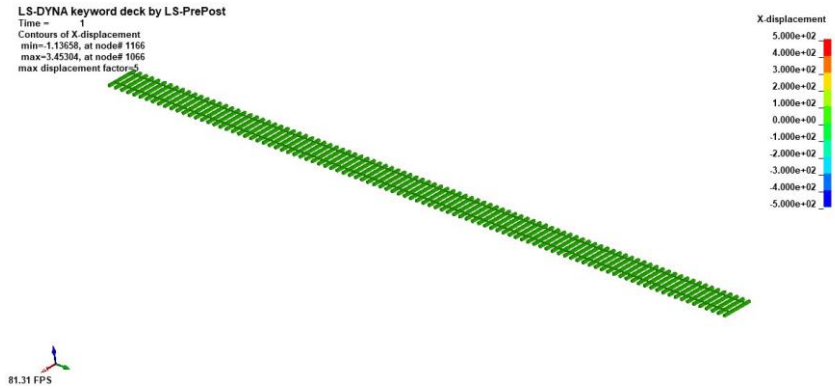
LS-DYNA keyword deck by LS-PrePost
Time = 1
Contours of X-displacement
min=-1.13658, at node# 1166
max=3.45304, at node# 1066
max displacement factor=5
X-displacement
5.000e+02
4.000e+02
3.000e+02
2.000e+02
1.000e+02
0.000e+00
-1.000e+02
-2.000e+02
-3.000e+02
-4.000e+02
-5.000e+02
81.31 FPS

(a)

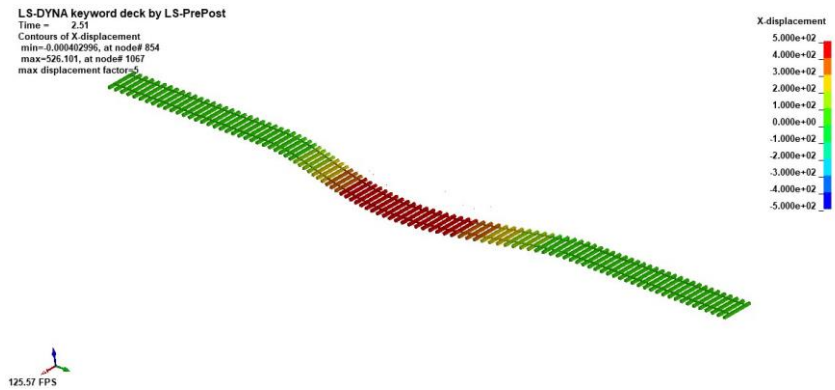
LS-DYNA keyword deck by LS-PrePost
Time = 2.51
Contours of X-displacement
min=-0.000402996, at node# 854
max=526.101, at node# 1067
max displacement factor=5
X-displacement
5.000e+02
4.000e+02
3.000e+02
2.000e+02
1.000e+02
0.000e+00
-1.000e+02
-2.000e+02
-3.000e+02
-4.000e+02
-5.000e+02
125.57 FPS

(b)

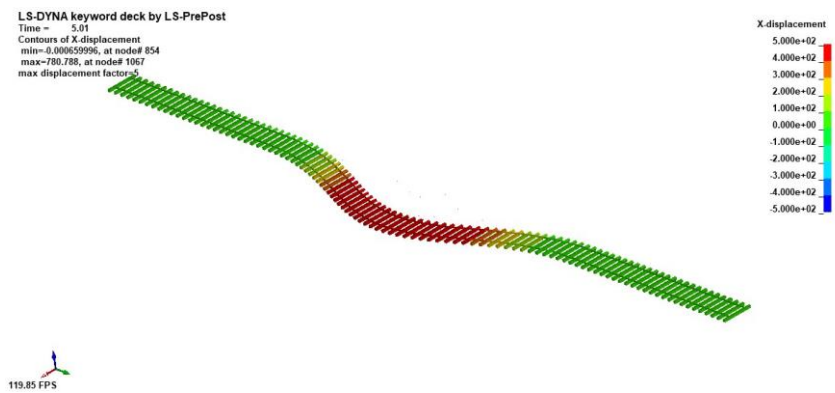
LS-DYNA keyword deck by LS-PrePost
Time = 5.01
Contours of X-displacement
min=-0.000659996, at node# 854
max=780.788, at node# 1067
max displacement factor=5
X-displacement
5.000e+02
4.000e+02
3.000e+02
2.000e+02
1.000e+02
0.000e+00
-1.000e+02
-2.000e+02
-3.000e+02
-4.000e+02
-5.000e+02
119.85 FPS

(c)

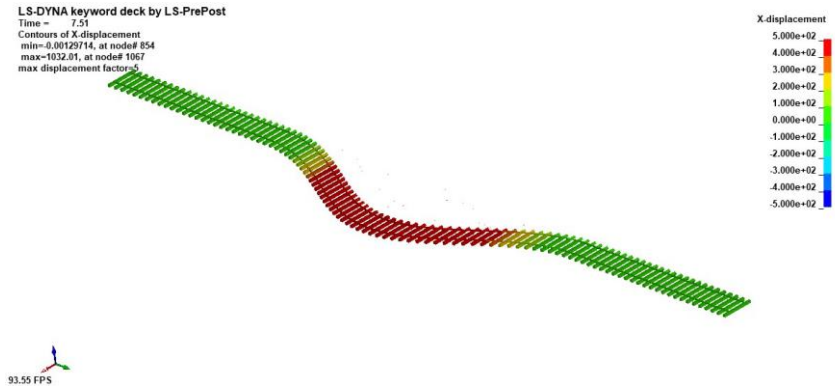

(d)

Figure 5.13 Buckling of timber sleepered track (Misalignment = 8mm, Lateral resistance = 200N/mm, W_p = 1mm) exposed to: (a) 20°C, (b) 50°C, (c) 100°C, and (d) 150°C.

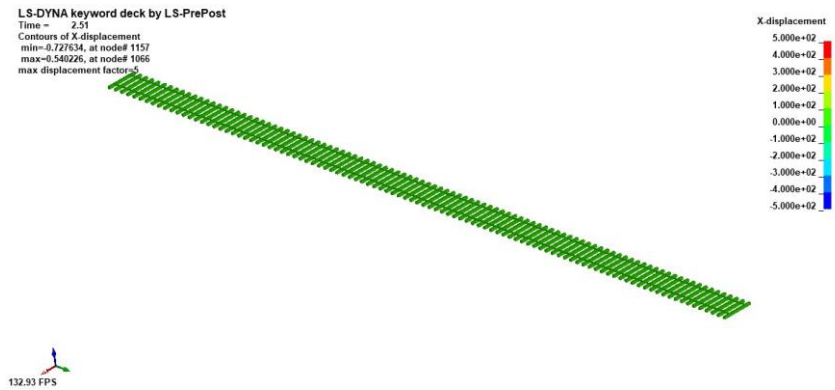

(a)

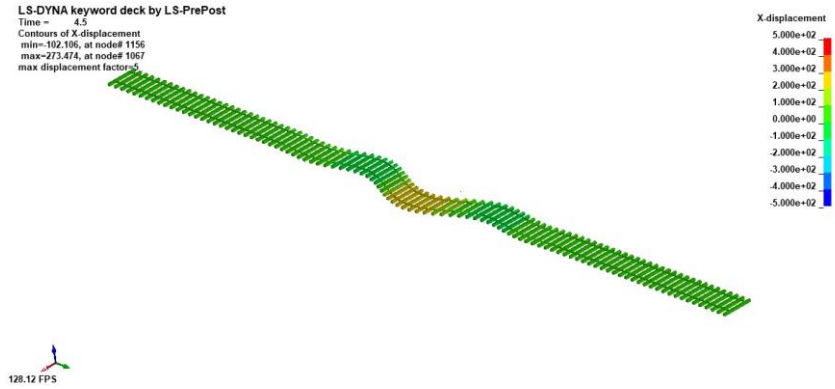

(b)

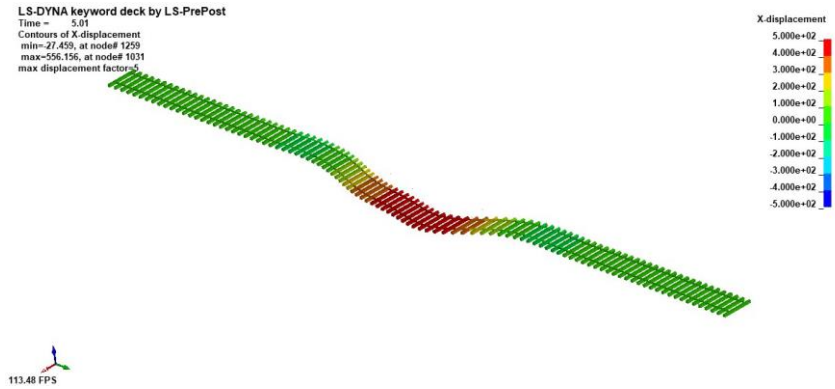

(c)

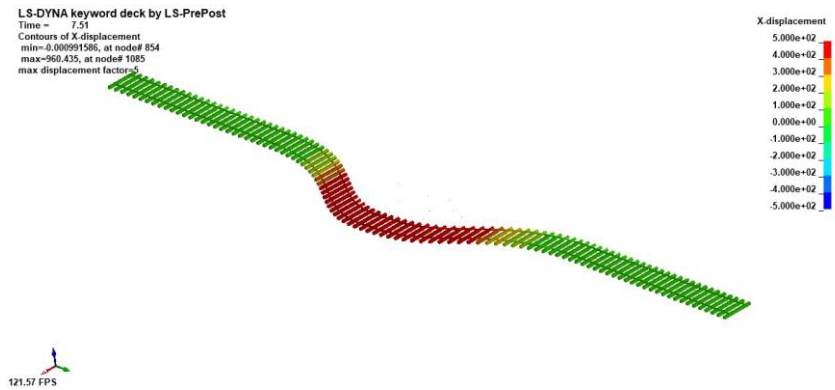

(d)

Figure 5.14 Buckling of timber sleepered track (Misalignment = 8mm, Lateral resistance = 2000N/mm, W_p = 1mm) exposed to: (a) 50°C, (b) 90°C, (c) 100°C, and (d) 150°C.

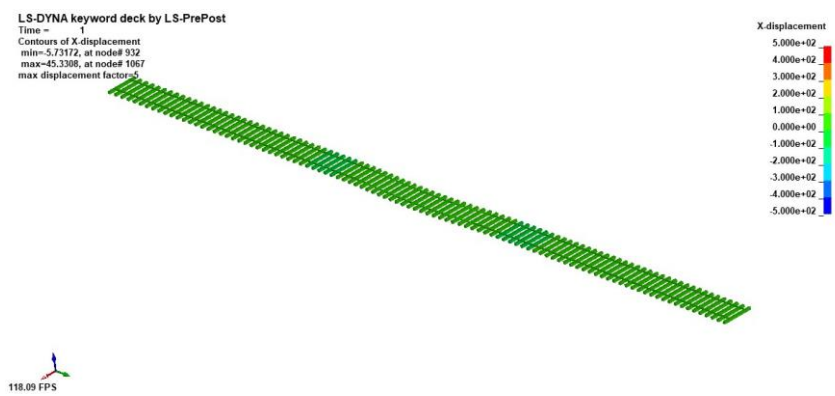

(a)

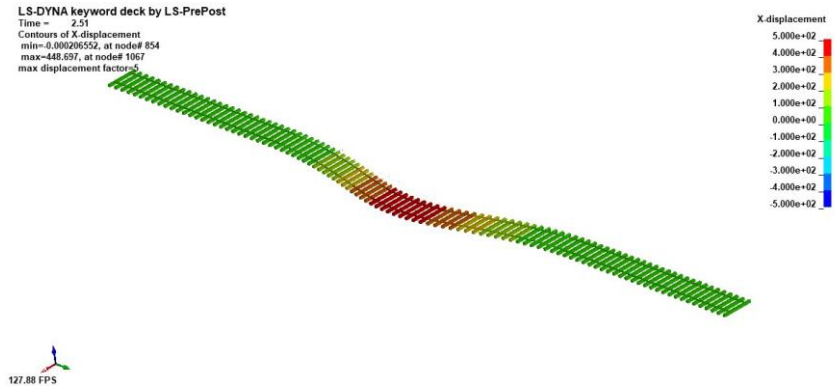

(b)

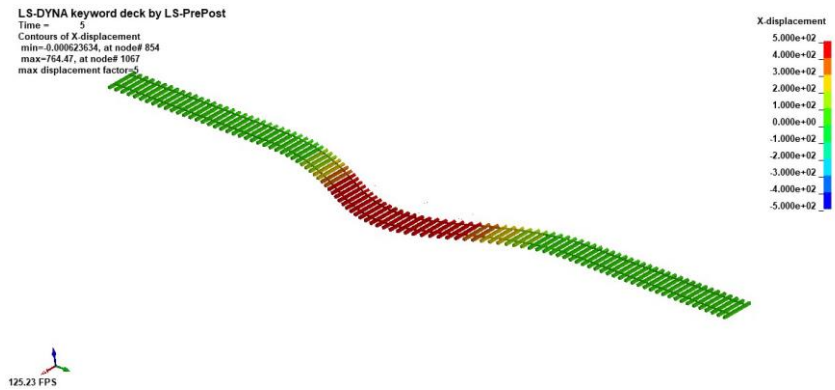

(c)

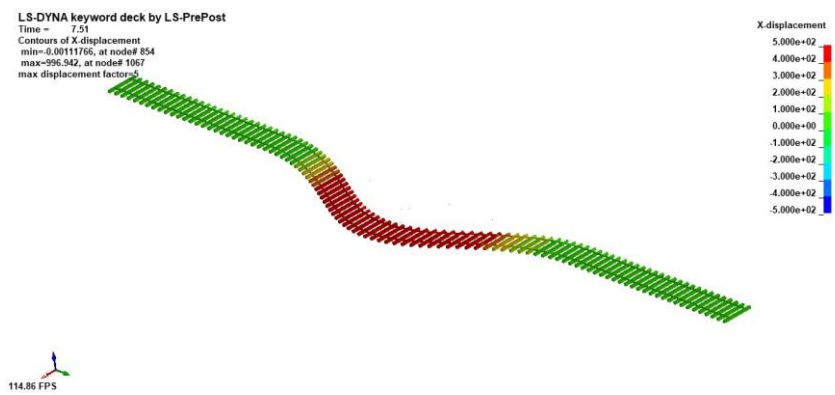

(d)

Figure 5.15 Buckling of timber sleepered track (Misalignment = 32mm, Lateral resistance = 200N/mm, W_p = 1mm) exposed to: (a) 20°C, (b) 50°C, (c) 100°C, and (d) 150°C.

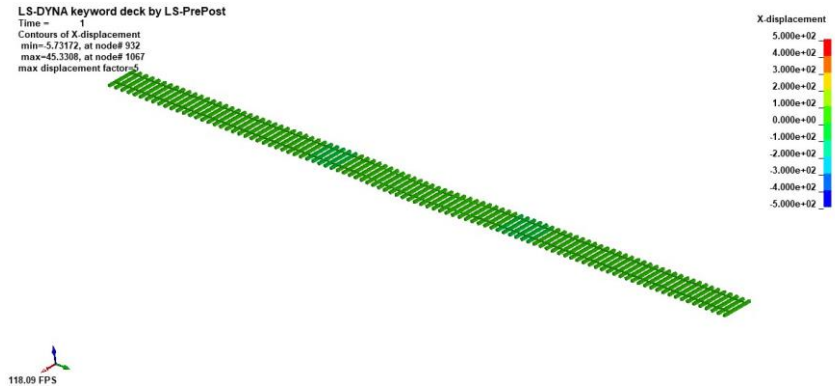
LS-DYNA keyword deck by LS-PrePost
Time = 1
Contours of X-displacement
min=-5.73172, at node# 932
max=45.3308, at node# 1067
max displacement factor=5
X-displacement
5.000e+02
4.000e+02
3.000e+02
2.000e+02
1.000e+02
0.000e+00
-1.000e+02
-2.000e+02
-3.000e+02
-4.000e+02
-5.000e+02
118.09 FPS

(a)

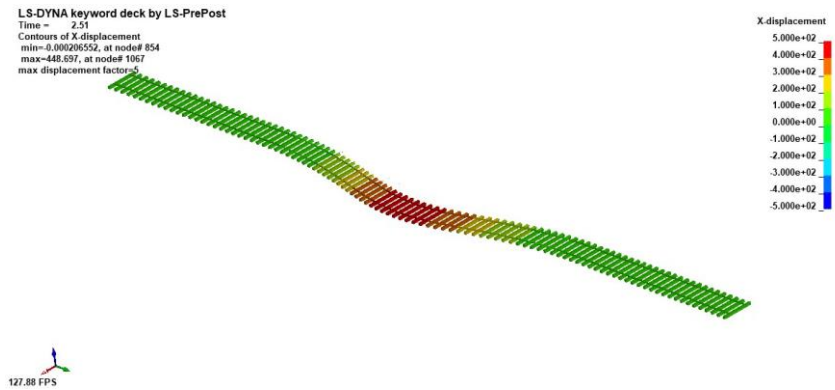
LS-DYNA keyword deck by LS-PrePost
Time = 2.51
Contours of X-displacement
min=-0.000206552, at node# 854
max=448.697, at node# 1067
max displacement factor=5
X-displacement
5.000e+02
4.000e+02
3.000e+02
2.000e+02
1.000e+02
0.000e+00
-1.000e+02
-2.000e+02
-3.000e+02
-4.000e+02
-5.000e+02
127.88 FPS

(b)

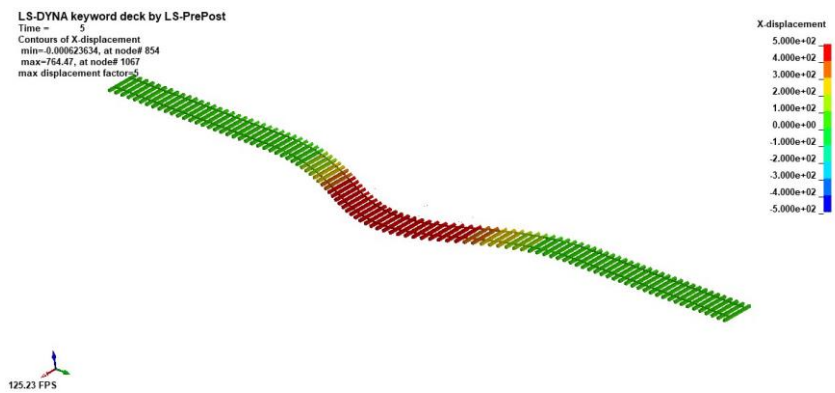
LS-DYNA keyword deck by LS-PrePost
Time = 5
Contours of X-displacement
min=-0.000623634, at node# 854
max=764.47, at node# 1067
max displacement factor=5
X-displacement
5.000e+02
4.000e+02
3.000e+02
2.000e+02
1.000e+02
0.000e+00
-1.000e+02
-2.000e+02
-3.000e+02
-4.000e+02
-5.000e+02
125.23 FPS

(c)

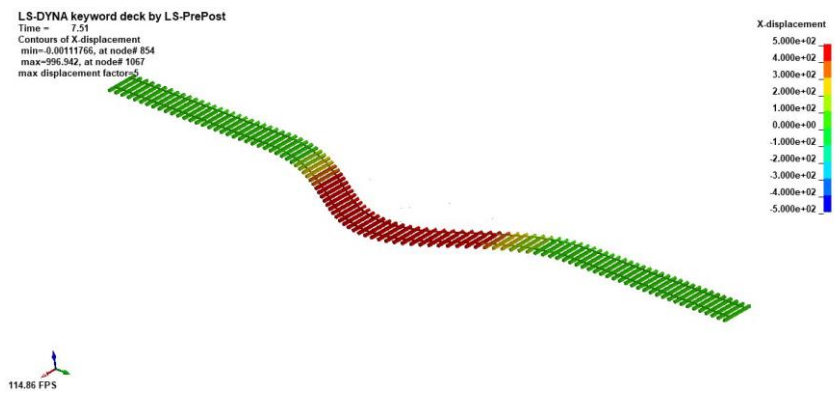

d)

Figure 5.16 Buckling of timber sleepered track (Misalignment = 32mm, Lateral resistance = 2000N/mm, W_p = 1mm) exposed to: (a) 20°C, (b) 50°C, (c) 100°C, and (d) 150°C.

5.5.2 Rail axial force

This study analyses the rail axial force induced by the change in rail temperature. To understand the physical behaviour of railway track buckling, the buckling failure mode should be investigated together with rail axial force that can be seen from the relationship between rail axial force and temperature rise above neutral. Figures 5.17-5.18 present the rail axial force of timber and concrete sleepered tracks exposed to a temperature rise above neutral. The cases presented are when the lateral resistance has 1mm displacement limit with the consideration of the initial misalignments of 8mm and 32mm.

The rail axial force-temperature relationships are presented in Figures 5.17-5.18. During the first stage or pre-buckling, the track is stable and has a very small lateral displacement due to the lateral restraint. The axial force increases due to the thermal expansion. The buckling temperature is measured when the axial compression reaches the buckling resistance as can be seen at the maximum temperature. The critical buckling force represents the maximum compressive axial force that the railway track can sustain due to

an increase in rail temperature. After this point, it is important to note that railway tracks undergo a large lateral deformation accompanied by axial contraction. The reduction in axial load is observed after reaching the buckling temperature. However, in the post buckling stage, the reduction in axial load can occur in different scenarios depending on track conditions. It is interesting that the axial force can be reduced progressively after buckling. This behaviour is likely to be observed in railway tracks with weaker lateral resistance such as timber sleepered tracks and is observed especially when the misalignment is large. This represents the progressive buckling failure. In addition, the sudden reduction of rail axial force can be observed in stronger tracks. After that, the rails constantly undergo further lateral displacement. Therefore, railway tracks are generally buckled in the snap-through phenomenon. Even though track with higher lateral stiffness can effectively prevent track buckling and prolong track stability under temperature increases, tracks that are buckled by large axial force tend to have larger self-excitation after buckling. It is important to note that progressive buckling should be avoided.

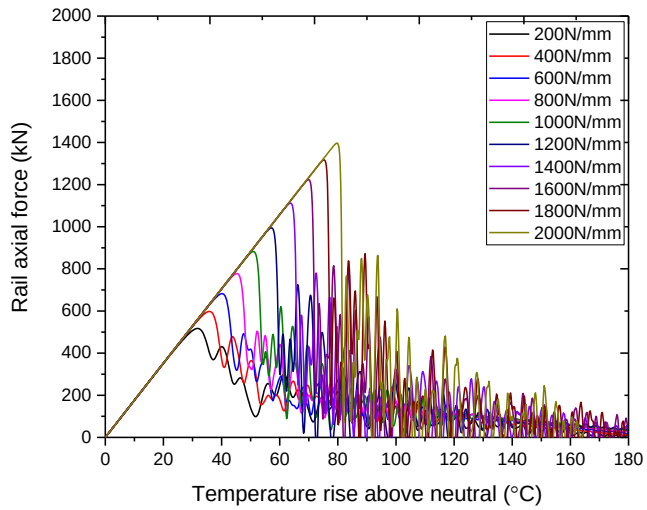

(a)

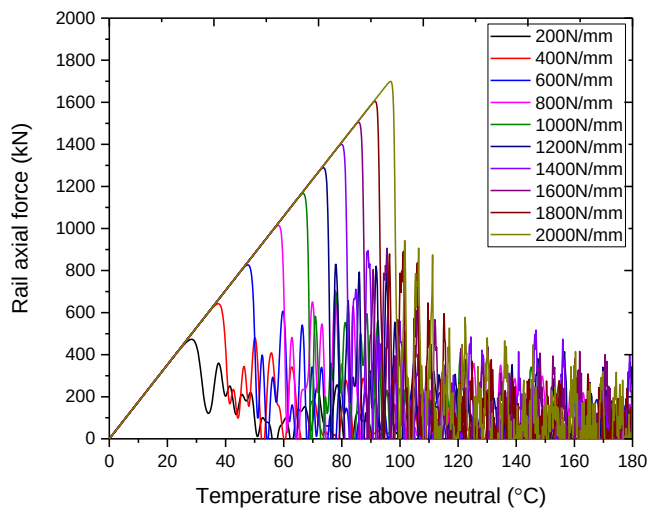

(b)

Figure 5.17 Axial force-temperature relationship of railway tracks with 8mmmisalignment: (a) timber sleepered tracks and (b) concrete sleepered tracks.

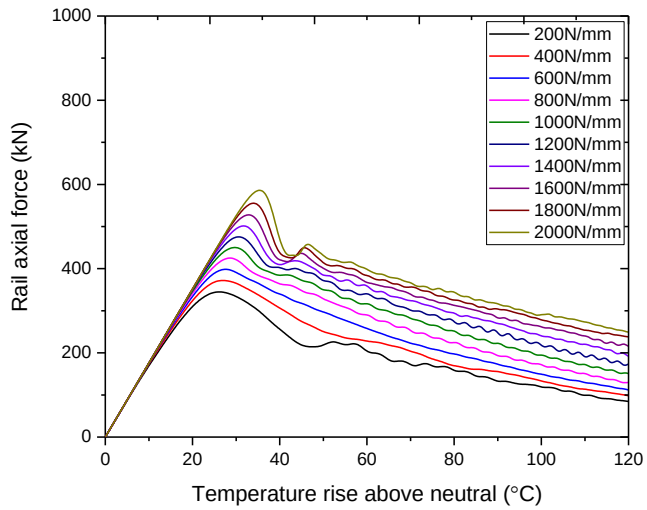

(a)

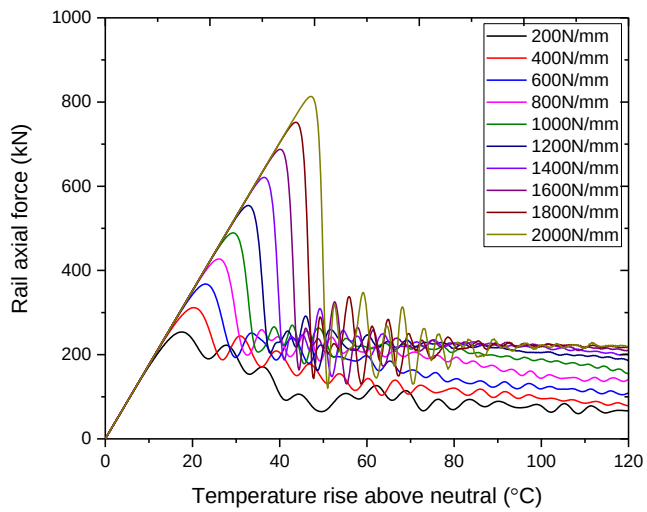

(b)

Figure 5.18 Axial force-temperature relationship of railway tracks with 32mm misalignment: (a) timber sleepered tracks and (b) concrete sleepered tracks.

5.5.3 Effects of lateral resistance

The buckling temperature and safe temperature over neutral of railway tracks are presented in Figures 5.19-5.20. The maximum temperature (T_{max}) and safe temperature (T_{min}) are compared within the same curves under the same conditions. The effects of 1mm and 2mm displacement limits on lateral resistance curves on buckling behaviour are demonstrated in Figures 5.19-5.20, respectively. It should be noted that the lateral resistance shown in the horizontal axis is calculated by the lateral resistance force divided by displacement limit. This implies that the lateral resistance force for 1mm displacement limit is lower than that for 2mm displacement limit. The perpendicular lines present the changes in buckling mechanism from progressive buckling (lower lateral resistance) to snap-through buckling (higher lateral resistance). The results show that the lateral resistance significantly improves the buckling strength for all cases as can be seen in the T_{max} curves while the T_{min} is less affected by lateral resistance. It is noted that, with the same lateral stiffness value, the higher displacement limit of the lateral resistance curve can potentially increase the buckling temperature. As for the case of 1mm displacement limit, the buckling temperature of concrete sleepered track is the highest and followed by 1 in 2, 1 in 3, 1 in 4 interspersed tracks and timber sleepered track, respectively. However, the inverse trends are shown when the lateral resistance is reduced to certain values. For instance, for the tracks with a misalignment amplitude of 8mm, the inflection point is around 350N/mm lateral resistance. Below this point, the timber sleepered and 1 in 2 interspersed track possesses greater buckling temperature than 1 in 3, 1 in 4 and concrete sleepered tracks. This is because the larger torsional fastening resistance of timber sleepers helps track to resist buckling as the lateral stiffness can no longer help resist track buckling. As for T_{min}, the trends are contrary

to T_{max} as the timber sleepered track has the highest T_{min} of all tracks. However, this T_{min} trend can potentially reduce the buckling regime leading to the likelihood of occurrence of progressive buckling failure especially for timber sleepered track. In Figure 5.19c and 5.19d, it is found that the crossing points between buckling temperature and safe temperature are observed when the buckling temperature is equal to the safe temperature. This shows the shifting paths from the snap-through buckling failure to progressive buckling failure. It can be seen buckling modes of tracks with the misalignment amplitude of 24mm are likely to be shifited from snap-through mode to progressive mode while the concrete sleepered tracks is still buckled in snap-throught mode. Meanwhile, the dash lines are not seen for timber sleepered, 1 in 3 and 1 in 4 tracks since these tracks with the mislignment amplitude of 32mm are all buckled progressively within this lateral resistance range.

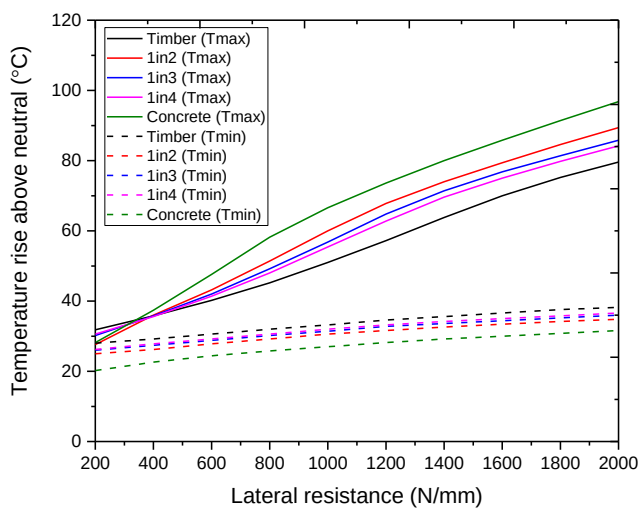

(a)

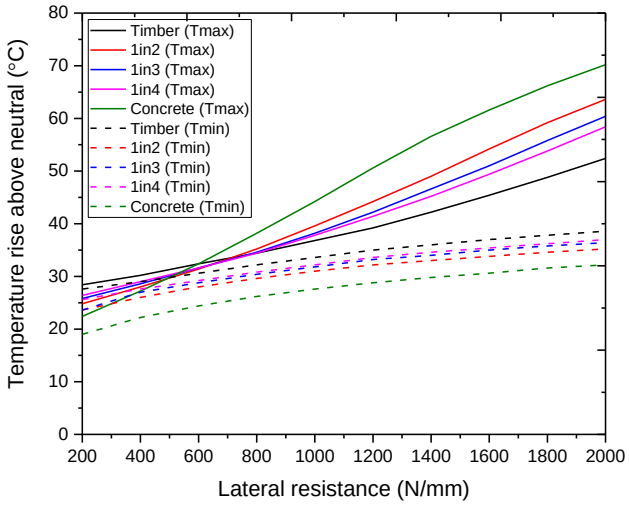
Temperature rise above neutral (°C)
Lateral resistance (N/mm)
Timber (Tmax)
1in2 (Tmax)
1in3 (Tmax)
1in4 (Tmax)
Concrete (Tmax)
Timber (Tmin)
1in2 (Tmin)
1in3 (Tmin)
1in4 (Tmin)
Concrete (Tmin)

(b)

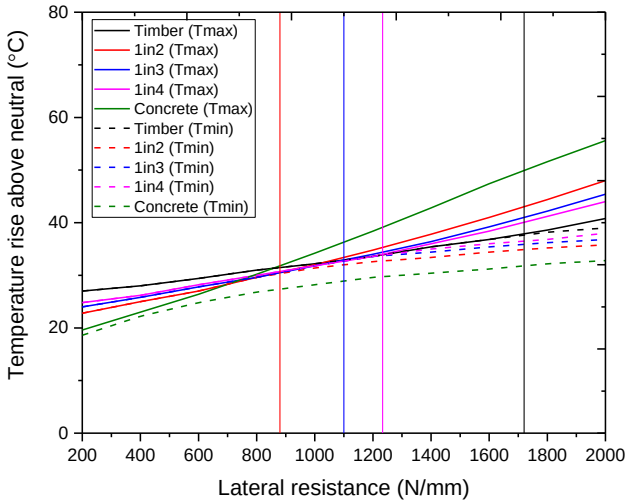
Temperature rise above neutral (°C)
Lateral resistance (N/mm)
Timber (Tmax)
1in2 (Tmax)
1in3 (Tmax)
1in4 (Tmax)
Concrete (Tmax)
Timber (Tmin)
1in2 (Tmin)
1in3 (Tmin)
1in4 (Tmin)
Concrete (Tmin)

(c)

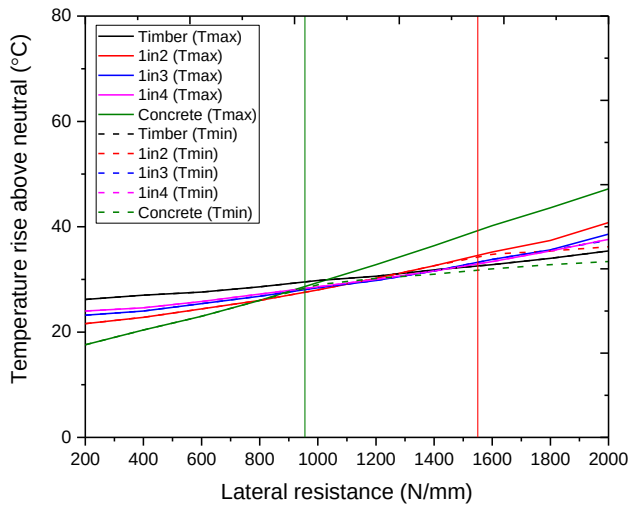

(d)

Figure 5.19 Buckling and safe temperatures of railway tracks with track lateral resistance with Wp = 1mm and lateral misalignment amplitude of: (a) 8mm, (b) 16mm, (c) 24mm, and (d) 32mm.

Figure 5.20 illustrates the buckling and safe temperatures of railway tracks with larger displacement limit of lateral resistance. As for 2mm displacement limit, the buckling strength has a similar trend to those for 2mm displacement limit case. It is noted that railway tracks generally have snap-through buckling mode, however, tracks can be buckled progressively when the initial misalignment amplitude is larger than 24mm (Figures 5.20c-d). The lateral resistance of 860N/mm, 619N/mm, 567N/mm, and 450N/mm are noted as the critical resistance for timber sleepered track, 1 in 4, 1 in 3, and 1 in 2 interspersed tracks, respectively. The buckling failure modes are shifted to progressive buckling whereas the concrete sleepered track is still buckled in snap-through failure mode within this range of lateral resistance. The progressive buckling of concrete sleepered track can be observed when the initial misalignment of 32mm is applied. The progressive buckling of timber sleepered, 1 in 4, 1 in 3, 1 in 2, and concrete sleepered tracks can occur when the lateral

resistance is less than 1340N/mm, 811N/mm, 971N/mm, 1040N/mm and 500N/mm, respectively.

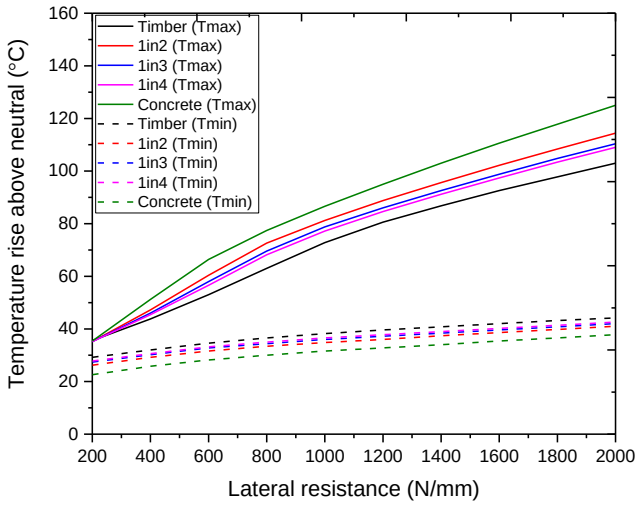

(a)

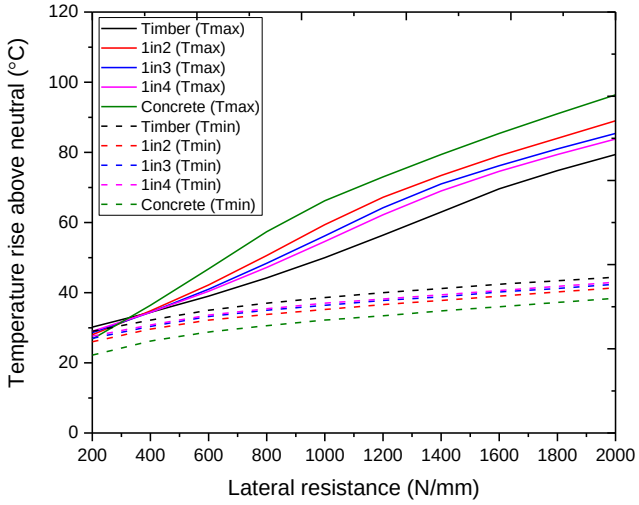

(b)

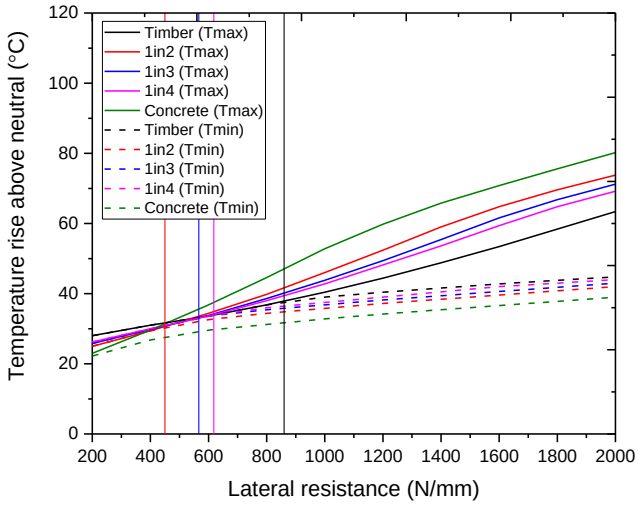

(c)

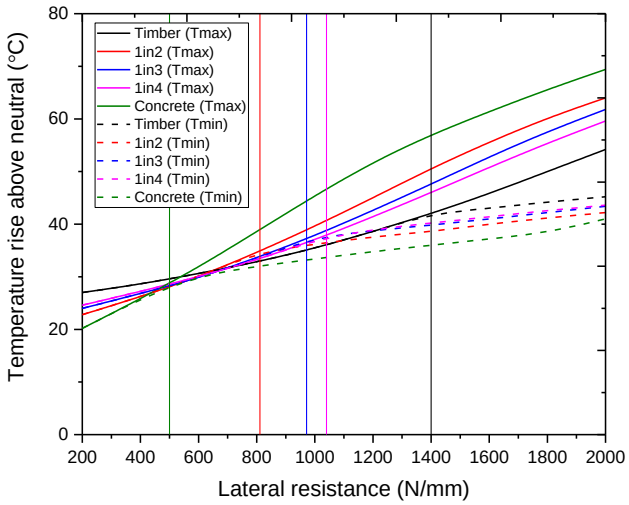

(d)

Figure 5.20 Buckling and safe temperatures of railway tracks with track lateral resistance with Wp = 2mm and initial misalignment amplitude of: (a) 8mm, (b) 16mm, (c) 24mm, and (d) 32mm.

5.5.4 Effects of track misalignment

The effects of lateral misalignments are presented in Figure 5.21. It can be clearly seen that, overall, buckling temperatures decrease as the misalignment amplitude increases. As for the 200N/mm lateral resistance tracks, interspersed methods can potentially increase the buckling temperature when the misalignment amplitude is high. However, the trends are not consistent when the lateral resistance of tracks are 200N/mm and 800N/mm (Figures 5.21a-b). When the lateral resistance is higher (Figures 5.21c-d), the interspersed method can help significantly increase the buckling temperature even if the misalignment amplitude is either small or large. It can be concluded that when the track is more stable, the method of interspersing can significantly improve the buckling resistance. Overall, the 2mm displacement limit yields larger buckling temperature and the trends are more consistent as the lateral resistance force increases.

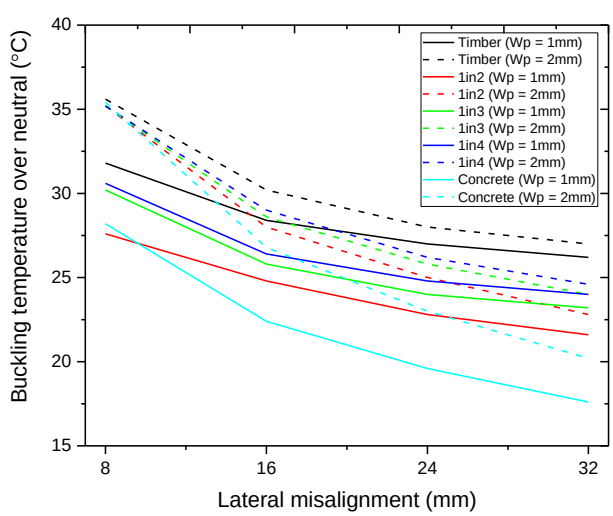

(a)

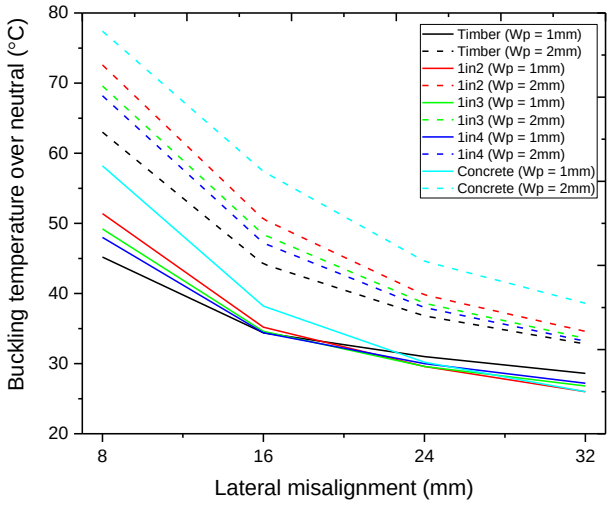
Buckling temperature over neutral (°C)
Lateral misalignment (mm)
Timber (Wp = 1mm)
Timber (Wp = 2mm)
1in2 (Wp = 1mm)
1in2 (Wp = 2mm)
1in3 (Wp = 1mm)
1in3 (Wp = 2mm)
1in4 (Wp = 1mm)
1in4 (Wp = 2mm)
Concrete (Wp = 1mm)
Concrete (Wp = 2mm)

(b)

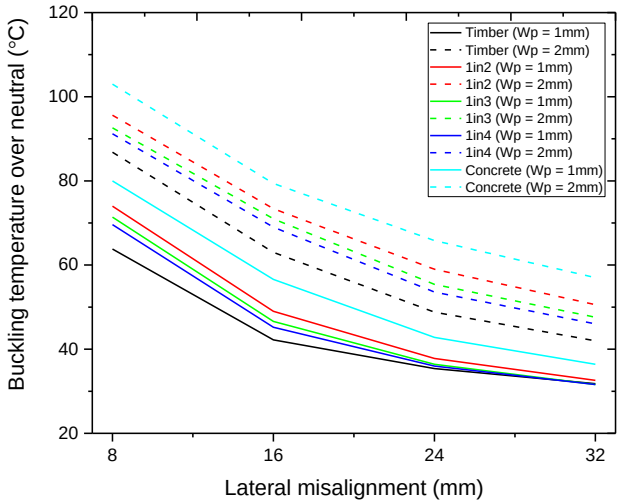
Buckling temperature over neutral (°C)
Lateral misalignment (mm)
Timber (Wp = 1mm)
Timber (Wp = 2mm)
1in2 (Wp = 1mm)
1in2 (Wp = 2mm)
1in3 (Wp = 1mm)
1in3 (Wp = 2mm)
1in4 (Wp = 1mm)
1in4 (Wp = 2mm)
Concrete (Wp = 1mm)
Concrete (Wp = 2mm)

(c)

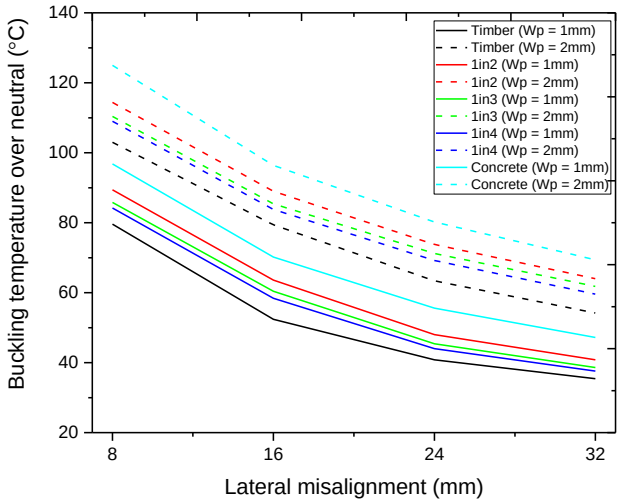

(d)

Figure 5.21 Effects of track lateral misalignment on buckling temperature of railway tracks with lateral stiffness of: (a) 200N/mm, (b) 800N/mm, (c) 1400N/mm, and (d) 2000N/mm.

Figure 5.22 presents the effects of track initial misalignment on safe temperature (T_{Bmin}) of railway tracks. It is clearly seen that the lateral misalignment has a very slight effect on safe temperature in comparison to buckling temperature. Interestingly, concrete sleepered track has the lowest safe temperature while timber sleepered track and interspersed tracks provide higher safe temperature. As for the case of 1mm displacement limit, the safe temperatures of concrete sleepered tracks are roughly between 19°C and 31°C while the safe temperatures of timber sleepered tracks are 28°C and 38°C. As for interspersed tracks, the safe temperatures are between those of concrete sleepered track and timber sleepered track. It is noted that increasing displacement limit of lateral resistance to 2mm can slightly increase safe temperature by less than 5°C in general. It can be concluded that torsional fastening resistance plays a significant role in safe temperature since the resistance on

timber sleepers is much larger than that of concrete sleepers due to the assumption that was made in Chapter 4.

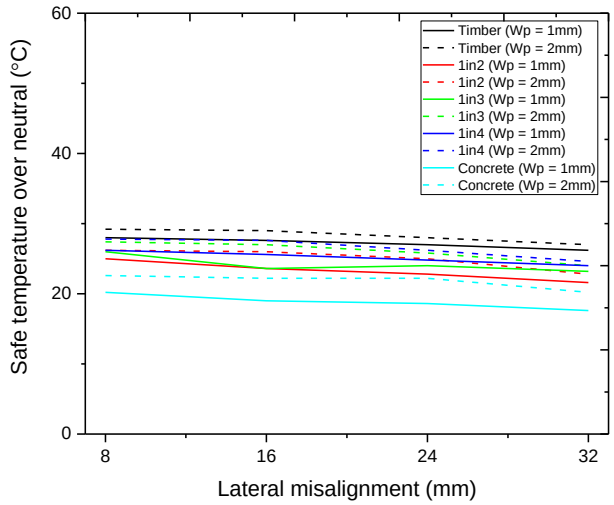

(a)

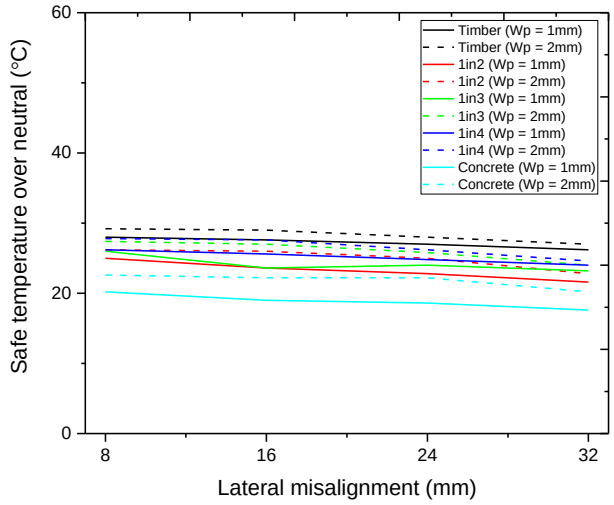

(b)

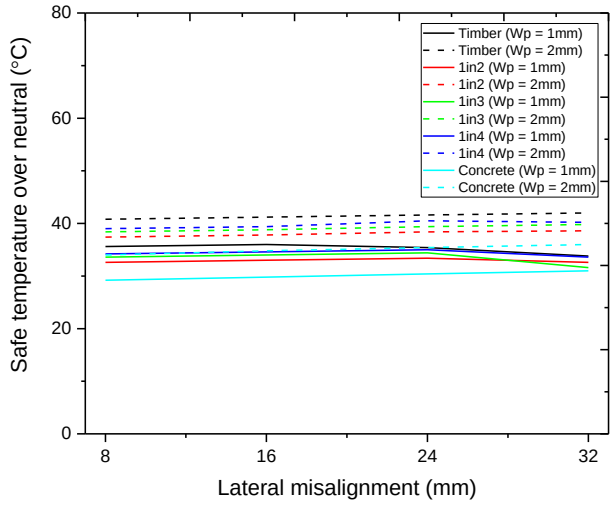

(c)

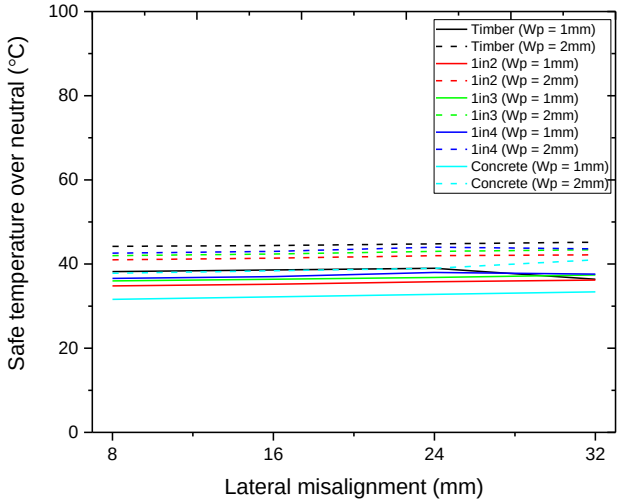

(d)

Figure 5.22 Effects of track lateral misalignment on safe temperature of railway tracks with lateral stiffness of: (a) 200N/mm, (b) 800N/mm, (c) 1400N/mm, and (d) 2000N/mm.

5.5.5 Buckling Criteria

Figures 5.23-5.24 present the allowable temperature over neutral temperature of railway tracks with 1mm and 2mm displacement limit of lateral resistance, respectively. The lateral resistance and lateral misalignment are taken into account. The allowable temperature is calculated based on the buckling criteria mainly depending on the differences between buckling temperature and safe temperature as previously presented in Chapter 3 (Esveld 1997). Even though interspersed tracks and concrete sleepered track tend to improve the buckling temperature, the allowable temperature may be slightly lower than timber sleepered track as seen in the red area in Figures 5.23-5.24. However, this is attributed to the fact that the difference between the buckling temperature and the safe temperature is considerably less than that in the case of the interspersed and concrete sleepered tracks, showing that the timber sleepered tracks are more likely to have a progressive buckling failure than the others. This means that timber sleepered tracks require less external energy to buckle the track while interspersed railway tracks can still provide better buckling strength for unloaded railway tracks.

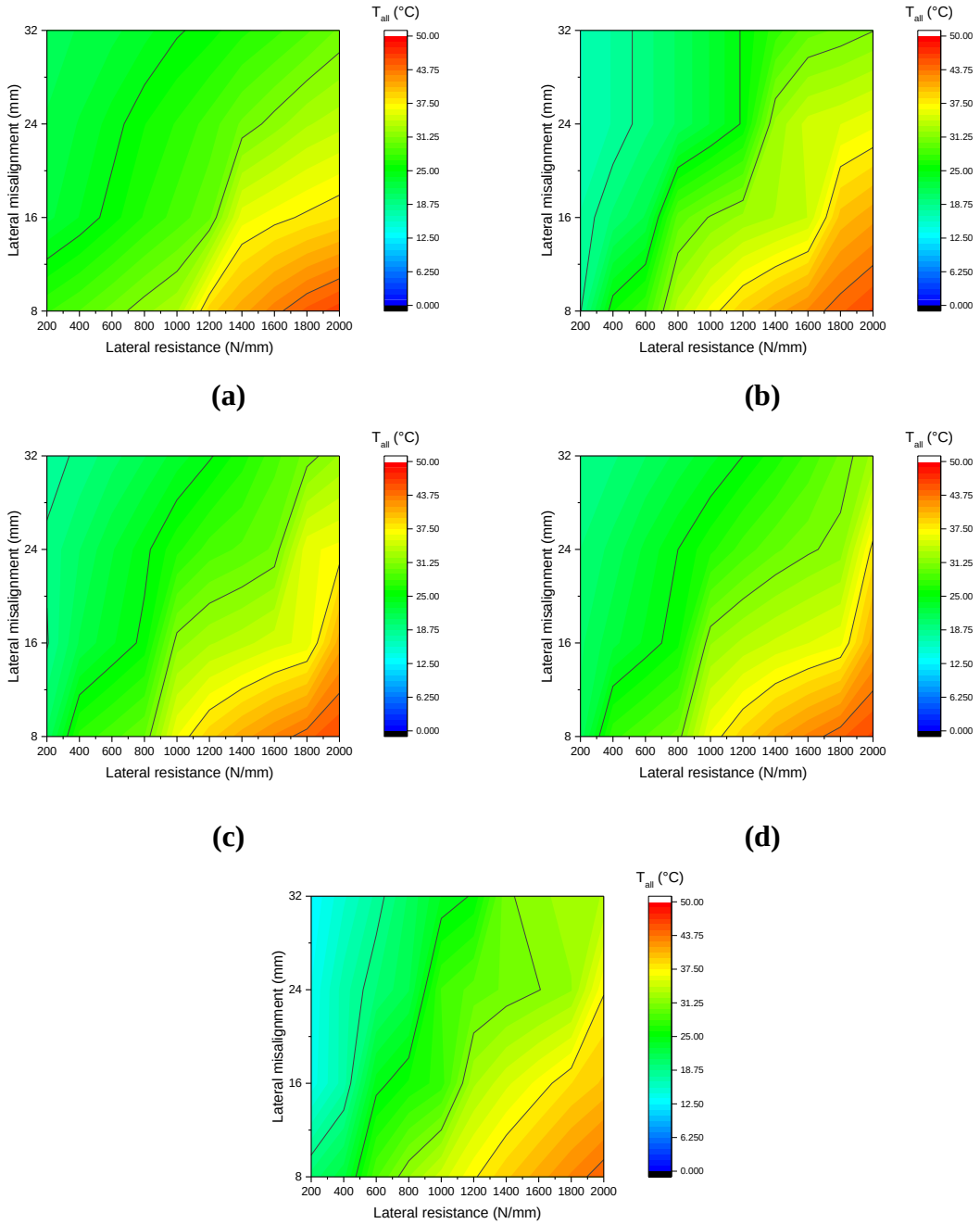

Figure 5.23 Allowable temperature considering lateral misalignment and lateral resistance with 1mm displacement limit: (a) timber sleepered track, (b) 1 in 2, (c) 1 in 3, d) 1 in 4, and (e) concrete sleepered track

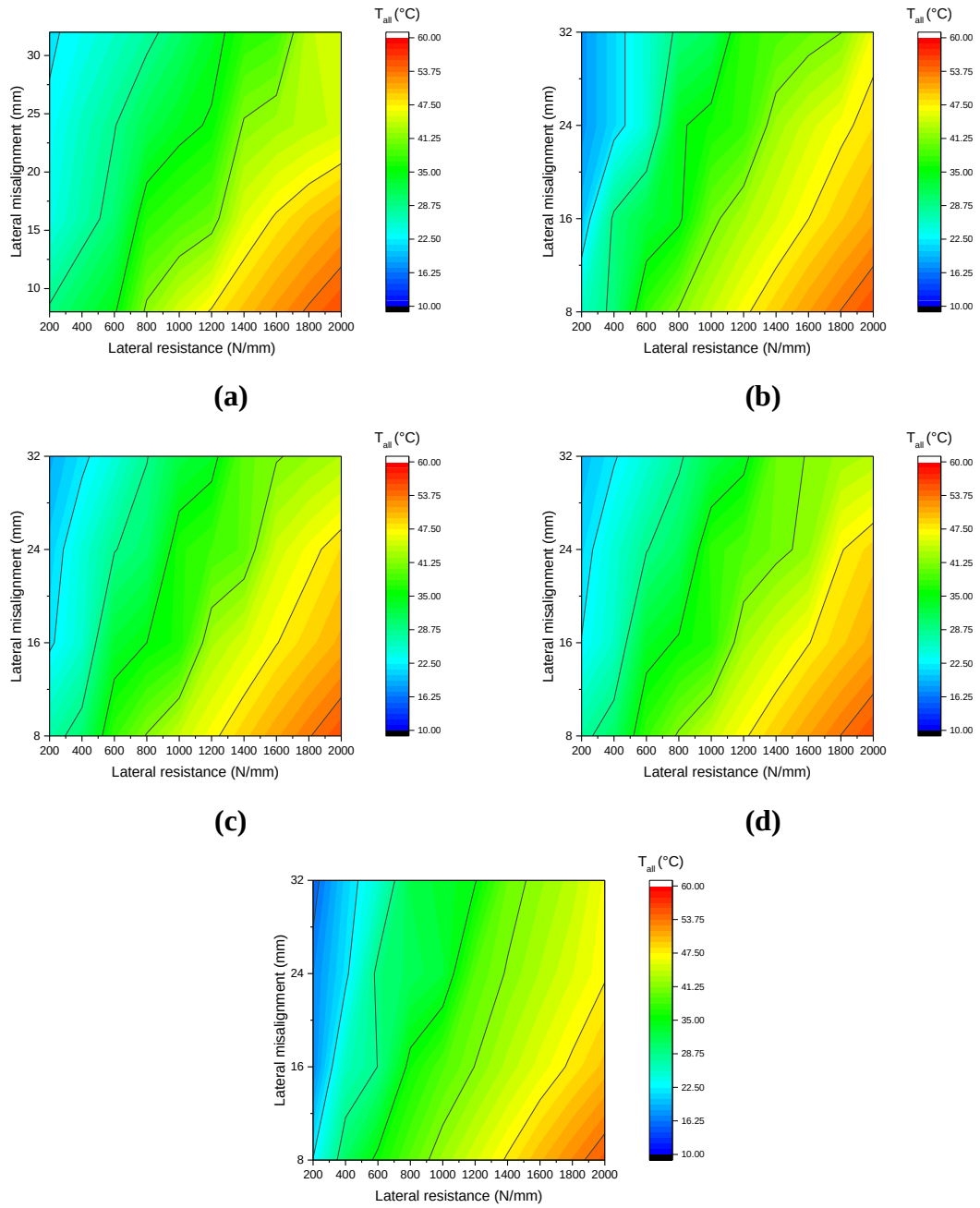

Figure 5.24 Allowable temperature considering lateral misalignment and lateral resistance with 2mm displacement limit: (a) timber sleepered track, (b) 1 in 2, (c) 1 in 3, (d) 1 in 4, and (e) concrete sleepered track.

5.6 Summary

This chapter presents the 3D finite element model of interspersed railway tracks developed to investigate the buckling behaviour using nonlinear analysis in LS-DYNA. Recently, only buckling behaviour of either plain timber sleepered track or concrete sleepered track have been studied. Nonetheless, nonlinear buckling analysis of interspersed railway tracks has never been fully studied. Chapter 4 has studied the effects of various parameters on buckling temperature of traditional and interspersed railway tracks using linear analysis. The obtained results have shown that the interspersed approach can help prevent track buckling by increasing buckling temperature when rotten sleepers are replaced by concrete sleepers. However, the results from Chapter 4 are limited due to the limitation of linear analysis while nonlinear analysis in this chapter can overcome the drawbacks and cover the full behaviour of ballasted tracks. The key findings of nonlinear analysis are as follows.

- Traditional timber sleepered tracks are likely to have progressive buckling failure while the interspersed approach can shift the buckling failure mechanism from progressive buckling to snap-through buckling.
- Torsional fastening resistance has significant effects on safe temperature, increasing the safe temperature of timber sleepered tracks more than concrete sleepered tracks.
- The replacement of timber sleepers by concrete sleepers tends to increase buckling temperature while reducing safe temperature due to its lower fastening torsional stiffness.

- In case of low lateral resistance, the buckling trends can be reversed as the ballast can no longer help mitigate the buckling. The torsional fastening resistance can rather help in this case and thus the timber sleepered track has higher buckling temperature than interspersed tracks.
- Initial lateral misalignment has a significant influence on buckling temperature. This means increasing misalignment results in buckling temperature reduction while it has less effect on safe temperature.
- For unloaded tracks where buckling temperature is the main indicator for buckling strength, the '1 in 2' interspersed track has higher buckling strength than '1 in 3' and '1 in 4' interspersed tracks and timber sleepered tracks as more timber sleepers are replaced by concrete sleepers. Plain concrete sleepered track provides higher buckling strength than all other tracks.

Nevertheless, the replacement of sleepers should be performed carefully since this activity can induce ballast disturbance resulting in a loose track as seen after many maintenance and renewal activities. The novel in-depth insight unprecedentedly instigates vulnerability and resilience of traditional and interspersed railway track systems exposed to extreme weather conditions. The method can be used as an indicative reference for innovative design and maintenance for stability and rail misalignment management of ballasted railway tracks. The insights will enhance the inspection of lateral resistance and support condition in ballasted railway track systems and mitigate the risk of delays due to unplanned maintenance.

As evidenced in Chapters 4 and 5 that the lateral resistance plays a significant role in buckling resistance to extreme temperature, next chapter will perform the DEM simulation

for the Single Sleeper (Tie) Push Tests (STPTs) considering the effects of progressive degradation of railway ballast to evaluate the lateral resistance of ballasted railway tracks. The actual lateral resistance force of ballasted railway tracks will be presented.

5.7 References

CAI, Z. 1994. *Modelling of rail track dynamics and wheel/rail interaction.* PhD Thesis, Queen's University.

CARVALHO, J., DELGADO, J., CALCADA, R. & DELGADO, R. 2013. A new methodology for evaluating the safe temperature in continuous welded rail tracks. *International Journal of Structural Stability and Dynamics*, 13**,** 1350016.

CRC FOR RAIL INNOVATION 2009. Track Stability Management – Literature Review: Theories and Practices Brisbane, Australia: CRC for Rail Innovation

CUADRADO, M., ZAMORANO, C., GONZÁLEZ, P., NASARRE, J. & ROMO, E. Analysis of buckling in dual-gauge tracks. 2008 2008. Thomas Telford Ltd, 177-184.

DE ROSA, A., ALFI, S. & BRUNI, S. 2019. Estimation of lateral and cross alignment in a railway track based on vehicle dynamics measurements. *Mechanical Systems and Signal Processing*, 116**,** 606-623.

FEDERAL RAILROAD ADMINISTRATION (FRA) 2010. Continuous welded rail (CWR); general. Federal Railroad Administration (FRA).

HALLQUIST, J. O. 2006. *LS-DYNA THEORY MANUAL*, Livermore Software Technology Corporation (LSTC).

JING, G. & AELA, P. 2020. Review of the lateral resistance of ballasted tracks. *Proceedings of the Institution of Mechanical Engineers, Part F: Journal of Rail and Rapid Transit*, 234**,** 807-820.

JUNIOR, E. P., DE JUNIOR, A. S. & DA SILVA, S. M. B. A. 2006. Tracing nonlinear equilibrium paths of structures subjected to thermal loading. *Computational Mechanics,* 38**,** 505-520.

LIVERMORE SOFTWARE TECHNOLOGY COPORATION (LSTC) 2018. *LS-DYNA KEYWORD USER'S MANUAL* LIVERMORE SOFTWARE TECHNOLOGY CORPORATION (LSTC)

NGAMKHANONG, C., WEY, C. M. & KAEWUNRUEN, S. 2020. Buckling Analysis of Interspersed Railway Tracks. *Appl. Sci.,* 10**,** 3091.

PUCILLO, G. P. 2019. Train-Induced Load Effects on the Thermal Track Buckling. Joint Rail Conference, April 9–12, 2019 Utah, USA. American Society of Mechanical Engineers Digital Collection.

SAMAVEDAM, G., KISH, A., PURPLE, A. & SCHOENGART, J. 1993. Parametric Analysis and Safety Concepts of CWR Track Buckling. United States. Federal Railroad Administration.

VILLALBA SANCHIS, I., INSA, R., SALVADOR, P. & MARTÍNEZ, P. 2018. An analytical model for the prediction of thermal track buckling in dual gauge tracks. *Proceedings of the Institution of Mechanical Engineers, Part F: Journal of Rail and Rapid Transit,* 232**,** 2163-2172.

YANG, Y. B., LIN, T. J., LEU, L. J. & HUANG, C. W. 2008. Inelastic postbuckling response of steel trusses under thermal loadings. *Journal of Constructional Steel Research,* 64**,** 1394-1407.

CHAPTER 6

LATERAL RESISTANCE OF BALLASTED RAILWAY TRACKS

6.1 Introduction

Chapters 4 and 5 have shown that the most important factor influencing the buckling strength of railway tracks is the lateral resistance of tracks commonly associated with the sleeper and the ballast. As mentioned in Chapter 3, the lateral resistance can vary widely depending on the conditions of the sleeper and the ballast. According to Chapters 3 and 4 on the track buckling analysis using the Finite Element Method (FEM), railway tracks can be modelled using a series of beams and springs to represent track components while reducing the simulation time. The lateral resistance of a ballasted track, which is represented by the lateral spring connected to the sleeper ends, is evaluated by the experiments of the Single Sleeper (Tie) Push Test (STPT) and pull test. This method has been proven to be the most suitable method to quantify the lateral resistance of tracks as recommended by AREMA (American Railway Engineering and Maintenance of Way Association, 2004). The resistance forces are calculated from the total contact force between the sleeper and the ballast against the movement of the sleeper in the lateral plane. The contact forces include those at three different locations: sleeper bottom, sleeper crib, and sleeper end force, as illustrated in Figure 6.1.

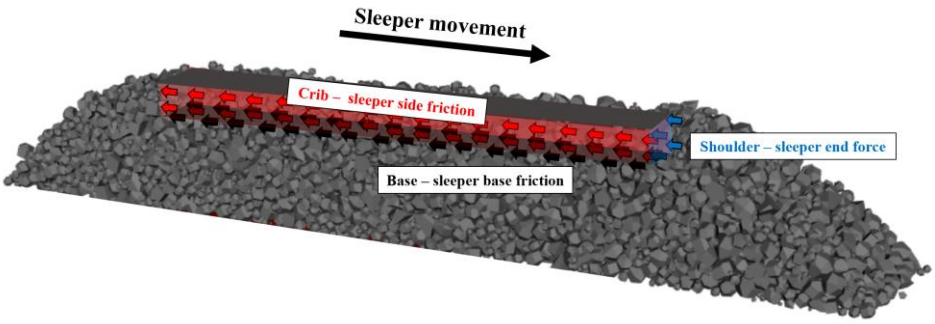

Figure 6.1 Contribution of sleeper–ballast contact force on lateral resistance.

Considerable research has been conducted on the STPTs of sleepers to obtain the lateral resistance–displacement curve of the sleepers for a ballasted track considering various factors for decades. However, a research gap has been found: to the best of my knowledge, the effects of the progressive fouling of the ballast on the track's lateral resistance has thus far never been investigated. More details about previous studies and research gap has been presented in Chapter 3. In this chapter, the layer of ballast with single sleeper is constructed according to the assumption that the lateral resistance of the ballasted track decreases in the stage of a loosely filled and tamped or stabilised track where buckling might occur in reality. It is important to Note that a railway track progressively degrades over time with usage, making the improvement of a ballasted track essential. More importantly, the lack of ballast support can significantly undermine the capacity of railway track, as evidenced in the past. For instance, in a track which is in poor condition, large voids and gaps can be easily observed between the sleepers and the ballast, usually caused by the wet track beds (highly moist ground) from natural water springs or poor drainage. The strength and drainage aspects of ballasted tracks are compromised by the increasing level of ballast fouling. This leads to considerably large particle movement, resulting in a relatively severe loss of support conditions.

As evidenced in the UK and worldwide, railway track buckling can occur even when the railway tracks are fully supported and the ballast layer seems to be in a good condition according to a visual inspection. In fact, degraded ballast particles and the accumulation of ballast breakdown or outside contamination, such as subgrade intrusion or coal dust, are often not seen visually (Sussmann et al., 2012, Anbazhagan et al., 2012). Their presence undoubtedly would have a negative impact on the vertical stiffness of the railway tracks

and cause potential track geometry defects. No quantifiable data currently exist on the extent of influence of a degraded ballast on the lateral stiffness of a ballasted track, and the percentage of fine particles generated in a fouled ballast decreases the lateral support through direct contact with the sleeper. Accordingly, there is a need to study and quantify the effect of the progressive degradation of the ballast influencing the lateral resistance by appropriately considering the contributions of the different frictional components in a ballasted track.

This chapter presents an analysis of the lateral resistance of a ballasted track by simplified DEM simulations. The simulations are conducted using the DEM BLOKS3D software established by the University of Illinois at Urbana-Champaign, USA, which is a collaborator with the University of Birmingham under the European Commission H2020-RISE Project No. 691135 “RISEN: Rail Infrastructure Systems Engineering Network. Although DEM has been widely used for STPT simulations, the effects of the progressive ballast fouling conditions on the lateral track resistance have not been quantified thus far. In this chapter, DEM is used to carry out the push test of single timber and concrete sleepers, considering different levels of fouling within the ballast depth profile. The influences of the ballast condition and vulnerability, due to the fouling levels compared with a clean ballast, on the lateral resistance are discussed. As such, a fouled ballast layer that cannot be inspected visually in the field can significantly reduce the track restraint and increase the likelihood of track buckling even when the degraded ballast is not in direct contact with the sleeper. Such quantitative insight can improve the track maintenance regimes in order to account for appropriate ballast support on the basis of realistic conditions. The outcome of this study can help track engineers to better understand how

different fouled ballast conditions relate to performance and help with the development of inspection criteria related to the ballast layer maintenance and renewal associated with the level of ballast degradation. It can be linked to the time-dependent behaviour of railway ballast degradation to appropriately maintain the performance of the ballast by ballast cleaning or renewal, particularly in summer.

6.2 Discrete Element Modelling (DEM)

The realistic shapes of railway ballast-crushed aggregate particles can be created in a DEM simulation by using the polyhedral elements. This element type can generate non-spherical particles and potentially provide better insight into inter-particle contacts by appropriately accounting for the corners and the sharp edges of the particles, which are essentially needed to correctly simulate the dilatancy angles in angular particle assemblies. More information about different particle models can be found in Chapter 2. In this study, the ballast shapes and their morphological properties are analysed using the imaging technology called 'Enhanced University of Illinois Aggregate Image Analyzer (E-UIAIA)' (Moaveni et al., 2013). The E-UIAIA can capture the realistic 3D shapes of ballast particles from three orthogonal views to quantify the detailed shapes and measurements of each particle including the Angularity Index (AI) and Flat and Elongated (F&E) ratio. AI simply presents an average of the angularity values of all the particles weighted by the particle weight, which measures the overall degree changes on the boundary of a 2D particle silhouette. The F&E ratio illustrates the ratio of the longest dimension of the particle to its minimum dimension, which is perpendicular to the longest dimension in the three orthogonal views. The ballast particles obtained by E-UIAIA are imported to the

BLOKS3D DEM software developed and extensively used at the University of Illinois at Urbana-Champaign in the last three decades (Ghaboussi and Barbosa, 1990, Zhao et al., 2006). The imported particles are then generated in BLOKS3D for the DEM simulation.

6.2.1 Ballast particle shapes

The ballast shapes and their corresponding geometric properties used in this study are presented in Table 6.1. It should be noted that the data were originally collected from the field. The percentage of particle proportion used and the average AI in this simulation are presented. Note that the proportions and the AI of each particle are evaluated using the Aggregate Image Analyzer (E-UIAIA). The average AI is calculated by taking a weighted average of the AI of each ballast shape, weighted by the percentage of the number of particles to match the AI curve of the field-collected ballast sample data (Hou et al., 2018). The average AI is approximately 430, which is considered a low AI, mostly representing the particles with smooth and rounded surfaces (Huang, 2010). This generally presents the ageing railway ballast with the particles having less angularity compared to the new ones. The ballast particles are generated on the basis of the particle distribution curve shown in Figure 6.2, which conforms to the American Railway Engineering and Maintenance-of-Way Association (AREMA) No. 24 standard specification.

Table 6.1 Imaging-based shape indices of ballast particles as discrete elements in DEM model.

No.	Ballast shape	Percentage of number of particles (%)	Angularity Index (AI)	Flat & Elongated ratio (F&E)
1		3.56	720	1:1
2		10.20	570	1:1
3		19.30	448	1:1
4		66.94	390	1:1
		Average	430	1:1

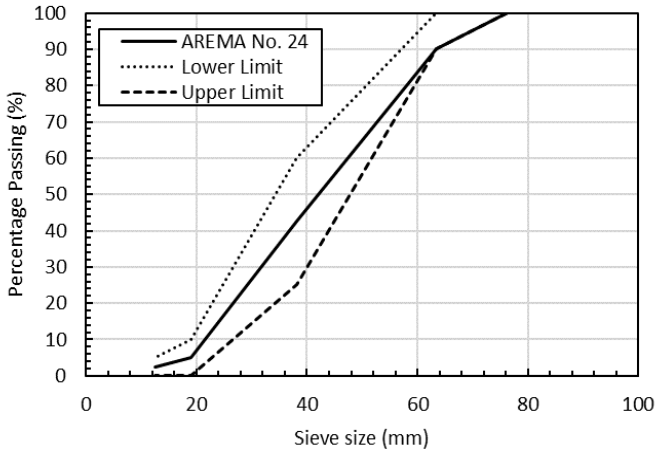

Figure 6.2. Ballast Particle Size Distribution (PSD) based on AREMA No. 24.

6.2.2 DEM parameters

The DEM model parameters consist of normal stiffness, shear stiffness, and surface friction that are applied between ballast particles. The DEM model parameters considered in this study are presented in Table 6.2. The model parameters in the table have been validated

previously against the experimental results of the direct shear and triaxial tests [36]. Note that the surface friction angle between the sleeper and the ballast set as 31° for a clean ballast and 27° for a fouled ballast. More details about the DEM parameters for the fouled ballast layer are presented in Section 6.3. This contact stiffness combination gave better DEM model predictions against the experimental results obtained in the laboratory. In terms of the contact between the sleeper and the ballast, the surface friction angles for both the timber and the concrete sleepers to the ballast are assumed to be equal at 30°, as calibrated previously for a concrete sleeper and a ballast contact. Note that the DEM parameters of the timber sleeper and the ballast has not been calibrated, it is assumed that they can be similar to those of the concrete sleeper. However, the surfaces of the concrete sleeper are smoother than those of the timber sleeper, and the assumption of the timber sleeper contact might slightly affect the results of the contact between the sleeper and the ballast. It is important to note that in the preliminary study on the lateral resistance, the surface friction angles of between 30° and 40° of the sleeper and the ballast contact were compared as, in general, the timber surfaces are relatively rough in comparison to concrete surfaces. However, it was found that the lateral resistance increased slightly by only approximately 5% upon the increase in the surface friction angle from 30° to 40°. Thus, the surface friction angle of 30° is used in this study for both the timber and the concrete sleeper cases.

Table 6.2 DEM parameters.

Parameters	Value	Unit
Normal stiffness	20	MN/m
Shear stiffness	10	MN/m
Surface friction angle (Clean ballast)	31	°
Surface friction angle (Fouled ballast)	27	°
Global damping	0	
Contact damping	0.4	

6.2.3 Physical model

In this study, a single span of ballast layer geometry with a mono-block sleeper is constructed on the basis of the typical dimensions shown in Figure 6.3. The dimensions of the established ballast layer model without a ballast crib and shoulder are illustrated with the sleeper dimensions. A timber sleeper with the dimensions of 250 mm × 150 mm × 2600 mm and a concrete sleeper with the dimensions of 260 mm × 235 mm × 2600 mm are separately placed on top of a 300-mm-thick ballast layer. The full width of these tracks with 400-mm-wide ballast shoulders and a 1:1.5 shoulder slope is modelled. The boundary in the longitudinal direction of the track is set as 600 mm, which is equal to the typical sleeper spacing. Thus, the model boundary area is set as follows: 600 mm long and 4600 mm wide. The material properties and dimensions of the sleepers are presented in Table 6.3.

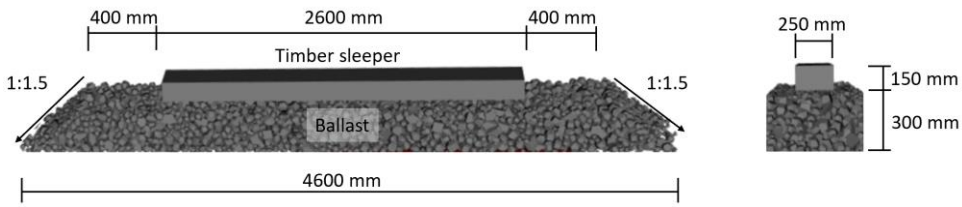

(a)

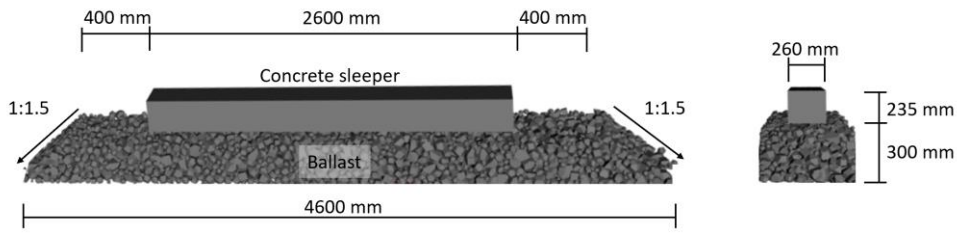

(b)

Figure 6.3 Sleeper and ballast layer geometry with no ballast crib and shoulder: (a) timber sleeper and (b) concrete sleeper.

Table 6.3 Sleeper characteristics.

Properties		Values	Units
Timber sleeper (Hardwood)			
Density		1100	kg/m^3
Elastic modulus		160000	MPa
Poisson's ratio		0.2	
Dimension	Length	2600	mm
	Height	150	mm
	Width	250	mm
Concrete sleeper			
Density		2740	kg/m^3
Elastic modulus		37500	MPa
Poisson's ratio		0.2	
Dimension	Length	2600	mm
	Height	235	mm
	Width	260	mm

that two cases of ballast layer geometries are considered. The ballast layer with no ballast crib and shoulder is first constructed as shown in Figure 6.4. This layer is set as an initial condition for another ballast layer geometry. Secondly, more ballast particles are generated into the first layer to create the ballast crib and shoulder. Note that for this case, the top height of the ballast is placed at the same level of sleeper depth. The schematic view of ballast layer with crib and shoulder is shown in Figure 6.4.

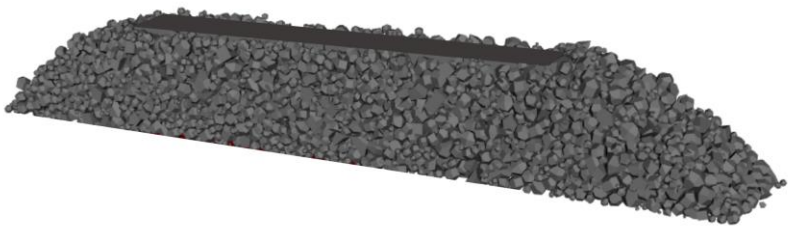

Figure 6.4 Schematic view of ballast layer with ballast crib and shoulder.

6.3 Ballast Fouling Mechanism

Figure 6.5 presents the ballast fouling phases and their mechanisms. It consists of three different phases starting from the clean ballast to the partially fouled ballast and ends up with the heavily fouled ballast. In Phase 1, the clean ballast, where each particle is still in contact with others, is presented. As there are voids between particles, finer materials from outside contamination easily fill these voids in Phase 2. The contacts between particles are still maintained while the contact strength can be reduced progressively as the number of finer particles in the voids keep increasing. In Phase 3, the ballast is heavily fouled when the voids are filled heavily by fine materials resulting in the elimination of particle contact. The movement of each ballast particle is constrained by the finer materials in the void. This normally occurs when the percentage of fouling particles in the ballast layer is higher than

50% (Indraratna et al., 2011). In this phase, the improvements including the renewal and the cleaning of the ballast layer are undoubtedly required.

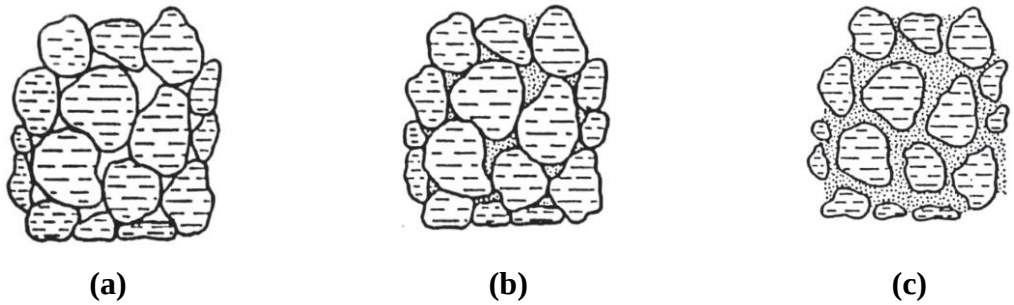

Figure 6.5. Critical ballast fouling phases: (a) Phase 1: clean ballast, (b) Phase 2: partially fouled ballast, and (c) Phase 3: heavily fouled ballast (Huang et al., 2009).

According to the previous experiments (Huang et al., 2009), three types of fine materials: coal dust, plastic clayey soil, and mineral filler, were considered to be the finer material applied into the voids of the ballast to evaluate the effects of different fouling agents on the ballast performance. It was found that coal dust provided the poorest mechanical properties and was reported to mostly reduce the aggregate assembly strength as compared to the others (Huang and Tutumluer, 2011). In general, in a DEM simulation, there are two approaches to represent the fouled ballast conditions. First, the direct approach is used to apply the actual new particle gradation of the fouled ballast. Note that once the ballast is fouled, more small particles are created that can significantly change the particle gradation. This leads to a considerably large number of ballast particles, resulting in the considerably high computational time and memory consumption. The other approach is the indirect method that assumes that the fouled ballast will still have large aggregate particles with the same number of particles as before fouling contacting each other at a considerably low surface friction angle; this method is adopted in this research as the modified DEM model parameter. This method allows dealing with new ballast type uniform gradations having

considerably fewer particles than the actual degraded ballast particle size distributions and provides faster simulation time. This approach is based on previous experiments using coal dust as a fine material in the triaxial and direct shear tests in the past (Huang et al., 2009). As coal dust acts as a lubricant which can reduce the friction between particles, a lower surface friction angle between two discrete ballast particles/elements in contact is adopted herein for the DEM simulations. It should be noted that the surface friction angle ranges from 31° for the clean ballast to 27° for the fouled ballast. This is based on the assumption that the void ratio and the compaction of the ballast are completely similar under both clean and fouled ballast conditions in the same profile track. However, in fact, when the ballast layer is fouled, the void volume have to be reduced (Sussmann et al., 2012).

This study considers the ballast fouling conditions, which are divided into three different levels from partially fouled to fully fouled: (1) 100-mm fouled layer at the bottom (Figure 6.6b), (2) 200-mm fouled layer at the bottom (Figure 6.6c), and (3) full-depth fouled ballast layer (Figure 6.6d). In general, after the breakdown of the ballast due to the load distribution from the sleeper, the ballast fouling process migrates from the top to the bottom and the fine aggregates accumulate at the bottom and form a fouled layer (Anbazhagan et al., 2012). This is represented by the first two cases of partially fouled layers. Note that this might not be the case if the soft subgrade causes mud pumping; the subgrade soil fines that intruded might be collected and observed at any depth profile in the ballast layer (Sussmann et al., 2012, Federal Railroad Administration, 2011). This case is represented by the assumption that the whole ballast layer is fouled. The schematic views of the different ballast layer conditions are shown in Figure 6.6.

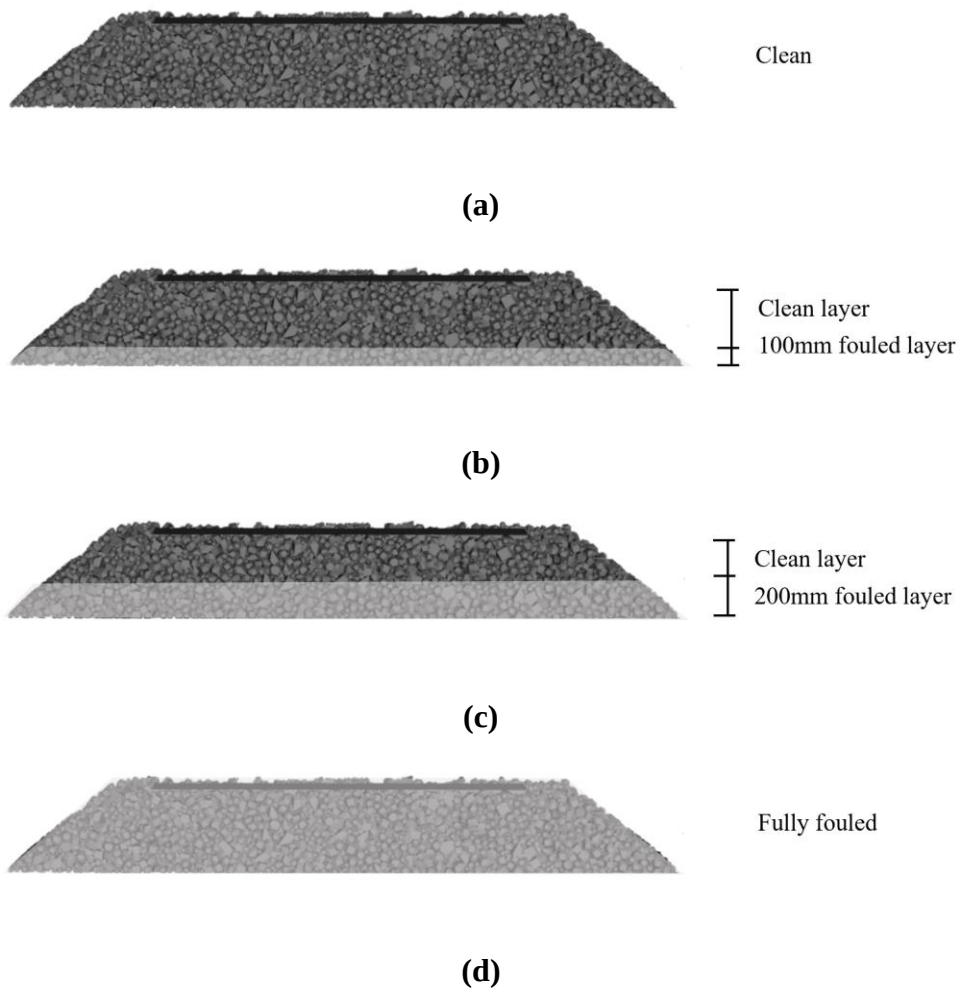

Figure 6.6 Schematic view of (a) clean ballast layer, (b) 100-mm fouled ballast layer, (c) 200-mm fouled ballast layer, and (d) fully fouled ballast layer.

6.4 Ballast Layer Preparation

The processing for preparing ballast layer modelling are:

1. As for the clean ballast layer, ballast particles are randomly dropped into the boundary area to generate the ballast layer. Note that approximately 12,805 ballast particles are initially formed. The ballast parameters are set for the clean ballast according to Table 6.2. As for the fully fouled ballast layer, the ballast layer preparation is set as that for the fully clean ballast layer except for the DEM contact parameters. In contrast, the number of

ballast particles with the contact parameters for the fouled ballast is decreased to generate the fouled ballast layer at the bottom for the 100-mm and the 200-mm fouled ballast layers.

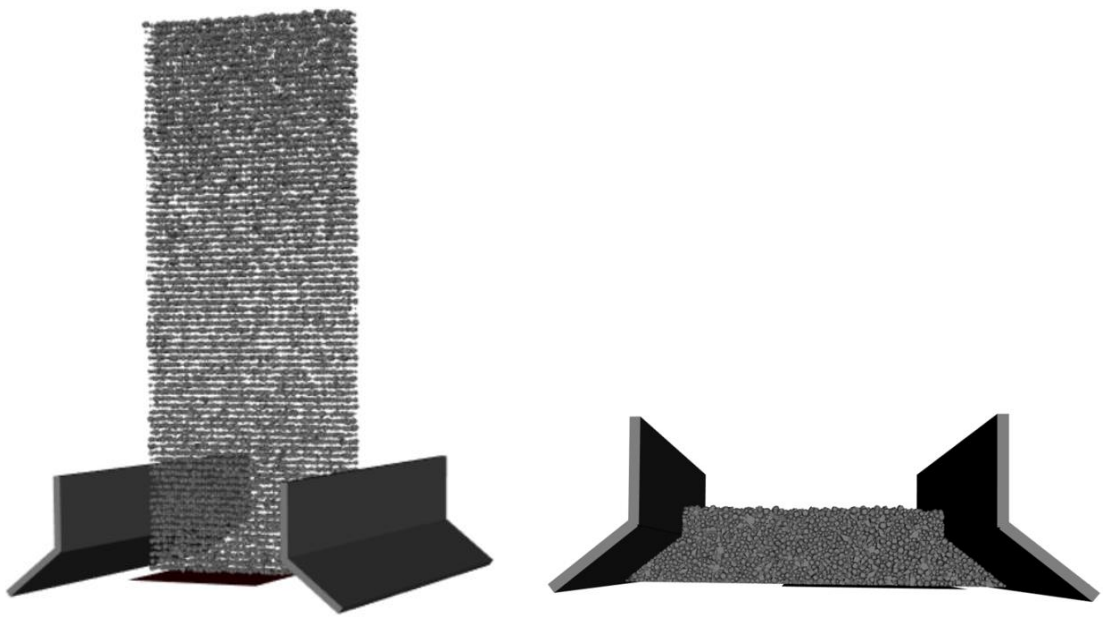

Figure 6.7 Ballast layer preparation step 1.

2. The ballast particles in the boundary area located over the target height are removed for the clean and the fully fouled ballast cases. In this case, the target depth of the ballast is set as 300 mm.

Regarding the partially fouled ballast, the ballast particles over the fouled layer, located over 100 mm and 200 mm, respectively, are removed, and then, the ballast particles with different contact parameters are added to generate the clean ballast layer on top of the fouled ballast layer. Lastly, the ballast particles over the target height of 30 m are removed.

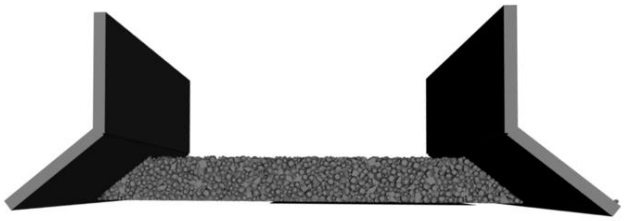

Figure 6.8 Ballast layer preparation step 2.

3. For all the cases, the non-deformable compaction plate is then pushed downward on top of the particles by applying the normal force of 100 kN, that was calibrated (Huang, 2010), to properly compact the ballast layer until it reaches the target void ratio and no particle movement observed. Note that approximately 38% target air void of the volume of the ballast layer is considered to represent a loose condition, as the target air void volume for the compacted ballast should reach 35% in the field (Sussmann, Ruel, and Chrismer 2012).

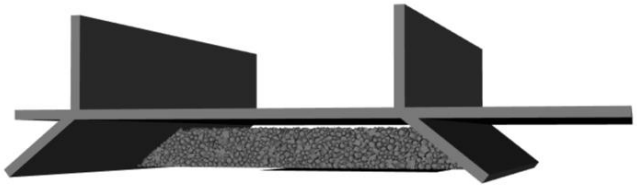

Figure 6.9 Ballast layer preparation step 3.

4. The sleeper, which is modelled as a non-deformable block, is then placed on top of the ballast layer. After the system is in equilibrium, the boundary boxes are then removed from the system. The sleeper with the ballast layer with no ballast crib and shoulder is ready for the sleeper push test simulation. It is important to note that the flexural behaviour of the sleeper is not taken into account so that the non-deformable master block can be appropriately considered in this study.

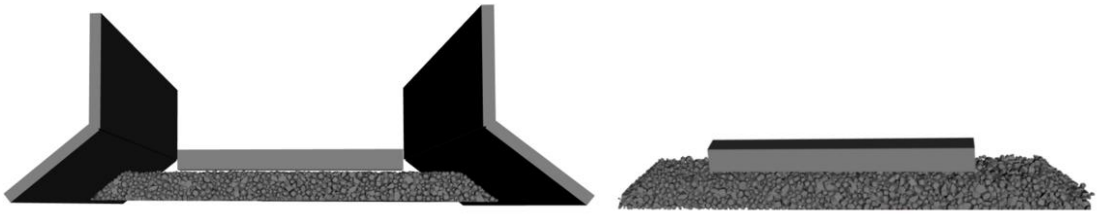

Figure 6.10 Ballast layer preparation step 4.

5. As for the ballast layer with the ballast crib and shoulder, the boundary box in Step 4 is kept. More ballast particles are then randomly dropped into the boundary area. It is noted that the ballast particles, which have the centroid over the depth of the sleeper, are removed. Thus, the ballast crib and shoulder heights are set as the depth of the sleeper.

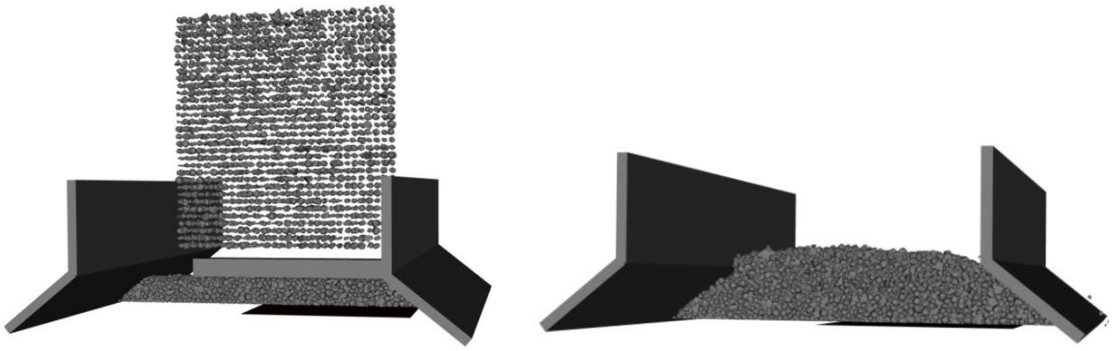

Figure 6.11 Ballast layer preparation step 5.

6. The boundary plates are removed from the system, and the sleeper with the ballast layer is ready for the sleeper push test simulation. Lastly, the sleeper is pushed transversally with the velocity of 0.5 mm/s. The sleeper is displaced laterally for approximately 3 mm, as the force is likely to be constant and not increase any further after 3 mm.

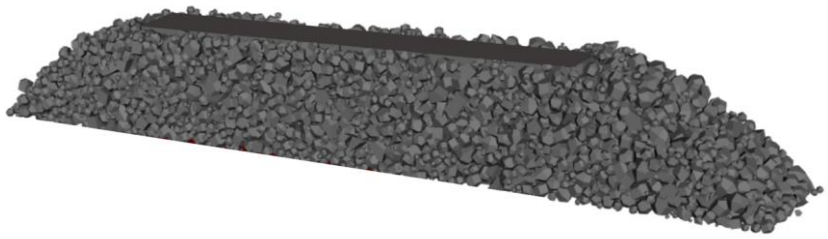

Figure 6.12 Ballast layer preparation step 6.

6.5 Results and Discussions

The lateral resistance of the ballasted tracks with the timber and concrete sleepers against the sleeper displacement is shown in Figure 6.13. The lateral force is computed by the summation of the contact forces between the sleeper and the ballast in the transverse direction. Note that the raw data, that originated from BLOKS3D, are smoothed using the adjacent averaging method to remove the spikes from the signals for a better comparison with each other. The slope of the lateral force–sleeper displacement represents the lateral stiffness of the ballasted track contributed by the sleeper–ballast contact. The initial stiffness, which is calculated from the maximum force at yield over the displacement limit, represents the lateral resistance (unit: N/mm). It is noted that the curves are likely to be bilinear which can fit to the original ones. The lateral force increases linearly as the sleeper displacement increases until it reaches a certain value or displacement limit. At that certain point, the sleeper displacement yields, and the lateral stiffness tends to be reduced. Note that the displacement limit can be observed at around 0.5–1 mm.

The results indicate that adding a ballast shoulder and crib can significantly increase the lateral resistance even though the sleeper displacement reaches the certain value or yield point. It is observed that the ballast and crib can help harden the lateral resistance of the

ballasted track, as the slope of the secondary stiffness of the track with the ballast crib and shoulder is higher than that of the track without the ballast crib and shoulder.

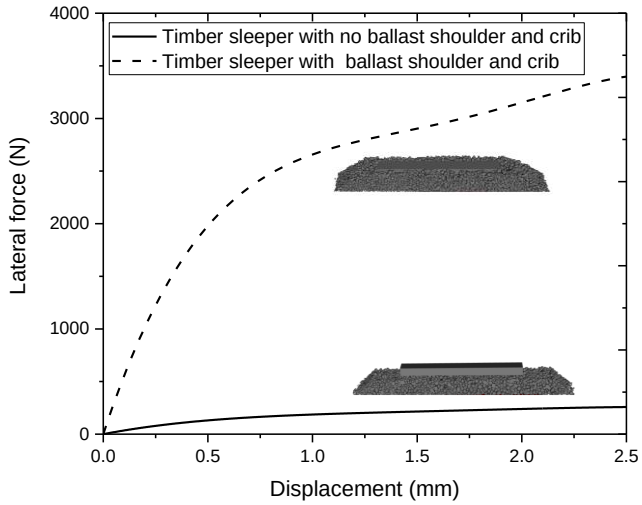

(a)

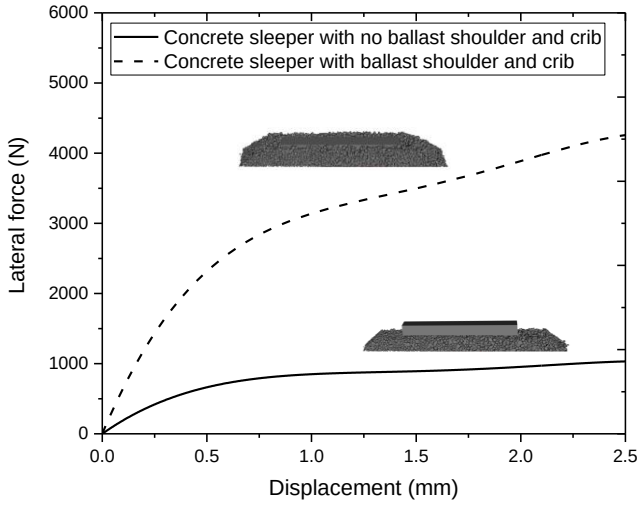

(b)

Figure 6.13 Lateral force–displacement: (a) timber sleeper and (b) concrete sleeper.

Note that the lateral force at the 2-mm sleeper displacement is generally recorded to represent the lateral resistance of the ballasted track in terms of the force, as the lateral force after this point tends to be constant or very slightly changed. The results of the original model of the clean ballast shown in Figure 6.14 reveal that the lateral force at the 2-mm concrete sleeper displacement is approximately 3.8 kN. The benchmarking values are categorised into six different cases depending on the conditions of the ballast: unballasted track, loosely filled track, tamped and lined track, stabilised track, dynamically stabilised track, and wet filled and fully stabilised track (Lichtberger, 2007), as presented in Figure 6.14. As the model is constructed in accordance with the loosely filled and tamped stage conditions, the lateral resistance of the concrete sleeper cases in this study matches well and falls within between the loosely filled (lateral resistance < 2.5 kN) and tamped stages (lateral resistance < 5.1 kN) as expected. This value is lower for the timber sleeper to be just above 3 kN (see Figure 6.13a).

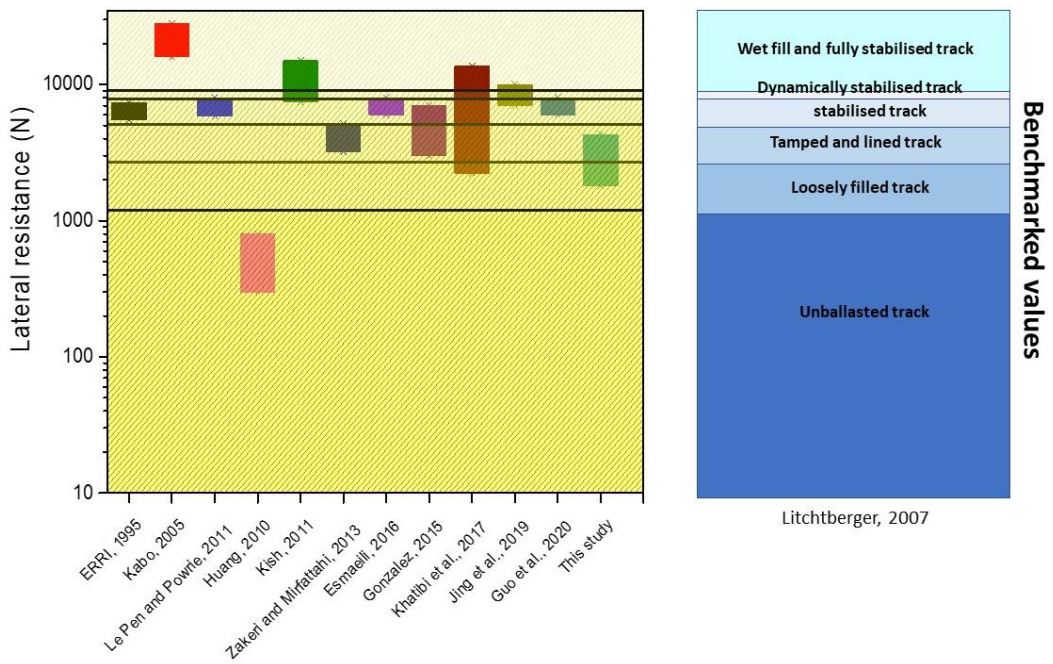

Figure 6.14 Lateral resistance of ballasted track at 2-mm sleeper displacement with benchmarked values

Figure 6.15 presents the lateral resistance percentage of the timber sleeper to the concrete sleeper over the sleeper displacement. It is observed that in the case of the ballast bottom only with no ballast shoulder and crib, the lateral resistance of the ballasted tracks with timber sleepers is approximately 20%–30% of that with concrete sleeper. This is directly related to the sleeper weight and shape that contributes considerably to the lateral resistance. Meanwhile, the lateral resistance percentage of the ballasted track with timber sleepers considering the ballast shoulder and crib is between 80% and 85% of that with concrete sleepers which are considerably larger than that in the previous case. This is because the sleeper side friction and the ballast shoulder end force help to restrain the sleeper movement and these parts are not considerably influenced by the sleeper weight and shape.

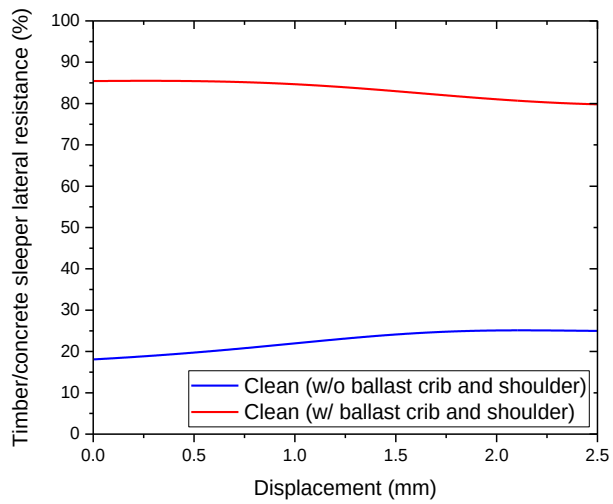

Figure 6.15. Timber/concrete sleeper lateral resistance ratio.

Figures 6.16 and 6.17 illustrate the lateral resistance of the ballasted track under fouled conditions. Note that the displacement limit, which is also known as the yield point, is between 0.5 mm and 1 mm, similar to that in the case of the clean ballast. It is obvious that the lateral resistance gradually decreases when the depth of the fouled layer increases. Heavier ballast fouling tends to reduce the lateral resistance while not changing the displacement limit, making the track softer with a decrease in the lateral stiffness. The reduction of the lateral resistance of the ballasted tracks is presented in Figure 6.18. This reduction of the lateral resistance because of the ballast fouling is calculated on the basis of the difference between the lateral resistance of the track with the clean ballast and that with the fouled ballast ($\frac{R_{clean}-R_{fouled}}{R_{clean}}$x100, where R is the resistance). Note that the resistance is measured when the sleeper displaces by 2 mm. The thicker the layer of the fouled ballast, the lower is the lateral resistance. For the timber sleeper, the resistance reductions are 13%–15%, 21%–25%, and 38%–48% for the tracks with a fouled ballast

thickness of 100 mm and 200 mm and the fully fouled track, respectively. While the reduction rates of tracks with concrete sleepers are likely to be higher than those of the timber sleepers, as 17%–21%, 23%–38%, and 39%–64% reductions are observed for tracks with a fouled ballast thickness of 100 mm, 200 mm, and 300 mm, respectively. As presented in Figure 6.18, tracks without a ballast shoulder and crib are likely to be more sensitive to the ballast fouling conditions, as the reduction rates in the lateral resistance are higher than those with the ballast shoulder and crib.

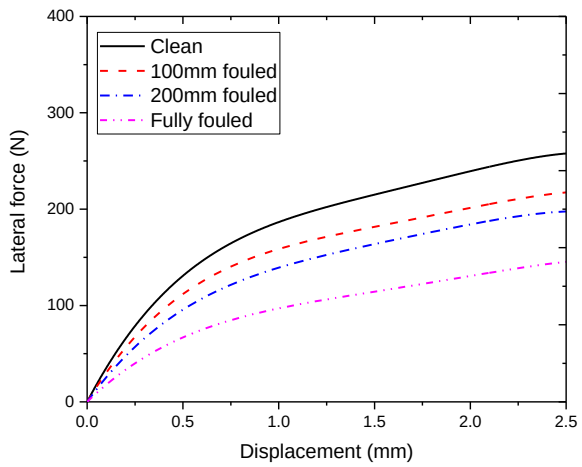

(a)

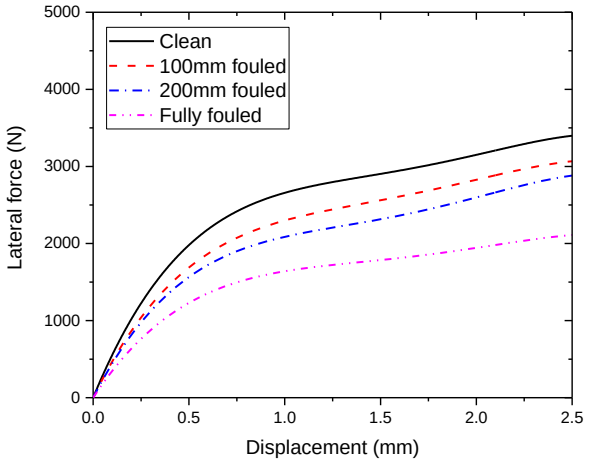

(b)

Figure 6.16. Lateral force–displacement of timber sleeper considering fouled ballast: (a) timber sleeper with no ballast shoulder and (b) timber sleeper with ballast shoulder.

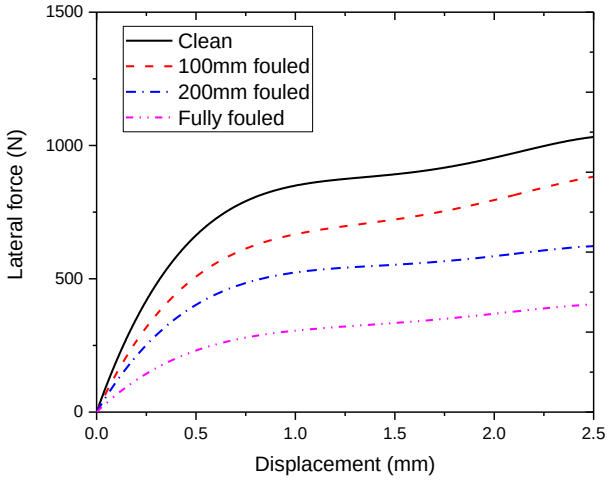

(a)

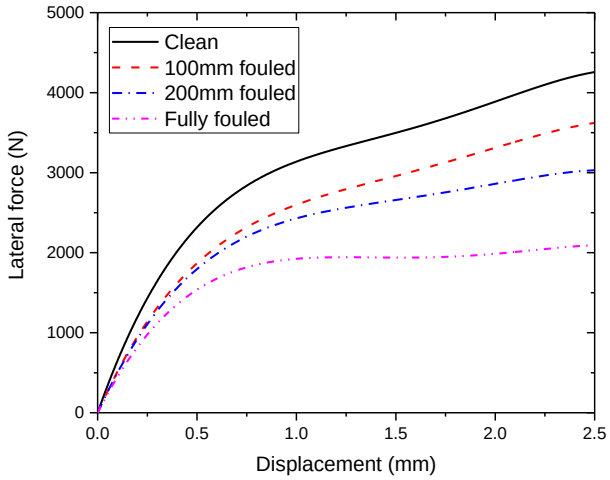

(b)

Figure 6.17. Lateral force–displacement of concrete sleeper considering fouled ballast: (a) concrete sleeper with no ballast shoulder and (b) concrete sleeper with ballast shoulder.

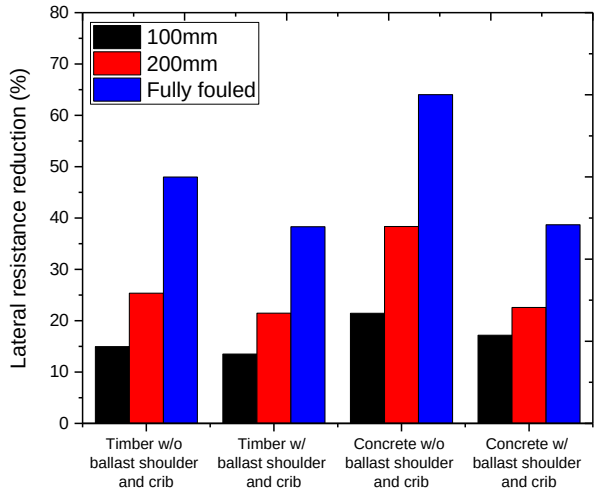

Figure 6.18. Lateral resistance reduction due to ballast fouling.

Figure 6.19 presents the contributions of each component for the lateral resistance. The results are derived from the case of the sleeper placed on the ballast bed with the ballast crib and shoulder. Note that the contributions include the sleeper base, ballast crib, and the

ballast shoulder, as previously presented in Figure 3.14. They are calculated from the percentage ratio of the component resistance to the total resistance ($\frac{R_{component}}{R_{total}}$x100). Note that the contributions are computed when the displacement of the sleeper is equal to 2 mm. As for the timber sleeper, the percentage ratios are 37%–47% for the sleeper base, 20%–34% for the ballast crib, and 30%–40% for the ballast shoulder. In contrast, the sleeper base plays a higher percentage contribution for the ballasted track with the concrete sleeper, and the percentage ratios are 56%–68% for the sleeper base, 20%–28% for the ballast crib, and 12%–16% for the ballast shoulder. This is attributed to the fact that the concrete sleeper has a greater weight and larger dimensions, resulting in higher normal forces and frictional resistance at the sleeper base. It is also noticeable that the ballast crib in the concrete sleeper case make a larger contribution to the lateral resistance than the ballast shoulder, while it is less in the timber sleeper case. These results match well with those of the previous studies on the lateral resistance of the ballasted track with the concrete sleeper. Note that the boundary area in the longitudinal direction of the rail is set as 600 mm in both the timber and the concrete sleeper cases, while the sleeper width of the timber sleeper is smaller than that of the concrete sleeper. This slightly influences the number of ballast particles and the ballast content in the crib area as the number of ballast particles for the concrete sleeper is less than that in the timber sleeper case because of the larger width of the concrete sleeper. This results in a closer gap from the concrete sleeper to the side boundary which could increasingly restrain the sleeper movement. In accordance, the sleeper spacing plays a role in the lateral resistance, as it changes the ballast content in the contact with the particles in the ballast crib. Reducing the sleeper spacing can increase the lateral resistance because of the better confinement of ballast crib. In conclusion, the lateral resistance contributions

provided by the ballast in the crib and shoulder mainly depend on the ballast layer geometry and the number of ballast particles in contact with the sleeper.

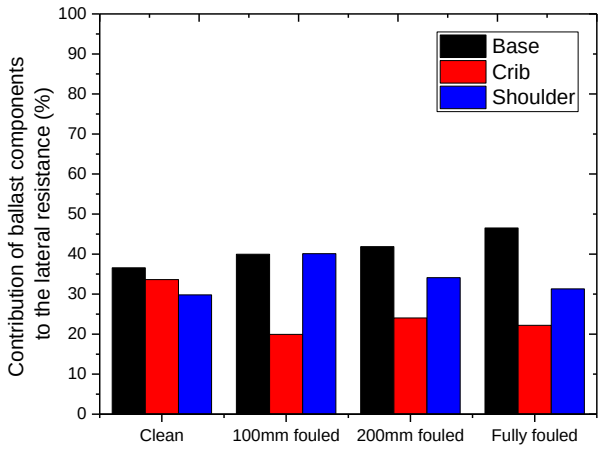

(a)

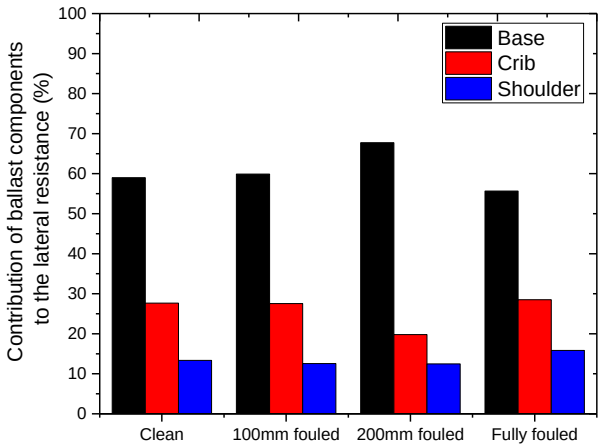

(b)

Figure 6.19. Contribution of each component: (a) timber sleeper and (b) concrete sleeper.

Figures 6.20 and 6.21 present the front and top views of the contact force distributions, illustrating the force chains in the ballast layer of the tracks and the visualisations for the

different fouling conditions when the lateral displacement of the sleeper reaches 2 mm. It should be noted that the ballast layer contact forces are shown for the full longitudinal width of the ballast with no concern about the ballast particles in the front obstructing the view of the ballast particles in the back. The darker and thicker areas represent the larger contact forces between particles, while the lighter areas represent a lower ballast particle contact force. In the figures, the sleeper is pushed from the left to the right, so the particle contact forces are concentrated on the right ends. It is obvious that the larger contact force areas result in a better support condition or resistance, while the lighter areas represent insufficient support or poor resistance. In accordance, for all the cases analysed, the larger ballast contact forces are observed at the bottom of the sleeper and near the right sleeper end, while the ballast around the crib area has less contact forces than the ballast below the sleeper and the ballast shoulder. The contact force chain intensities for the track with the timber sleeper are generally less than those for the concrete sleeper. To counter the sleeper movement, the clean ballast case has the highest contact forces between the ballast particles and is followed by those of the 100-mm fouled, 200-mm fouled, and fully fouled, respectively; therefore, the clean ballast layer can better restrain the sleeper movement. This trend is similar for both the timber and the concrete sleeper cases. In other words, the more severe the fouling conditions are, the lesser are the contact forces, and the ballast particles provide lower lateral resistance for the sleeper movement. In summary, when the ballast is degraded and fouling starts to accumulate from the bottom-up, the ballast support becomes considerably less sufficient to provide the required lateral restraint to arrest the movement of the sleeper.

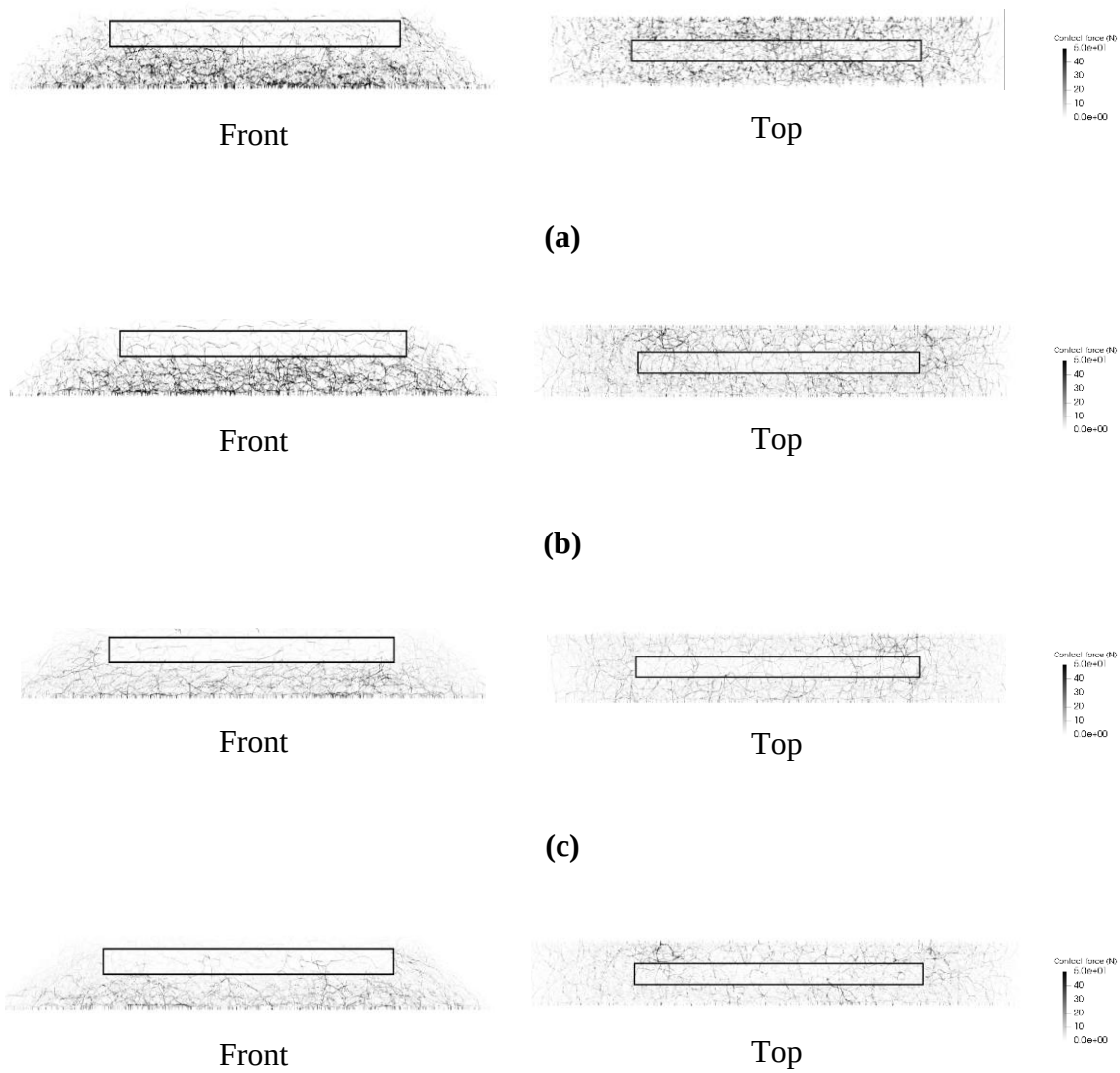

Figure 6.20 Contact force chain of ballast layer with timber sleeper with different conditions: (a) clean ballast, (b) 100-mm fouled ballast, (c) 200-mm fouled ballast, and (d) fully fouled ballast.

Front Top

(a)

Front Top

(b)

Front Top

(c)

Front Top

(d)

Figure 6.21 Contact force chain of ballast layer with concrete sleeper with different conditions: (a) clean ballast, (b) 100-mm fouled ballast, (c) 200-mm fouled ballast, and (d) fully fouled ballast.

6.6 Summary

This chapter presents the DEM simulation of STPTs considering the ballast fouling conditions. Note that the study of the effect of the ballast fouling condition on a track's lateral vulnerability has not been conducted in the past. The coal dust is represented as a finer material or fouling agent filling in the voids to represent the fouling conditions of the ballast layer. In the simulation, the fouled ballast layer is created by adopting the DEM contact parameters based on the assumption that each particle interaction has less friction. The DEM parameters for the fouled ballast layer have been calibrated previously against the direct shear and triaxial tests of the fouled ballast. Fouling is considered to start from the bottom of the ballast layer in different zones and is applied all the way to the top to represent the completely fouled ballast layer condition. According to the findings, the sleeper base plays a significant role in the lateral resistance, particularly for heavier and larger sleepers such as concrete sleepers. The results show that ballast fouling significantly reduces the lateral resistance of the ballasted track even if the fouled ballast is observed in the bottom layer where there is no contact to the sleeper. The ballast fouling condition can reduce the lateral resistance by up to approximately 48% for the timber sleepers and 64% for the concrete sleepers if the ballast layer is fully fouled. This is the new insight that has never been reported elsewhere.

In accordance, a depth profile fouling investigation of the ballast layer is therefore very important, as the ballast fouling conditions, often unseen or noticed from the ballast surface, can undermine the lateral stability of a railway track. This might shift the buckling failure mode from snap-through to progressive buckling, because of the reduction in the

lateral resistance in the same track profile, and increase the risk of track buckling. The results will be used further in Chapter 7 for the full-track buckling analysis to potentially evaluate the buckling temperature and phenomena of the railway track under these conditions. The study findings are intended to help with the development of the inspection criteria for the ballast lateral resistance and support conditions, to improve the safety and the reliability of the rail network, and mitigate the risk of delays due to the track buckling leading to the unplanned maintenance.

6.7 References

AMERICAN RAILWAY ENGINEERING AND MAINTENANCE-OF-WAY ASSOCIATION 2004. Manual for Railway Engineering.

ANBAZHAGAN, P., BHARATHA, T. P. & AMARAJEEVI, G. 2012. Study of Ballast Fouling in Railway Track Formations. *Indian Geotechnical Journal,* 42**,** 87-99.

FEDERAL RAILROAD ADMINISTRATION 2011. Heavy Axle Load Revenue Service Mudfouled Ballast Investigation. *RESEARCH RESULTS REPORT* U.S. Department of Transportation.

GHABOUSSI, J. & BARBOSA, R. 1990. Three-dimensional discrete element method for granular materials. *International Journal for Numerical and Analytical Methods in Geomechanics,* 14**,** 451-472.

HOU, W., FENG, B., LI, W. & TUTUMLUER, E. 2018. Evaluation of Ballast Behavior under Different Tie Support Conditions using Discrete Element Modeling. *Transportation Research Record: Journal of the Transportation Research Board,* 2672**,** 106-115.

HUANG, H. 2010. *Discrete Element Modeling of Railroad Ballast Using Imaging Based Aggregate Morphology Characterization.* Doctor of Philosophy PhD Thesis, University of Illinois at Urbana-Champaign.

HUANG, H. & TUTUMLUER, E. 2011. Discrete Element Modeling for fouled railroad ballast. *Construction and Building Materials,* 25**,** 3306-3312.

HUANG, H., TUTUMLUER, E. & DOMBROW, W. 2009. Laboratory Characterization of Fouled Railroad Ballast Behavior. *Transportation Research Record: Journal of the Transportation Research Board,* 2117**,** 93-101.

INDRARATNA, B., SU, L. J. & RUJIKIATKAMJORN, C. 2011. A new parameter for classification and evaluation of railway ballast fouling. *Canadian Geotechnical Journal,* 48**,** 322-326.

LICHTBERGER, B. 2007. The lateral resistance of the track. *European Railway Review.* Plasser & Theurer.

MOAVENI, M., WANG, S., HART, J. M., TUTUMLUER, E. & AHUJA, N. 2013. Evaluation of Aggregate Size and Shape by Means of Segmentation Techniques and Aggregate Image Processing Algorithms. *Transportation Research Record: Journal of the Transportation Research Board,* 2335**,** 50-59.

SUSSMANN, T. R., RUEL, M. & CHRISMER, S. M. 2012. Source of ballast fouling and influence considerations for condition assessment criteria. *Transportation Research Record: Journal of the Transportation Research Board***,** 87-94.

ZHAO, D., NEZAMI, E. G., HASHASH, Y. M. A. & GHABOUSSI, J. 2006. Three-dimensional discrete element simulation for granular materials. *Eng Comput* 23**,** 749-70.

CHAPTER 7

INFLUENCES OF BALLAST DEGRADATION ON BALLASTED TRACK BUCKLING

7.1 Introduction

This chapter analyses the buckling temperature and buckling regime for ballasted railway track considering the influences of ballast degradation. The 3D modelling of railway tracks developed in Chapter 5 is used in this chapter. The lateral resistance curves for ballast lateral spring obtained in Chapter 6 are then applied in this chapter to analyse the buckling phenomena of ballasted tracks with the consideration of ballast degradation. Even though the buckling phenomena were previously performed in Chapter 5, the properties and resistances of components of railway tracks were based on parametric studies with no link to the realistic condition of railway ballast. In chapter 6, it was found that the lateral stiffness of ballasted tracks not only depends on ballast layout geometry but also the ballast condition itself. The ballast degradation can potentially undermine the lateral resistance even though the degraded ballast particles are located at the bottom of the ballast layer where there are no direct contacts to the sleeper.

It was previously found that the fouled ballast particles can be accumulated at the bottom layer due to ballast breakdown or outside contamination, and it is well known that this significantly influence track geometry and alignment leading to track degradation (Anbazhagan et al., 2012, Sussmann et al., 2012). It is important to note that ballast fouling can be built up in the ballast profile from the bottom all the way up to the top, representing completely fouled ballast layer (Sussmann et al., 2012). Chapter 6 presented the lateral force of sleeper-ballast contacts against the movement of sleepers, considering the progressive ballast degradation with different levels of ballast fouling. It was found that progressive ballast fouling could progressively reduce the lateral force of sleeper-ballast

contact. The obtained results from Chapter 6, showing lateral force and sleeper displacement, are further used in this chapter as the input curves for lateral springs connected to sleeper ends.

This chapter investigates the buckling phenomena using advanced three-dimensional finite element modelling of ballasted railway tracks based on the assumptions that ballast fouling is accumulated and formed from the ballast base. The conditions of ballast are divided into 4 stages: clean, 100 mm fouled, 200 mm fouled, and completely fouled. This chapter provides new insights regarding the coupled effects of ballast degradation and track misalignment. The buckling temperature and buckling regime are also presented under different actual ballast conditions. The results suggest that the reduction of lateral resistance due to ballast degradation may increase the risk of track buckling significantly. The results with allowable temperature can be mapped with weather forecast to obtain buckling predictions and lateral ballast inspection to properly plan for ballast renewal.

7.2 Modelling

Ballasted railway tracks with the standard gauge, that have been built and validated in Chapters 4-5, are used in this chapter. It should be noted that the properties of track components are based on

Table 7.1 while the lateral spring properties are derived in accordance with the lateral force-displacement of sleepers obtained in Chapter 6. It is noted that the properties are based on the nominal values used previously in normal track conditions. It is important to note that the lateral force-displacement curves are linked to the lateral spring mapping of ballast performances in lateral plane as shown in Figure 7.1. The simplified model, including the

original FEM model with the consideration of ballast fouling conditions, is presented in Figure 7.2. This chapter considers three cases of ballast fouling conditions: 100-mm fouled layer (Figure 7.2a), 200-mm fouled layer (Figure 7.2b) and fully fouled condition (Figure 7.2c).

Table 7.1 Material properties.

Parameter list	Characteristic value	Unit
Rail (UIC60)		
Modulus	2×10^5	MPa
Density	7850	kg/m^3
Poisson's ratio	0.25	
Thermal expansion	1.17×10^{-5}	1/°C
Timber sleeper [150x250x2600mm]		
Modulus	1.60×10^4	MPa
Shear modulus	3.93×10^3	MPa
Density	1100	kg/m^3
Poisson's ratio	0.2	
Torsional fastening resistance	225	kNm/rad
Concrete sleeper [235x260x2600mm]		
Modulus	3.75×10^4	MPa
Shear modulus	1.09×10^3	MPa
Density	2740	kg/m^3
Poisson's ratio	0.2	
Torsional fastening resistance	75	kNm/rad

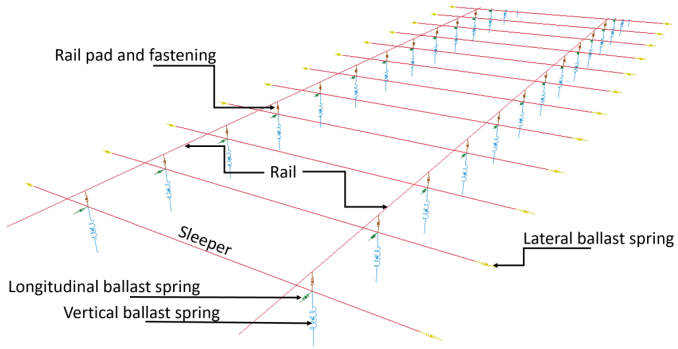

(a)

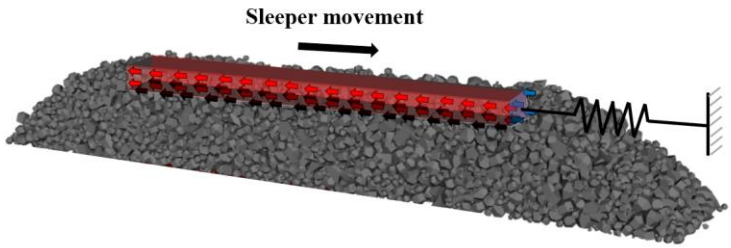

(b)

Figure 7.1 (a) Finite Element modelling of ballasted railway track (b) Nonlinear lateral ballast spring representing sleeper-ballast lateral resistance.

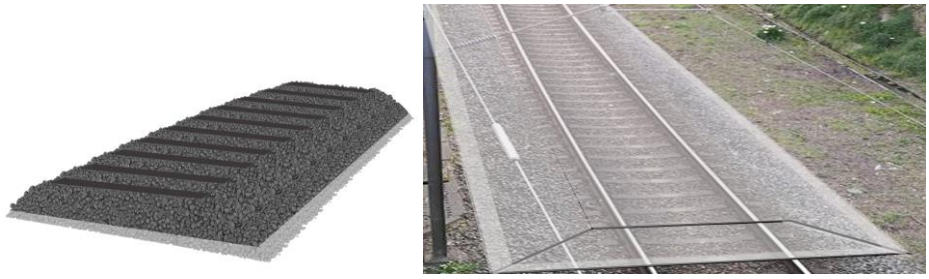

(a)

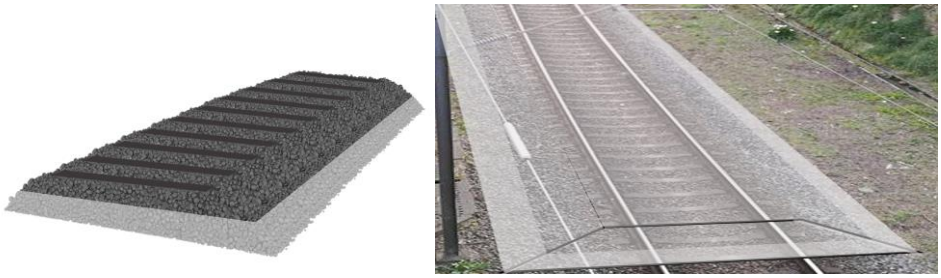

(b)

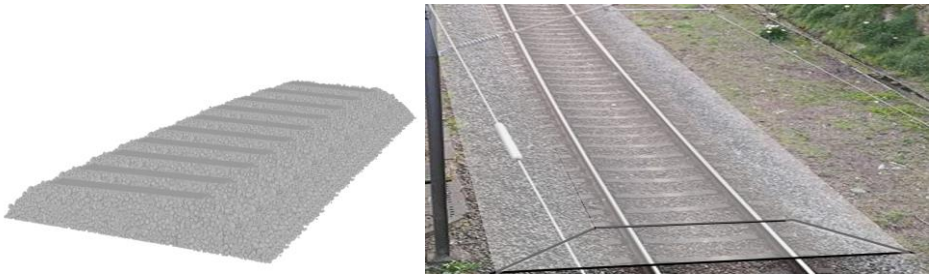

(c)

Figure 7.2 Ballast fouling conditions: (a) 100 mm fouled layer (b) 200 mm fouled layer (c) fully fouled.

7.3 Simulation Approach

In the nonlinear buckling analysis, the solution method uses the nonlinear approach with the BFGS quasi newton algorithm in LS-DYNA. This iterative method is used for solving unconstrained nonlinear optimisation problems. Linear analysis is not considered in this chapter as this approach disables nonlinear properties to be used while the lateral curves obtained in Chapter 6 are highly nonlinear. Hence, this chapter considers only nonlinear buckling analysis for simulations. This approach is more accurate than linear analysis since it includes the nonlinearities and covers both pre- and post-buckling of a structure. It should be noted that this approach must include structural imperfections in the model to be able to theoretically buckle railway tracks. The initial misalignments of between 8 and 32 mm are applied to the rails at mid-tracks. It is noted that the allowable misalignment can be over

30 mm depending on class of track (CRC for Rail Innovation, 2009, Federal Railroad Administration (FRA), 2010).

According to previous STPT simulations on ballast lateral resistance in Chapter 6, load-displacement curves have been obtained. It should be noted that the original curves can be fitted well with bilinear curves as presented in Figure 7.3 for both timber and concrete sleepers. The displacement limit, which is the inflection of stiffness, is set as 0.5mm as it can be clearly detected as a yield point. The original curves are fitted with bilinear curves using the linear polynomial fit method. The equations obtained for lateral force-displacement curves representing linear properties of lateral springs are presented in Table 7.2. It is found that both initial and secondary stiffness tend to be smaller when ballast is heavily fouled.

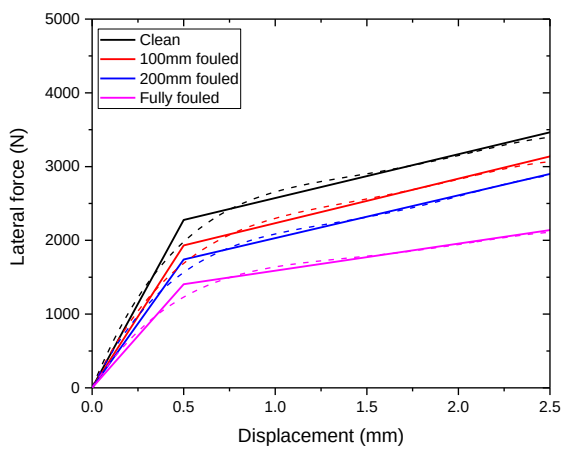

(a)

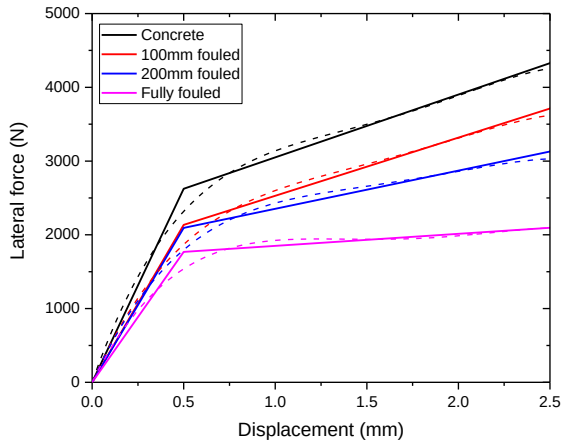

(b)

Figure 7.3 Lateral force-displacement curve for: (a) Timber sleepers (b) Concrete sleepers.

Table 7.2 Lateral force-displacement equations.

Case	Timber	Concrete
Clean	x<0.0005: 4553691x x≥0.0005: y = 1980+593691x	x<0.0005: 5264000x x≥0.0005: y = 2197+852224x
100 mm fouled	x<0.0005: 3861480x x≥0.0005: y = 1629+603480x	x<0.0005: 4270000x x≥0.0005: y = 1740+788404x
200 mm fouled	x<0.0005: 3479527x x≥0.0005: y = 1450+579527x	x<0.0005: 4184000x x≥0.0005: y = 1834+517878x
Fully fouled	x<0.0005: 2809340x x≥0.0005: y = 1221+367340x	x<0.0005: 3538000x x≥0.0005: y = 1687+163138x

y = lateral force (N), x = lateral displacement of sleeper (m)

A temperature of 200 °C is applied to the system using the keyword LOAD_THERMAL_LOAD_CURVE in LS-DYNA. The thermal expansion is applied to

the rails using the keyword MAT_ADD_THERMAL_EXPANSION. The following parameters also are considered.

- Fouling area of ballast represented by unconstrained length: 6-30 m
- Initial track misalignment (imperfection): 8-32 mm.
- Lateral ballast resistance considering 4 scenarios: Clean ballast, 100 mm fouled ballast, 200 mm fouled ballast and fully fouled ballast.

7.4 Results and Discussions

7.4.1 Buckling temperature

Firstly, buckling temperature (T_{max}) is analysed considering different unconstrained lengths and ballast conditions. The results are presented together with maximum rail buckling force at the temperature that can buckle railway tracks. Figure 7.4 presents the buckling temperature over neutral and rail axial force of ballasted track with timber sleepers. Considering the unconstrained length, the buckling temperatures are compared. The overall results show that railway tracks are generally buckled within the same ranges when the unconstrained length is larger than 18 m whereas railway tracks with 6 m and 12 m unconstrained lengths of 6 m and 12 m are clearly buckled with much higher temperature. As for the track with unconstrained lengths of 6 m and 12 m, the buckling temperature for all ballast conditions have different trends depending on the initial misalignment amplitude. It is found that buckling temperature of track with 6 m unconstrained length is lower than that with 12 m unconstrained length when the misalignment is equal to 8 mm (Figure 7.4a) while in other cases (Figure 7.4b-7.4d),

railway tracks with 6 m unconstrained length tend to buckle later that that with 12 m unconstrained length. This is because the effects of unconstrained length on the misalignment curves since the track with 6-m unconstrained length tends to be the curved track instead of straight track that can largely reduce the stability and buckling temperature. This implies that the further use of the unconstrained length method for spot replacement optimisation should be proposed on the straight track to maximise the benefit of the spot replacement method. As for misalignment, larger initial track misalignments yield a lower buckling temperature. The buckling temperature of railway tracks with unconstrained length of 12 m tends to be smaller when the initial misalignment becomes larger. More importantly, progressive ballast degradation has a significant effect in reducing buckling temperature. It is observed that buckling temperatures of railway tracks with partially fouled ballast are lower than those with clean ballast. However, there is no significant change in buckling temperature when fouled ballast is accumulated from 100 mm to 200 mm. On the other hand, the buckling temperature drops suddenly when the ballast is fully fouled that includes ballast crib and shoulder. This is due to the fact that, for the partially fouled ballast conditions, the fouled ballast is located at the bottom layer which is not directly contacted to the sleeper bottom showing the quite close trend in buckling temperatures for the cases of partially fouled of 100 mm and 200 mm. These trends can be clearly seen in concrete sleeper so the contribution of the bottom sleeper is greater than other parts (Figure 7.5).

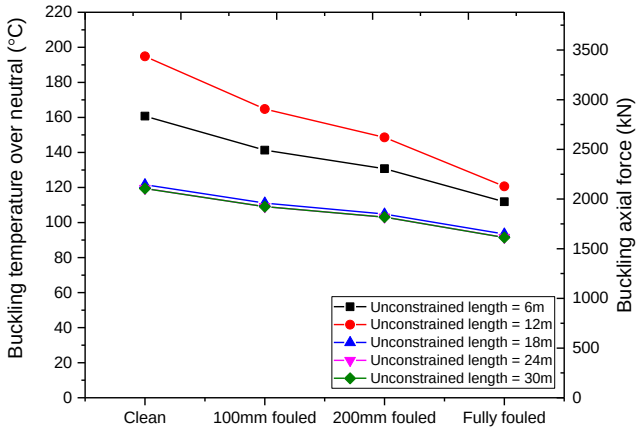
Buckling temperature over neutral (°C)
Buckling axial force (kN)
Clean
100mm fouled
200mm fouled
Fully fouled
Unconstrained length = 6m
Unconstrained length = 12m
Unconstrained length = 18m
Unconstrained length = 24m
Unconstrained length = 30m

(a)

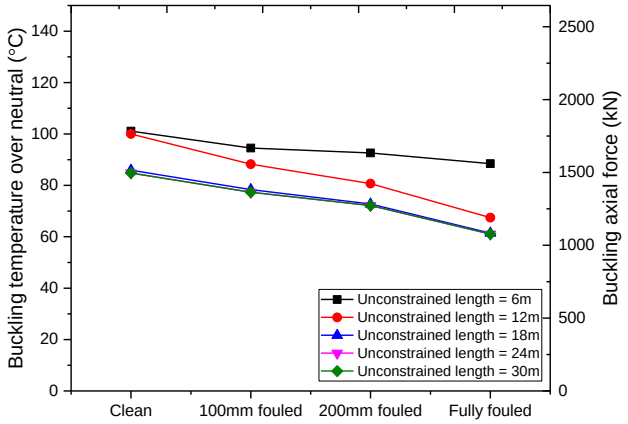
Buckling temperature over neutral (°C)
Buckling axial force (kN)
Clean
100mm fouled
200mm fouled
Fully fouled
Unconstrained length = 6m
Unconstrained length = 12m
Unconstrained length = 18m
Unconstrained length = 24m
Unconstrained length = 30m

(b)

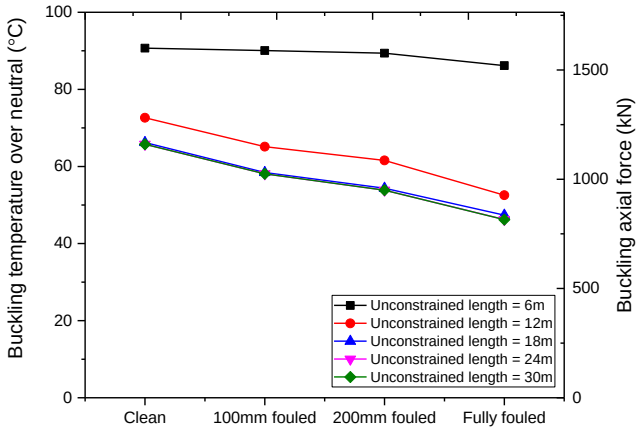

(c)

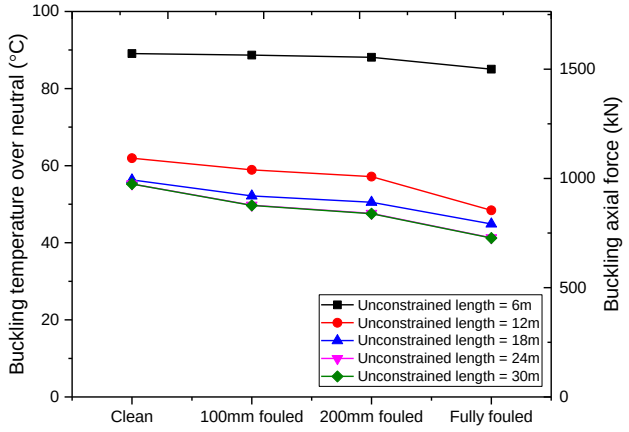

(d)

Figure 7.4 Buckling temperature over neutral and buckling axial force of railway tracks with timber sleepers: (a) misalignment = 8 mm (b) misalignment = 16 mm (c) misalignment = 24 mm (d) misalignment = 32 mm.

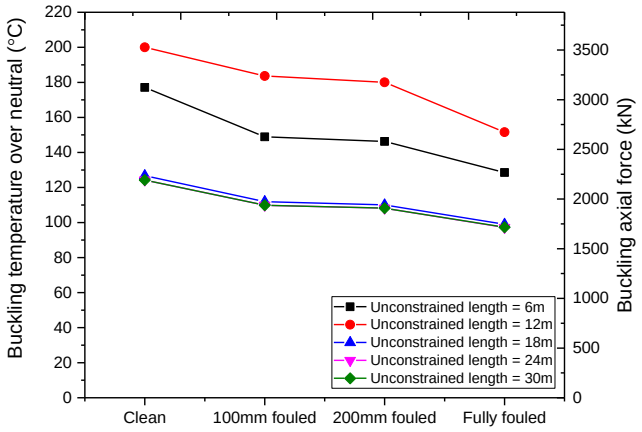
Buckling temperature over neutral (°C)
Buckling axial force (kN)
0
20
40
60
80
100
120
140
160
180
200
220
0
500
1000
1500
2000
2500
3000
3500
Clean
100mm fouled
200mm fouled
Fully fouled
Unconstrained length = 6m
Unconstrained length = 12m
Unconstrained length = 18m
Unconstrained length = 24m
Unconstrained length = 30m

(a)

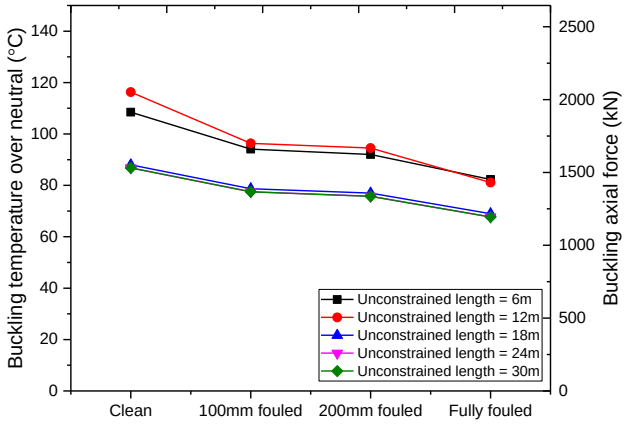
Buckling temperature over neutral (°C)
Buckling axial force (kN)
0
20
40
60
80
100
120
140
0
500
1000
1500
2000
2500
Clean
100mm fouled
200mm fouled
Fully fouled
Unconstrained length = 6m
Unconstrained length = 12m
Unconstrained length = 18m
Unconstrained length = 24m
Unconstrained length = 30m

(b)

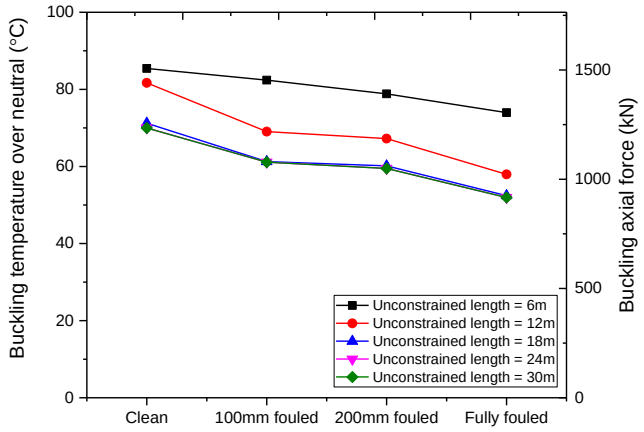

(c)

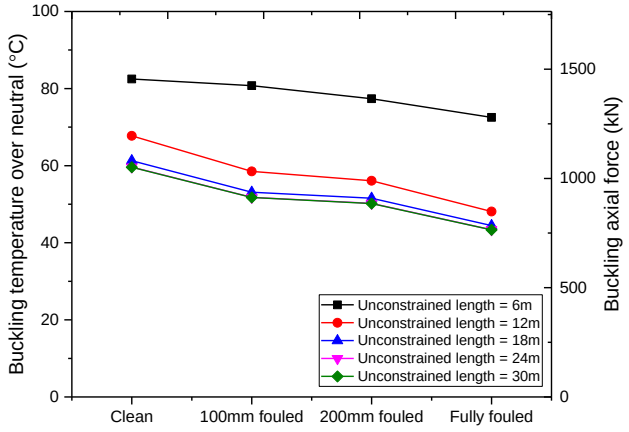

(d)

Figure 7.5 Buckling temperature over neutral and buckling axial force of railway tracks with concrete sleepers (a) misalignment = 8 mm (b) misalignment = 16 mm (c) misalignment = 24 mm (d) misalignment = 32 mm.

7.4.2 Rail axial force

The rail axial force over rail temperature of railway tracks with concrete sleepers is presented in this section. It should be noted that maximum axial force, where track buckling

occurs, can be used to detect buckling temperature using the linear relationship equation between axial force and increased temperature. The safe temperature can be calculated in the post-buckling stage. After buckling, if snap-through buckling occurs, the axial force is reduced immediately until it reaches a level where the track excites constantly. After that level, railway track becomes stable. It is noted that the safe temperature can be calculated by drawing a trend line of axial force in the post-buckling stage when the tracks are stable. This can be drawn backward until this line intersects with the rail axial force curve in the pre-buckling stage. The projection of this intersection point is the rail axial force that might buckle the track at minimum or safe temperature. Meanwhile, the axial force of progressive buckling track is not suddenly reduced but progressively reduced, so that the safe temperature cannot be seen, as in snap-through buckling. More information about safe temperature evaluation can be found in Chapter 5.

Figure 7.6 illustrates the rail axial force against the increase in rail temperature of railway tracks with clean ballast considering its unconstrained lengths of 6 m and 30 m, respectively. This figure compares axial force of rails in railway tracks with the misalignment amplitudes between 8 mm and 32 mm. As for track with 6 m unconstrained length, the buckling failure mode can be either progressive or snap-through depending on the size of misalignment (Figure 7.6a). When railway tracks have big size of misalignment (24 mm and 32 mm), buckling failure mode is likely to be progressive mode as there is no sudden drop of axial force after buckling while the snap-though can be observed when track has 8 mm and 16 mm misalignments since the peak and sudden drop in axial force can be clearly detected. In railway tracks with larger unconstrained length (Figure 7.6b), the buckling mode tends to be snap-through buckling failure. For a similar unconstrained

length, rail axial forces for all cases are likely to be the same once the tracks become stable after buckling.

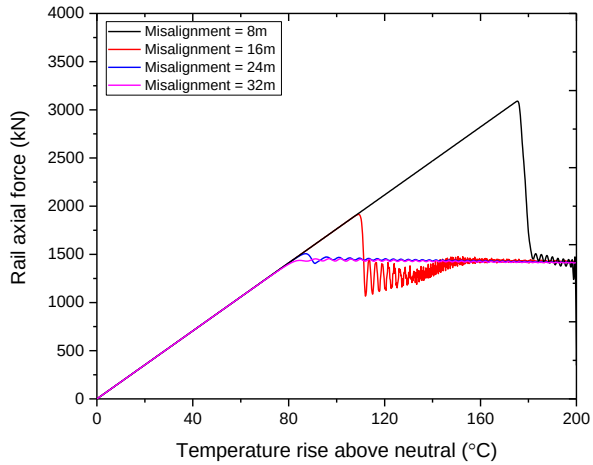

(a)

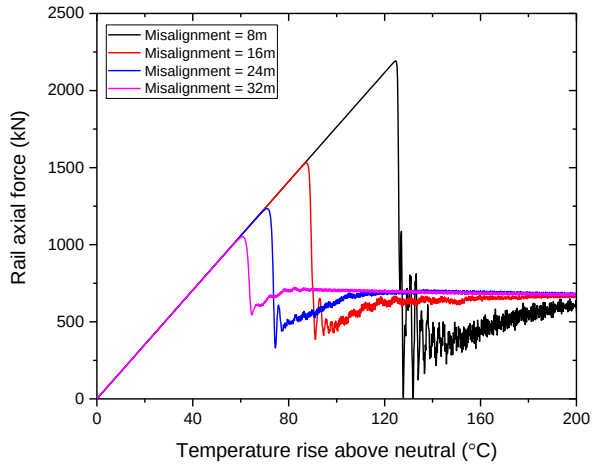

(b)

Figure 7.6 Rail axial force – temperature rise above neutral of tracks with concrete sleepers and clean ballast: (a) 6 m unconstrained length (b) 30 m unconstrained length.

Figure 7.7 compares the rail axial force temperature rise among different unconstrained lengths considering ballast fouling conditions. It is clear that ballast fouling also has a significant influence in rail temperature reduction in both pre- and post-buckling for all cases especially when the ballast is fully fouled due to the reduction of axial buckling force. Safe temperature is also significantly reduced when ballast is fully fouled, however, safe temperature is not affected much for 100 mm fouled ballast thickness. Moreover, large rail excitations in the post-buckling stage are not observed when the misalignment is large (Figure 7.7b and Figure 7.7d) while they are seen when 8 mm misalignment is considered especially when the unconstrained length of railway tracks is 30 m (Figure 7.7c),

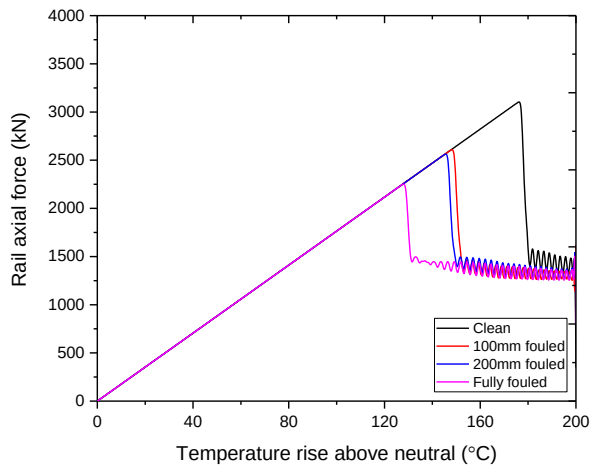

(a)

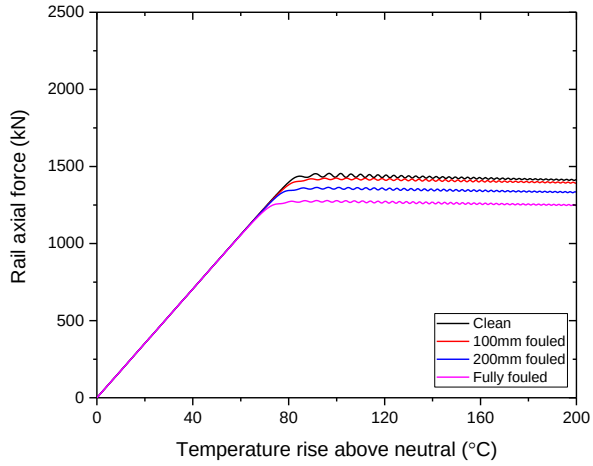
Rail axial force (kN)
Temperature rise above neutral (°C)
Clean
100mm fouled
200mm fouled
Fully fouled

(b)

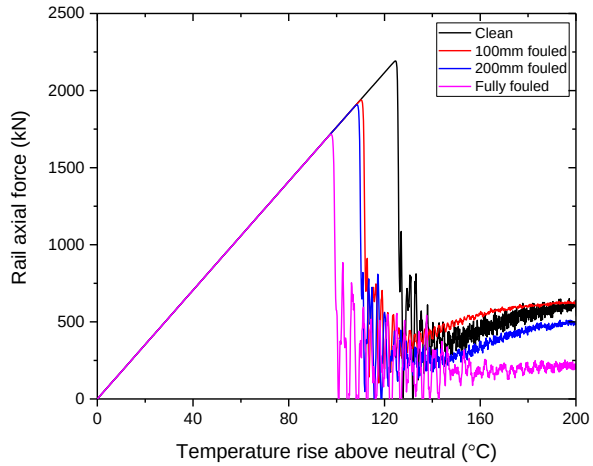
Rail axial force (kN)
Temperature rise above neutral (°C)
Clean
100mm fouled
200mm fouled
Fully fouled

(c)

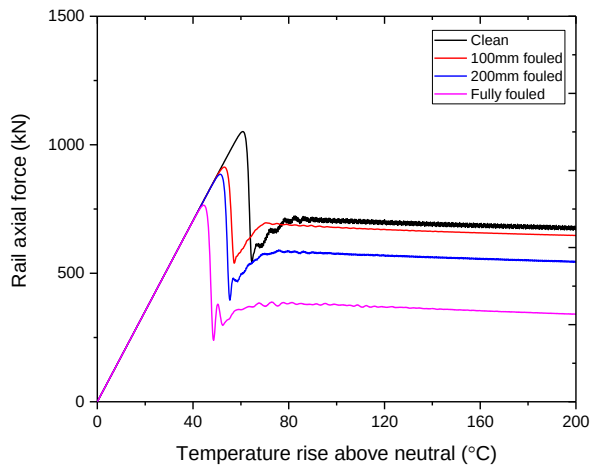

(d)

Figure 7.7 Rail axial force – temperature rise above neutral of tracks considering ballast fouling conditions: (a) 6 m unconstrained length, 8 mm misalignment (b) 6 m unconstrained length, 32 mm misalignment (c) 30 m unconstrained length, 8 mm misalignment (d) 30 m unconstrained length, 32 mm misalignment.

7.4.3 Safety criteria and allowable temperature

Safety criteria of railway track buckling can be determined from the buckling temperature and safe temperature (European Rail Research Institute Committee D202, 1995). The buckling temperature and safe temperature for each railway track condition with timber and concrete sleepers are presented in Figure 7.8 and Figure 7.9, respectively. The graphs provide a clearer classification of buckling failure modes. If both temperatures are clearly separated from each other within the same condition, the snap-through buckling is presented. Meanwhile, progressive buckling is observed when both temperatures are crossed and overlay each other. As seen in Figure 7.8, railway tracks with purely timber sleepers tend to be easily buckled in progressive modes especially when the ballast is fouled. Figure 7.8a illustrates that progressive buckling can occur when the size of

misalignment is larger than 16 mm. In Figure 7.8b-e, it is shown that if the misalignment amplitude is larger than 24 mm, railway tracks with timber sleepers are buckled in progressive buckling mode when ballast is fouled while it is still buckled in snap-through mode when ballast is completely clean. As for railway tracks with concrete sleepers, generally, they tend to be buckled in snap-through mode. However, buckling failure mode can be shifted from snap-through to progressive modes for railway tracks with 6 m unconstrained length when the amplitude misalignment increases to 24 mm as seen in Figure 7.9a. The results confirm those obtained in Chapter 5 that purely timber sleepered tracks have higher safe temperature than purely concrete sleepered tracks due to their higher torsional fastening stiffness while the buckling temperature of timber sleeper tracks are still higher than concrete sleepered tracks. For this reason, timber sleepered tracks are likely to have or close to progressive buckling mode. From both figures, it can be concluded that safe temperature is not affected by track misalignment but largely affected by torsional resistance. Hence, it is recommended to use the stiffest fastener for timber sleeper: elastic fastener and followed by eight spikes per plate, four spikes per plate, and two spikes per plate, respectively.

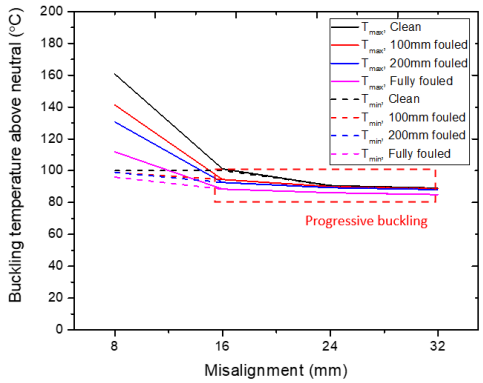

(a)

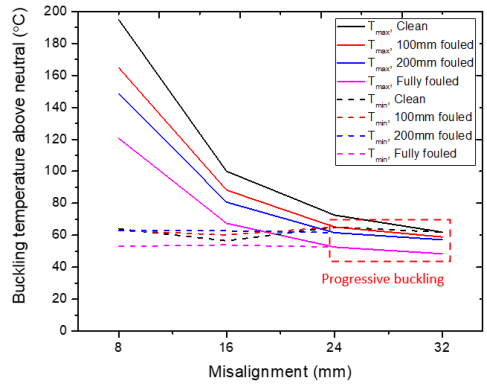

(b)

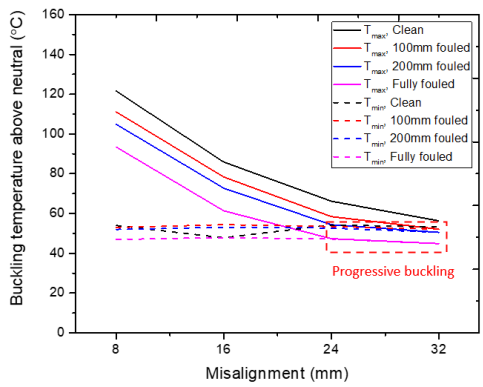

(c)

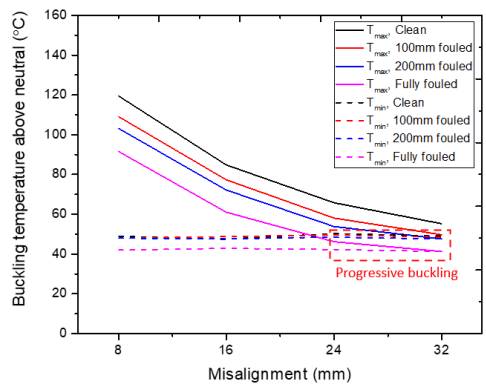

(d)

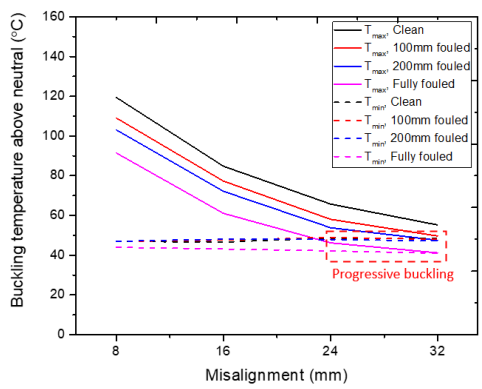

(e)

Figure 7.8 Buckling temperature and safe temperature of railway tracks with timber sleepers: (a) unconstrained length = 6 m (b) unconstrained length = 12 m (c) unconstrained length = 18 m (d) unconstrained length = 24 m (e) unconstrained length = 30 m.

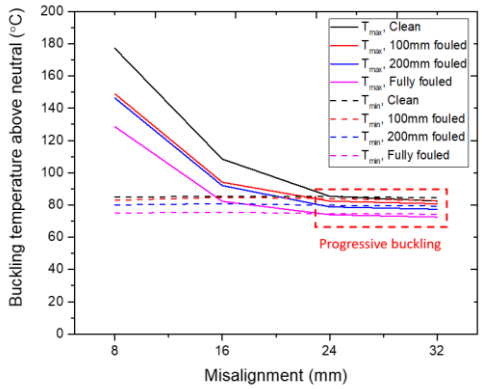

(a)

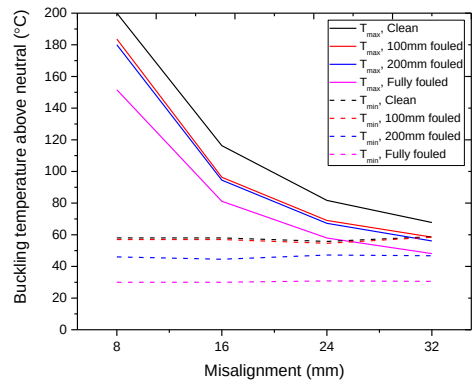

(b)

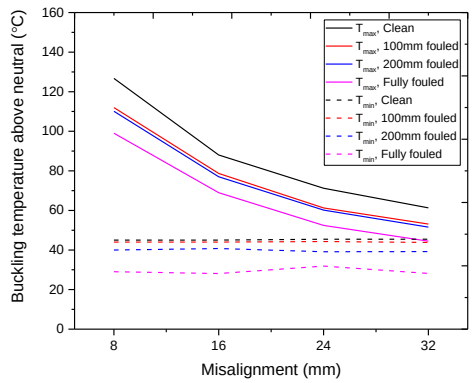

(c)

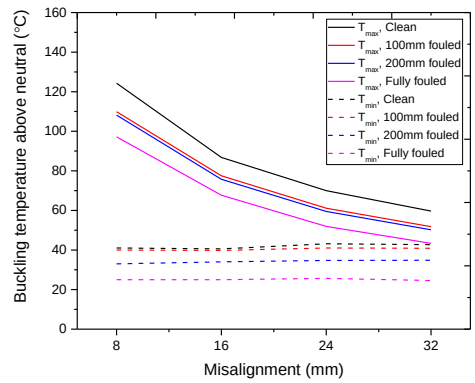

(d)

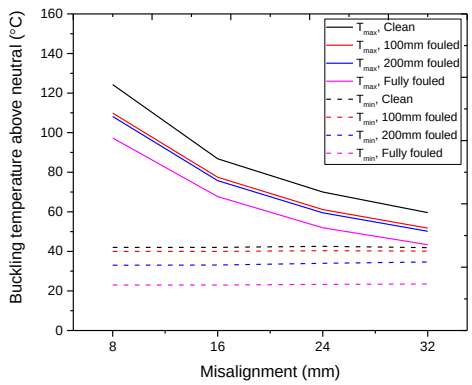

(e)

Figure 7.9 Buckling temperature and safe temperature of railway tracks with concrete sleepers: (a) unconstrained length = 6 m (b) unconstrained length = 12 m (c) unconstrained length = 18 m (d) unconstrained length = 24 m (e) unconstrained length = 30 m.

The allowable temperature above neutral (T_{all}), can be evaluated using Table 3.1 in Chapter 3. It should be noted that the different buckling criteria present different formulas for allowable temperature calculation based on ΔT or buckling failure modes which are largely relevant to safe temperature.

The allowable temperature rises over neutral for railway tracks with timber and concrete sleepers are shown in Figure 7.10 and Figure 7.11, respectively. It is clearly seen that fouled ballast can significantly reduce the allowable temperature, which increases the likelihood of track buckling. However, allowable temperature of railway tracks with timber sleepers seems to be higher than those with concrete sleepers even though buckling temperature of those with timber sleepers is lower. This is because allowable temperature is calculated mostly based on safe temperature, which is significantly influenced by torsional resistance, especially when the difference between buckling and safe temperature is low. However, the difference between T_{max} and T_{min} for concrete sleeper is much higher than timber sleeper so that more buckling energy is needed to buckle the concrete sleepered at the safe temperature level. Moreover, the allowable temperature of degraded ballasted tracks is significantly lower than railway tracks with clean ballast where snap-through buckling can occur. Moreover, high misalignment coupled with fouled ballast that occurs in the larger area can greatly reduce the allowable temperature leading to more risk to buckling. It is important to note that the allowable temperature can be lower than 30 °C which can be usually observed in summer. For this reason, train speed on degraded railway tracks should be limited in summer to avoid the additional energy that can increase the risk of track buckling especially on timber sleepered tracks. Meanwhile, on unloaded track, railway tracks with purely timber sleepers are at more risk of track buckling.

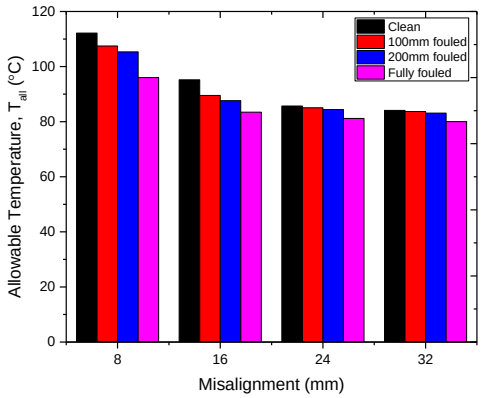

(a)

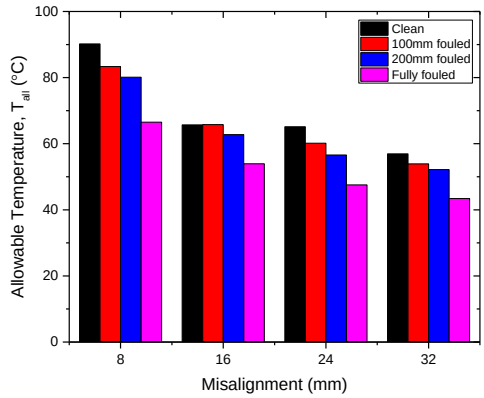

(b)

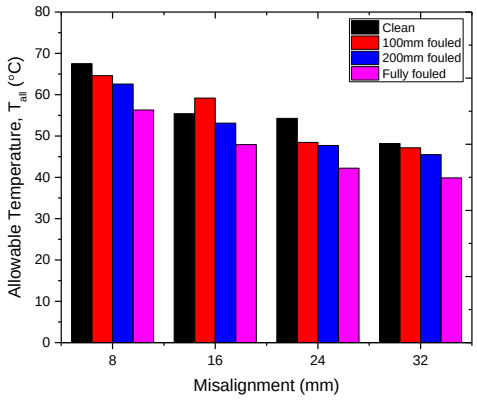

(c)

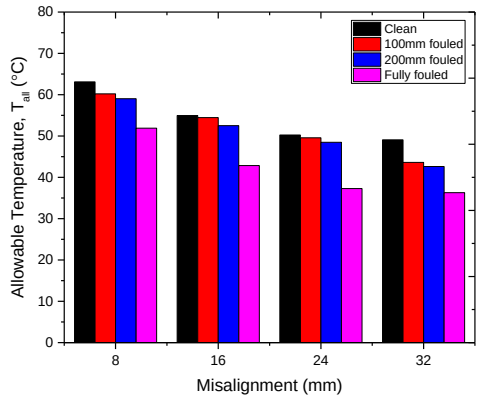

(d)

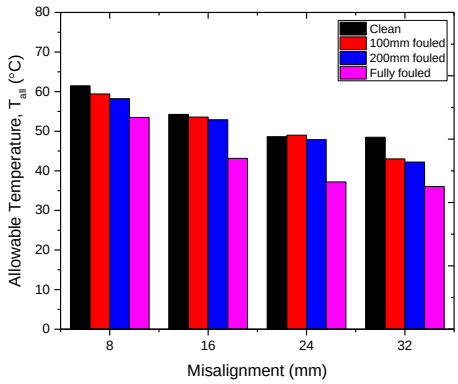

(e)

Figure 7.10 Allowable temperature rise of railway tracks with timber sleepers: (a) unconstrained length = 6 m (b) unconstrained length = 12 m (c) unconstrained length = 18 m (d) unconstrained length = 24 m (e) unconstrained length = 30 m.

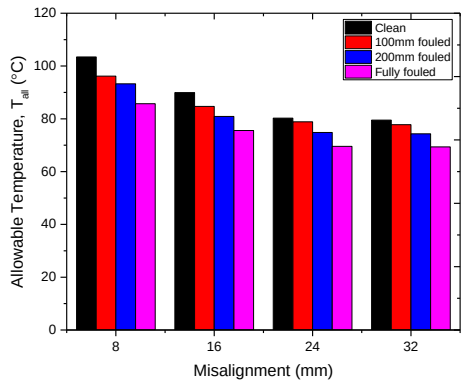

(a)

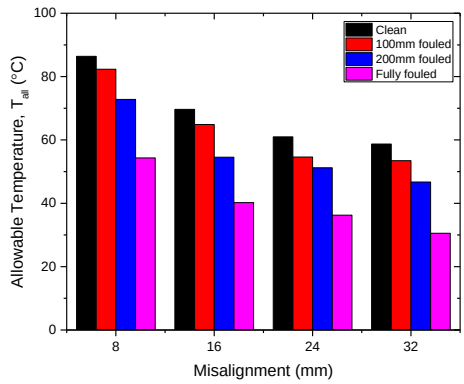

(b)

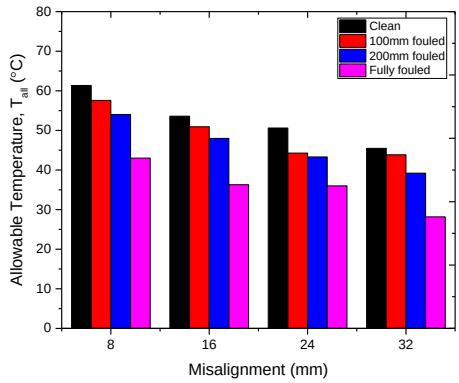

(c)

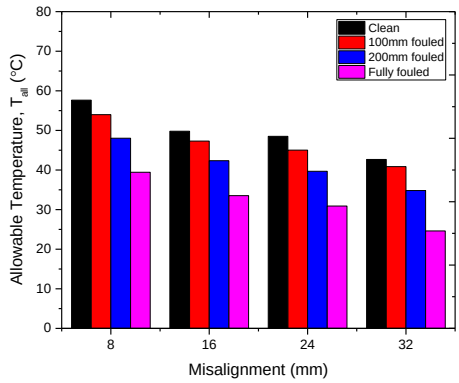

(d)

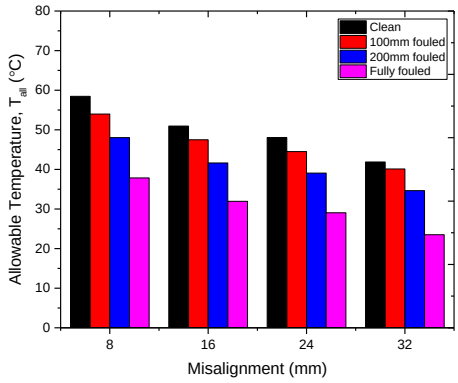

(e)

Figure 7.11 Allowable temperature rise of railway tracks with concrete sleepers: (a) unconstrained length = 6 m (b) unconstrained length = 12 m (c) unconstrained length = 18 m (d) unconstrained length = 24 m (e) unconstrained length = 30 m.

7.5 Summary

This chapter presents the 3D finite element models previously developed in Chapter 4 combined with the lateral spring properties obtained in Chapter 5. It aims at investigating the buckling behaviour of ballasted railway tracks considering the progressive ballast degradation. The lateral resistance curves obtained from previous simplified DEM simulations at different stages of ballast conditions have been applied as an input at sleeper ends for track buckling analysis. The following are the new insights from this chapter.

- Reducing the unconstrained length to 12 m or 20 spans can potentially reduce the risk of track buckling for all ballast conditions. The results show an agreement with the recommended approach in Chapter 4. This finding can help optimise the proper strengthening method for buckling strength by restraining the sleeper at optimised spans.

- Generally, snap-through buckling occurs with high temperature especially for ballasted track with new clean ballast. Nevertheless, in the same track profile, the buckling failure mode can be shifted from snap-through to progressive when a track is progressively degraded including larger track lateral misalignment and ballast fouling conditions. This progressive degradation can significantly reduce the allowable temperature.

- The risk of track buckling is far greater for railway tracks with fouled ballast conditions even if the fouled ballast is hidden in the bottom layer where there is no direct contact to sleeper. This illustrates that buckling strength of ballast track is reduced over time due to the progressive degradation of ballast leading to buckling.

- When the ballast layer is completely fouled, the allowable temperature of rails falls between 20 °C and 30 °C. This clearly shows that track buckling can occur during summer when the temperature can hit this level.

This study confirms that inspection of ballast profile is essential even though ballast condition seems to be good according to a visual inspection, as the hidden degraded ballast in the bottom layer can still undermine the buckling strength, resulting in increasing vulnerability to track buckling. The insights will enhance the inspection of ballast conditions in railway systems and mitigate the risk of delays due to unplanned maintenance, thus paving a robust pathway for a practical impact on societies.

It is obvious that the ballast fouling can result in a significant reduction of the buckling strength. Hence, prevention of ballast breakage, which is a major cause of ballast fouling, is essential. Next chapter will study the effects of Under Sleeper Pads (USPs), which is a resilient material attached underneath the sleeper, on the dynamic responses of ballasted railway tracks. The performance of USP to reduce stress on the ballast will be investigated.

7.6 References

ANBAZHAGAN, P., BHARATHA, T. P. & AMARAJEEVI, G. 2012. Study of Ballast Fouling in Railway Track Formations. *Indian Geotechnical Journal,* 42**,** 87-99.

CRC FOR RAIL INNOVATION 2009. Track Stability Management – Literature Review: Theories and Practices Brisbane, Australia: CRC for Rail Innovation

EUROPEAN RAIL RESEARCH INSTITUTE COMMITTEE D202 1995. Improved knowledge of forces in CWR track (including switchws). *Report2, review of existing experimental work in behaviour of CWR track.* Utrecht, Netherlands: European Rail Research Institute

FEDERAL RAILROAD ADMINISTRATION (FRA) 2010. Continuous welded rail (CWR); general. Federal Railroad Administration (FRA).

SUSSMANN, T. R., RUEL, M. & CHRISMER, S. M. 2012. Source of ballast fouling and influence considerations for condition assessment criteria. *Transportation Research Record: Journal of the Transportation Research Board***,** 87-94.

CHAPTER 8

UNDER SLEEPER PADS (USPs)

SUBJECTED TO EXTREME IMPACT LOADING

8.1 Introduction

At present, there are many types of resilient materials used in railway systems, such as rail pads, Under Ballast Mats (UBMs), and Under Sleeper Pads (USPs) to provide and improve track resilience of ballasted tracks. USPs were initially used back in the 1980s and have been widely developed and used heavily in central Europe, such as in Austria, the Czech Republic and Germany while several countries have carried out pilot trials such as Sweden, Australia, and China. The main objectives of using USPs, that have been recently found, are to moderate track stiffness, and to reduce ground-borne vibrations and ballast breakage. The previous study also initially considered USPs to possibly improve track lateral resistance (Sol-Sánchez et al., 2014). It was found that USPs not only improve load distribution but also increase lateral resistance, showing good performance in improving buckling strength to tackle extreme temperature (Sol-Sánchez et al., 2014). It has been well known that USP can significantly reduce the maintenance cost of ballasted track resulting in economic benefits. It should be noted that previous studies on the dynamic responses using finite element modelling of train-track interaction considering USP have been presented under serviceability conditions (Paixão et al., 2015, Alves Ribeiro et al., 2015). However, in fact, railway tracks may face extreme impact loading especially when excited by a high-speed train travelling over short-pitch rail defects, rail joints, coupled defects or crossings. Moreover, the impact loading can increase to about 1000kN when the short and long wavelength defects are coupled, as evidenced in the paper written by (Kaewunruen and Chiengson, 2018). For instance, 10mm dipped rail joint in depth coupled with 100mm track settlement depth can generate a dynamic factor greater than 7. It is important to note that impact load is the major cause of ballast breakage. It has been evidenced in Chapters

6 and 7 that ballast fouling, which is a consequence of ballast breakdown, significantly undermine lateral resistance of ballasted railway tracks resulting in reduction the buckling and safe temperature of railway tracks. It is obvious that USP can help to redistribute the load on the ballast under static, quasi-static and normal dynamic loads, while this aspect of extreme impact loading has not been investigated in the past. It is interesting to adopt USPs to prevent ballast breakage from extreme impact loading conditions. Hence, this chapter covers the sleeper and ballast behaviours with USP under both serviceability and extreme impact loading conditions. The insights can be used to improve the standard design of USPs for the purposes of ballast breakage prevention and maintaining lateral track resistance.

This chapter thus presents a 3D finite element modelling of prestressed concrete sleepers with USPs using LS-DYNA. A three-dimensional finite element modelling of validated full-scale railway prestressed concrete sleeper, that has been established before in ANSYS (Kaewunruen and Remennikov, 2006b, Kaewunruen and Remennikov, 2008, Kaewunruen and Remennikov, 2007), is extended in LS-DYNA and presented with the insertion of USP. The model is constructed according to the Australian Standard (Standards Australia, 2003a, Standards Australia, 2003b). The calibrated finite element model has been extended to include ballast support and in situ boundary conditions (British Standards Institution, 2016). The impact analysis has been validated against the drop mass impact tests of sleeper with no USP in the past (Kaewunruen and Remennikov, 2007). After the validation with the low-intensity impact load, various cases with different impact loads and USP are then considered. In this study, impact loads of up to 1000kN are applied to the system in order to study the performance of USP under not only serviceability but also extreme cases. The initial velocities of drop mass corresponding to the actual impact loads from drop mass

impact tests are applied to the system to generate different impact events. The dynamic responses of railway concrete sleepers with USPs to high-intensity impact loading conditions are presented in this chapter. This chapter focuses on the sensitivity of impact loads to the dynamic responses of prestressed concrete sleepers and ballast with USP. The dynamic responses including von Mises stress, maximum displacements and accelerations of concrete sleepers and ballast considering various types of USP are highlighted. Additionally, an alternative use of a very stiff USP is proposed for possible use to trade off the benefits and drawbacks of USPs. This study will help track engineers to consider the use of USPs as an insertion element in railway track in areas prone to extreme impact loading.

Figure 8.1 USP glued to the sleeper (Kaewunruen et al., 2017).

8.2 Life Cycle Cost Analysis (LCCA)

The elastic materials, such as rail pads, USPs, UBMs, have advantages mainly in adapting the vertical stiffness of railway track. The other aims of using elastic materials are to attenuate noise and vibration in railway track leading to reducing the maintenance cost of such tracks. These elastic materials can improve track resilience, which is likely to reduce

the annual maintenance cost. However, these elements have a short life span of about 20 years due to the effects of the environment such as temperature, oxidation or hydrolysis (Deutsche Bahn and Hans-Joerg, 2011). In addition, using another elastic material in railway tracks means adding another element causing a significant increase in the initial construction and investment costs. Thus, it is necessary to economically evaluate the long-term effects and the feasibility of using these materials in railway systems.

Life Cycle Cost Analysis (LCCA) (Langdon, 2007) has been introduced to the transportation decision-making process to help evaluate the feasibility and outcome of the projects. The purpose of this method is to evaluate the overall cost for the projects over their lifetime. Hence, this method is adapted to determine the benefit of using USP elements in the long term considering the overall construction and maintenance costs of railway tracks. Moreover, this method has economic effects during the life span of the resilience materials. This section presents an example of LCCA of ballasted railway tracks with and without USPs considering the annual maintenance cost and discount rate.

This study uses previous data on the cost of railway tracks used in Europe from the open literature (Guedelha, 2012) and assumes some parameters related to the UK data for LCCA. The comparisons of initial construction and annual maintenance costs of railway tracks between tracks with and without USPs were described in the research paper written by Guedelha (2012). It is noted that the 700km ballasted track with an axle load of 32T for high-speed trains was considered in that study. The construction cost of this track with and without USPs is shown in Table 8.1. According to the table, the initial construction cost increases by 10% for railway tracks with USPs.

Table 8.1 Initial cost construction (Guedelha, 2012).

Track types	Initial cost per km (€)	Total construction cost (€)
Construction of railway track without USPs	500,000	350,000,000
Construction of USPs only	50,010	35,007,000

Table 8.2 shows the annual maintenance cost of railway tracks with and without USPs. It is interesting to note that using USPs can significantly reduce the maintenance cost by about 50%. The annual depreciation can be also decreased by using USPs. Surprisingly, about €11,083,333 of total cost reduction is noted. In conclusion, even though the construction cost of railway tracks with USPs is relatively high, USPs can significantly reduce annual maintenance cost of railway track. This leads to important long-term cost benefits.

Table 8.2 Maintenance cost.

Cost	Annual maintenance cost (€)
Annual maintenance cost without USPs	17,000,000
Annual maintenance cost with USPs	8,750,000
Annual depreciation cost without USPs	14,000,000
Annual depreciation cost with USPs	11,666,667
Annual maintenance cost reduction	8,750,000
Depreciation cost reduction	2,333,333
Total cost reduction (annual earning)	11,083,000

An example of LCCA in railway systems with USPs is presented based on the data in Table 8.1 and Table 8.2. In this study, the discount rate of 6% is assumed based on UK

data, and this is used to determine the present value of future cash flows (Grout 2003). Two railway tracks, with and without USPs, are compared to determine the long-term outcomes of USPs. It is assumed that only annual maintenance and depreciation costs are taken into consideration. The present values of these projects considering 6% discount rate are presented in Figure 8.2. It is seen that railway track with USP obviously has lower annual maintenance costs, even if the investment cost is higher.

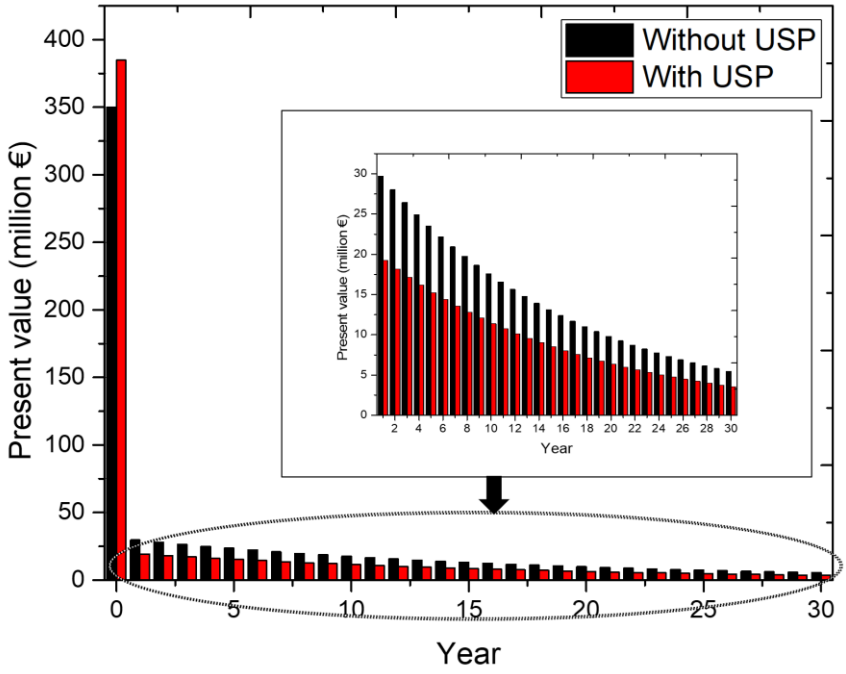

Figure 8.2 Comparison of the annual cost of railway tracks with and without USP.

Figure 8.3 shows the cumulative net present value (NPV) of both projects over 30 years. This shows the cumulative costs of the projects throughout their life cycle, considering construction and maintenance costs. It is observed that there is a crossing point between both projects at about year 3.26, which means that it takes about 3.26 years to compensate

the initial construction cost by using USPs. The NPV of railway track with USPs is slightly offset by a reduction in maintenance cost over time.

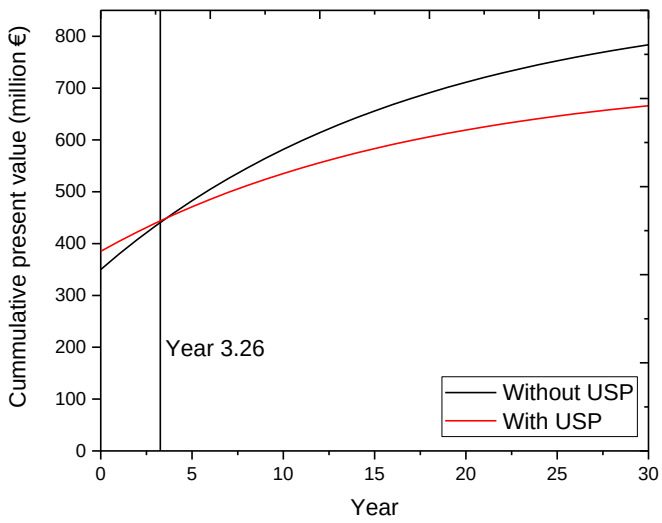

Figure 8.3 Cumulative present values (NPV) of two projects.

8.3 Finite Element Modelling (FEM)

The general-purpose finite element analysis package ANSYS was first used to develop a 3D finite element model of a full-scale railway prestressed concrete sleeper for static analysis. The model of Austrak broad gauge sleeper is built with the dimensions shown in Table 8.3. Concrete was modelled using SOLID65 solid elements where each node has three degrees of freedom (translation in x, y and z). The modulus of elasticity of concrete was estimated based on AS3600 (Standards Australia, 2001) with the compressive strength of 80 MPa (f'_c). As for prestressing wire, LINK8 truss element was considered to withstand the initial strain attributed to prestressing forces, by assuming a perfect bond between these elements and concrete. Note that this truss element cannot resist neither bending moments

nor shear forces. Since bond slip was barely observed under any failure modes of prestressed concrete sleeper (Kaewunruen and Remennikov, You et al., 2019), the perfect bond between pre-stressing wires and concrete was assumed using the shared node method. The 0.2% proof stress is 1,700 MPa and the ultimate stress is 1,930 MPa. The static and dynamic moduli of elasticity of pre-stressing wire are 190,000 MPa. As for the alternative support in the experiments based on Australian standard (Standards Australia, 2003a), the polymeric materials can be used to represent the support condition instead of the real ballast particle. This can equally and uniformly distribute the pressure underneath the sleeper with no effects of particle discontinuities. In this chapter, the ballast support is reasonably represented by 6-layer rubber mat which has been calibrated and proven to be a reasonable alternative method to replicate the actual ballast bed. It was clearly shown that the natural frequencies and corresponding mode shapes of track with ballast bed and 6-layer rubber mat were quite close to each other showing the accuracy of this alternative as ballast support (Kaewunruen, 2007). For dynamic analysis, the original model in ANSYS was then transferred to LS-Dyna with the insertion of USP, as shown in Figure 8.4.

In this model, the support condition is constrained in a vertical direction on the bottom nodes of the rubber mat layer. The contacts between each layer are modelled using *CONTACT_AUTOMATIC_SURFACE_TO_SURFACE which is a contact algorithm establishing contact when one surface penetrates another surface. Note that this contact algorithm provides high accuracy when coarse mesh is defined. It should be noted that mesh convergence analysis has been analysed and it has been found that mesh sizes are between 20mm and 50mm for sleeper depending on the location. The properties of materials are shown in Table 8.4.

After model preparation, USP is inserted between the sleeper and rubber mat layer. Four different types of USPs are considered by applying the bedding modulus to the model. It should be noted that bedding modulus is normally calculated by the relationship between surface pressure (N/mm^2) and deflection (mm) which can be obtained from the experiment. The classification of USP relies on the thickness and elastic modulus which are directly related to bedding modulus. Thus, the elastic modulus of USP is the bedding modulus multiplied by its thickness.

The bedding moduli of USP generally vary from less than 0.10 N/mm^3 (very soft) to 0.35 N/mm^3 (stiff), depending on the type of usage. Note that three main types of USPs - soft, medium stiff, and stiff are first considered. Additionally, a very stiff USP, which has a bedding modulus of $1N/m^3$, is also proposed as an alternative for possible use in the future. In this chapter, the 10 mm USPs are considered for all types.

Table 8.3 Sleeper dimension (Austrack Broad Gauge Sleeper).

Gauge length	Total length	At rail seat (mm)			At mid-span (mm)		
		Top width	Bottom width	Depth	Top width	Bottom width	Depth
160	2.695	224	250	210	224	250	180

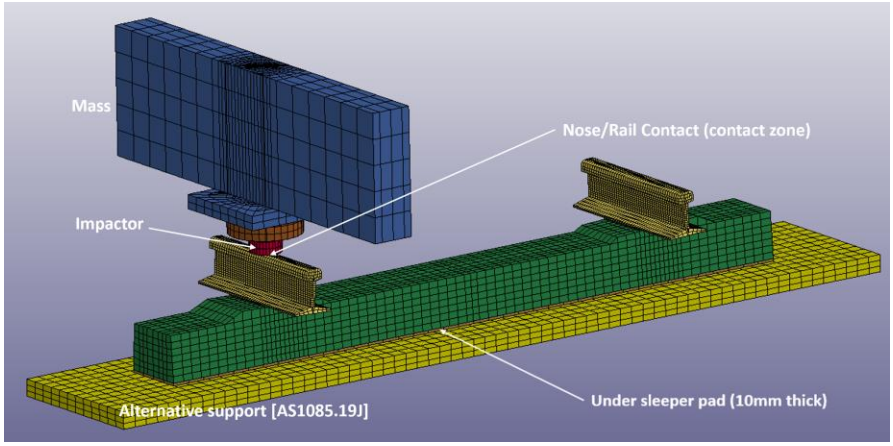

Figure 8.4 Finite element model of sleeper with USP.

Table 8.4 Material properties.

Parameter		Characteristic value	Unit
Rail (UIC60)			
Modulus, E_r		2×10^5	MPa
Poisson's ratio, v_r		0.25	-
Density, d_r		7850	kg/m^3
Concrete sleeper			
Modulus, E_s		3.8×10^4	MPa
Poisson's ratio, v_r		0.2	-
Density, d_r		2400	kg/m^3
HDPE rail pad			
Modulus, E_r		1250	MPa
Poisson's ratio, v_r		0.42	-
Density, d_r		8960	kg/m^3
Under sleeper pad			
Thickness		10	mm
Poisson's ratio, v_r		0.45	-
Density, d_r		1100	kg/m^3
Bedding modulus, C	Soft	0.15	N/mm^3
	Medium stiff	0.25	

	Stiff	0.35	
	Very stiff	1.00	
Rubber mat			
Thickness		60	mm
Modulus, E_s		250	MPa
Poisson's ratio, v_r		0.45	-
Density, d_r		1100	kg/m^3

8.3.1 Model validation

In this study, the extended finite element model was calibrated using vibration data from the impact test results (Kaewunruen and Remennikov, 2006b, Standards Australia, 2001). For verification purposes, the drop height of the mass of 600 kg is 0.1m as a comparison case. The simulation results from FEM are achieved by assigning the initial velocity to the drop mass to generate an impact event, similar to the actual drop tests (Kaewunruen and Remennikov, 2007, Kaewunruen and Remennikov). The initial velocity is applied to the drop mass instead of applying the gravity as this is much more convenient and easier for adaptation than varying the weight of drop mass to generate similar impact forces to the actual tests. The in-situ conditions of railway concrete sleeper are replicated. The accelerations of sleeper at both rail seat and mid span are compared with the experimental results. The validation results are presented in Figure 8.5. It can be seen that the trends of peak acceleration responses are quite close to each other, although there is certain phase difference. It is concluded that this finite element model is acceptable and sufficient for further use in impact response prediction of the prestressed concrete sleeper. The strength of concrete is then tuned to appropriately find the actual value to also compare this with other experimental results obtained from modal tests.

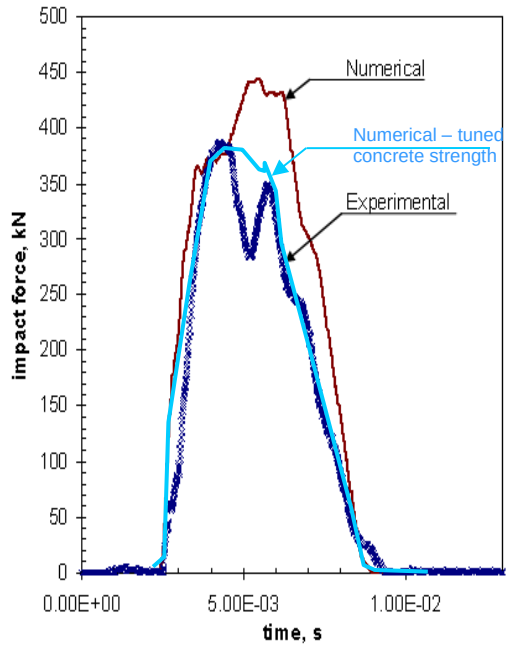

(a)

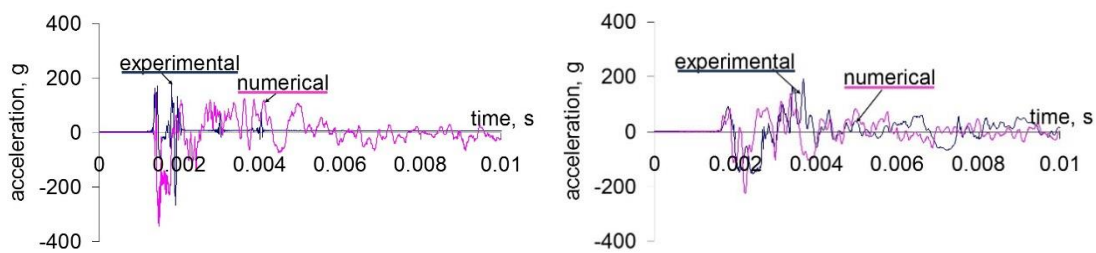

(b)

Figure 8.5 Comparison between numerical and experimental results: (a) contact shock load and (b) acceleration at rail seat (top) and mid-span (bottom).

8.4 Results and Discussions

8.4.1 Mode shapes and frequencies

These sleeper models have been validated against impact tests in Section 8.3.1. Moreover, the vibration characteristics of sleeper models are validated with the impact hammer

excitation technique, which is a non-destructive method to obtain the fundamental mode shapes and corresponding frequencies via frequency response function (Kaewunruen and Remennikov, 2006a). The eigenvalue analysis is used for solving the fundamental mode shapes of sleepers. The free-free condition is considered in both numerical and experimental approaches. The experimental modal analysis using impact hammer excitation technique is used to identify mode shapes and their corresponding frequencies over the frequency range between 0 and 1600 Hz that are believed to cover the fundamental vibration modes. The modal parameters are identified by the Frequency Response Function (FRF) curve which is obtained by the acceleration response of the sleeper with respect to the impact force excited by impact hammer. The signals are processed using DATS modal analysis software. The experimental results show strong agreement with the eigenvalue analysis in finite element analysis with less than 5% difference, as seen in Table 8.5.

Table 8.5 Mode shapes and natural frequencies (dynamic strength, $f'_{c,d}$= 90 MPa).

Mode no.	Mode shapes	Natural frequencies (Hz)		Difference (%)
		Experiment	Numerical	
1	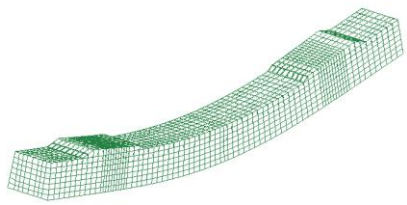 (1st bending)	112.64	107.29	4.75
2	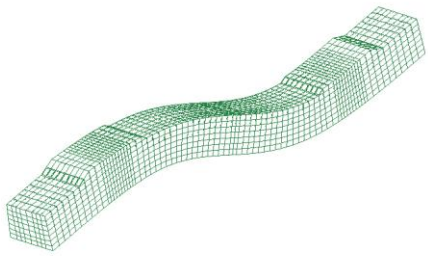 (2nd bending)	312.50	299.46	4.17
3	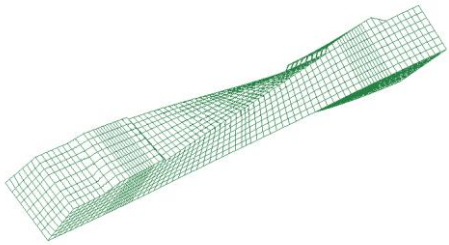 (1st twisting)	436.60	427.45	2.09
4	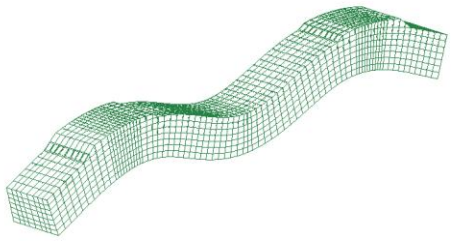 (3rd bending)	605.51	581.52	3.74

8.4.2 Impact loads

In this study, 3 types of typical USPs: soft, medium stiff, and stiff, are considered. It is widely recommended that medium stiff and stiff USPs are used for prolonging the service life of railway track. However, it has been reported that these typical USPs may cause negative effects on railway track especially on sleepers according to the field measurement data (Kaewunruen, 2012). This study proposes a very stiff pad with a bedding modulus of 1N/mm^3, which has never been used in the past. In this analysis, the initial velocities of 0.74 m/s (A), 1.94 m/s (B), and 3.14 m/s (C) of drop mass are applied to generate different impact force intensities on railway sleepers. Figure 8.6 presents the time histories of impact forces triggered by different velocities of drop mass. It is clearly seen that impact forces reduce significantly by about 10% when using USPs. It is interesting to note that pulse duration increases when USP is used because the support becomes softer, resulting in impact energy reduction. By comparing different types of USPs it is clear that the support plays a role in impact responses since the impact magnitude reduces as does overall track stiffness, whilst pulse duration is inversely proportional to the stiffness (Cai, 1994) when softer USP is used. It should be noted that the pulse durations are generally in the range of 3-4 ms. The impulse, which is the integral of force over time, is then calculated and represents the average impact force during collision. The impact forces and impulses of different applied initial velocities to sleepers with and without USP are shown in Table 8.6. It should be noted that despite pulse durations increasing when USPs are used, the impulse significantly decreases since the area under the relationship between force and time decreases as clearly seen in Figure 8.6. It is concluded that the impact event of sleeper vibration with stiffer support can be stopped quicker compared to that with softer support.

Importantly, strain rate plays a significant role in the dynamic problem since the strength of material can increase dramatically resulting in no cracks being observed in sleepers under single impact event. Strain rate can significantly increase the dynamic strength of concrete by about 20% compared to static strength, resulting in higher sleeper capacity (Wakui and Okuda, 1997, Ngamkhanong et al., 2019). Nonetheless, cracks can be seen after applying a number of cycles of impact loads. As this study only considers a single impact event, the linear elastic properties of sleepers are capable for use in this analysis (Kaewunruen and Remennikov, 2009).

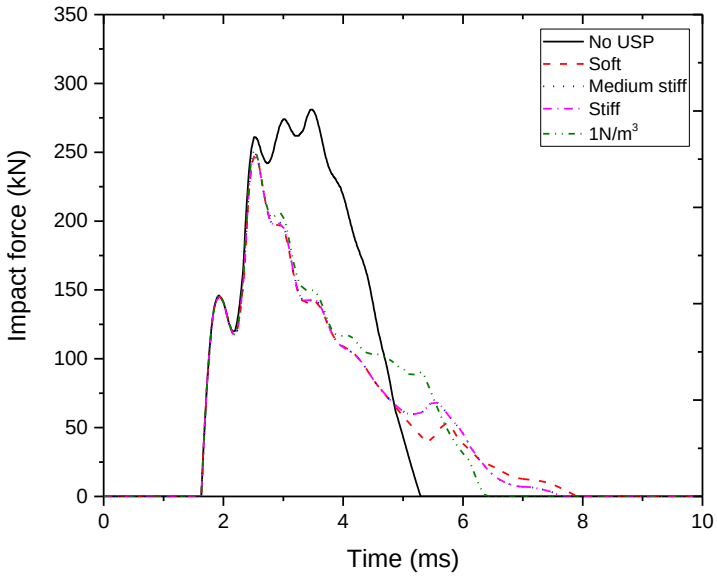

(a)

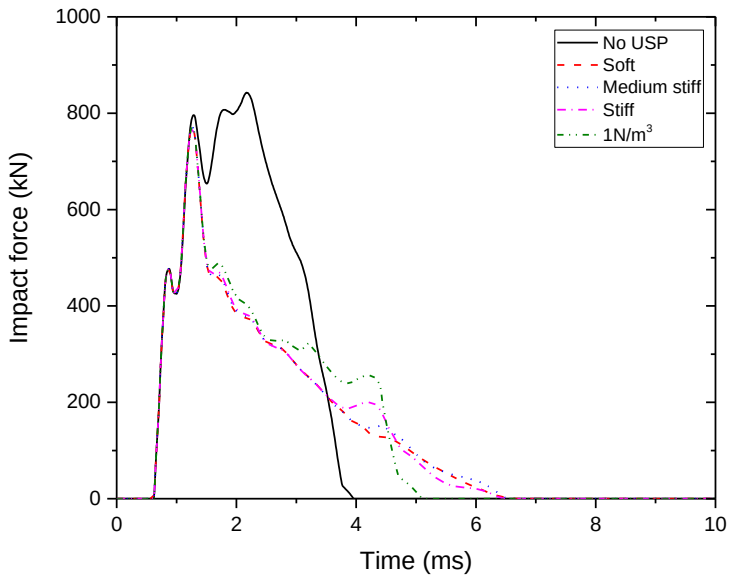

(b)

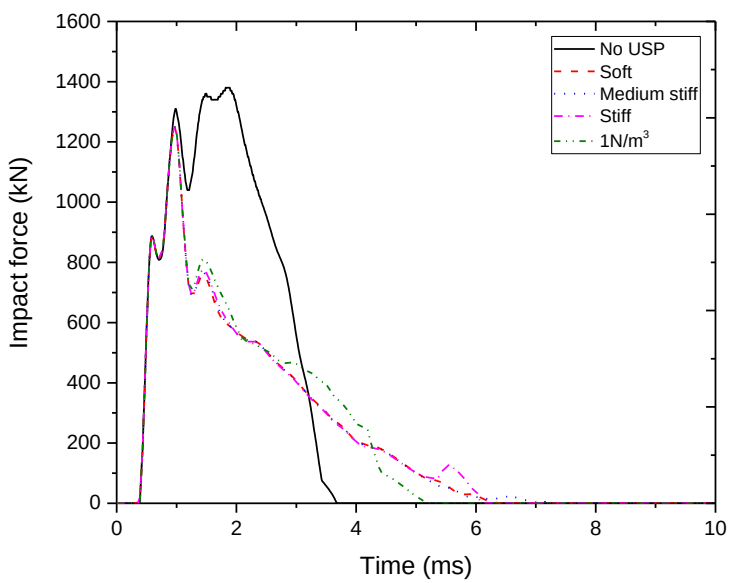

(c)

Figure 8.6 Impact loads of with initial velocities of drop mass of (a) 0.74 m/s (A), (b) 1.94 m/s (B), and (c) 3.14 m/s (C).

Table 8.6 Contact force and impulse.

Case	Initial velocity (m/s)	Contact force (kN)		Reduction (%)	Impulse (kNs)		Reduction (%)
		Without USP	With USP		Without USP	With USP	
A	0.74	288	249	11.43	647	552	14.68
B	1.94	843	772	8.41	1766	1415	19.88
C	3.14	1380	1252	9.31	2888	2291	20.67

8.4.3 Sleeper responses

The comparison of von Mises stress contour caused by the self-weight between sleepers with and without USP is presented in Figure 8.7. Note that von Mises stress is considered to determine the overall response instead of particular component. It can be seen that the stress concentration at soffit of concrete sleepers is less than that with USP especially at rail seat. This shows that USP plays an important role in load distribution along the sleeper length. However, the actual maximum von Mises stress occurs at both top (under the rail surface) and soffit of sleeper at rail seat when the load is applied. Although it is clearly seen in Figure 8.7 that the von Mises stress at soffit can be redistributed and reduced by USPs, the von Mises stress starts increasing slightly on the top of the sleeper after applying load when USP is used.

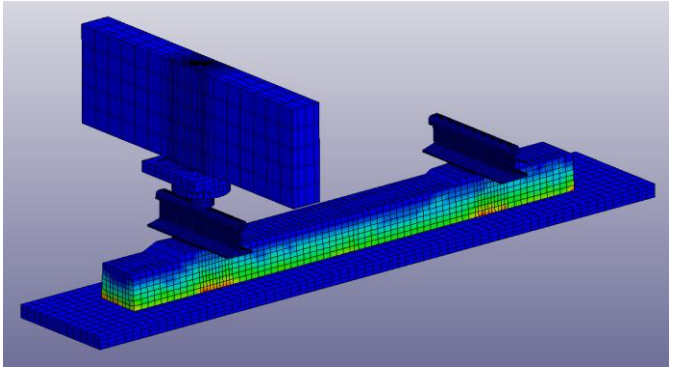

(a)

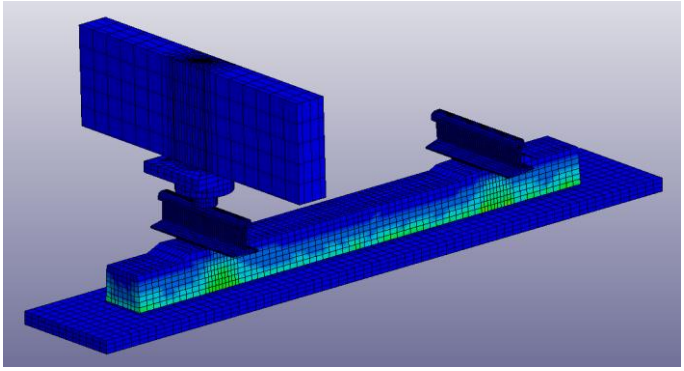

(b)

Figure 8.7 Von Mises stress contour of sleeper: (a) without USP and (b) with USP.

The effects of different types of USPs on the von Mises stress of the prestressed concrete sleepers subjected to extreme impact loads on top of sleeper are presented in Figures 8.8-8.10. The measured element is located on top of sleepers where the maximum stress occurs. It is found that stiff USP results in redistributing the loading area along the sleepers and slightly increases the maximum and overall von Mises stress responses. Moreover, USPs slightly expand the stress contour and extend the impact duration as shown in Figure 8.8. Even though using USP can obviously decrease the contact force and impulse, maximum von Mises stresses of sleeper at both rail seat and mid-span slightly increase when using USP. The configurations of time histories of von Mises stress in Figure 8.8 can be seen in Figure 8.9. It is found that the stress on sleepers without USP disappears much quicker

than that with USP as there is a greater free vibration response after impact loading. Figure 8.10 shows that maximum von Mises stress obtained from time history responses. It is seen that maximum von Mises stress can increase from about 33 MPa to 38 MPa which is around a 14% increase, when USP is used. However, the type of USP does not obviously reflect any significant difference in von Mises stress responses in both rail-seat and mid span. However, a very stiff USP (1 N/mm^3) still has a better overall performance on von Mises stress than other USPs.

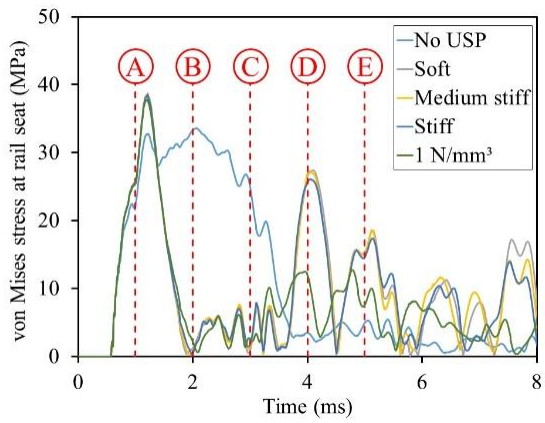

(a)

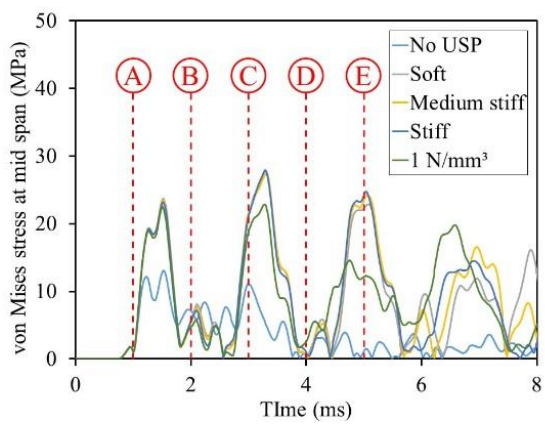

(b)

Figure 8.8 von Mises stress under impact load case C: (a) rail seat and (b) mid span.

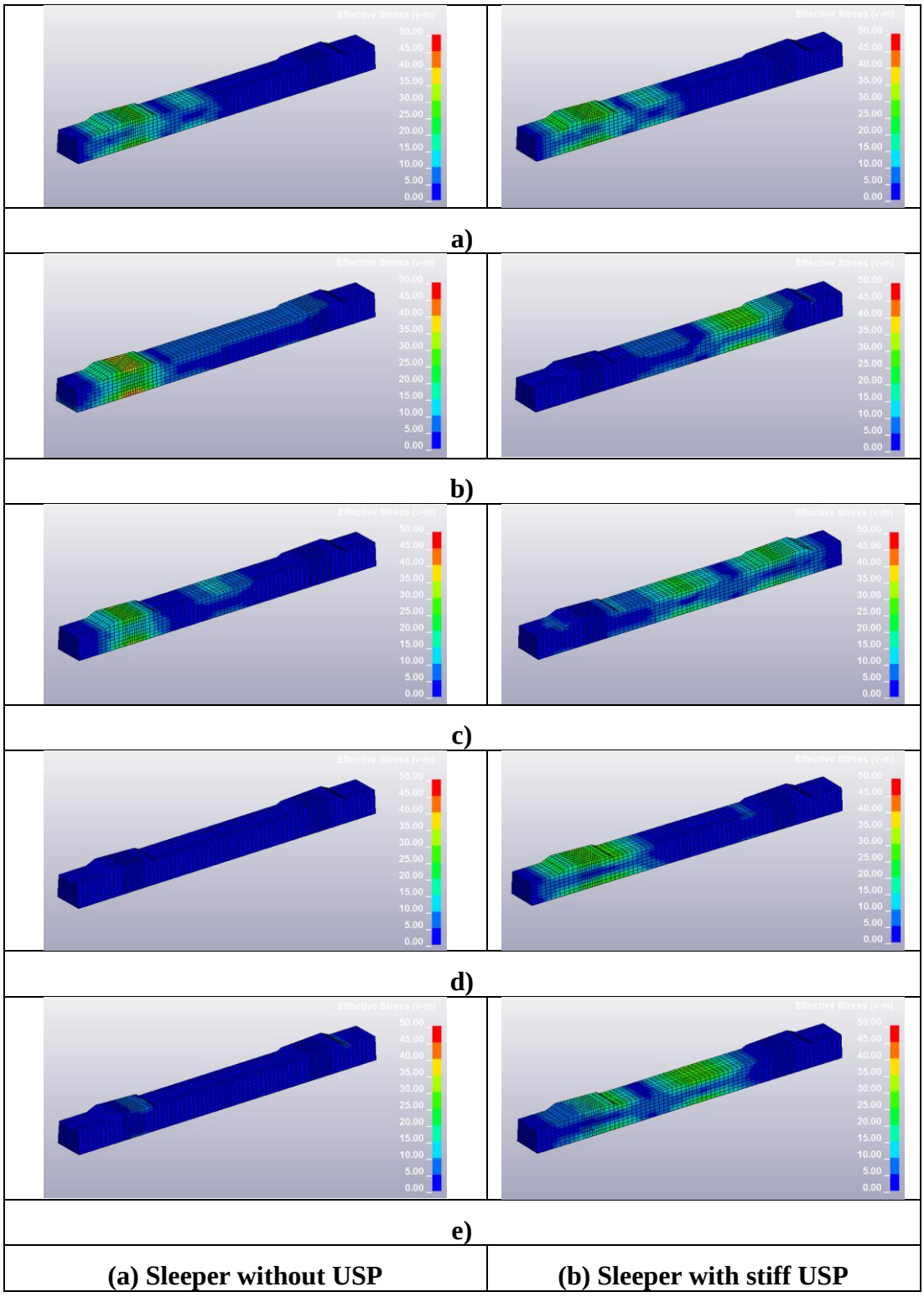

Figure 8.9 Stress contour of sleeper with USP under impact load case C at each time point.

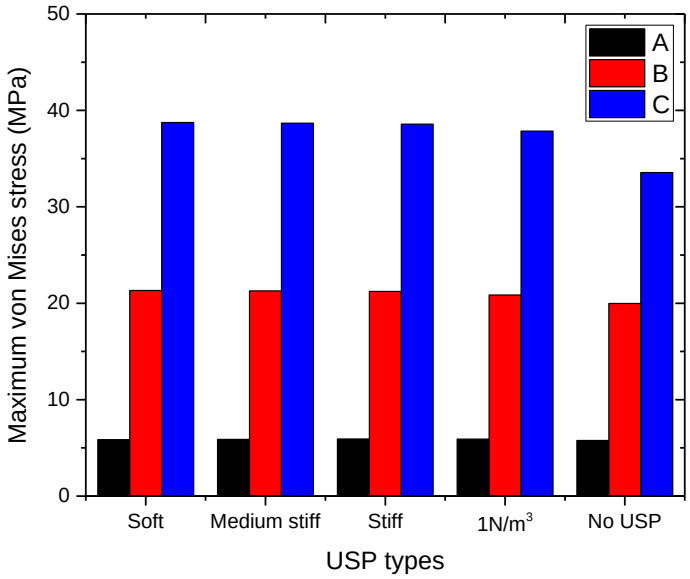

(a)

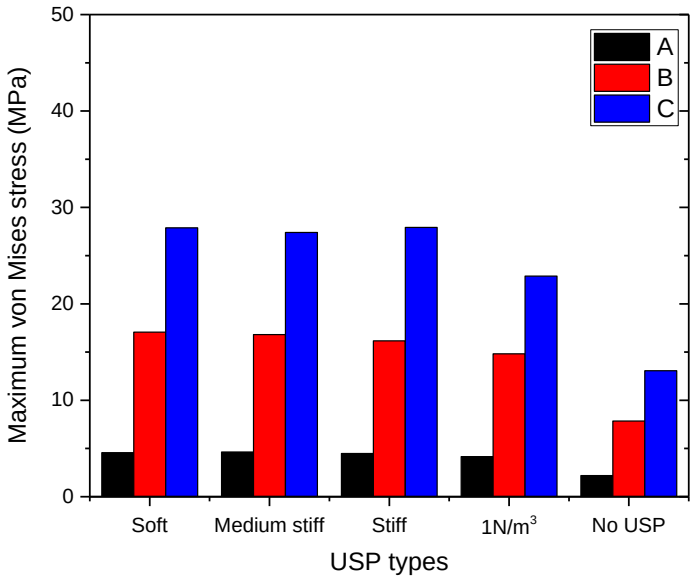

(b)

Figure 8.10 Maximum von Mises stress at: (a) rail seat and (b) mid span.

Figure 8.11 shows the maximum sleeper displacement ratio. Although it is noticeable that using USPs can obviously decrease the contact force and impulse, displacements of sleepers at both rail seat and mid-span can notably increase as well as von Mises stress. On this ground, USPs are likely to have negative effects on sleeper responses at both rail seat and mid span. This is because USPs affect the overall track characteristics by reducing track stiffness and softening the track especially at support. Even though, different USP types do not present any significant changes in von Mises stress response, sleepers with stiffer USP have lower displacement than that with softer USP. It is noticeable that sleepers with USP especially softer pad tend to have worse performance when higher impact load is applied. As for soft USPs, about 4.5-7.5 times higher sleeper displacement is observed while about 3-4 times higher sleeper displacement is observed when stiff USP is used. Moreover, greater impact load results in greater displacement ratio. This shows that USP can worsen the sleeper responses when impact load intensity is higher. However, as for a very stiff USP, about 2% displacement enlargement is observed in all load cases. Thus, an alternative USP has better performance than typical types in terms of sleeper responses. It can be also concluded that shorter impact events may have less severe responses than longer impact durations despite the maximum impact force being higher.

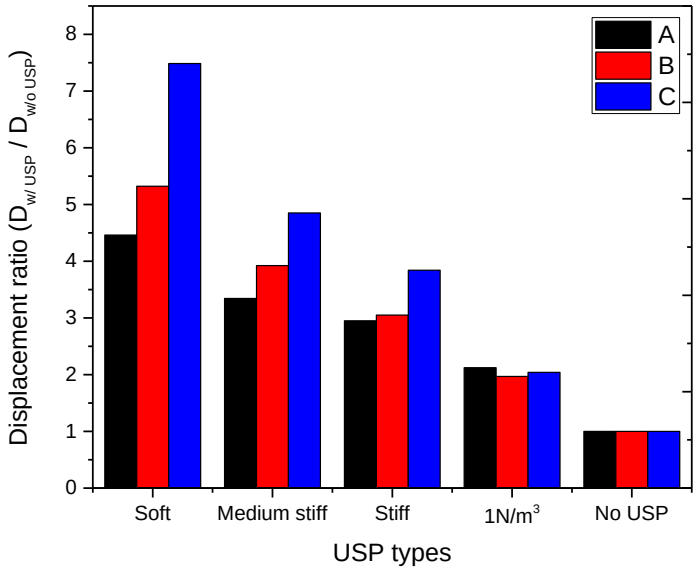

Figure 8.11 Sleeper maximum displacement ratio at rail seat

The acceleration vibrations are also presented in terms of insertion loss. Figure 8.12 presents the insertion loss against one-third octave frequency band of concrete sleepers due to USPs. Insertion loss is calculated by the logarithm of acceleration ratio of sleepers without USP with respect to that with USP under similar impact load event in terms of decibels (dB) (insertion loss $=10\log(\frac{A_{woUSP}}{A_{wUSP}})$). It can clearly be seen that USP can increase sleeper vibrations at certain frequency ranges as the insertion loss increases by softer USP. Thus, USPs tend to have greater effect on acceleration amplitude vibrations of sleepers, especially when greater amplitude of impact load is applied as seen in Figure 8.12c. This is due to the reduction of support stiffness of track by applying USP.

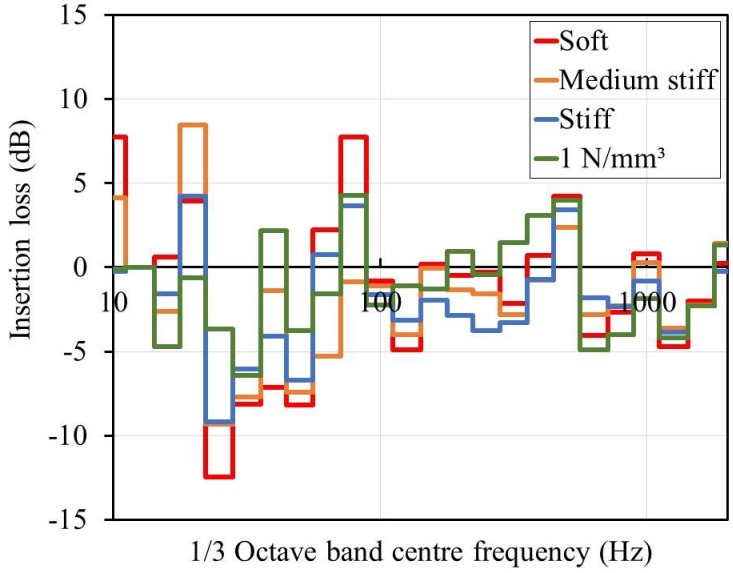
15
10
5
0
-5
-10
-15
10
100
1000
Insertion loss (dB)
1/3 Octave band centre frequency (Hz)
Soft
Medium stiff
Stiff
1 N/mm³

(a)

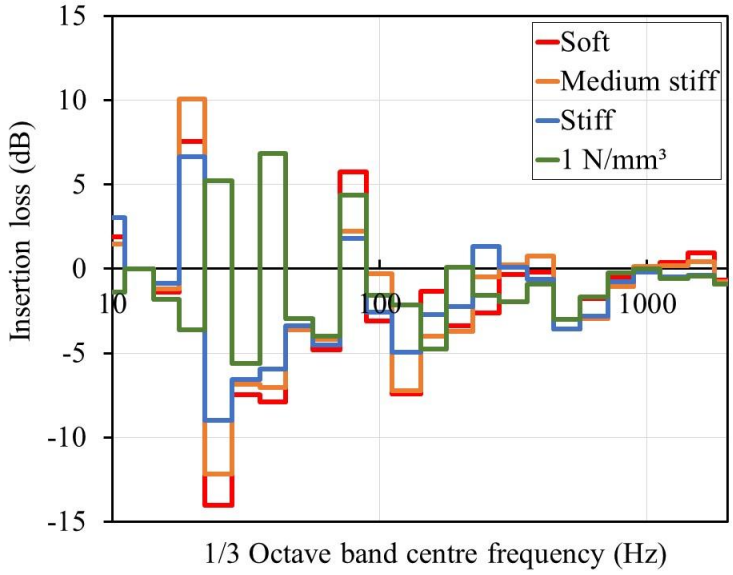
15
10
5
0
-5
-10
-15
10
100
1000
Insertion loss (dB)
1/3 Octave band centre frequency (Hz)
Soft
Medium stiff
Stiff
1 N/mm³

(b)

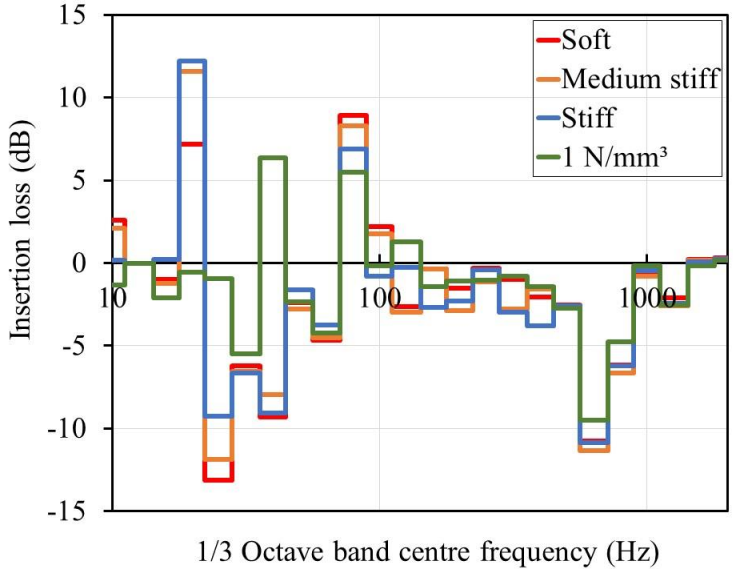

(c)

Figure 8.12 Insertion loss due to USP under load cases: (a) case A, (b) case B, and (c) case C.

8.4.4 Ballast responses

This section presents the ballast responses, which is the main aim of using USP, under impact loads to study the stiffness adaptation on railway track. It is noted that ballast is modelled as a continuum support which is assumed to be a packed assembly of particles and combined as a continuous mass in order to reduce the memory consumption and computational time. Hence, this study assumes that the ballast fully supports the sleeper with a continuous contact. In order to reduce the stress transferred from sleeper to ballast, several methods, such as USP, frame and half frame sleepers, have been previously studied and used in the field. According to previous studies (Kaewunruen, 2012, Sol-Sánchez et al., 2014), USP can obviously increase the contact area between sleeper and ballast, resulting in stress reduction on the ballast. It can reduce the stress concentration at certain points and help spread the stress to a wider area. However, the numerical analyses of this

aspect have not been fully investigated especially when railway tracks are subjected to an extreme impact loads. Figure 8.13 presents the sleeper-ballast contact forces under different load cases. It is obviously seen that USPs can potentially reduce the contact force between sleeper and ballast. It is found that sleeper-ballast contact forces can be reduced by about 70-95% using normal USP while an alternative USP (very stiff pad) can decrease contact force by 60-70% (Figure 8.14). Note that the softer USPs have a slight better effect in reducing contact force between sleeper and ballast compared to the stiffer pads. On this ground, it can be concluded that a very stiff pad can be an alternative option for use as a USP since it still has a positive effect in ballast response reduction while decreasing the negative effect on sleeper vibration compared to the traditional USPs.

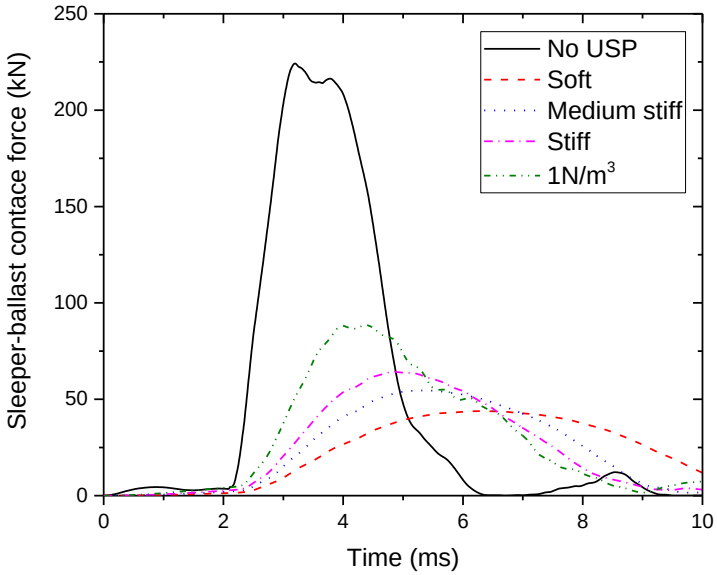

(a)

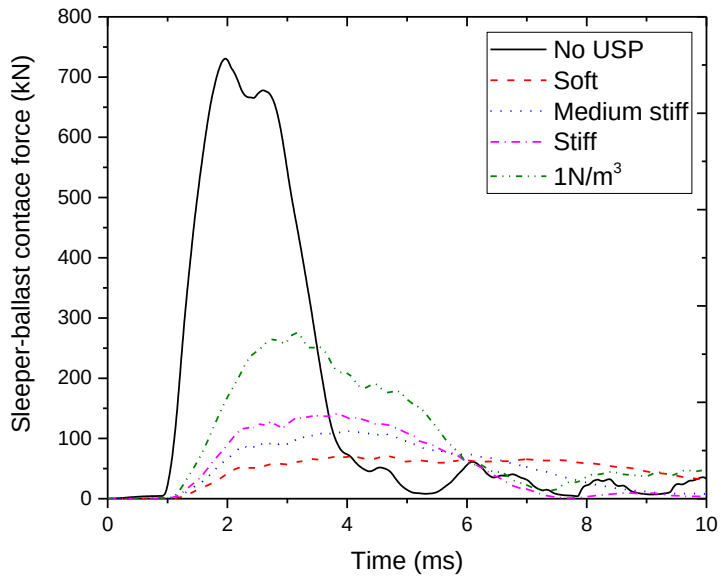

(b)

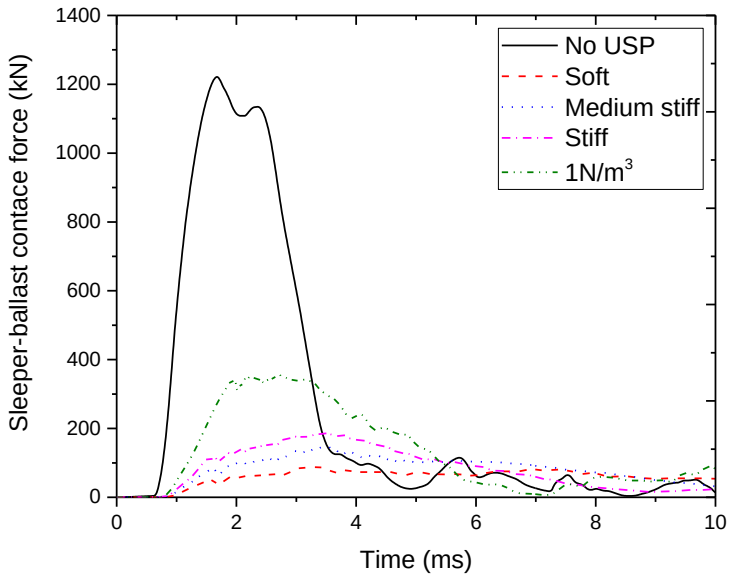

(c)

Figure 8.13 Sleeper-ballast contact force: (a) case A, (b) case B, and (c) case C.

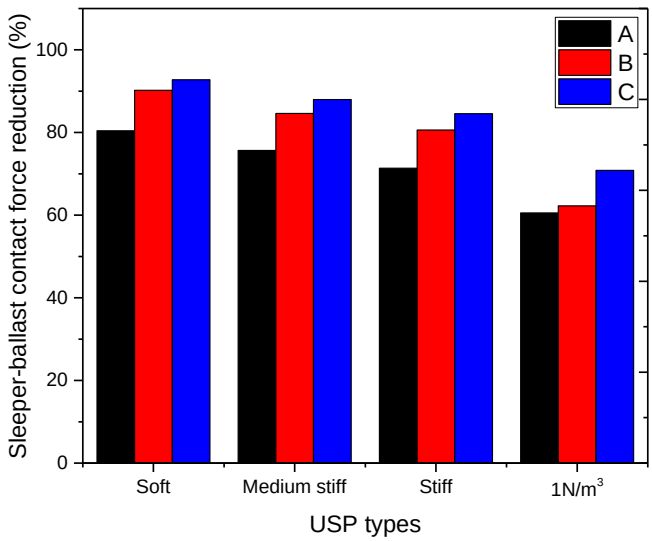

Figure 8.14 Sleeper-ballast contact force reduction.

Figure 8.15 illustrates the distribution of contact pressure on ballast under impact load at two time steps of impact event: at maximum contact force for sleeper without and with typical stiff USP (Figure 8.15a). It is clear that USP can significantly reduce the contact stress especially at concentrated rail seat, although the contact stress is redistributed over a wider area and prolong the impact duration. In addition, at rail seat, soft USP has more benefit in contact stress reduction between sleeper and ballast compared to other USPs as clearly seen in Figure 8.15. As for a very stiff pad, even though the stress responses have longer responses, the overall stress can be significantly reduced especially in the first half of impact events where the maximum stress occurs. As evidenced here, it is obvious that USPs can help prevent ballast pulverisation and breakage, which is a main cause of ballast fouling, resulting in maintaining its lateral resistance for restraining track stability.

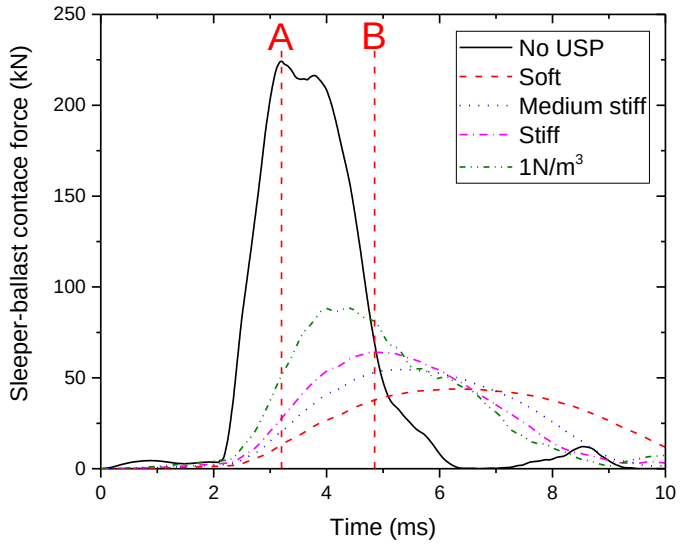
A
B
No USP
Soft
Medium stiff
Stiff
1N/m3
Sleeper-ballast contace force (kN)
Time (ms)
0
50
100
150
200
250
0
2
4
6
8
10

(a)

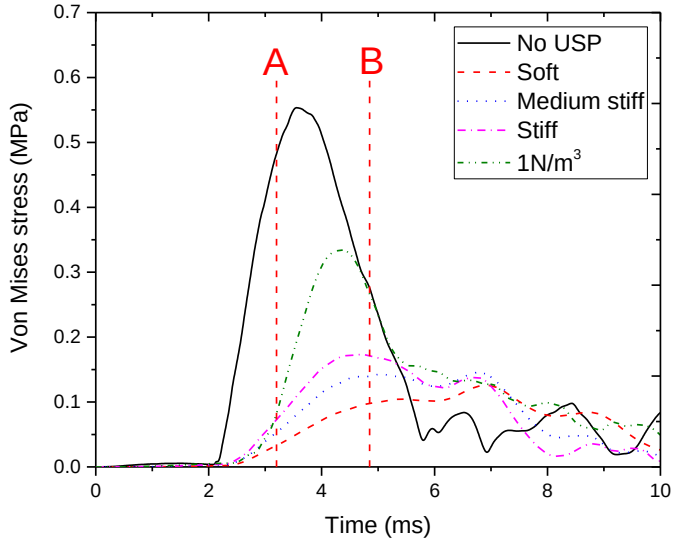
A
B
No USP
Soft
Medium stiff
Stiff
1N/m3
Von Mises stress (MPa)
Time (ms)
0.0
0.1
0.2
0.3
0.4
0.5
0.6
0.7
0
2
4
6
8
10

(b)

No USP	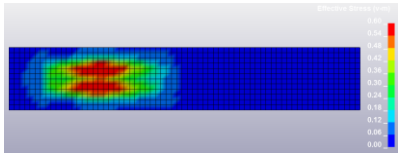	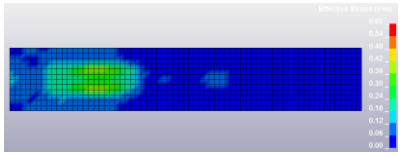
Soft USP	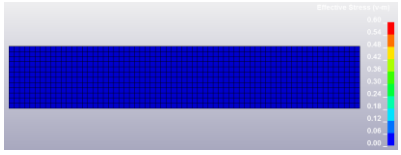	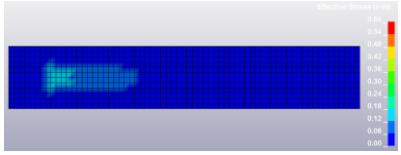
Medium stiff USP	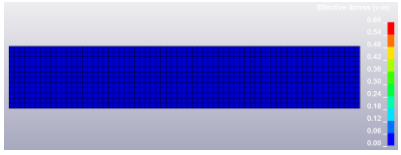	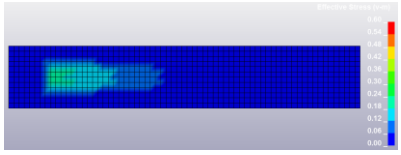
Stiff USP	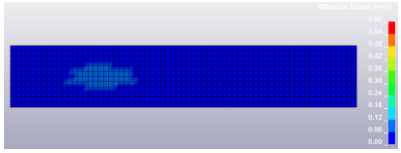	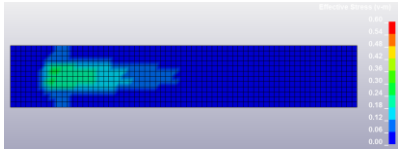
1 N/mm^3	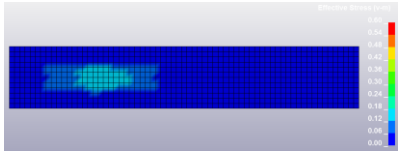	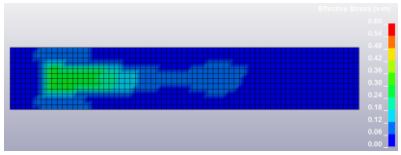
	A	**B**

(c)

Figure 8.15 Ballast responses: (a) sleeper-ballast contact force, (b) von Mises stress at rail seat over time, and (c) von Mises stress distributions.

8.5 Summary

Recently, elastic components have been used as an additional element in railway track to improve its resilience and prolong service life. This can help improve track performance and attenuate noise, vibration, and impact load. Under Sleeper Pads (USPs) attached underneath sleepers have been proposed for use in the field to reduce track vibration. It is highlighted that USP can redistribute the transferred load, and increase contact area leading to reducing stress concentration. It can also help increase lateral resistance of ballasted

tracks as confirmed by STPTs. However, the short service life of USPs is a concern leading to the need to study economic outcomes and its life cycle. Life cycle cost analysis (LCCA), which is a decision-making process to help determine the present and future values of the projects, is used for analysing the cost benefit of using USP based on the data in the literature. This chapter first presents the life cycle and feasibility of using USP in railway track in terms of long-term cost. It can be concluded that although railway track with USPs have higher initial costs than that without USPs, the cumulative cost of the project decreases significantly as a results of lower annual maintenance costs. However, due to the limited studies and data in this field, it is recommended that more factors, such as uncertainty, risk, operation cost, should be also taken into account when these data exist in the future.

The emphasis of this chapter is also on the effects of USPs on the dynamic responses of prestressed railway concrete sleeper subjected to extreme impact loading using Finite Element Modelling (FEM). An experiment prototype of drop mass test for single sleeper in the past was conducted and USP was then inserted to study its effects on sleeper due to impact loading. Three main typical types of USPs: soft, medium, and stiff were considered in this study. An alternative called ‘very stiff pad’ with the bedding modulus of 1 N/mm^3, was also studied in order to ascertain its feasibility for use as USP. The initial velocities were applied to drop mass to generate impact events on the rail. The models were validated against the experimental results. The initial velocities applied to the mass corresponded to the drop mass of 600kg with the variations of height. This study is the first to consider the influences of an extreme impact loads on railway track responses taking the coupling track defects into account. It is noted that an impact load of about 1000kN that can be found at

the location of the coupling track defects was applied to the model. The results show that the USPs can significantly reduce contact forces by about 8-12%. Although this study has found that sleepers with USPs tend to have lesser flexures, contact forces and impulse under the similar drop mass, and sleepers with USP could experience larger displacement and acceleration amplitude vibrations. The higher the impact load, the higher sleeper vibration. The results confirm field measurement data on rail joints on Austimer track (Illawarra Line in NSW Australia) that the sleeper vibration can increase at rail joint due to impact load. However, the main advantage of using USP is to reduce the load distributed to ballast. It results in minimising ballast breakage and pulverisation. As for the ballast responses, it is interesting that softer USPs effectively provide better load distribution performance on ballast compared to stiffer ones, although, the USPs may have negative effects on sleeper responses under impact loads. However, a proposed very stiff USP with a bedding modulus of 1 N/m^3 can still reduce the ballast responses by 60-70% while it has lower negative responses on sleeper vibrations. Importantly, USPs can obviously help to maintain the lateral resistance of the tracks by reducing the stress transmitted to the ballast from the impact loads, which are the cause of ballast fouling. As evidenced in Chapters 6 and 7 that the ballast fouling from impact loads causes a significant reduction in track stability leading to higher risk of track buckling, the results in this chapter shows that USPs may also indirectly help to reduce the risk of track buckling. Furthermore, the outcome of this study provides a significant evidence for a very stiff USP that can potentially reduce the negative effects on sleepers. It can be concluded that the applications of USPs should be done careful especially in areas prone to extreme impact load corresponding to a high-speed train travelling over short-pitch rail defects, rail joints, coupled defects and crossings

since the USPs could trade off the desired benefits by increasing the dynamic responses of sleepers with USPs. The new findings from this study will improve the design of USPs for particular areas prone to aggressive impact load and to help track engineers to make better decisions on the usage of USPs in railway networks.

8.6 References

ALVES RIBEIRO, C., PAIXÃO, A., FORTUNATO, E. & CALÇADA, R. 2015. Under sleeper pads in transition zones at railway underpasses: numerical modelling and experimental validation. *Structure and Infrastructure Engineering,* 11**,** 1432-1449.

BRITISH STANDARDS INSTITUTION 2016. BS EN 16730:2016 Railway applications — Track —Concrete sleepers and bearerswith under sleeper pads. UK: BSI Standards Limited.

CAI, Z. 1994. *Modelling of rail track dynamics and wheel/rail interaction.* PhD thesis, Queen's University.

DEUTSCHE BAHN, A. & HANS-JOERG, T. 2011. State of the art review of mitigation measures on track. *Deliverable D,* 3.

GUEDELHA, P. L. 2012. Materiais elásticos como elementos de protecção em vias balastradas.

KAEWUNRUEN, S. 2007. *Experimental and numerical studies for evaluating dynamic behaviour of prestressed concrete sleepers subject to severe impact loading.* Doctor of Philosophy, University of Wollongong.

KAEWUNRUEN, S. 2012. In situ performance of under-sleeper pads (USPs) at glued insulated joints (GIJs). *Technical Rep. TR,* 208.

KAEWUNRUEN, S., AIKAWA, A. & REMENNIKOV, A. M. 2017. Vibration attenuation at rail joints through under sleeper pads. *Procedia Engineering,* 189**,** 193-198.

KAEWUNRUEN, S. & CHIENGSON, C. 2018. Railway track inspection and maintenance priorities due to dynamic coupling effects of dipped rails and differential track settlements. *Engineering Failure Analysis,* 93**,** 157-171.

KAEWUNRUEN, S. & REMENNIKOV, A. 2007. Low-velocity impact analysis of railway prestressed concrete sleepers. 23rd Biennial Conference of the Concrete Institute of Australia: Design, Materials, and Construction, October, 18-20 Adelaide, Australia. 659-668.

KAEWUNRUEN, S. & REMENNIKOV, A. 2006a. Non-destructive testing (NDT): A tool for dynamic health monitoring of railway track structures. *Materials Australia,* 39**,** 14-16.

KAEWUNRUEN, S. & REMENNIKOV, A. 2006b. Nonlinear finite element modelling of railway prestressed concrete sleeper. *10th East Asia-Pacific Conference on Structural Engineering and Construction.* Bangkok, Thailand.

KAEWUNRUEN, S. & REMENNIKOV, A. 2007. Experimental and numerical studies of railway prestressed concrete sleepers under static and impact loads. *Civil Computing,* 3**,** 25-28.

KAEWUNRUEN, S. & REMENNIKOV, A. M. 2008. Experimental simulation of the railway ballast by resilient materials and its verification by modal testing. *Experimental Techniques,* 32**,** 29-35.

KAEWUNRUEN, S. & REMENNIKOV, A. M. 2009. Progressive failure of prestressed concrete sleepers under multiple high-intensity impact loads. *Engineering Structures,* 31**,** 2460-2473.

LANGDON, D. 2007. Life Cycle Costing (LCC) as a contribution to sustainable construction: a common methodology. *Literature Review, Davis Langdon Management Consulting*.

NGAMKHANONG, C., LI, D., REMENNIKOV, A. M. & KAEWUNRUEN, S. 2019. Dynamic capacity reduction of railway prestressed concrete sleepers due to surface abrasions considering the effects of strain rate and prestressing losses. *International Journal of Structural Stability and Dynamics,* 19**,** 1940001.

PAIXÃO, A., ALVES RIBEIRO, C., PINTO, N., FORTUNATO, E. & CALÇADA, R. 2015. On the use of under sleeper pads in transition zones at railway underpasses: experimental field testing. *Structure and Infrastructure Engineering,* 11**,** 112-128.

SOL-SÁNCHEZ, M., MORENO-NAVARRO, F. & RUBIO-GÁMEZ, M. C. 2014. Viability of using end-of-life tire pads as under sleeper pads in railway. *Construction and Building Materials,* 64**,** 150-156.

STANDARDS AUSTRALIA 2001. Design of concrete structures. Australia: Australian Standard.

STANDARDS AUSTRALIA 2003a. Railway track material *Part 14: Prestressed concrete sleepers.* Australia: Australian Standard.

STANDARDS AUSTRALIA 2003b. Railway track material. *Part 19: Resilient fastening assemblies.* Australia: Australian Standard.

WAKUI, H. & OKUDA, H. 1997. A study on limit state design method for prestressed concrete sleepers. *Doboku Gakkai Ronbunshu,* 1997**,** 35-54.

YOU, R., GOTO, K., NGAMKHANONG, C. & KAEWUNRUEN, S. 2019. Nonlinear finite element analysis for structural capacity of railway prestressed concrete sleepers with rail seat abrasion. *Engineering Failure Analysis*, 95**,** 47-65.

CHAPTER 9

CONCLUSIONS AND RECOMMENDATIONS

9.1 Introduction

This doctoral thesis aims at investigating the buckling phenomena of ballasted railway tracks under extreme temperatures to clearly understand this vulnerability in order to improve a ballast track's resilience to extreme temperatures. The critical reviews in Chapters 2 and 3 discussed previous research work done over the past decades and existing research gaps. In order to achieve the main aim and objectives, several research activities have been carried out at the University of Birmingham, while some parts have been carried out in collaboration with the University of Illinois of Urbana-Champaign in the USA through European Commission Project No. 691135. This project aims to improve response and resilience of rail infrastructure systems to climate change, extreme events from natural and human-made hazards, and future operational demands. The research findings and recommendations for future research are summarised in this chapter.

9.2 Research Findings

As stated in Chapter 1, to achieve the main aim of this doctoral thesis, the objectives are successfully accomplished. The first research objective is to identify the existing research gap related to the vulnerability to extreme heat and the buckling phenomena of ballasted railway tracks. Insufficient research and questions arising from the literature review are first identified. It is necessary to conduct the studies that needed to be expanded and had not been resolved in the past.

The critical literature review investigates the past and current studies related to the resilience and behaviour of ballasted railway tracks under extreme temperatures. The past

research regarding methodologies is adopted for improvement for a better understanding and new outcome of this doctoral thesis. The research objectives are achieved using three main methodologies. The parametric studies conducted are described in Chapters 4 and 5 to identify the critical parameters and buckling phenomena. A cost-effective method to improve the buckling strength and the resilience of the existing railway tracks is also proposed. Note that this study uses different numerical approaches based on the different purposes to potentially understand structural behaviour of railway tracks under elevated temperature. Chapter 4 uses linear eigenvalue analysis to first study the influence of each parameter. This method can clearly help to identify the most critical parameters and largely save the computational time. However, this method has limitation as it can only include linear property. To overcome the limitation in Chapter 4, nonlinear analysis is used in Chapter 5. This approach considers nonlinear property so that the results provide higher accuracy than the previous one, but the computational cost is also relatively high. Thereafter, the coupling method FEM-DEM (Finite Element-Discrete Element Modelling) is carried out to first evaluate the lateral vulnerability of ballasted railway tracks using DEM in Chapter 6, and then, the buckling phenomena are investigated at the corresponding vulnerable railway tracks using nonlinear FEM in Chapter 7. Lastly, in Chapter 8, Under Sleeper Pads (USPs) are adopted using FEM to improve track resilience and protect the ballast from extreme impact loads.

9.2.1 Parametric studies to identify critical parameters influencing buckling strength

The objective is to identify the critical parameters related to the buckling phenomena. The previous studies have presented various critical factors in relation to the buckling

phenomena due to extreme heat. However, the past research has not covered all the phenomena and the behaviours that can be observed in real life. This doctoral thesis presents the 3D finite element model of the traditional ballasted and interspersed railway tracks to identify the critical parameters and components and to investigate the buckling phenomena under extreme heat. Parametric studies have been conducted to accomplish the objectives of this doctoral thesis. The traditional timber sleepered track, which buckles easily, is first built, and then, the timber sleepers are replaced by the concrete sleepers to build the interspersed railway tracks and the concrete sleepered tracks. Five railway tracks, namely timber sleepered, '1 in 2', '1 in 3', '1 in 4', and concrete sleepered tracks, are built to compare their buckling resistances to extreme heat. Two methods, namely linear analysis and nonlinear analysis, are used to evaluate the buckling phenomena of ballasted railway tracks considering various parameters.

In the linear analysis, the buckling shape and the corresponding buckling temperature are analysed considering the variation of lateral resistance, torsional resistance, and unconstrained length. The buckling path could not be obtained by the linear analysis, as this method can only analyse the buckling temperature at the bifurcation point; thus, the buckling mechanism cannot be evaluated. It is noted that buckling failure mechanism can be obtained by buckling path. The lateral resistance of the ballasted railway tracks plays a significant role in determining the buckling strength. The torsional resistance of the fastening system can also influence the buckling strength when the lateral resistance is low. It is important to minimise the length of the weaker area (unconstrained length) and keep the tracks restrained laterally, as these can significantly help to increase the buckling temperature. Importantly, the reducing unconstrained length to 12 m of the railway tracks

can significantly increase the buckling temperature. Note that the constrained length has no effect when it is larger than approximately 24 m. Under the same unconstrained length, increasing the lateral resistance results in more wave cycles of the sinusoidal buckling shape with a higher buckling temperature.

In comparison to the linear analysis, the buckling temperatures obtained from the nonlinear analysis are considerably lower. The safe temperature can be evaluated in the nonlinear analysis as the buckling path and buckling failure mode are obtained. The nonlinearities including the geometric and the material properties are included in the nonlinear analysis. The overall trends obtained by the parametric study is similar to that obtained by the linear analysis. However, deeper knowledge can be obtained by the nonlinear analysis. The key findings show that, in the same track profile, the interspersing approach can shift the buckling failure mechanism from progressive buckling to snap-through buckling. Even though the torsional fastening resistance has a slight effect on the buckling temperature, it can significantly increase the safe temperature that in turn helps the timber sleepered tracks to tackle the extreme heat. However, interspersed and concrete sleepered tracks obviously help to increase the buckling strength because of the higher lateral resistance from the concrete sleepers. In the case of the unloaded track, despite the fact that the timber sleepered tracks might have a higher safe temperature than the interspersed and concrete sleepered tracks, the timber sleepered tracks require less buckling energy to buckle the track at the safe temperature level. This is attributed to the fact that the difference between the buckling temperature and the safe temperature is considerably less than that in the case of the interspersed and concrete sleepered tracks, showing that the timber sleepered tracks are more likely to have a progressive buckling failure than the others.

9.2.2 Coupling method FEM-DEM for lateral vulnerability influencing track buckling phenomena

According to the findings derived from the parametric studies, track buckling occurs when the tracks lack ballast support. It can be concluded that the major factor affecting the buckling strength is the lateral resistance from the sleeper–ballast interaction. Although the lateral resistance of the ballasted railway track has been investigated through the Single Sleeper (Tie) Push Test (STPT) by using both experimental and numerical approaches, a research gap has been found: to the best of my knowledge, the effects of the progressive fouling of the ballast, which is usually seen in the field, on the track's lateral resistance has thus far never been investigated. Note that, after the ballast breakdown, the ballast fines migrate from the top to the bottom and starts to accumulate at the bottom of the ballast layer. The ballast fouling is usually caused by the impact load. The study used Discrete Element Modelling (DEM), which has been proven to be an effective tool to analyse the realistic particle interaction of the ballast, to conduct the STPTs of the ballasted railway tracks considering the progressive fouling of the ballast. The results show that the ballast fouling significantly reduce the lateral resistance of the ballasted track even if the fouled ballast is observed in the bottom layer where there is no direct contact with the sleeper. This implies that the lateral resistance is progressively reduced over time. The ballast fouling condition can reduce the lateral resistance by up to approximately 48% for the timber sleepers and 64% for the concrete sleepers if the entire ballast layer is fully fouled. This is the new insight that has never been reported elsewhere. Thereafter, the obtained lateral force–displacement curves of the sleepers under different fouling conditions are applied to the FEM model to investigate the buckling temperature by using the nonlinear

analysis. The ballast degradation is coupled with the initial track misalignment. The new findings show that, in the same track profile, the buckling failure mode be shifted from the snap-through to the progressive buckling mode when this progressive degradation includes a larger track lateral misalignment and a higher depth of the fouled ballast layer. It is obvious that ballast fouling can significantly reduce both the buckling and the safe temperatures of the tracks until the risk level, as the allowable temperature can fall from between 40°C and 60°C to between 20°C and 30°C for the long CWR track. This doctoral thesis has proven that the risk of track buckling is far greater for railway tracks with fouled ballast conditions even if the fouled ballast is hidden in the bottom layer where there is no direct contact with the sleeper. The outcome will enhance the development of the inspection criteria for the ballast lateral resistance and support conditions, improve the safety and reliability of the rail network, and mitigate the risk of delays due to the track buckling leading to unplanned maintenance. On this ground, the control of sleeper-ballast contact stress is essential to reduce ballast deterioration and eventually ballast fouling which can result in poorer lateral track resistance.

9.2.3 Under Sleeper Pad (USPs) for ballast protection from extreme impact loads

As aforementioned, ballast fouling, whose main cause is the ballast breakdown from impact loads, can significantly reduce the buckling strength of ballasted railway tracks showing that the prevention of ballast breakage is very crucial. This study proposes the use of Under Sleeper Pad (USP) as an alternative to prevent ballast breakage. Even though previous studies have shown that the sleepers with traditional USPs could have lesser flexures, contact force, and impact energy, sleeper vibration could be slightly amplified by

installing USPs. This doctoral thesis proposes a new type of USP with a higher bedding modulus representing a 'very stiff USP' to ascertain the drawbacks of the traditional ones. The emphasis of this doctoral thesis is on the effects of USPs on the dynamic responses of railway concrete sleepers subjected to extreme impact loading by using FEM. An experimental prototype of the drop mass test for single sleepers is conducted, and a USP is then inserted to study its effects on the sleeper under extreme impact loading. It is noted that numerical modelling is first validated with previous experiment using the case of low-intensity impact load.

The results reveal that the sleeper with the traditional USP might have larger vibration than that without the USP. However, USPs could help decrease the stress transmitted to the ballast under impact loads. This clearly shows that USPs can help to minimise ballast breakage, which undermines track stability. However, the negative effects on amplified sleeper vibration due to the installation of USPs should be observed carefully. It is found that the higher the impact load is, the larger is the sleeper vibration amplitude. Nevertheless, a very stiff USP can help to reduce the negative effects on the sleeper vibration as compared to the traditional USPs, while it can still significantly reduce the stress transmitted to the ballast. The outcome of this study provides significant evidence for a very stiff USP that can potentially lead to minimising ballast breakage. It can be concluded that the applications of USPs should be carried out carefully, particularly in the area vulnerable to extreme impact loads corresponding to a high-speed train travelling over short-pitch rail defects, rail joints, coupled defects, and crossings, as the USPs could trade off the desired benefits by aggravating the dynamic behaviour of the sleepers with USPs. Hence, the use of a very stiff USP is recommended at the areas prone to extreme impact

loads. This benefit combined with its effect on improving the lateral resistance leads to a better railway track stability. The new findings from this study will improve the design of USPs for particular areas prone to an aggressive impact load and to help track engineers to make better decisions on the usage of USPs in railway networks.

9.3 Recommendations for Future Research

Despite the several findings reported in this doctoral thesis, future studies are needed to further extend the knowledge and translate the outcome of this study into real-life practice. The outcomes of this study have enhanced the need for future research as follows:

- This study proposes an alternative cost-effective approach to improve the buckling strength of ageing ballasted railway tracks. It is suggested that the replacement of rotten sleepers should be done every 20 spans or 12 m to considerably increase the buckling resistance of the ballasted railway tracks. This spot replacement method can significantly improve the buckling strength if these new spans are fully restrained in the lateral plane. To improve the lateral resistance, the ballast must be well filled and fully stabilised. However, the aim of spot replacement is to improve the stability of the existing railway tracks, which only requires the sleepers to be replaced so that the activities related to the ballast are not conducted. Note that the emphasis is placed on the sleepers which are needed to be fully restrained laterally. On the basis of the results of interspersed track buckling, it is found that replacing a timber sleeper by a concrete sleeper, which is assumed to have 40% larger lateral resistance, can increase the buckling temperature by 25%. To achieve the target, the lateral resistance of the spot replacement must be higher than that of the existing

spans. According to some previous literatures, there are some methods that can potentially help to improve the lateral stability, e.g. frictional sleeper, ladder sleeper, and nailed sleeper. Nonetheless, the sleeper replacement activity should be performed very carefully to avoid the ballast disturbance that may lead to less ballast compaction.

- Obviously, it is evidenced that ballast fouling causes a significant reduction in the buckling strength of the vulnerable ballasted railway tracks. Moreover, the inspection and the monitoring of the ballast are needed across the ballast profile to maintain a good support condition. The time-dependent degradation data of the railway ballast should be evaluated in order to map the data with the obtained results in this doctoral thesis to appropriately maintain the performance and stability of the ballast by ballast cleaning or renewal, or sleeper restraint. The appropriate linking data between the monitoring of the time-dependent degradation of the ballast from the field and the results presented here will potentially help to move from the scheduled preventive maintenance to a more rational predictive maintenance approach.
- This doctoral thesis focused on the extreme heat alone on the unloaded ballasted railway tracks. Various factors have been taken into account for evaluating their influences on the buckling phenomena of the misaligned railway tracks. In fact, trains running over the unstabilised track can have an impact on the buckling phenomena by adding the forces in both the vertical and the lateral directions. They may increase the likelihood of track buckling, particularly when the wheel and the track are defected. It is recommended to include the dynamic train loads on the

tracks in the future research. A train-track Multi Body Simulation (MBS) should be performed earlier to obtain the wheel–rail contact forces that will be applied further in the buckling analysis. Note that the effects of the wheel–rail irregularities can be included in MBS.

- This doctoral thesis used the rubber layers to replicate a realistic ballast according to the Australian Standard in order to reduce the computational time and only focus on the stress concentration on the top layer of the ballast. The results have shown that USPs can obviously help to reduce stress from the extreme impact loads on the ballast. However, it is recommended to extend the FEM model to further investigate the stress distribution through the ballast profile to the underlying layers under impact loads, which are known to be the major cause of ballast fouling. However, this doctoral thesis focused on the single impact event, which could rarely break the ballast particle. In fact, railway tracks generally experience fatigue or multiple impact loads that can actually break the ballast particles after a number of cycles.
- As aforementioned, an alternative USP, with a slightly larger bedding modulus than that of the traditional USPs, is proposed and found to provide better performance under impact loading conditions. However, this is just the beginning for an improved understanding of an alternative USP. This type of USP has never been manufactured and placed in any standards. Therefore, additional laboratory and field measurements are needed to verify the results obtained in this doctoral thesis.